NASA TM-X-69910

X-401-72-332

EARTH OBSERVATORY SATELLITE
(EOS)
DEFINITION PHASE REPORT

VOLUME 1

PRICES SUBJECT TO CHANGE

AUGUST 1971

GSFC ——— GODDARD SPACE FLIGHT CENTER ———
GREENBELT, MARYLAND

EARTH OBSERVATORY SATELLITE
(EOS)

DEFINITION PHASE REPORT

Study Manager
Wilber B. Huston

August 1971

Approved by: _____

Dr. R. A. Stampfl
Assistant Director for Projects
(Advanced Projects)

GODDARD SPACE FLIGHT CENTER
Greenbelt, Maryland

NOTICE

This report presents the results of technical studies conducted during 1971 by the Goddard Space Flight Center of an Earth Observatory Satellite (EOS) system.

These studies were reviewed by an EOS Mission Review Group (EOSMRG) comprised of technical experts in their particular fields. Copies of the complete Definition Study are available and may be obtained by contacting:

> Mr. Wilber B. Huston
> EOS Study Manager
> Goddard Space Flight Center
> Greenbelt, Maryland   20771
> Tel: 301/982-2488

The GSFC study is a part of the effort leading to the identification and evaluation of different options for future earth observation systems. This activity will be continued. User Agency review and coordination will be conducted prior to any decision to proceed with development.

Release of these reports is for general information only and should not be construed as a commitment by NASA management to either the EOS configuration or mission options identified therein.

ii

FOREWORD

This report covers the results of the Earth Observatory Satellite (EOS) System Definition Studies conducted at the Goddard Space Flight Center (GSFC). These studies show that the concept of an Earth Observatory Satellite series in a near-earth, sun-synchronous orbit would make a unique contribution to the goals of a coordinated program for acquisition of data for environmental research with applications to earth resource inventory and management. This report provides the technical details for the proposed development of sensors, spacecraft, and a ground data processing system with a launch goal of early 1976. Volume 2 contains the Appendixes to this report.

This Definition Phase Study and the results presented represent the concerted efforts of the following individuals:

Wilber B. Huston	Study Manager
William R. Bandeen	Study Scientist
Clarence Cantor*	System Engineer
Charles R. Laughlin	System Engineer
Kenneth W. Stark	Mechanical Systems

Staff

William L. Alford	Ground Data Processing
James L. Cooley	Orbit Analysis
Thomas R. Cooney*	Sensor Technology
Joseph Epstein	Isotope Power Systems
Paul M. Feinberg	Spacecraft Data Systems
David B. Friedman	Documentation
Joseph F. Fry	Power System
Dr. Per Gloersen	Sensor Technology
Isidore L. Goldberg	Sensor Technology
Robert J. Goss	Launch Vehicles
Dr. Arun K. Guha	Attitude Control System
Leonard Hardis	Mission Analysis
Abe Kampinsky	Sensor Technology
George C. Keller	Space Shuttle System
Francis J. Logan	Space Communications

* Retired from Government Service - May 1971

Henry Maurer, Jr.	Spacecraft Testing
Marvin S. Maxwell	Spacecraft Data Systems
Edwin G. Moses	Power Systems
Harvey Ostrow	Sensor Technology
Carl Powell	Tape Recorders
Dr. Allan Sherman	Thermal Control
Dr. Thomas J. Smugge	Sensor Technology
Albert A. Yetman	Orbit Adjust System
Dr. Thomas T. Wilheit	Sensor Technology

User Group Consultants

S. R. Addess	USDI/USGS
Dr. John Apel	NOAA/AOML
Dr. William Davis	USDC/NOAA
Dr. S. Q. Duntley	Scripps Institution of Oceanography
Dr. R. W. Fary, Jr.	USDI/USGS
Dr. Kirby Hansen	NOAA/AOML
Dr. W. Kellogg	NCAR
John E. Masterson	NCAR
Dr. Robert H. Miller	USDA
John W. Sherman	SPOC
Dr. Alan Strong	NOAA/NESS
John Tyler	Scripps Institution of Oceanography
Comdr. Donald Walsh	USN
H. Yotko	SPOC
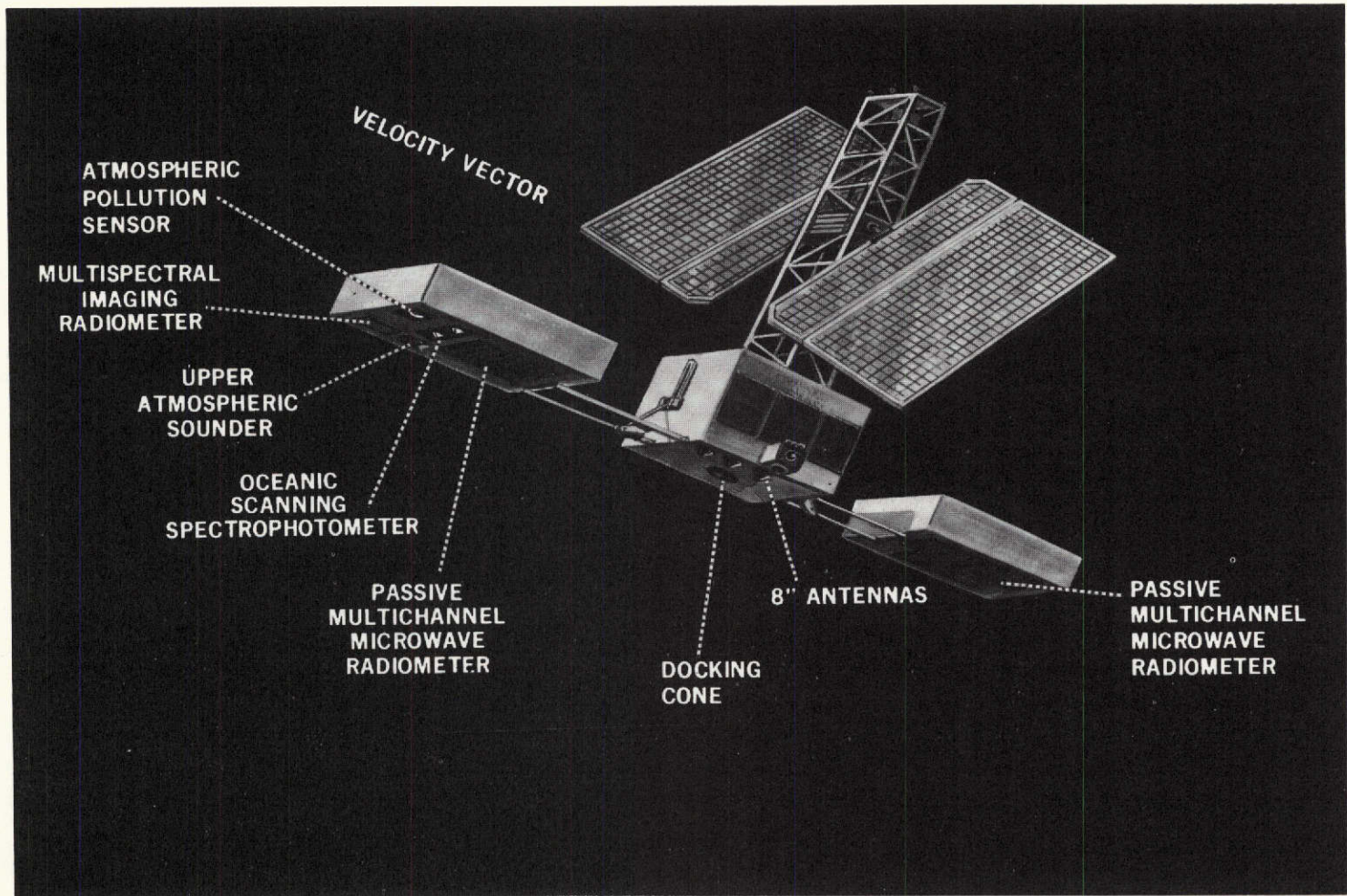
Frontispiece. Artist's Conception of EOS A

CONTENTS

VOLUME 1

SECTION 1

INTRODUCTION

SECTION 1

INTRODUCTION

This report describes the results of the Earth Observatory Satellite (EOS) Definition Study performed at the Goddard Space Flight Center. The EOS system will provide a space platform for testing experimental sensors and spacecraft subsystems for acquisition of data for environmental research and for development of space applications in earth resources, environmental management and meteorology. Emphasis is placed on combining instruments into payload combinations that will complement one another synergistically.

As presently authorized, the ERTS and Nimbus programs will launch their final flights in 1973 and 1974, respectively. With completion of these flight programs, an important capability for gathering data for the earth observation disciplines will have come to an end. To meet the continuing and future needs of these disciplines, the EOS program is directed toward the goal of an earth observatory satellite which would not only continue the terrain survey and meteorological research previously provided by ERTS and Nimbus, but would initiate new programs in the study of oceanographic phenomena and environmental quality.

NASA and other Government agencies have recently expanded their research efforts on applications of data which can be acquired by remote sensing from space. To assure maximum coordination of requirements, an interagency group, the Earth Resources Survey Program Review Committee (ERSPRC), has been established. The Benefits Studies Subcommittee of ERSPRC has supported the present study by providing consultants on sensor applications which meet the data needs of the earth observation disciplines. In the course of the study an extensive effort has been devoted to the definition of sensors for EOS payloads which are within the state-of-the-art and could be available for an initial flight in 1976. The study also includes an examination of the future course of sensor development and of the ways in which this development could influence the evolution of future earth observation spacecraft. Instruments which could be ready for flight by 1980 are identified. In the payloads considered for EOS A and B, the major spacecraft allocation has been to facility-type payloads designed to meet the needs of user agencies. A portion of the spacecraft has also been reserved for support of sensors which are currently under development in the NASA Advanced Applications Flight Experiments (AAFE) program.

In the conduct of the study, a preliminary spacecraft configuration has been designed which establishes the feasibility of the spacecraft system. This design utilizes a configuration which can be realized in various sizes related to the diameter of the NASA complement of launch vehicles, 8-feet (Delta), 10-feet (Atlas or Titan) and 15-feet (Space Shuttle). For early flights, it is concluded that a Delta-launched spacecraft is adequate to the mission goals, but the course of sensor development is such that a larger spacecraft will very likely be required before 1980. The configuration studied is capable of accommodating this growth without major structural redesign.

In the body of the report, Section 2 provides a summary of principal results. Section 3 traces the development of the Earth Observation Mission during the past 10 years and describes the role of the Earth Observatory Satellites. Section 4 provides a review of sensors which can contribute to the goals of the EOS mission. The implications of interdisciplinary and multispectral aspects of earth observation studies and the rationale for multisensor payloads are discussed in Section 5. Section 6 outlines the constraints which sensor field of view and earth coverage requirements place on the orbital altitude. Details of the spacecraft and subsystem characteristics required to support the EOS sensors are given in Section 7. The relationships between launch vehicle capability and spacecraft characteristics are reviewed in Section 8. The data transmission and processing systems for EOS are described in Sections 9 and 10. Section 9 deals with the data transmission links and the NASA network of tracking and data acquisition stations. Section 10 discusses the relationship of the ERTS ground data processing to the EOS ground data processing system.

This Definition Phase Report defines the role of the Earth Observatory Satellite in meeting the goals of the nation's program in the earth observation disciplines and provides a basis for proceeding with the EOS system design.

SECTION 2

EOS STUDY SUMMARY

SECTION 2

EOS STUDY SUMMARY

ILLUSTRATIONS

TABLES

SECTION 2

EOS STUDY SUMMARY

2.1 BACKGROUND

Since the launch of the first weather satellite in 1960, TV cameras and radiometric instruments aboard satellites such as TIROS and Nimbus have been providing remote sensing data about the Earth and its atmosphere. Although these satellites were designed primarily for meteorological studies, the sensor data on earth surface features have nonetheless found many applications in the earth resources disciplines.

The Earth Resources Technology Satellites (ERTS A and B), scheduled for launch in 1972 and 1973, will be the first unmanned satellites designed to make observations from space as part of the Earth Resources Survey Program. The payloads of ERTS A and B are designed primarily for terrestrial survey, thus the investigation of problems involving the ocean survey will be left untouched.

With the launches of Nimbus E and F in 1972 and 1974 respectively, there will be a number of advances in remote sensing technology, including, for the first time, experiments sensing emissions in the microwave part of the electromagnetic spectrum for imaging ocean and land surfaces and for sounding the lower atmosphere. The major thrust of the Nimbus research and development program, however, will have been directed toward observations for describing the initial conditions which are used in models for long range numerical forecasts.

Presently, there is no authorized and funded satellite program for research and development in Earth Observations beyond 1974. Agency planning for follow-on missions initially considered two programs, ERTS C through F, and Nimbus G and H. GSFC Working Groups on Meteorology and on Earth Resources in late 1969 and early 1970 reviewed the nature of the ongoing programs in the earth observations disciplines, especially the data needs of User Agencies, and the contribution which remote sensing from space could make to these programs. These Working Groups identified a number of key areas in which interdisciplinary measurements from space by advanced techniques is both important and feasible in the time frame following ERTS B (1973) and Nimbus F (1974) (see Table 2.1-1).

Table 2.1-1

Key Areas for Making Earth Observation Interdisciplinary
Measurements from Space

A. Sea Surface Phenomena
B. Structure and Phenomena of the Atmosphere above 30 km
C. Cloud Structure and Composition
D. Spectral, Spatial, and Temporal Characteristics of Significant Earth Surfaces Features
E. Interactions Between Different Levels in the Earth-Atmosphere System
F. Atmospheric Pollution

The Working Group reports also made the following recommendation:

". . . strong consideration should be given to combining the Nimbus G
and H and ERTS E and F missions into a single Earth Observations
mission."

2.2 SCOPE OF THE EOS STUDY

This report describes the results of a Definition Phase Study of the Earth Observatory Satellite
(EOS) System which implements the recommendations of the GSFC Working Groups. The scope
of the study is illustrated in Figure 2.2-1, in which the study is viewed in terms of a number of
related elements which, taken together, support the earth observations disciplines. The flow
of Figure 2.2-1 also illustrates some of the rationale of the study. User needs lead to sensors
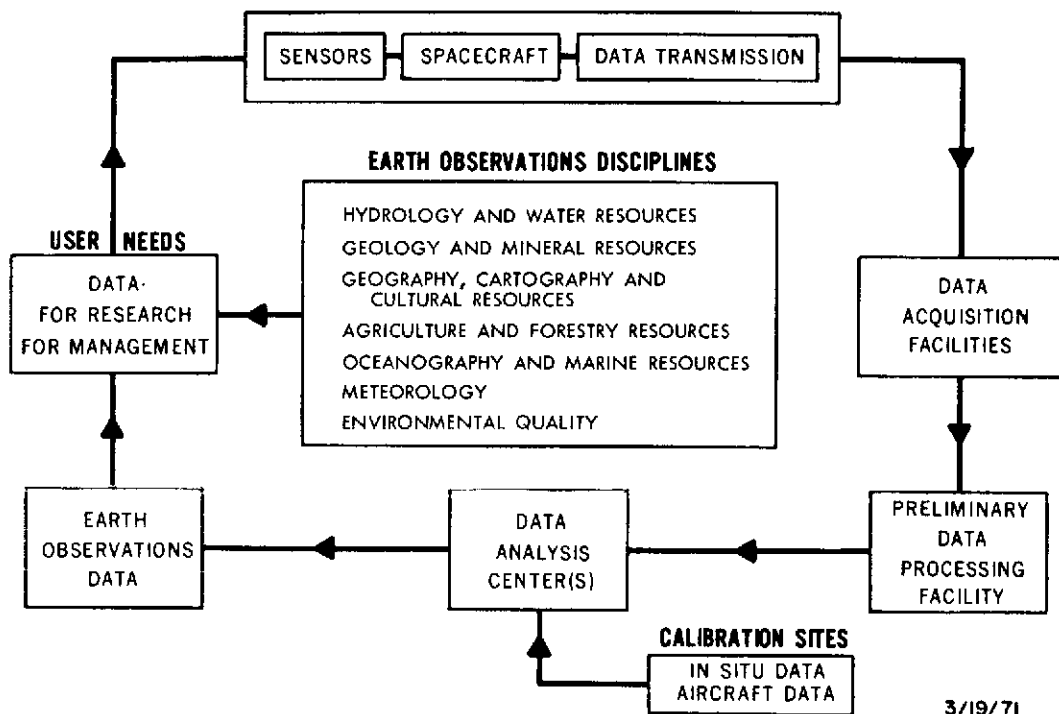
Figure 2.2-1 The EOS Study Scope

which in turn dictate the characteristics of the space observatory. A key element of the
observatory is its data storage and transmission system which must reflect not only the character-
istics of the sensor data but also those of the existing NASA data acquisition network and of
the proposed evolution of this net. The ground processing of the data is also considered in order
to develop guidelines for optimum use of the ERTS Ground Data Processing Systems and to
support development of user oriented data analysis centers (with supporting calibration-site data)
in the mid-to-late seventies.

The study has explored a number of options and identified a number of key trade-off elements
which are dealt with in the body of the report. Out of these tradeoffs have emerged a clear
definition of requirements and a program plan for meeting these requirements beginning with a
first launch in 1976.

2.3 USER GROUP PARTICIPATION

Government agencies as well as private industry and institutions have recently expended consider-
able effort in defining requirements for data of the types to be acquired from Earth Observatory
Satellites. These studies have identified the seven Earth Observation Discipline areas listed in
Table 2.3.1. It is convenient to consider the first four listed under the general term
Terrestrial Resources. Terrestrial Resources grouped with Oceanography and Marine
Resources will, in this report, be termed Earth Resources.

Table 2.3-1

Earth Observation Disciplines

	1. Hydrology and Water Resources	
Terrestrial Resources	2. Geology and Mineral Resources	
	3. Geography, Cartography, and Cultural Resources	Earth Resources
	4. Agriculture and Forestry Resources	
	5. Oceanography and Marine Resources	
	6. Meteorology	
	7. Environmental Quality	

National requirements and the NASA program in these disciplines are being coordinated through
the interagency Earth Resources Survey Program Review Committee (ERSPRC). Through the
Benefits Studies Subcommittees of ERSPRC, the GSFC EOS Study Team has had the benefit of
advice on sensors and their applicability to meeting the needs of user groups. This assistance
has involved the identification of measurement parameters in each of the Earth Observation
disciplines, and in formulating the payloads outlined in this report.

2.4 EARTH OBSERVATION SENSORS

In the course of the study a comprehensive review of sensor development was conducted. The
review identified sensors that are within the state of the art, and could be available for flight
in 1976. These key sensors are listed in Table 2.4-1.

Two of the sensors have been proposed by Principal Investigators for development in the Advanced
Applications Flight Experiments (AAFE) program. The other five make up the Earth Observations
Facility payload which is considered to meet the needs of an interagency group of data users
in the earth observations disciplines. A brief note on each of the seven sensors follows—more
detail is given in Section 4.

1 SEA SURFACE TEMPERATURE IMAGING RADIOMETER

Five channels in the infrared and visible will provide precise daily global measure-
ments of sea surface temperature at high (~2 km) spatial resolution, with correction
for atmospheric effects in the line of sight. The data will contribute to our knowledge
of ocean currents and the energy exchanges at the air-sea interface. This instrument

2-9

will also provide measurements of components of the radiation budget of the earth-atmosphere system.

Table 2.4-1

Key EOS Sensors

Sensor Type	Facility Payload	Principal Investigator Payload
1. Sea Surface Temperature Imaging Radiometer	X	
2. Cloud Physics Radiometer	X	
3. Oceanic Scanning Spectrophotometer	X	
4. Thematic Mapper	X	
5. Passive Multichannel Microwave Radiometer	X	
6. Upper Atmospheric Sounder		X
7. Atmospheric Pollution Sensor		X

2   CLOUD PHYSICS RADIOMETER

Two visible and three infrared channels scanned from horizon to horizon will provide information on the physical characteristics and distribution of the cloud cover over the globe. The multispectral approach will permit the determination of such factors as cloud top pressure level, cloud thickness, droplet size, the density of condensed water and the distinction between ice clouds and those made up of liquid water droplets.

3   OCEANIC SCANNING SPECTROPHOTOMETER

Ten to twenty narrow spectral bands in the visible spectrum will measure sea surface color, providing data needed for identification of nutrient rich and sterile areas of the oceans and their temporal changes. Data from this instrument together with the Sea Surface Temperature Imaging Radiometer will provide information on oceanic circulation and ecological processes, and possibly certain types of pollution, such as oil slicks.

4   THEMATIC MAPPER

With seven spectral bands in the visible and selected atmospheric windows in the infrared, this instrument will provide data primarily for terrestrial resources survey. With an instantaneous field of view for 66 meters, and a 100 n.m. swath, the Thematic Mapper would continue and extend the earth resources surveys initiated with ERTS A and B. The addition of two infrared channels in particular will extend the ability to detect and distinguish the signature of agricultural and forest resources, and of natural thermal sources.

5 PASSIVE MULTICHANNEL MICROWAVE RADIOMETER

This instrument, operating in a number of bands to be selected in the wave length range between 1 and 11 cm will afford a global all-weather capability to measure such parameters as sea state, sea surface temperature, precipitation over the oceans, and the extent and nature of sea ice, as well as soil moisture and properties of snow and ice cover over the land.

6 UPPER ATMOSPHERIC SOUNDER

Several candidate sensors are under study which can determine temperature profiles in the atmosphere above 30 km, determine the nature and distribution of atmospheric components such as ozone or water vapor, and contribute to our understanding of the dynamics and photochemistry of this region.

7 ATMOSPHERIC POLLUTION SENSOR

Several types of instruments are under development for the detection and measurement of gases associated with atmospheric pollution. The sensor data, based on the Remote Gas Filter Correlation Analyzer, (AAFE 71-18) are representative of the payload allocation required for atmospheric pollution monitoring.

2.5 MISSION

With the assistance of the user group representatives, a list of measurement parameters relevant to the goals of the earth observation disciplines has been developed. In conjunction with the seven key EOS sensors listed in Table 2.4-1 the list of measurement parameters is shown as a matrix in Table 2.5-1. Specific measurement parameters are grouped under the four earth observation discipline areas of Table 2.3-1. The three symbols, P, S, and C, denote levels of correspondence between data and the goals of the EOS disciplines.

P identifies a primary measurement of a given parameter

S identifies a sensor providing supporting data which (although its nature is of primary importance to a given parameter) is considered to be secondary because of a shortcoming in one or more characteristic, (e.g. spatial or spectral resolution may be somewhat less than optimum.)

C identifies a sensor making measurements essentially of correlative importance with respect to other primary or supporting measurements.

The matrix illustrates a key consideration in planning for the EOS mission, the interdisciplinary aspect of the data:

1. Each facility sensor, while serving a primary purpose, provides correlative data for other disciplinary areas.

2. Each disciplinary area is supported by more than one sensor.

The seven sensors included in Table 2.5-1 illustrate the broad range of values of sensor characteristics which must be factored into the design requirements of the Earth Observatory Satellite. Six of these characteristics are listed in Table 2.5-2. Payload weight, power, and size are major design drivers in that they characterize the size of the spacecraft. Data rate, instantaneous field of view (IFOV) and the presence or absence of a cooled detector are key considerations in the design of the spacecraft data system, the attitude stabilization system and certain geometrical factors related to the angle between the orbit plane and earth-sun axis.

Table 2.5-1

EOS Mission Matrix

	S.S. Temp. I. Rad.	Cl. Physics Rad.	Oceanic S. Spectro.	Thematic Map.	P.M. Microwave Rad.	U.S. Sounder	A. Pollution
OCEAN SURVEY							
Sea Surface Temperature	P		C	C	P		
Sea Surface Roughness	C				P		
Sea Surface Composition (Color)	C		P				
Sea Surface Phase (Ice vs. Liquid)	C				P		
Sea Surface Pollution	C		P	C			
Cloud Cover Survey	P				C		
Precipitation Survey	C	P			P		
Radiation Budget Over the Oceans	P				C		
Shoal and Coastal Mapping	C		C	P			
Sea Surface Currents	C		C	C			
Sea Surface Geopotential Figure	C		C				
ENVIRONMENTAL QUALITY							
Atmospheric Pollution	C					C	P
Sea Surface Pollution	C		P				
TERRESTRIAL SURVEY							
— Agriculture and Forestry							
Terrain Mapping	C			P			
Soil Moisture	C			C	S		
Snow/Ice Survey	C			P	S		
Atmospheric Pollution	C						P
— Geology and Mineral Resources							
Earth Surface Composition	C			P			
Soil Moisture	C			C	S		
— Geography, Cartography, and Cultural Res.							
Terrain Mapping	C			P			
Soil Moisture	C			C	S		
Snow/Ice Survey	C			P	S		
Atmospheric Pollution	C						P
— Hydrology and Water Resources							
Terrain Mapping	C			P			
Soil Moisture	C			C	S		
Snow/Ice Survey	C			P	S		
METEOROLOGY							
Sea Surface Temperature	P		C	C	P		
Sea Surface Winds (Inferred fm. Roughness)	C				P		
Sea Surface Phase (Ice vs. Liquid)	C				P		
Cloud Cover Survey	P	P			C		
Precipitation Survey	C	P			P		
Cloud Composition (Ice vs. Liquid Water)	C	P			C		
Cloud Thickness	C	P					
Cloud Density of Condensed Water	C	P			C		
Cloud Drop Size Parameter	C	P			C		
Cloud Top Pressure Level	C	P					
Upper Atmospheric Temperature	C					P	
Upper Atmospheric Composition[5]	C					P	
Soil Moisture (Garp-Scale)	C			C	P		
Snow-Ice Survey	C			C	P		
Radiation Budget	P	C					
Atmospheric Pollution	C						P

Table 2.5-2

EOS Sensor Characteristics

	WT. (LB.)	POWER (W)	AREA (FT^2)	DATA (MB/S)	IFOV (DEG.)	COOLER
SEA SFC. TEMP. IM'G. RAD.	45	30	1.3	0.33	0.11	YES
CLOUD PHYSICS RAD.	70	40	1.9	.22	.14	YES
OCEANIC SCANNING SPECTRO.	45	60	3.7	.5	.11	NO
THEMATIC MAPPER	265	70	10	30	.004	YES
PASSIVE MULT. MICR. RAD.	513	355	58	.01	$1.2/10$	NO
UPPER ATM. SOUNDER	56	27	1.3	.01	.03	YES
ATM. POLLUTION SENSOR	30	10	.7	.01	5	YES
TOTALS	1024	557	77	--	--	--

In the course of the study, a preliminary design was made of a spacecraft which could support the full complement of sensors shown in Table 2.5-2. Such a spacecraft would weigh about 3800 lb. (1700 kg.), a weight currently requiring a launch vehicle of the Titan class. Since the current ERTS/Nimbus spacecraft has payloads up to 500 lb. (227 kg.), its capability for the EOS mission was also investigated. An analysis was also made of a spacecraft which would make use of the 8-foot diameter and payload capabilities of the Delta 2910 launch vehicle. A comparison of the results of the analysis is shown in Table 2.5-3

Table 2.5-3

Spacecraft Design Analysis Comparison

	ERTS	EOS-A,B	EOS. (GROWTH)
LAUNCH VEHICLE	5' DELTA	8' DELTA	TITAN
CAPABILITY (LB)	2100	2600	3800+
S/C WEIGHT	1400	1950	2600
PAYLOAD AVAIL	500**	650	1200+
POWER (W)	260*	550*	900*
S/C	100	200	250
PAYLOAD	160	350	650
EARTH VIEW AREA (FT^2)	17	100	145
DATA RATE (MB/S)	15	30	100
ATTITUDE DET. (DEG)	0.1	0.002	0.002

*BEGINNING OF LIFE, ORBITAL AVERAGE

**LIMITED BY SPACECRAFT STRUCTURE

On the basis of the data of Table 2.5-3 it was considered that a spacecraft of the 2600 lb (1200 kg) class would make a significant contribution to the Earth Observation Disciplines in the 1976 time period. This spacecraft is henceforth designated EOS A and B in this report.

It was further concluded that a spacecraft of the class labeled EOS (Growth) in Table 2.5-3 with greater payload capability, and increased power will very likely be required by 1980. Factors considered in reaching this conclusion include:

●The probable course of sensor development

●Extension of the areas of terrestrial data collection from the North American land mass to an expanding group of the member states of the United Nations

●The availability of increased launch capability in the Space Shuttle.

Because of this potential a major factor in the evaluation of candidate configurations for the EOS mission was the capability of accommodating the growth from EOS A and B at 2600 lb (1200 kg) to a projected EOS C and D at 3800 lb (1700 kg). The configuration selected is capable of accommodating this growth without major redesign. It is shown in Figures 2.5-1 and 2.5-2 with illustrative payloads.

Before considering the spacecraft in more detail, it is useful to consider candidate payloads for EOS A and B, as well as a potential payload for a follow on ERTS spacecraft which was considered in the course of the study. Although the programmatic elements required to develop such a mission are beyond the scope of the present report, an additional ERTS mission appears to be a feasible and worthwhile interim flight between ERTS B in 1973 and EOS A in 1976. These payloads are shown in Table 2.5-4.

Table 2.5-4

Candidate Payloads

	ERTS-C	EOS-A	EOS-B
(1) SEA SFC. TEMP. IMAGING RAD.	X	X	X
(2) CLOUD PHYSICS RAD.		X	X
(3) OCEANIC SCANNING SPECTRO.	X	X	X
(4) THEMATIC MAPPER	X (MSS+ 1 RBV)		X
(5) PASSIVE MULTICHAN. MICRO-WAVE RAD.		X	
(6) UPPER ATMOS. SOUNDER		X	X
(7) ATMOS POLLUTION SENSOR		X	X
FUTURE SENSORS (e.g., RADAR, POLARIMETER, LIDAR, SUNGLITTER PHOTOMETER, ADVANCED CAMERA, ETC.)			X

The sensors for the suggested interim ERTS C mission permit a continuation of the terrestrial survey studies begun with ERTS A and B, as well as initiating an oceanographic program. Comparison with the Mission Matrix of Table 2.5-1 shows that EOS A is a mission with Oceanographic-Meteorological emphasis, while the EOS B has a Terrestrial Resource-Meteorological Emphasis.
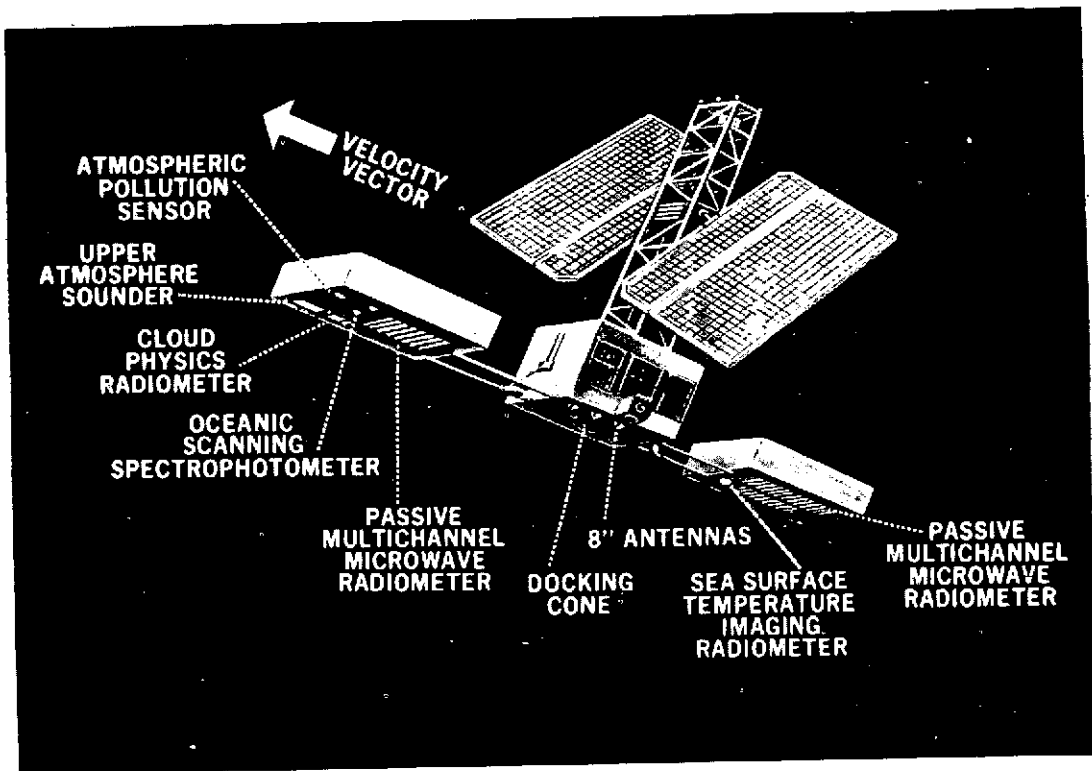
2-14

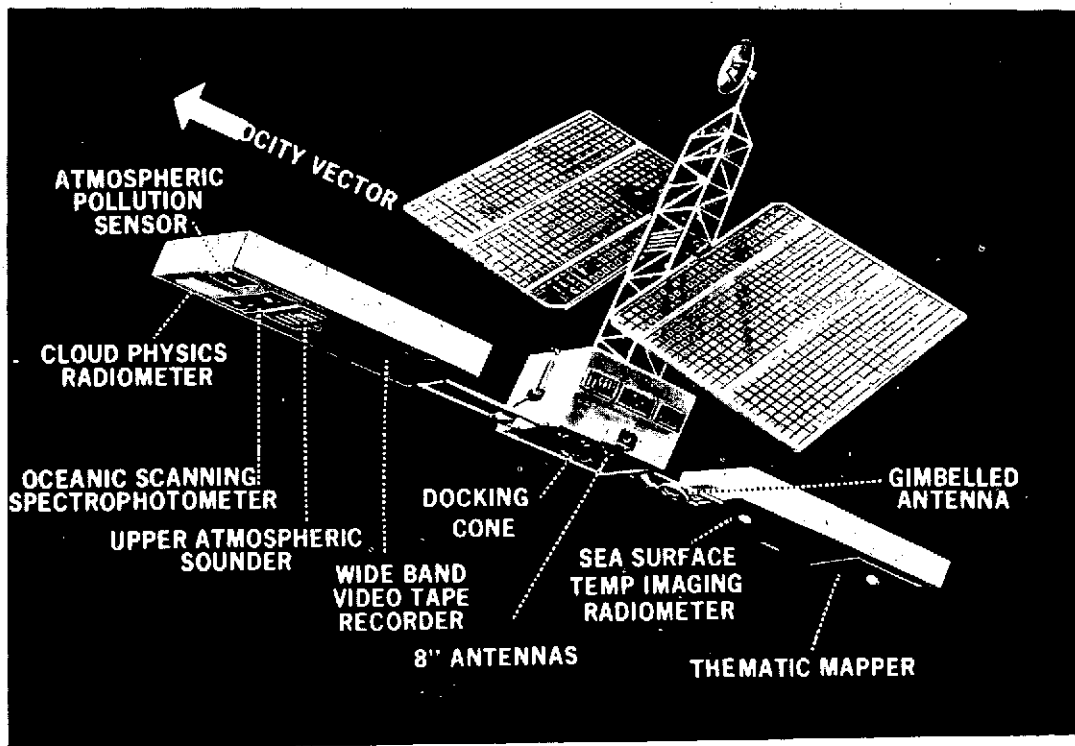Figure 2.5-1   EOS A Configuration Study

Figure 2.5-2   EOS C Configuration Study

EOS A and B together accomplish measurement of all the parameters listed in the earth observation mission matrix.

2.6 SPACECRAFT

The basic spacecraft configuration for EOS is made up of three sections. The main section, or central body and two deployable sensor mounting bay sections. The two bays are folded during launch in a back-to-back arrangement against a tower structure which supports the solar arrays.

Primary features of the configuration and the spacecraft sybsystems for EOS A and B include

- Large ratio of earth viewing area to spacecraft weight (0.04 ft^2/lb, 0.008 m^2/kg)

- Efficient utilization of Delta shroud envelope

- Three axis stabilization by proven techniques

- Precision attitude determination (to 0.002 degrees) to permit geographical referencing of terrain data

- Operation in orbits between 400 and 600 nm (740-1100 km)

- Ability to select solar illumination angles by permitting nodal crossing times between 0900 and 1500

- Compatibility with Shuttle operations when available

- Modularity design to facilitate subsystem checkout and integration and to permit flexability in choice of sensors

- Compatibility with the Data Relay Satellite when available

2.6.1 POWER SYSTEM

The power system is a direct energy transfer system that utilizes oriented solar arrays for the power source and nickel-cadmium batteries for power storage. A regulated bus voltage of plus 28V ±2% with a negative ground has been selected in order to make efficient use of the silicon transistors currently used in high power transmitters. This choice of power bus is consistent with the plans for the operational meteorological satellites (TIROS-N). The solar array capacity is oversized at the beginning of life so that the rated power is available after two years of operation.

2.6.2 COMMAND AND DATA HANDLING

EOS command and data processing can be handled by four subsystems.

1. A command system similar to that on the Nimbus/ERTS spacecraft with 512 commands any of which can be stored in 127 locations.

2. A Versatile Information Processor (VIP) for low data rate sensors, on-off functions, and housekeeping. The data rate is adjustable up to 12.5 kb/s. Real time data is transmitted over a low power VHF link. A narrow band tape recorder is used for storage and recorded data (32 to 1 playback) is multiplexed with other data on the S-band link.

3. A Manipulated Information Rate Processor (MIRP) will be used to sample and format medium data rate sensors, especially the oceanographic and meteorological sensors requiring global data collection at rates up to 0.5 mb/s. Sampling is synchronized with sensor scan and the data are buffered and formatted to reduce peak data rates. Total MIRP output rate is approximately 1.2 mb/s. One orbit storage is provided by a 32 track tape recorder with 24 to 1 playback. Real time and recorded data are transmitted over an S-Band link.

4. The Multi-megabit Operation Multiplexer (MOMS) is used on EOS only when high data rate sensors such as the Thematic Mapper are included in the payload. Depending on scan efficiency, and resolution the sensor will generate data at a peak rate between 30 and 80 mb/s. The MOMS will digitize to 8 bit accuracy and buffer so that the average rate is 30 mb/s or less and the data can be accommodated on a 30 MHz bandwidth S-Band link. A video tape recorder with 1 to 1 playback will provide up to 30 minutes of storage.

2.6.3 COMMUNICATIONS

The EOS Communications System consists of three subsystems.

- VHF Subsystem

- S-Band Real Time Data, Ranging and Command Subsystem

- S-Band 30 mb/s Data Subsystem

In addition a K-Band data subsystem may be needed for future spacecraft if data rates of up to 100 mb/s are required.

The VHF subsystem is similar to that on Nimbus 4. It is used to transmit the VIP data, as on acquisition aid for high gain ground tracking antennas and a backup method for orbital determination via the minitrack system.

The S-Band Realtime Data, Ranging, and Command Subsystem is used for transmission of medium rate (MIRP) real time data, and playback of low rate data (VIP). It is also used for orbit determination and the EOS Command System.

The S-Band 30 mb/s Data Subsystem consists of two 30 MHz channels that can carry two independent 30 mb/s data channels via fixed earth pointing antennas. The two channels can be selected in orbit from any of the following channels

a. Real time 30 mb/s sensor data (Thematic Mapper)

b. Playback (1-1) of 30 mb/s sensor data

c. Playback (24-1) of medium rate data

Quadriphase modulation would be used to contain the r.f. transmission bandwidth to within 30 MHz.

Provision could also be made to transmit any one 30 mb/s channel to a Local Readout Ground Station (LRGS) via a higher gain, steerable S-Band antenna (EOS-C). The spacecraft configuration provides mounting area for an oriented K-Band antenna for 100 mb/s data to the ground, or on the tower, for a data link with a Data Relay Satellite System.

2.6.4 ATTITUDE CONTROL SYSTEM (ACS)

Conceptually the ACS may be regarded as an updated version of the Nimbus/ERTS type of attitude control. Signals to appropriate control circuits from the rate gyros and horizon scanners activate cold gas jets for initial capture (and recapture), momentum wheel desaturation, and coarse control. Stabilization with respect to the local vertical is maintained within 0.5 degrees in each axis. Rate perturbations are limited by gyro to less than ±0.005 degrees per second. Telemetry of attitude sensor, and torquer data, coupled with modelling of known bias and error sources will permit medium accuracy attitude determination to within 0.1 degree by after the fact ground computations. This accuracy is within the resolution element of all of the ocenaographic and meteorological data to be obtained from the EOS sensors.

2.6.5 PRECISION ATTITUDE DETERMINATION

For EOS missions with high resolution sensors such as the Thematic Mapper on EOS B, it is necessary to relate the sensor data to geographical coordinates. Precision attitude determination provides an attractive alternate, or supplement, to the landmark techniques developed for ERTS data processing. Inertial attitude is continuously measured by a star sensor and precision 3-axis gyro combination. The telemetered data can permit inertial attitude determination to within 0.002 degrees. At an altitude of 1000 km, this error corresponds to 30 meters at the subsatellite point. The accuracy of ephemeris determination in the 1976-1977 time period is expected to lie within 30 and 100 meters. Geographical referencing of sensor data to within a resolution element will be feasible if ephemeris accuracy of 30 meters can be achieved on an operational basis.

2.6.6 ORBIT ADJUST

Orbit adjust capability is required by the Thematic Mapper on EOS B to meet the required synchronized repetition cycle for the satellite subtrack. It is utilized to correct the initial orbit for residual errors of the launch vehicle system, and to provide drag makeup. Orbit adjust is not required on missions containing only global type sensors with broad swath, for Example EOS A. For this reason the orbit adjust system is designed as a separate module to permit easy inclusion when required. A blowdown hydrazine system using Shell 405 catalyst type thrusters is planned. Each is sized for a nominal 5 pound (2.2 kg) force output, and is capable of producing a minimum impulse of 0.15 lb-sec.

2.6.7 THERMAL CONTROL AND COOLING

Thermal control of the EOS spacecraft is accomplished by a system of fixed and louvered radiation areas, heat pipes, multilayer insulation, and thermal control coatings. Preliminary calculations indicate there are no basic problems in maintaining the proper temperature environment; an auxiliary heater may be required in sensor mounting bays during minimum power operations. The controlled environment is $25^\circ \pm 10^\circ C$ throughout, except for the battery locations in the control body which is controlled to $20^\circ \pm 10^\circ C$ to extend battery life.

Some of the EOS sensors (Table 2.5-2) have IR detectors which require cooling, in some instances to 90K. The feasible choices include

- Passive radiator cooler

- Solid cryogenic cooler

- Vuilleumier refrigeration cycle

A detailed review of these options, with a discussion of trade-off considerations is included in Section 7.8. The spacecraft configuration is such that any of the three methods is feasible. Further study during the spacecraft system design will determine an optimum cooling system.

2-18

2.6.8 WEIGHT AND POWER BUDGET

A summary of the weight and power allocations for EOS A and B, and for EOS C and D is shown in Table 2.6-1. For comparison, the allocation for ERTS A is also shown.

Table 2.6-1

Weight and Power Budget

	ERTS A		EOS A & B		EOS C & D	
	Power [1] W	Weight LB	Power [1] W	Weight LB	Power [1] W	Weight LB
SPACECRAFT						
Structure	–	249	–	675	–	865
Power	–	304	–	325	–	510
Command & Data Hdlg	52	110	85	180	105	210
Communications	5	99	35	70	65	150
Attitude Control	36	271	65	315	65	325
Oribit Adjust	2	137	–	120	–	160
Thermal	5	86	15	85	15	110
Harness	–	136	–	180	–	270
Total Spacecraft	100	1404	200	1950	250	2600
PAYLOAD	160 [2]	460	250 [3]	650 [4]	500 [3]	1200
TOTAL	260 [2]	1864	450 [3]	2600	750 [3]	3800

1 Orbital Average
2 Beginning of Life
3 End of Life
4 Capability at proposed orbital altitude of 530 n.m. (980km)

2.7 ORBIT

A comprehensive analysis of orbit characteristics for earth observations missions was performed during the definition of the ERTS mission. For that mission the swath width of the terrain mapping sensor (100 nm, 185 km) and a requirement for a 10 percent overlap in imagery at the equator effectively led to a revisit time of 18 days, a period such that there are $13\frac{17}{18}$ orbits per day. Descending nodes migrate westward on succeeding days, and the imagery on day n is repeated within 10 nm (18 km) on day n+18.

A review of the requirements which the EOS payloads place on the orbit (Section 6) confirms the ERTS rationale, in general, and illustrates the value of expressing period not in minutes but as a fraction showing the number of orbits per day for example

$$N = n \pm \frac{c}{M}$$

where

N = orbital frequency (orbits/day)

n = orbital frequency to the nearest integer

c = integer which determines the ground trace pattern

M = number of days to obtain full earth coverage

As noted for ERTS, n=14, c=1, and M=18. The EOS B payload has the Thematic Mapper with 100 nm. (185 km) swath, as in ERTS. It also has the Oceanic Imaging Spectrophotometer with a swath of 400 nm (740 km) and a revisit time of 4 days. The multiple swathing characteristics of orbits where c in the foregoing equation is not unity are useful for such a payload mix, recommended for EOS B is c=4, M=17, thus the number of orbits per day, N is

$$N = 14 - \frac{4}{17}$$

$$= 13\frac{13}{17}$$

2.8   LAUNCH VEHICLE

The sun-synchronous orbits required for the EOS missions are currently most easily accessible from launches at the Western Test Range (WTR). Of the launch vehicles currently projected at WTR only the Delta is in the NASA complement. The Delta 2910 with 8-foot diameter shroud is projected to have a capacity of 2500 lb (1140 kg) at 600 nm. This capability has been used in planning for EOS A and B. A growth Delta in the 1980 time period, or the Space Shuttle System will permit larger payloads to the same orbit. A goal of 3800 lb (1730 kg) for EOS C and D is reasonable.

2.9   TRACKING AND DATA ACQUISITION

For collection of terrain survey data over the continental United States the three ERTS stations, MOJAVE, ALASKA and NTTF (at GSFC) are required for real time data readout. Limited collection of terrain data from sites in other nations can be accomplished by recording and readout during nighttime passes, but any comprehensive program of collection of thematic mapping data can better be accomplished by direct readout. The existing network of NASA tracking stations can support a broad program; coverage is illustrated in Figure 2.9-1

The bandwidth available for EOS data links is a key factor in limiting the amount of data which can be handled. The Multifunction Receiver System at antenna sites will be operational in the EOS time period, and the data links for EOS A and B utilize this system. Some EOS unique equipment is required at any site selected to support EOS. This equipment comprises wideband tape recorders, quadriphase demodulators and a spacecraft simulator. Oceanographic and meteorological data will normally be collected on a global basis and read out to the United States sites. The real time MIRP mode can however be used if there are international users for regional data.

2.10   GROUND DATA PROCESSING

The facility for processing the EOS data is based on the NASA Data Processing Facility (NDPF) for ERTS. The EOS NDPF will be a user oriented facility with the flexibility to process data with a variety of formats and data rates. Output will include

Film data, black and white and color

Computer compatible digital tapes

Data will be geometrically and radiometrically corrected, and rectified to standard map projections, such as Universal Mercator or Polar Sterographic. The facility will be organized to support

Figure 2.9-1.   Potential Regions of Real-Time Data Readout at NASA Tracking Stations
at Orbital Altitude 600 n. m. (1100 km)

Primary Users (in general Government Agencies and prime investigators) directly. Through the
secondary data centers support can be given the general user community. The computing and
film processing equipment developed for ERTS can be utilized for EOS with minimal changes.
Much of the software is also directly transferable. Some augmentation of the digital processing
capability is required.

SECTION 3

MISSION OF THE EARTH OBSERVATORY SATELLITES

SECTION 3

MISSION OF THE EARTH
OBSERVATORY SATELLITES

PRECEDING PAGE BLANK NOT FILMED

SECTION 3

MISSION OF THE EARTH OBSERVATORY SATELLITES

3.1 INTRODUCTION

This section outlines the background of the Earth Observatory Satellite (EOS) Mission, and discusses the goals of the mission in relation to the objectives of the nation's interagency programs in the Earth Observations disciplines These programs, especially those in the areas of Ocean Survey, Terrestrial Survey, Meteorology, and Environmental Quality affect the life and welfare of every living creature, and the future of man himself.

It has been projected that the world's population will nearly double by the end of this century. This growth will put increased demands on our life support system. There will be vastly increased demands for living space, mineral resources, energy, food, and pure water, and an increasing pollution of the air we breathe and the environment that must support us, with possible effects upon weather and climate. It is becoming increasingly important to assess and decide how best to manage the available resources and environment effectively. Effective management requires observations and inventory of Earth resources and critical environmental parameters on a timely and continuing basis.

3.2 BACKGROUND

It is probable that an optimum earth resource observation system will include a coordinated array of surface, balloon, aircraft and satellite sensors.

The Earth Resources Technology Satellites (ERTS) A and B, scheduled to be launched in 1972 and 1973, respectively, will be the first unmanned satellites designed to make observations from space as part of the Earth Resources Survey Program. Their instrumentation, consisting of a high spatial resolution Multi-Spectral Scanner (MSS), a three-color Return Beam Vidicon (RBV), and a data collection system is primarily designed to acquire data for terrestrial survey. The sensors and data system are not adapted to ocean survey applications, and thus leave untouched the investigation of problems involving about 70 percent of the globe.

The Earth Resources Experiment Package (EREP) of the manned Skylab orbital facility, scheduled for launch in 1973 will include a multispectral photographic facility, a visible-infrared spectrometer, a 13-band multispectral scanner, a microwave radiometer/scatterometer/altimeter, and a passive L-band radiometer operating near 1.4 GHz. These experiments will be in operation at intervals spread over about 120 days and will be used to determine the extent to which Earth resources data can be obtained from selected test sites. Ocean surveys (and terrestrial surveys) will, however, be secondary on Skylab as there are some forty-seven experiments in astronomy and other disciplines making demands on the capabilities of the mission.

The program which has acquired observations of the Earth from space over the longest period is the Meteorology Program. Nimbus 4, launched on 8 April 1970, was the latest of a series of fourteen TIROS and Nimbus research satellites orbited, beginning with TIROS 1 on 1 April 1960. The cameras and radiometric instruments carried on these satellites, remotely sensing the Earth and atmosphere in the infrared, visible, and ultraviolet portions of the electromagnetic spectrum, have obtained data that have been applied in many different ways to broaden our knowledge of the meteorology of our planet. Among these applications have been:

- Cloud cover imaging
- Storm tracking
- Surface temperature determination

PRECEDING PAGE BLANK NOT FILMED

- Cloud top height inference
- Radiation balance studies
- Mean tropospheric moisture inference
- Mean stratospheric temperature mapping
- Solor ultraviolet measurements
- Vertical soundings of temperature, water vapor, and ozone

These applications have led to many discoveries concerning the organization and movement of cloud patterns and their relationship to meteorological processes; the radiative properties of the atmosphere and clouds and of land and ocean surfaces in the visible and infrared; and the intensities and fluctuations of the solar ultraviolet at wavelenghts important to the photochemical processes affecting the generation and destruction of ozone. The meteorological literature is replete with papers discussing the almost endless variety of applications of these data, either alone or more often in combination with other satellite or conventional data, both for research and for operational forecasting of the weather. An outstanding example of the latter is the use of the vertical sounding data from Nimbus 3 and Nimbus 4 since May 1969 in the numerical weather prediction model at the National Meteorological Center (NMC) of the National Oceanic and Atmospheric Administration (NOAA). Nimbus television and infrared data have also found a number of applications in the earth resources disciplines, such as:

- Mapping of snow cover
- Surveys of Arctic and Antarctic ice
- Tracking large dust storms
- Delineation of flood areas
- Geological studies of fault systems and mountain locations in the antarctic

In addition to the remote sensors flown to date on meteorological satellites, balloon and buoy tracking and data collection experiments were successfully demonstrated on both Nimbus 3 and Nimbus 4.

Nimbus E, scheduled to be launched in mid-1972, will for the first time carry experiments sensing emission in the microwave part of the spectrum, both for imaging ocean and land surfaces and for sounding the lower atmosphere. Also Nimbus E will carry the first experiment designed expressly for Earth Resources survey, i.e., a Surface Composition Mapping Radiometer (SCMR) to sense reststrahlen features near 10μm and, hence, to distinguish between"acidic" and "basic" surface materials. The payload of Nimbus F, scheduled to fly in 1974, will include advanced vertical sounders (sensing in the 15μm and 4.3μm carbon dioxide bands and the 5 mm oxygen band), an Earth radiation budget experiment, a differential doppler constant-level balloon tacking system, a single-channel microwave scanning radiometer primarily intended to map sea ice, and a two-channel multispectral imaging infrared radiometer.

Thus, the Research and Development meteorological satellite program, beginning with the TIROS series and continuing with the Nimbus series through Nimbus F, has developed, or is currently developing, a vast array of sensors which may be divided into the following six categories:

a. Framing devices (television cameras).

b. Non-scanning radiometers (omnidirectional or low spatial resolution).

c. Scanning multispectral radiometers (medium-to-high spatial resolutions).

d. Data collection and moving platform (e.g., balloon/buoy) location systems.

e. Indirect vertical atmospheric sounders.

   f. Instruments to monitor the direct radiation from the sun (e.g., ultraviolet radiation important in the photochemistry of ozone).

Descriptions of the various experiments flown on the TIROS and Nimbus meteorological satellites are given in the User's Manuals or User's Guides published for each satellite (e.g., Reference 1).

The space technology represented in categories a. - through - e. above and the techniques of data analysis and interpretation developed in the R&D satellite program, in large part have been or are being incorporated into the NOAA (formerly ESSA) operational meteorological satellite system. These developments have emphasized the remote sensing of the troposphere and lower stratosphere, the regions having the most immediate impact upon weather processes affecting man's environment. These developments will also provide the technology upon which the space-based part of the Global Atmospheric Research Program (GARP) of the mid-1970's will draw to provide world-wide measurements of the mass, wind, and moisture fields from the surface to 10 mb (a height of ~31 km) (References 2.3). In contrast to the other categories, sensors in category f. heretofore have been intended solely for research purposes without any parallel prospect of their being incorporated into a an operational system.

3.3 EARTH OBSERVATIONS AFTER 1974

It seems apparent that with the launch of Nimbus F in 1974 a significant milestone will have been reached in the applications of space techniques to meteorology, Up to that point the major thrust of the Nimbus program will have been focused on making observations for the purpose of describing the initial conditions which must be used in the models for long range numerical forecasts. Specifically, techniques to measure the mass and motion fields on a global scale will have been developed to a degree such that they will be utilized in observing systems for the GARP. However, it is expected that the first global experiments for the GARP will only be the first attempt at making long range weather forecasts and that many gaps in our knowledge of atmospheric processes will render this first attempt less than perfect. In a Pre-Phase A Study (see Attachment A), the GSFC Meteorology Working Group (METWG) identified the following five specific areas requiring further research involving the application of advanced observing techniques from near Earth satellites beyond Nimbus F:

   a. Sea Surface Phenomena

   b. Structure and Phenomena of the Atmosphere Above 30 km

   c. Cloud Structure and Composition

   d. Spectral, Spatial, and Temporal Characteristics of Significant Earth Surface Features

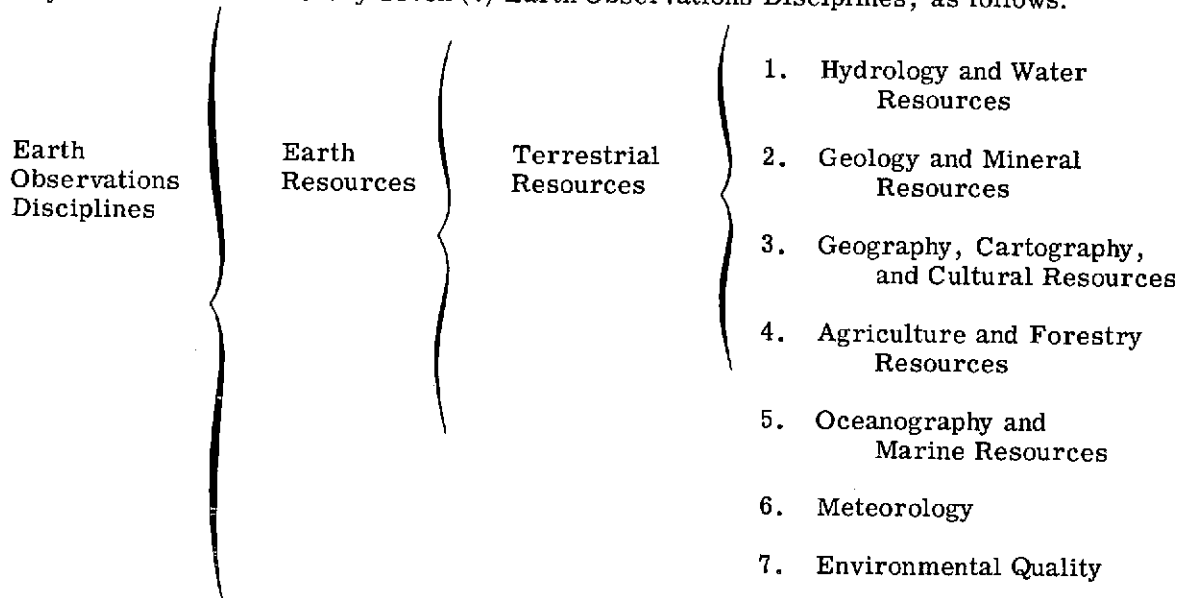   e. Interactions Between Different Levels in the Earth-Atmosphere System

In that study it was noted that sea surface temperature and roughness measurements under a. above were also of importance to the discipline of Oceanography; that soil moisture measurements under d. above were also of importance to the disciplines of Agriculture, Hydrology, and Geology; and that ice and snow cover under d. were also of importance to Hydrology and (over water) to Oceanography. The study concluded, therefore, that because of the apparent overlap of meteorlogial and Earth resources missions, strong consideration should be given to combining the Nimbus G and H and ERTS E and F missions into single Earth observations missions.

In a similar Study (see Attachment B), the GSFC Earth Resources Working Group also required sea temperature and roughness measurements, but added a third sea surface phenomena measurement, viz., ocean color, and also required soil moisture and ice and snow surveys, but added high spatial

resolution multispectral thematic mapping for the disciplines of Hydrology, Geology, Geography, and Agriculture. In both the Earth Resources Working Group and the Meteorology Working Group Reports it was concluded that the need for passive microwave radiometers and/or radars for sea surface temperature, sea surface roughness, soil moisture, and ice and snow sensing, with their requirements for large antennas and large amounts of power, probably precluded the use of the current Nimbus-ERTS type of spacecraft and that probably a wholly new and larger Earth Observatory Satellite would be required.

3.4   THE ROLE OF EOS

In the recent past, Government agencies, as well as private industry and institutions, have expanded considerable effort on requirements for the use of data of the types to be acquired from Earth Observatory Satellites. We identify seven (7) Earth Observations Disciplines, as follows:

Earth Observations Disciplines — Earth Resources — Terrestrial Resources —

1. Hydrology and Water Resources

2. Geology and Mineral Resources

3. Geography, Cartography, and Cultural Resources

4. Agriculture and Forestry Resources

5. Oceanography and Marine Resources

6. Meteorology

7. Environmental Quality

National requirements in these disciplines are being coordinated with the help of:

Department of Commerce National Oceanic and Atmospheric Administration	Hydrology, Oceanography, Meteorology, Environmental Quality
Department of Defense, Department of the Navy Department of the Army (Corps of Engineers)	Oceanography Hydrology
Department of the Interior U.S. Geological Survey	Hydrology, Geology, Geography
Department of Agriculture	Agriculture and Forestry
Environmental Protection Agency	Environmental Quality

The making of interdisciplinary measurements from space, employing advanced observing techniques in the time frame immediately following ERTS B (1973) and Nimbus F (1974), is considered to be both important and feasible in the following areas:

3-8

a. Sea Surface Phenomena

   (1) Temperature
   (2) Roughness
   (3) Composition (chemical, biological, particulate)
   (4) Phase (ice/liquid)
   (5) Pollution
   (6) Currents

b. Structure and Phenomena of the Atmosphere Above 30 km

   (1) Temperature
   (2) Composition (water vapor, ozone, trace constituents, dust)

c. Cloud Structure and Composition

   (1) Ice vs. liquid clouds
   (2) Thickness
   (3) Density of condensed water
   (4) Drop size parameter, precipitation
   (5) Cloud top pressure level

d. Spectral, Spatial, and Temporal Characteristics of Significant Earth Surface Features

   (1) Soil moisture
   (2) Snow/ice survey
   (3) Thematic mapping (visible and infrared)

e. Interactions Between Different Levels in the Earth Atmosphere System

   (Utilize measurements performed in other areas)

f. Atmospheric Pollution

   (1) Gaseous
   (2) Particulates

The overall mission of the Earth Observatory Satellite will be to serve as an advanced Earth observations platform for making interdisciplinary measurements in these areas. In this capacity, the EOS will provide a space platform for the orbital test of experimental sensors, measurement techniques, and spacecraft systems for the acquisition of data for research, and for the development of applications of these data and techniques to problem areas in resources and environmental management and in meteorology. Emphasis should be placed on orbiting payload combinations where the individual instruments complement one another synergistically. The quasi-operational use of data by appropriate agencies should be encouraged if such use is indicated during the intitial research phase of one or more of the instruments provided the primary research nature of the satellite is not comprised.

In view of the emphasis of ERTS and A and B on terrestrial survey and of the strong meteorological satellite research and development program over many years, the mission of EOS-A may be stated as:

● Provide a facility for the conduct of experimental research and development of advanced space systems for the earth observations disciplines in the latter half of the 1970-1980 decade.

3-9

- Emphasize space observations of oceanographic phenomena and interactions of the ocean surface with the atmosphere to meet urgent needs for research data and the development of advanced operational sensors for the oceanographic and meteorological disciplines.

- Initiate a program to develop and test space sensors to monitor indicators of environmental quality, such as atmospheric pollution, on global and other appropriate scales.

- Provide a flexible data management system having the capability of providing data in appropriate formats and quantities on a timely basis, primarily for research purposes but also (as may be indicated during the initial research phase of one or more of the instruments) for quasi-operational use by appropriate agencies on a real-time basis.

- Develop a new spacecraft with an evolutionary design, adaptable to supporting a wide variety of earth observations sensors and combinations of sensors.

Specific sensors addressed to these goals, both those considered feasible now as well as others considered promising for the near future but requiring additional developmental work before being ready for orbital flight, are discussed in the following Section.

3.5 REFERENCES

1. Nimbus IV User's Guide, 1970: Prepared by the Nimbus Project, Goddard Space Flight Center, Greenbelt, Md., 214 pp.

2. COSPAR Working Group VI, 1969: Systems Possibilities for an Early GARP Experiment. Report to the Joint Organizing Committee (JOC) (January), 55pp.

3. National Academy of Sciences, 1969: Plan for U.S. Participation in the Global Atmospheric Research Program. U.S. Committee for the GARP, 79 pp.

SECTION 4

SENSORS

SECTION 4

SENSORS

ILLUSTRATIONS

TABLES

SECTION 4

SENSORS

4.1 INTRODUCTION

The payloads selected for Earth Observation research spacecraft have, in general, been made up of sensors initially proposed and developed by Principal Investigators. Each sensor has reflected man's continuing need for fundamental knowledge. In the case of the meteorological program the data have led to quasi-operational uses and then, to an operational program where the spacecraft payload has served as a data gathering facility to support the requirements of a particular user, the nation's weather forecasting services.

For the initial flights (ERTS A and B) in the Earth Resources Program, the payload developed in consultation with the user agencies, is considered a facility to serve the needs not of a single user but of a broad spectrum of user agencies and groups.

For the EOS missions the principal allocation of weight, power, and earth viewing area will also be to the facility concept, but a portion of the capability of each spacecraft should be reserved for studies initiated by Principal Investigators.

The present section constitutes a review of remote sensing techniques and instruments which are candidates for EOS missions. The discussion is in two parts. Sections 4.2 through 4.8 deal with techniques which could be available for an initial flight in 1976. The balance of the section deals with sensors which hold considerable promise for various required measurements in Earth surveys, but need further development, or require power and weight capabilities beyond these considered applicable to early EOS missions.

Of the seven sensors identified for early flights, five are recommended for selection in Facility-type payloads for EOS A and B. They are;

> Sea Surface Temperature Imaging Radiometer
> Cloud Physics Radiometer
> Oceanic Scanning Spectrophotometer
> Thematic Mapper
> Passive Multichannel Microwave Radiometer

Two other sensors,
> Upper Atmospheric Sounder and
> Atmospheric Pollution Sensor

are representative of studies proposed by Principal Investigators in the Advanced Applications Flight Experments (AAFE) program, and are particularly addressed to two of the earth observation goals for the mid-seventies. For each of the seven sensors there is a discussion of the measurements to be made, and their role in meeting the goals of the earth observations disciplines as well as a discussion of the sensor characteristics. In a number of key areas it is evident that regular, repetitive, global, remote sensing from space can make a unique contribution to ongoing programs.

The measurements of interest are spread across the electromagnetic spectrum from the visible through the infrared to radio frequencies. In many instances interpretation of the earth signature in a particular frequency band requires measurements at a number of different frequencies to separate various effects. Frequently, simultaneous measurements from two or more sensors are required, a subject dealt with in more detail in Section 5, Payloads. Necessary for most applications are supplemental calibration and surface truth data gathered from such sources as a ship, a field trip, a crop survey, or a related sensor in an aircraft.
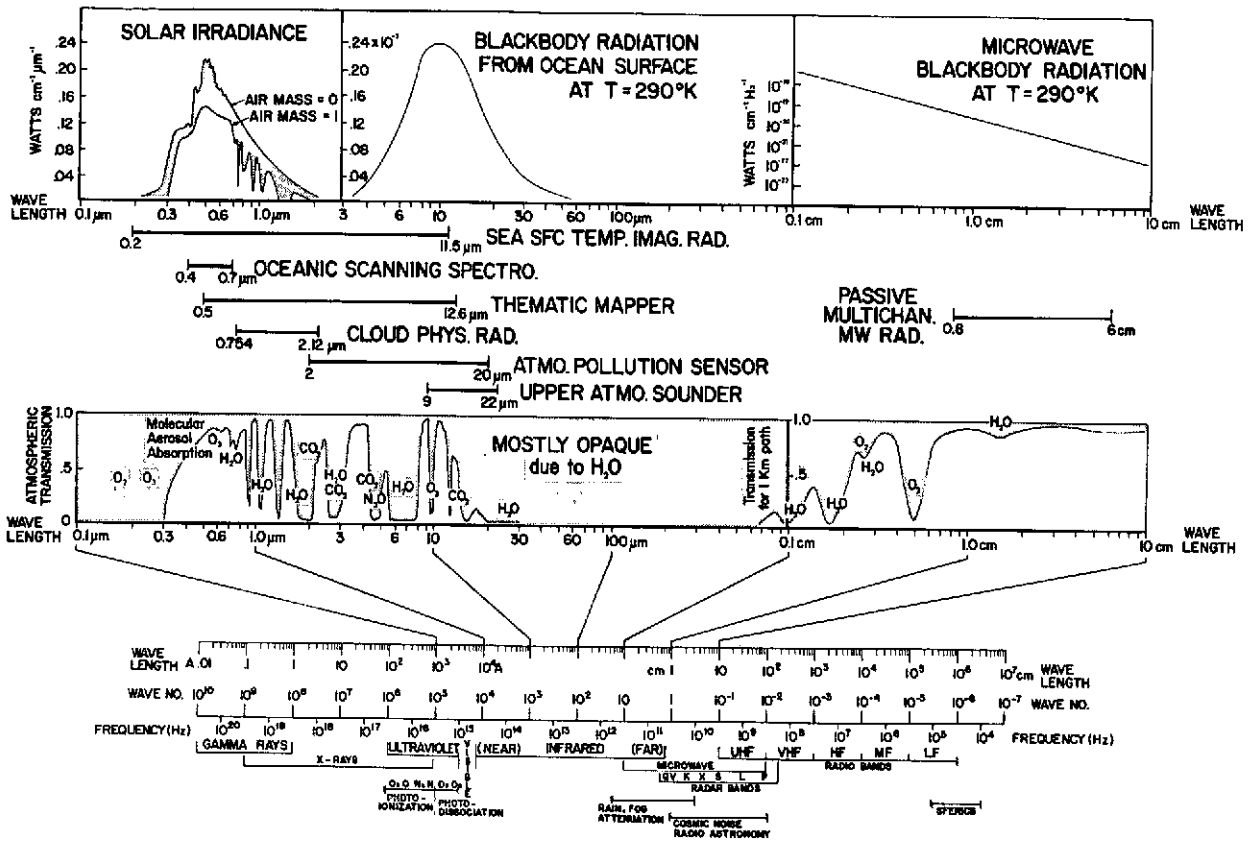
Figure 4.1-1   EOS Sensors and the EM Spectrum

The region of the electomagnetic spectrum covered by the seven key EOS sensors is summarized in Figure 4.1-1, which also shows some of the physical phenomena associated with the spectrum, the nature of atmosphere absorption and transmission in the portions of the spectrum of interest in the present study, and a comparison of the magnitudes of important energy sources, solar irradiance, and black body radiation.

In the sections that follow, sensors have been given generic names, both for convenience and to avoid the use of titles of particular instruments which are under development by a number of user groups. Technical details on sensors are given as preliminary design data, and are used in establishing the requirements which the payload places on such key spacecraft characteristics as earth viewing area, power, data rate, detector cooling, and attitude control.

4.2 SEA SURFACE TEMPERATURE IMAGING RADIOMETER

4.2.1 INTRODUCTION

A knowledge of water surface temperature and its distribution is of significance to a number of scientific communities. Such information is particularly useful in locating fishing grounds, in charting ocean and lake surface currents, and in monitoring heat budget and thermal exchange between water and the atmosphere. To establish meaningful relationships as to surface currents and successful fishing probabilities accurate surface temperature measurements are needed. For currents, surface temperature gradients are most important whereas for fishing operations absolute temperatures are also required. While daily coverage of a given area may eventually be required, especially in coastal areas, weekly coverage would be adequate for initial evaluation and research. Current NOAA sensors on satellites provide 7.5 km (4 nautical mile) resolution in the 10.5 - 12.5μm band and by 1972 this resolution will be improved to 0.8 km (1/2 nautical mile) using the Very High Resolution Radiometer (VHRR). With ERTS-B, 250 meter resolution in the 10.5 - 12.5μm band will become possible in selected areas every 18 days. However, since none of these systems have the capability of compensating for the effects of the atmosphere, temperature estimates with errors in the order of $\pm$ 2 K are the best that can be obtained (1). A combined "limb darkening" atmospheric correction must be applied to these satellite data, empirically tailored to each satellite, so that the data can be used for mapping sea surface temperatures over extensive ocean areas. Therefore, it is important to incorporate measurement techniques in the sensory system to compensate for atmospheric effects (including clouds) so as to obtain more reliable measurements of water surface temperature. The Surface Composition Mapping Radiomerer (SCMR) scheduled to fly on Nimbus-E in 1972 will have three channels, one sensing in the 10.2μm - 11.2μm band another in the 8.3μm - 9.3μm band and a third in the 0.8μm - 1.1μm band. All channels will have an instantanous field of view of 0.6 mr and will be registered with one another. This instrument will provide the opportunity, for the first time, of testing that part of the multispectral technique discussed in Section 4.2.2 having to do with correcting for the water vapor in the instantaneous field of view (utilizing the data from the 10.7μm and 8.8μm channels.) The third channel on the SCMR, which is also in the near-infrared region, can also serve in the daytime to identify the presence of clouds in the instantaneous field of view.

4.2.2 FIVE CHANNEL SYSTEM FOR SURFACE TEMPERATURE DETERMINATION

Anding, Kauth and Turner in a theoretical study (2) have demonstrated the feasibility of accurate sea-surface temperature sensing from space. Their technique will be augmented on EOS by performing simultaneous radiometric measurements in five spectral bands: 3.6 - 4.1, 6.5 - 7.0, 8.85 - 9.35, 10.5 - 11.5, and 0.2 - 4.0μm. Cloudy atmosphere may be sorted out, and the effects of non-cloudy atmospheres on the observed radiance can be nearly entirely compensated making sea surface temperature determinations possible to an accuracy of 0.15 K. The infrared window at 11μm occurs near the peak intensity of the long-wave Earth radiation. Under cloud-free conditions its only appreciable attenuation is by atmospheric water vapor. At nadir Earth viewing from space, this attenuation can lower the apparent Earth viewed temperature by 1 K to 4 K, the 4 K representing a moist tropical atmosphere. By sensing at two other wavelengths where outgoing radiation is again only reduced by water vapor, but in varying degrees, a correction may be applied to the 11μm data, thereby increasing its accuracy significantly. The 9.0μm wavelength region is intermediate between the strong absorption channel at 6.5 - 7.0μm and the 11μm window channel. Within the two regions, 7.0μm to 9.5μm and 10.0μm -12.0μm investigated by Anding et al [2] the band pair which gave the best results for water vapor correction, in regard to linearity and minimum scatter, is presented in Figure 4.2-1.

The maximum difference between cloud and water surface emittance occurs near 4.0μm as shown in Figure 4.2-2. Therefore particularly at night, use of information in this wavelength would provide the necessary information to estimate fractional cloud cover. A drawback in the use of radiances at 5.0μm is the appreciable water vapor absorption occuring at that wavelength.
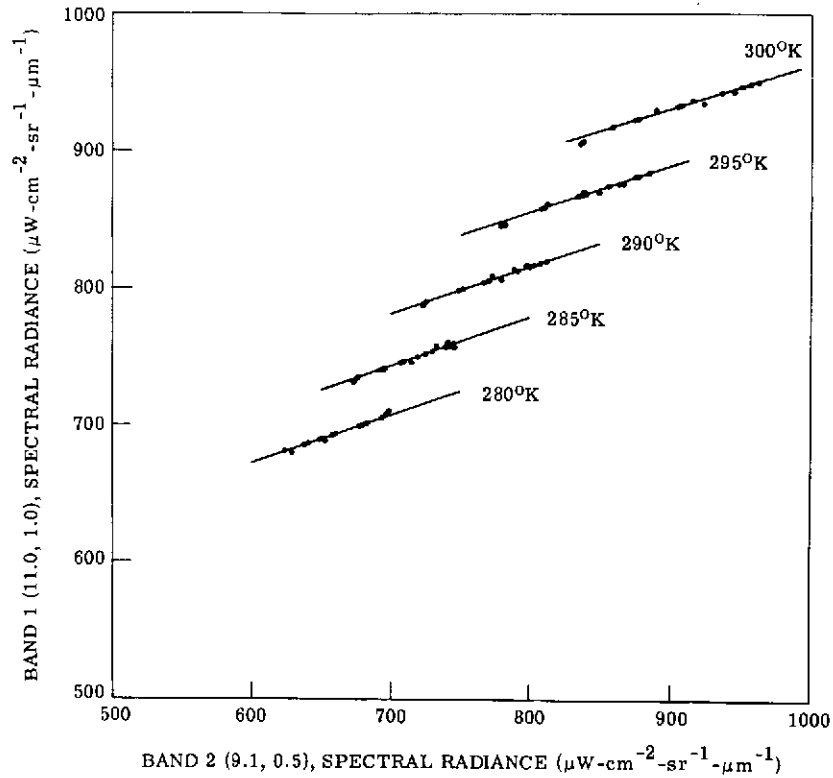
Figure 4.2-1. Spectral Radiance in Band 1 versus that in Band 2 as a function of Atmospheric State. Parameters = Zenith Angle at Target and Sea-Surface Temperature
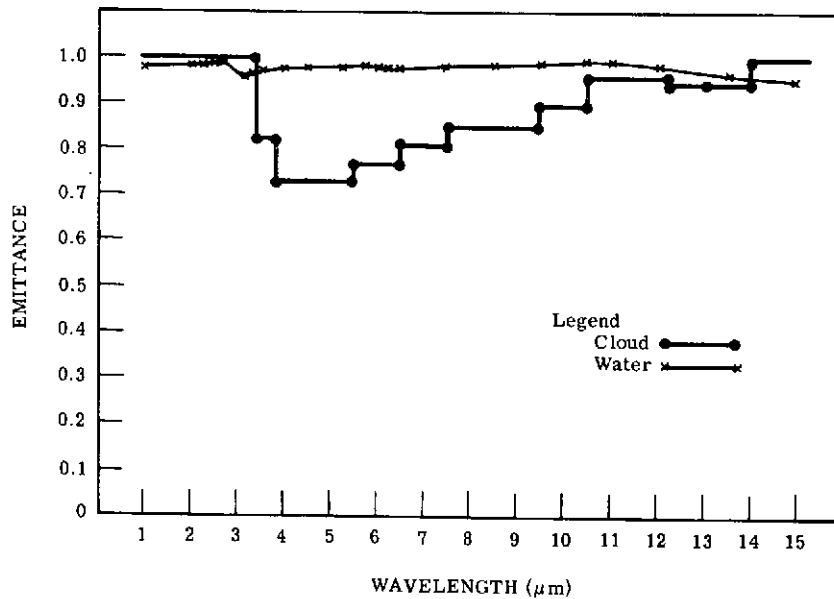

Figure 4.2-2. Spectral Emittance of Liquid Water and Opaque Water-Drop Cloud

4-12

A recommended alternative is the use of radiances in the 3.6-4.1μm window. The use of combined 3.7μm and 11μm radiances for inferring sea surface temperature was recently investigated theoretically by Smith and Rao.[3] The Infrared Temperature Profile Radiometer (ITPR) to be flown on Nimbus-E will obtain radiances in these two windows. Smith and Rao studied the use of these radiance measurements for determining sea surface termperatures, a necessary part of the analysis of the ITPR data to yield vertical temperature profiles. They concluded that the multispectral approach allows surface temperatures to be determined even when the instrumental field of view contains broken clouds, and that sea surface temperatures determined from multispectral observations will be much more accurate and reliable, especially on small spatial scales, than those currently obtained with single window channel measurements. Semi-transparent clouds, particularly high thin cirrus, have been suspected as elusive contaminants on all satellite sea surface temperature measurements to date. The Anding et al[2] model indicates that their presence will easily be detected by the proposed sensor. Further, in studies of a multispectral technique using data from three channels (6.4-6.9μm, 0.2-4.0μm, and 10-11μm) of the Nimbus-2 Medium Resolution Infrared Radiometer (MRIR), Shenk and Szekielda (4) and Shenk and Salomonson (5) report good results in the use of the 6.4 - 6.9μm data to infer the presence of thin cirrus during night or day and of the 0.2 - 4μm data to "tag" the presence of clouds in the instantaneous field of view during the daytime; and after thus determining cloud-free lines of sight, in the subsequent use of the radiances in all three spectral intervals to correct for the effect of the intervening atmosphere in deducing the true ocean surface temperature. Shenk and Salomonson (5) conclude that their technique is capable of determining sea surface temperature to an accuracy of approximately ± 1 K. They furthur conclude that increased accuracies would result from the use of higher spatial resolution data (IFOV of the MRIR is about 55km at the sub-satellite point) and additional channels, such as one sensing in a part of the spectrum where there is weak water vapor absorption to yield more information on the moisture content of the lower troposphere. An example of a sea surface temperature map produced by means of this method is shown in Figure 4.2-3. During daytime passes the 0.2 - 4μm channel will readily detect clouds. Therefore, measurements from this channel would indicate when the 11.0μm information was not from sea surface emission. Such simultanteous data channels act as a filter to sort out accurate sea surface measurements in cloud-free areas. Furthermore, the broadband 0.2-4 μm channel will be useful in measuring the albedo and assessing the radiation budget of the Earth-atmosphere system.

The effects of the atmosphere on the spectral radiance emanating from the sea surface can be significant and must be compensated if accurate sea surface temperatures are to be obtained from space. The give channel sensor will compensate almost completely for atmospheric effects in cloud-free areas.

4.2.3 SENSOR DESIGN

The design of an instrument which achieves the goals of ocean surface temperature measurement outlined in Section 4.2.2 is based on the following parameters:

> Spacecraft altitude - 1000 km
> Instantaneous field of view (IFOV) - 2 km x 2 km
> Ground velocity of the spacecraft - 6.36 km/sec
> Spectral bands:
> > 0.2 - 4.0μm
> > 3.6 - 4.1μm
> > 6.5 - 7.0μm
> > 8.85 - 9.35μm
> > 10.5 - 11.5μm
> Scan angle - 102 (± 51 from nadir)

The scanning will be accomplished by rotating a mirror through 360°. One scan of the earth's surface will be made for each 360° rotation of the mirror. The rotational speed to provide
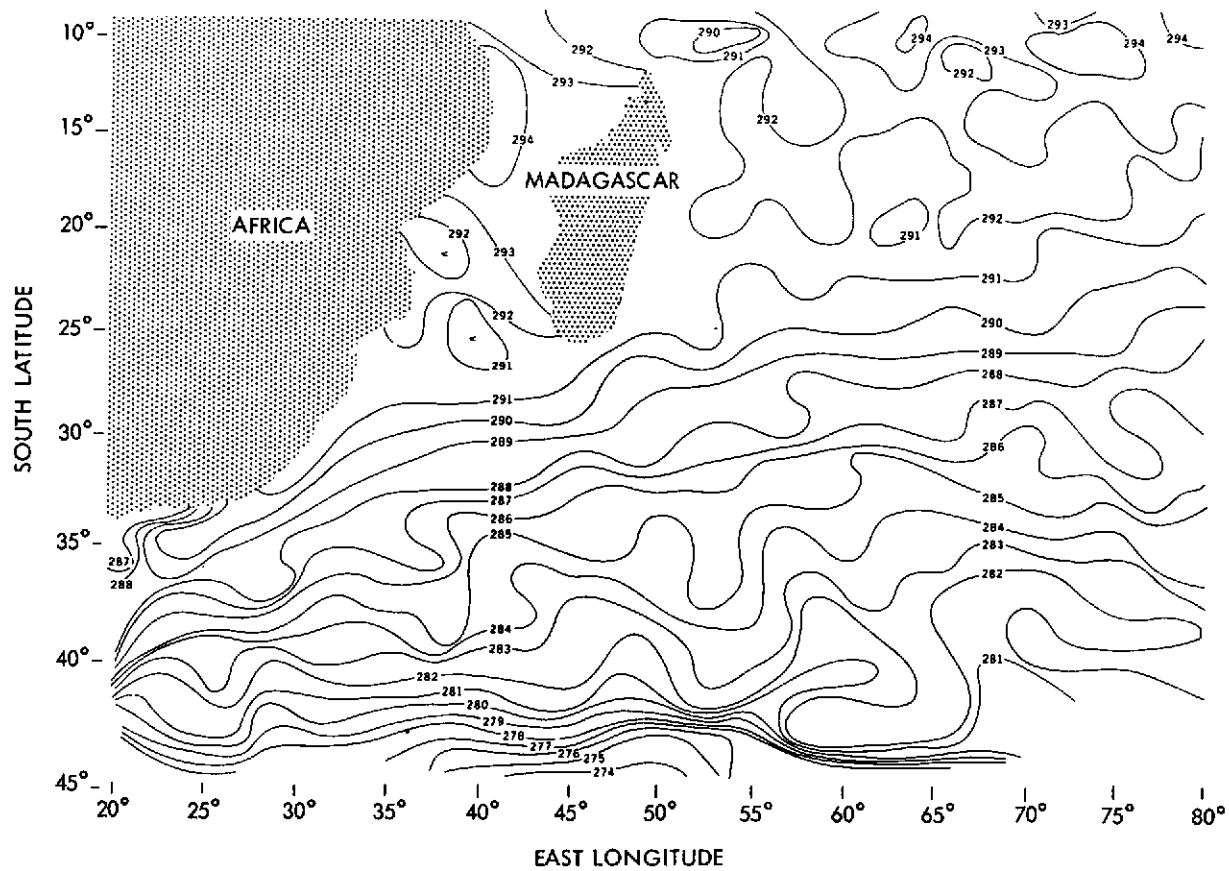
Figure 4.2-3.   Sea Surface Temperature Distribution over the Indian Ocean from June 14
thru July 7, 1966.   (From Nimbus 2 MRIR Data using a Three-Channel
Analysis Technique - after Shenk and Szekielda [5])

contiguous ground coverage will be 3.13 scans/sec and the scan efficiency will be 0.278. The rotational axis of the mirror will be parallel to both the optical axis of the telescope and the velocity vector of the spacecraft similar to the HRIR configuration.

The design was based on the 8.85 - 9.35μm band since the combination of energy available and the precision of measurement required makes this the most critical. Calculations which follow show that we can, for the 8.85 - 9.35μm band, obtain an NEΔT of 0.15 K with an aperture of 52 cm^2(8.8 cm diameter primary mirror). The analysis assumes the sea surface to be a 290°K black body with an emissivity of one. The diffraction limit of a 8.8 cm mirror is well within that required for the 10.5 - 11.5μm band which is the most critical with respect to optical resolution.

In the 10.5 - 11.5μm band, and again assuming a 290 K blackbody, the instrument will provide an NEΔT of 0.09K. For colder temperatures the instrument will be less sensitive. For example, for a blackbody at a temperature of 200K the NEΔT will be 0.33 K in this spectral band.

An analysis of the 3.6-4.1μm spectral band indicates that the following performance would be obtained:

Equivalent Blackbody Temperature	NEΔT
(Kelvins)	(Degrees C)
290	1.3
260	4.7
220	50.0

The rapid fall-off in performance at the colder temperatures in this spectral band is due to the decrease in radiance for a blackbody at the lower temperatures.

In the spectral band from 6.5 - 7.0μm a 50m thick cloud at 12 km altitude gives a radiance, N_λ, of 65 x 10^{-6} watts/cm^2-ster-μm reference (2). This is equivalent to a blackbody temperature of 225 K. The instrument as proposed with provide an NEΔT of 0.83 K for a 225 K blackbody. Similarly, in the spectral band from 4.65 - 5.15μm which may be substituted for the 3.6 - 4.1μm band, a 50μm thick cloud at 12 km altitude gives a radiance, $N\lambda$, of 50 x 10^{-6} watts /cm^2-ster-μm. This is equivalent to a blackbody temperature of 260 K and the instrument will provide an NEΔT of 1.05 K.

Detailed calculations were not made for the 0.2 - 4.0μm band since the energy available and the detector sensitivity in this region permits the presence of clouds to be easily detected.

It is proposed to use a silicon diode for the 0.2 - 4.0μm band since a diode is simpler to design into the system than a PMT when sensitivity is not a problem. Hg Cd Te detectors which will require cooling to 90 K will be used for the thermal bands. The spectral bands will be isolated from the total energy received by dichroic type filters.

A simple all reflective optical system will be required for the telescope since it is used essentially on axis. A single field stop will be used. If we assume a focal length of 30 cm this field stop will be 0.024 inch by 0.024 inch in size. It will be necessary to reduce the size of the field stop as related to the detector in the thermal bands since the noise in the detector is proportional to the square root of the detector area. The calculations have been based on a reduction in size of approximately eight. An immersion lens at the detector to give an effective f number of 0.3 will be satisfactory.

A "DC restore" technique will be required for each of the five video channels. In addition a calibration is required at frequent intervals for the thermal channels. Since the field of view of

the instrument rotates through 360° and the active video only occurs during 27.8% of this time it will be possible to locate a suitable calibration source on the housing of the instrument. This will permit calibration to take place once each scan line. A scan monitor system will be required for synchronization and to provide a video start signal.

The data rate will be approximately one megabit per second. This is based on five video channels two samples per IFOV and digitizing to ten levels. Since the active video only occurs during 27.8 percent of the total scan cycle the data can be buffered to reduce the data rate to about 0.33 megabits per second.

The size of this instrument will be about 8" x 8" x 24". The estimated weight is 35 pounds and the estimated power required is 30 watts. These figures are for the scanner and do not include estimates for multiplexing and signal processing. In addition, a cooler will be required for the four Hg Cd Te detectors. The size and weight estimates do not include a cooler. To facilitate review, the design calculations for an SSTIR are incorporated here:

Size of primary aperture

$$Ap = \frac{A_d^{1/2} \, \Delta f_n^{1/2}}{D^* \, \Omega (NER) \, e_0}$$

where

A	–	area of the detector
Δf_n	–	noise bandwidth
D*	–	measure of detector sensitivity
Ω	–	instantaneous field of view (IFOV)
NER	–	noise equivalent radiance
e_0	–	optical efficiency

The following values were used in the above equation to calculate Ap:

$A^{\frac{1}{2}}$	–	7.6×10^{-3} cm
Δf_n	–	9.2×10^3 Hz
D*	–	10^{10} cm Hz$^{\frac{1}{2}}$/watt
Ω	–	4×10^{-6} steradians
NER	–	1.14×10^{-6} watts/cm^2 – ster
e_0	–	0.2

These values give a required collecting area of 52 cm^2. If we assume a 40% central obscuration for the secondary mirror the diameter of the primary mirror is 8.8 cm.

$$\Delta f_n = \frac{\alpha \, RK}{2\Omega^{1/2} \, e_s}$$

where

α	–	scan angle in radians – 1.745
R	–	scans/sec – 3.2
K	–	factor to account for the filter passband and amplifier noise – 1.82
Ω	–	IFOV – 4×10^{-6} steradians
e_s	–	scan efficiency – 0.278

Table 4.2-1

Sea Surface Temperature Imaging Radiometer

Design Parameters	
IFOV, km	2.0
Scan, deg	±51
Swath, nm (km)	1550 (2870)
Nodal Crossing (LMT)	0900, 1200, 1500
Revisit Time, Days	1

Spectral Channels (Approx.)

Wavelength (μm)	Parameter	Measurement
(1) 10.5 - 11.5	IR Window	Sea surface temperature from multispectral analysis in clear skies
(2) 8.85 - 9.35	Water Vapor Continuum	
(3) 6.5 - 7.0	Water Vapor Absorption	Thin cirrus tag, multispectral analysis
(4) 3.6 - 4.1	IR Window	Cloud tag (night) multispectral analysis
(5) 0.2 - 4.0	Solar Radiation	Cloud tag (day) multispectral analysis
		Also, chan's (1) and (5): Radiation budget; correlative imagery for other measurements

Sensor Characteristics

Date Rate, Mb/s	0.33
Power, watts	30
Weight, lb (kg)	45 (20)
Proj. Area ft^2 (m^2)	1.3 (0.12)

The spectral radiance of the earth in the wavelength range from 8.85 - 9.35μm (assuming the sea surface to be a 290 K blackbody with an emissivity of one) is 4.05 x 10^{-4} watts/cm^2 - ster. For a T of 0.15 K the NER is then:

$$\text{NER} = \frac{14.388}{\lambda T}\frac{\Delta T}{T}N_\lambda$$

where

T   –   absolute temperature = 290K
ΔT   =   0.15K
λ –   wavelength in   m = 9.1
N_λ –   spectral radiance = 4.05 x 10^{-4} watts/cm^2 - ster

Using the above values the NER = 1.14 x 10^{-6} watts/cm^2 - ster.

4.2.4 SUMMARY

The preliminary design of a sea-surface temperature imagering radiometer (Section 4.2.3), summarized in Table 4.2-1, shows that the sensor is small and could be accommodated as the single sensor on a SATS class spacecraft. For many oceanographic purposes, however, such as detection of ocean currents and assessment of nutrient rich or nutrient free areas, simultaneous measurements of ocean temperature and ocean color are required and the single sensor space-craft provides a severe limitation. Assessment of sea surface conditions by microwave radio-metry will also benefit from correlative infrared measurement of sea surface temperature.

4.2.5. REFERENCES

1. Smith, W. L., P. K. Rao, R. Koffler, and W. R. Curtis 1970: The Determination of Sea-Surface Temperature from Satellite High Resolution Infrared Window Radiation Measurements. Mo. Weather Review, 98, 604-611.

2. Anding, D., R. Kauth and R. Turner, 1970, "Atmospheric Effects on Infrared Multispectral Sensing of Sea Surface Temperature from Space, "Willow Run Laboratories University of Michigan, Contract NAS 12-2117, 98 pages.

3. Smith, W. L. and P. K. Rao, 1971: Sea Surface Temperature Measurements from Satellites. Paper presented at the 5th Symposium on Temperature. Its Measurement Control, Science and Industry, June 21-24, 1971, Washington, D. C.

4. Shenk, William E. and Karl-Heinz Szekielda, 1971: Satellite Ocean Temperature Analysis of the Indian Ocean, Paper presented at the Symposium on the Indian Ocean and Adjacent Seas-Their Origin, Science, and Resources, January 12-18, 1971, Cochin, India.

5. Shenk, William E. and Vincent V. Salomonson, 1971: A Multispectral Technique to Determine Sea Surface Temperature Using Nimbus 2 Data. (To be published in the Journal of Physical Oceanography.)

4.3 CLOUD PHYSICS RADIOMETER

4.3.1 INTRODUCTION

Hanel [1] proposed that cloud top pressure levels could be sensed using the 2.0μ CO_2 band. Yamamoto and Wark [2] and, independently, Chapman[3] proposed using the oxygen "A" band. As is often the case, what once were thesis and antithesis have now become synthesis. This experiment is designed to infer the cloud top pressure level, the density and phase of the condensed water in the cloud, a drop size parameter, and the clouds' thickness, both optical and geometrical. This would be accomplished by measuring the solar energy reflected from clouds in five spectral intervals. One is in the 0.7619μm oxygen "A" band at 0.763μm. Another is used as a reference and is just outside the band at 0.754μm. Two more intervals are similarly in and just out of a carbon dioxide band at 2.06μm. These channels are at 2.06μm and 2.12μm, respectively. The fifth channel is at 1.6μm.

Several earlier experiments have helped to establish the feasibility and general form of the preposed experiment. These experiments include the hand-held spectrograph flown on Gemini-Titan 5 [4,5]; and early aircraft instrument, flown aboard a NOAA RB-57 aircraft; and the engineering model of a terminated Nimbus-D experiment, which was flown aboard the NASA CV 990 [6].

Numerous measurements of the reflection, absorption, and other optical properties of water and ice have been made. These are summarized and anlayzed in [7]. A filter wedge spectrometer which was developed for Nimbus D has been flown for some time in high altitude aircraft, i.e., the NASA CV-990 and B-57B. Numerous spectra of different cloud types have been obtained. These measurements are presented in [8,9,10]. In addition, there have been many theoretical studies [11,12,13] in support of this experiment, so that the concepts suggested have solid experimental and theoretical bases.

4.3.2 SCIENTIFIC OBJECTIVES

4.3.2.1 Specific Objectives. The specific objectives of this experiment are to make radiance measurements with a suitable radiometer in 5 spectral intervals 0.754, 0.763, 1.61, 2.06, and 2.12μm and to collect adequate "ground truth" about the clouds being observed. This ground truth would consist of the pressure level of the clouds' top, its thickness, and some determination of the particle size distribution, particle density and phase. Presumably this ground truth would be obtained by means of an appropriately instrumented aircraft.

The radiometer's specifications as to spectral bandwidth, radiometric and wavelength calibration and accuracy requirements will be discussed in detail below.

The final specific goal is to reduce the radiometric data and correlate it with the actual observations of the cloud parameters and theoretical calculations.

4.3.2.2 Additional Applications. If the specific objectives of this experiment are achieved to the desired accuracy, these data can be used in a number of additional applications; several of which are discussed below.

The Global Atmospheric Research Program (GARP) is an international cooperative program of research whose goals are to increase understanding of the general circulation of the atmosphere and to develop the physical and mathematical basis of extended weather prediction. The World Weather Watch (WWW) is a program sponsored by the World Meteorological Organization (WMO) and its member nations for expanding the world weather observing network, improving the global telecommunications system, and facilitating data collection through establishment of world meteorological criteria. The two programs are essentially the arms of a world weather program, GARP being the research arm and WWW the operational arm.

Detailed knowledge of the altitude distribution and composition of clouds is required for these programs because of the importance of clouds to radiative transfer and the thermodynamic and dynamic interaction of clouds and the environment. Calculations indicate an extreme sensitivity of the atmospheric state to the amount and distribution of clouds. Their determination thus represents one of the important links in a complete theory of the general circulation. Accurate global observations of cloud distributions will be important in developing comprehensive theories and again, later in checking the accuracy of numerical calculations. It is also possible to calculate albedo and the solar and thermal flux divergences of the atmosphere.

The report of the GARP study conference [14] specifically mentions the need for investigations designed to improve our understanding of basic atmospheric radiative processes, particularly the investigation of radiative transfer in clouds.

4.3.3 TECHNICAL DISCUSSION

4.3.3.1 The Physics of Clouds. If all clouds had the same droplet size distribution and number density, and if they were composed of spherical water drops, the determination of the cloud-top altitudes and thicknesses would be fairly straightforward. One would only need to measure the reflected solar radiation at two wavelengths, one inside the oxygen absorption band and the other outside the band. The reflected radiation outside the band, R_1, would not be affected by the oxygen absorption and would therefore be a measure of the maximum reflectance of the cloud in this spectral region, while the reflected radiation inside the band, R_2, would be partially absorbed by the oxygen that intervenes between the sun, the cloud, and the satellite.

Given the zenith angle of the sun and the nadir angle of the direction of view of the instrument, the measured reflectance outside the oxygen band would depend only upon the thickness of the cloud. At the same time, the ratio of the cloud reflectance within the band to that outside of it would yield the transmittance of the atmosphere above the cloud, which would be strongly dependent upon the cloud-top altitude and only weakly dependent upon the cloud thickness.

The transmittance in the clear atmosphere above the cloud, $T_2^{(a)}$, can be calculated by the method shown by Wark and Mercer[15] the transmittance in the cloud, $T_2^{(c)}$, can be calculated by the multiple scattering technique discussed by Saiedy, Jacobowitz, and Wark [5] . The product of the two transmittances, T_2, would be the observed transmittance so that by inverting the procedure the cloud-top altitude and thickness could be deduced directly from the measured reflectances, R_1 and R_2.

Clouds, however, do not have the same droplet size distribution and number density so that these determinations cannot be made from two channels alone.

Figure 4.3-1 presents a striking example of the limitations imposed by the use of a single absorption band. The observations were obtained chronologically, with a hand-held spectrograph used from a NOAA aircraft [4] and from the Gemini 5 spacecraft; with a spectrometer carried on a NOAA aircraft [6]; and with a more advanced spectrometer carried on a NASA aircraft [6] . In each case the sun was overhead and the instrument was pointed downward. The clouds were very bright with $R_1=0.72$. The quantities shown are the ratios of the true cloud-top pressure, obtained from in situ measurements, to the apparent cloud-top pressure derived from cloud models.

All observations fit along a "main sequence" except for one observation. This was a thick cirrostratus cloud in a weak occluded front in the Pacific, observed on June 20, 1968. All other clouds were of the dense variety (cumulus congestis, stratus, thick altostratus and altocumulus, and cumulonimbus spreading out to form altostratus). The explanation for the disparity of this one observation lies in some unknown combination of water concentration and drop-size distribution.
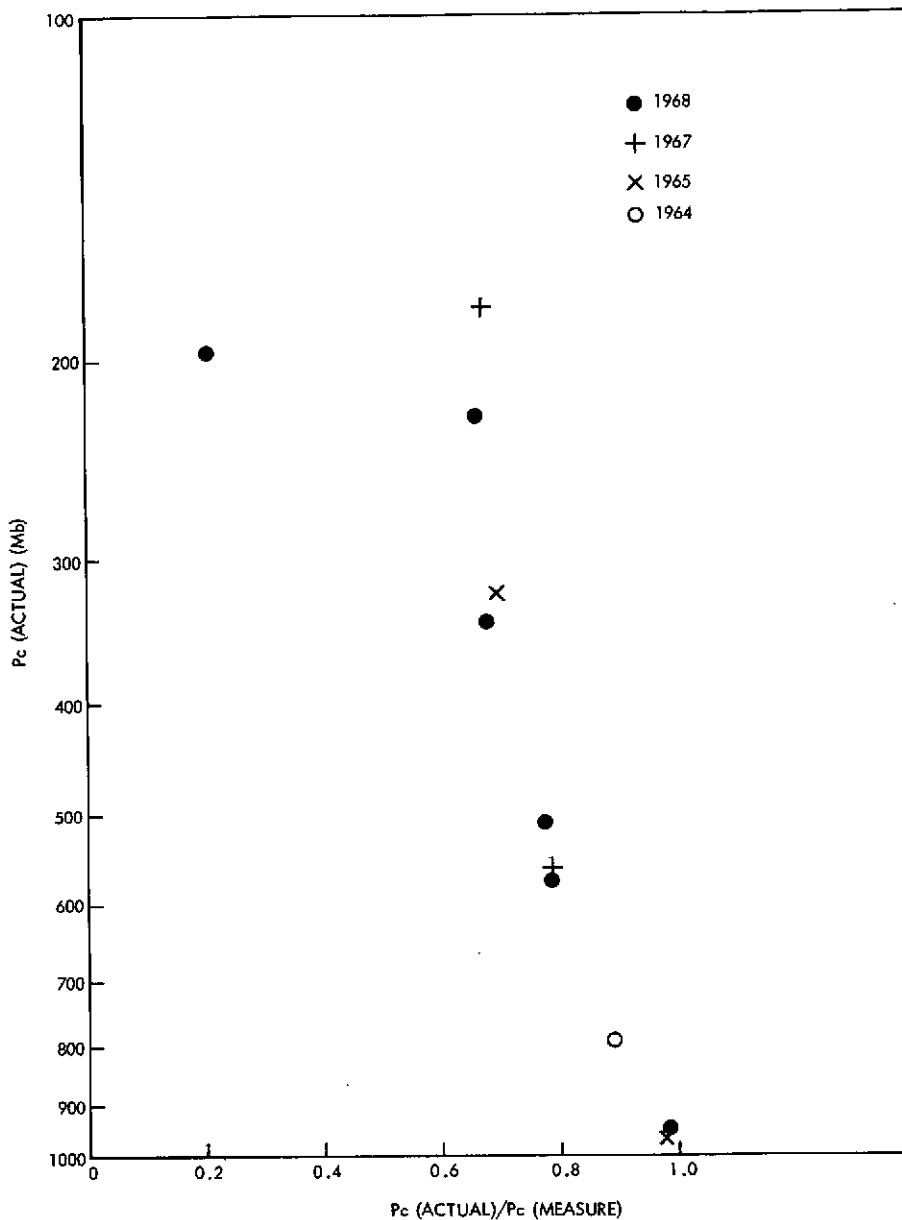
Figure 4.3-1.   Relationships Between Actual and Measured Cloud-Top Pressures
from Four Aircraft Expeditions

One must therefore use two spectral intervals whose measured reflectances and transmittances are linearly independent of one another in order to obtain independent information about the optical properties of the clouds observed. It was suggested that two spectral intervals in the oxygen band be used. However, measurements of the transmittances in two such intervals for cirrus clouds were identical to those for stratus clouds. In other words, the second absorbing channel did not yield an independent piece of information that could be used to differentiate between high and low clouds. Because of this, a second interval in a different part of the spectrum was sought.

Consideration of the advantages and disadvantages of various spectral intervals led to the choice of the 2.06μm CO_2 band and the "window" to the long wavelength side of this band at 2.12μm.

In this region, the imaginary part of the index of refraction "n_i" is 3×10^{-4} which results in an absorption by the liquid water, with a consequent reduction in the mean penetration of the cloud and a reduction in the maximum reflectance.

Calculations based upon the matrix techniques of Twomey, Jacobowitz and Howell (12) show the reflectance of a cloud to be related through empirical expressions to d, p, and the size parameter $(r + o_r)$ for any combination of sun and view angles. Likewise, the transmittance that results for the calculations show that it can be related empirically to P_c, d, p, and $(r + o_r)$;

where 1)   The pressure altitude of the cloud-top is P_c.
This should be known to about 200 meters.

2)   The geometric thickness of the cloud is d. This is known with decreasing accuracy for increasing thickness.

3)   The density of liquid water is p. This should be known to a few tens of percent, excluding rain drops.

4)   The size parameter of the cloud droplets is $(r + o_r)$ with r being a mean radius and o the dispersion. This should be known within ten percent.

Cloud scattering is a strong function of particle size at $1.6\mu m$ and $2.1\mu m$ wavelengths. Because of absorption in the solid or liquid cloud particles, cloud scattering is a strong function of particle size — small particles scattering efficiently and large particles inefficiently. In a visual display, ice crystal clouds at $2.1\mu m$ will be nearly black, while water droplet clouds will range in brightness from very white to grey, depending upon droplet size. At $1.6\mu m$ all water droplet clouds will be very bright while ice crystal clouds will range from grey to black, again depending upon particle size. The data at these two wavelengths can thus be analyzed to obtain cloud composition information. This can be done by both visual interpretation and more precisely by photometric analysis.

The single scattering albedo W_0 for ice crystals at $2.1\mu m$ ranges between about 0.9 and 0.5. Relative reflectance of such clouds is shown by the curves at the top of Figure 4.3-2. Ice crystal clouds reflect quite inefficiently with reflectance values for a given optical thickness confined to a narrow range of values. Consequently it is not possible to determine ice crystal size accurately at this wavelength.

Because of the smaller values of the absorption coefficients for water and ice and the small differences between them, the situation is somewhat different at $1.6\mu m$. The single scattering albedo is nearly 1 for all water droplet clouds. Reflectance curves for these clouds are shown at the bottom of Figure 4.3-2. The single scattering albedo range for ice crystal clouds at this wavelength is about $0.98 \geq W_0 \geq 0.6$. As shown, these clouds reflect less efficiently than water clouds. At $1.6\mu m$, reflectance data provide less accurate information on water droplet size than at $2.1\mu m$ but much better information on ice crystal size.

4.3.3.2 Sensor Requirements. The principal channels for studies of the physics of clouds are as follows:

Channel	Center Wavelength	Bandwidth
1	$.754 \pm .001\mu m$	$.005\mu m$
2	$.763 \pm .0005\mu m$	$.005\mu m$
3	$1.61 \pm 0.002\mu m$	$.072\mu m$
4	$2.06 \pm .02\mu m$	$.050\mu m$
5	$2.125 \pm .02\mu m$	$.032\mu m$
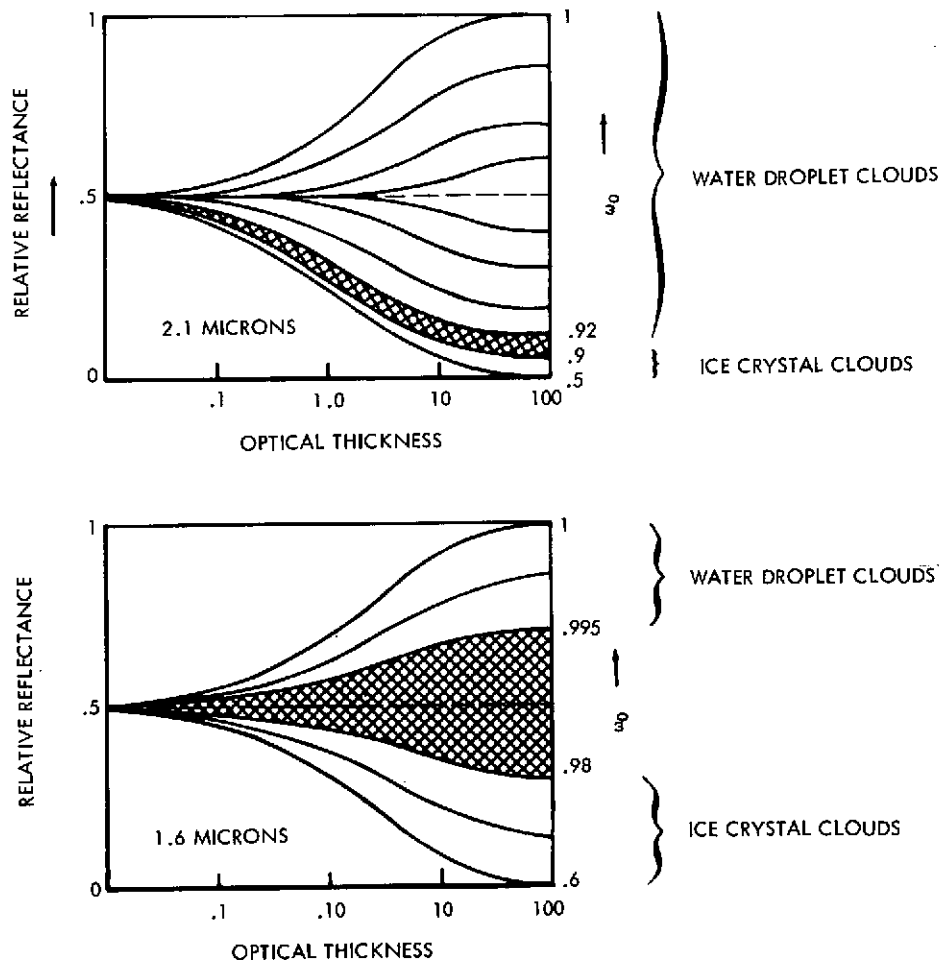
Figure 4.3-2.   Estimated Cloud Reflectances at 1.6 and 2.1 Micrometers

Earlier versions of this experiment have used narrower bandwidths; however, it is now believed that the wider bandwidths are as useful and simplify the instrument design.

The radiometric accuracy required is 2% absolute for the out-of-band channels and 0.1% relative accuracy for all of the channels. This requires digitization of the data to 10 bit accuracy. [The currently favored radiometric calibration method is to diffuse the sun's energy, using a transmission or reflection element.]

Wavelength calibration should nominally be within the tolerances quoted for the center wavelengths of the channels. Since the atmosphere has numerous absorption bands in this spectral region whose centers and widths are well known, the proposed wavelength calibration method is simply to do a spectral scan through the 0.75 - 2.2μm region.

Detectors for this spectral region with high D*'s are readily available. Silicon photodiodes are available for the short wavelength channels and lead sulfide can be used for the longer wavelength channels.

The accuracy requirements of this experiment are fairly high so that a signal-to-noise ratio (S/N) of about 100 is required; however, the sun is a "bright" source and clouds are good reflectors, so that this S/N may be achieved with only modest size collecting optics. The exact size, of course, is quite dependent on field-of-view and electronic bandwidth requirements.

There are many readily available techniques to achieve the spectral resolution required. They range from all filter to all grating, and an interferometer could be used. Again the specific technique would depend on many factors.

4.3.3.3 Supporting Efforts. Twomey, Jacobowitz, and Howell [12] have performed calculations for size distributions and size parameters for the "A" band part of the experiment. However, specific calculations for the $2\mu m$ region using the appropriate size parameters and index of refraction values have not been done. These will be carried out in the near future. Calculations also need to be made for ice clouds in both wavelength regions.

Atmospheric transmission values for the "A" band have been determined by Wark and Mercer [15] . However, the atmospheric transmittance of 2μ CO_2 band to the required accuracy has yet to be determined.

The values of the optical constants of water and ice as summarized by [7] indicate that there is some discrepancy in the measurements. These discrepancies are believed not to be significant for the experiment; however, future measurements and analysis may prove this is not the case.

In addition to the radiances measured by the radiometer, independent measurements of the cloud's physical characteristics are necessary. The important parameters are: (1) the cloud top pressure level, (2) the cloud's thickness (geometrical and/or optical), (3) the droplet size distribution, (4) the density of the cloud (expressed in drops per unit volume or mass per unit volume), (5) the phase of the cloud particles (water or ice).

Presumably these measurements would be done from an appropriately instrumented aircraft. The exact instrumentation would depend on a number of factors.

A similar experiment is being proposed for SKYLAB and will be conducted by NOAA's National Environmental Satellite Service. NASA aircraft data from GSFC's filter wedge spectrometer will be investigated as further supporting activity.

4.3.3.4 Sensor Design. A preliminary design of a Cloud Physics Radiometer is based on the following parameters:

Spacecraft altitude — 1000 km
Instantaneous field of view — (IFOV) — 2.5 x 2.5 km
Ground velocity of the spacecraft — 6.36 km/sec
Spectral bands:

CENTER WAVELENGTH	BANDWIDTH
0.754 μm	0.005 μm
0.763 μm	0.005 μm
1.61μ m	0.072 μm
2.06μ m	0.050 μm
2.125 μm	0.032 μm

Scan angle — 102° (±51° from nadir)

The scanning will be accomplished by rotating a mirror through 360°. One scan of the earth's surface will be made for each 360° rotation of the mirror. The rotational speed to provide contiguous ground coverage will be 2.55 scans/sec and the scan efficiency will be 0.278. The rotational axis of the mirror will be parallel to both the optical axis of the telescope and the velocity vector of the spacecraft (similar to the HRIR configuration).

The design is based on the 0.763μm band since this is the most critical channel. The calculations in this section show that the noise equivalent change in reflectance (NEΔR) is 0.1% with an aperture of 207 cm² (17.7 cm diameter primary mirror). It is also shown that we can obtain a NEΔR considerably better than 0.1% in all of the infrared bands. A 17.7 cm diameter primary mirror would require a focal length for the system of about 53 cm. For an IFOV of 2.5 x 2.5 milliradians the field stop would be 1.33 x 1.33 mm.

It is proposed to use photomultipliers as detectors in the 0.754 and 0.763 μm spectral bands. In As detectors will be used for the other three bands. These will require cooling to 120° K. During the design study for this instrument a trade — off analysis should be made between the cooled In As detectors and various types of detectors which can operate at ambient temperatures such as lead sulfide.

The spectral bands will be isolated from the total incoming energy by means of a grating spectrometer. Assuming that the optical efficiency of the spectrometer is 80% an overall optical efficiency of 50% is expected.

A DC restore technique will be required for each of the five video channels. In addition, a calibration is required at frequent intervals. Since the field of view of the instrument rotates through 360° and the active video only occurs during 27.8% of this time it should be possible to locate suitable calibration sources on the housing of the instrument. This would permit calibration to take place once each scan line. A scan monitor system will be required for synchronization and to provide a video start signed.

The size of the insrtument will be approximately 10" x 10" x 28". The estimated weight is 70 pounds and the estimated power required is 40 watts. A cooler has not been included in these estimates.

To facilitate review, the design calculations are given below:

The size of the primary aperture was based on the 0.763μm band. As is shown in the calculations for the Oceanic Scanning Spectrophotometer (Section 4.4.3.2), the area of the primary aperture is given by the relation

$$A = \frac{4 e N_{\lambda_T} \Delta f}{S \left(N_{\lambda_s} \right)^2 \Omega e_0}$$

where

A = area of primary aperture (cm²)
S = responsivity of the PMT in amps/watt
N_{λ_S} = spectral radiance of the earth due to a change in reflectance of 0.1% as seen from the satellite in watts / cm² – ster
N_{λ_T} = total spectral radiance as seen from the satellite
Ω = solid angel subtended by the IFOV of the instrument in steradians.
Δf = noise bandwidth of the system
e_0 = optical efficiency
e = charge on an electron

Using the following values:
S = 30 x 10⁻³ amp/watt
N_{λ_s} = 1.53 x 10⁻⁷ watts/cm² – ster (assumes a solar zenith angle of 37°),
Ω = 6.35 x 10⁻⁶ steradians

$$\Delta f = 5830 \text{ Hz}$$
$$e_o = 0.5$$
$$e = 1.6 \times 10^{-19} \text{ coulombs}$$

we get a required area for the primary aperture of 207 cm². Allowing for an obscuration of 40% for the secondary mirror we would have a primary 17.7 cm in diameter.

The noise bandwidth is determined from the following:

$$\Delta f = \frac{R K \alpha}{2 \Omega^{1/2} e_s}$$

where
α = scan angle in radians = 1.745
R = scan rate in scans/sec = 2.55
e_s = scan efficiency = 0.278
$\Omega^{1/2}$ = 0.0025
K = factor to account for the filter pass band and amplifier noise = 1.82
Δf = 5830 Hz

The following calculations show the performance of the instrument in the infrared bands. The noise equivalent power (NEP) was determined for the three spectral bands:

$$NEP = \frac{\sqrt{a_d \Delta f}}{D^*}$$

where

D^* = 3 x 10¹¹ cm Hz^{1/2}/watt
Δf = 5830 Hz
A_d = 0.133 x 0.133 cm (2.12μm)
A_d = 0.133 x 0.213 cm (2.06μm)
A_d = 0.133 x 0.298 cm (1.61 μm)
NEP = 3.4 x 10⁻¹¹ watts (2.12 μm)
NEP = 4.27 x 10⁻¹¹ watts (2.06μm)
NEP = 5.08 x 10⁻¹¹ watts (1.61μm)

The total power on the detector (P_λ) is determined from the following equation:

$$P_\lambda = N_\lambda \, d\lambda \, \Omega \, A_p \, e_o$$

where
A_p = area of the primary mirror in cm²
N_λ = incident radiant energy in watts/cm² - μm — ster
$d\lambda$ = spectral bandwidth in μm
N_λ = 0.0028 watts/cm² - μ m - ster (2.12 μm)
N_λ = 0.0030 watts/cm² - μ m - ster (2.06 μm)
N_λ = 0.0076 watts/cm² - μ m - ster (1.61 μm)
$d\lambda$ = 0.032 μm (2.12) μm)
$d\lambda$ = 0.050 μm (2.06 μm)
$d\lambda$ = 0.072 μm (1.61 μm)
P_λ = 583 x 10⁻¹⁰ watts (2.12) μ m
P_λ = 972 x 10⁻¹⁰ watts (2.06 μm)
P_λ = 3560 x 10⁻¹⁰ watts (1.61 μm)

$$NE\Delta R = \frac{NEP}{P_\lambda}$$

4-26

NEΔR = 0.06% (2.12 μm)
NEΔR = 0.04% (2.06 μm)
NEΔR = 0.014% (1.61 μm)

The data rate will be approximately 0.64 megabits per second. This is based on five video channels, two samples per IFOV and digitizing to ten levels. Since the active video only occurs during 27.8% of the total scan cycle, the data can be buffered to reduce the data rate to about 0.22 megabits per second.

4.3.4 SUMMARY

The preliminary design (Sec. 4.3.3.4) of a Cloud Physics Radiometer for EOS is summarized in Table 4.3.1. Although a potential candidate for a SATS class spacecraft, the information return is greatly enhanced if the radiometer is flown in conjunction with the sea surface temperature imaging radiometer and the passive multichannel microwave radiometer.

Table 4.3-1

Cloud Physics Radiometer

Design Parameters		
IFOV, km	2.5	
Scan, deg	±51	
Swath, nm (km)	1550 (2870)	
Nodal crossing (LMT)	0900, 1200, 1500	
Revisit time, days	1	

Spectral Channels (Approx.)		
Wavelength, μm	Parameter	Measurement
(1) 0.754 ± 0.0025	Visible Window	Ice vs liquid clouds
(2) 0.763 ± 0.0025	O_2 absorption	Thickness of Cloud
(3) 1.61 ± 0.036	IR Window	Droplet size parameter
(4) 2.06 ± 0.025	CO_2 absorption	Density of condensed water
(5) 2.12 ± 0.016	IR Window	Cloud top pressure level

Sensor Characteristics		
Data rate, mb/s	0.22	
Power, watts	40	
Weight, lb (kg)	70 (32)	
Proj. Area, ft² (m²)	1.9 (0.17)	

4.3.5 REFERENCES

1   Hanel, R., J. Geophys. Res. 66, 1300, (1961).

2   Yamamoto, G. and D.Q. Wark, J. Geophys. Res., 66, 3596 (1961).

3   Chapman, R.M., Planet Space Sci., 9, 70, (1962).

4   Saiedy, F., D.T. Hilleary, and W.A. Morgan, Appl. Opt., 4, 495, (1965).

5   Saiedy, F., H. Jacobowitz, and D.Q. Wark, J. Atmos. Sci., 24, 63, (1967).

6   Wark, D.Q. "Indirect Measurements of Cloud-Top Altitudes" IUGG/WMO Symposium
     on Radiation, Berger, Norway 22-28 August, 1968, (Summaries published by WMO).

7   Irvine, W.M., and J.B. Pollack, Icarus, 8, 324, (1968).

8   Blau, H.H., Jr., and R.P. Espinola, Appl. Opt., 5, 555, (1966).

9   Espinola, R.P. and H.H. Blau, Jr., J. Geophys. Res., 70, 6263, (1965).

10   Hovis, W.A. Jr., and M. Tobin, Appl. Opt., 6, 1399, (1967).

11   Twomey, S., H. Jacobwitz, and H. Howell, J. Atmos. Sci., 23, 289, (1966).

12   Twomey, S., H. Jacobowitz, and H. Howell, J. Atmos. Sci., 24, 70, (1967).

13   Plass, G.N. and G.W. Kattawar, Appl. Opt., 7, 361, (1968).

14   Global Atmospheric Research Programme (GARP) Study Group, 1967: Report of a
     Study Conference held at Stockholm, Sweden, 28 June - 11 July 1967. Jointly organized
     by the ICSU/IUGG Committee on Atmospheric Sciences and COSPAR and co-sponsored by
     the World Meteorological Organization, 144 pp.

15   Wark, D.Q. and D.M. Mercer, Appl. Opt., 4, 839, (1965).

4.4 OCEANIC SCANNING SPECTROPHOTOMETER

4.4.1 INTRODUCTION

To a casual observer at the surface the ocean appears blue, although some will contend that the Pacific is green. Other colors, of course, often are noted visually, particularly the browns and greens, in the vicinity of many coastal areas. The more subtle variations in hue are emphasized when the observation level is increased to aircraft or orbital altitudes. Col. John Glenn, for example, on the first manned Mercury flight in 1961 reported seeing the Gulf Stream from the color contrast between the warm current and the adjacent shelf water. Large-scale ocean fronts also have been detected by optical sensors on geosynchronous satellites.

The color of the oceans is determined primarily by the reflective, absorptive, and scattering properties of the water as well as the atmosphere above. The ocean color variations are related to the biological, chemical, sediment, nutrient, and pollutant content of the water. Reflective properties of the water also vary with the dynamic motion of the surface, the presence of an ice canopy, and, in shoal areas, the composition of the bottom and depth of the water.

Accordingly, oceanographers consider ocean color and clarity measurements an important part of water mass analysis. Indications of these factors have been collected as a routine aspect of oceanographic observation. For this purpose a Forel scale was developed to standardize and facilitate reporting water color. The Forel scale includes eleven categories from blue to green. Determination of the color involves lowering a Secchi disc to one meter below the surface of the water and comparing the apparent color with one of the eleven samples which make up the scale.

Although many such observations have been taken over the past decades, relatively little is known concerning the distribution of sea color. In part, this lack of knowledge is attributable to the fact that color, particularly that related to biological activity, occurs in rather small patterns and varies at a relatively high rate so that the low sampling rate available to ships may be inadequate to observe changes. Lepley (1) who recently attempted to apply archival Secchi disc records to a world-wide analysis of water clarity and color found many deficiencies in the data and was required to make many assumptions in order to complete the study. In addition application of the Secchi disc and Forel scale is subjective in that it is necessary to visually match the colors and it is obviously difficult to maintain the disc at the required one meter depth at sea.

The appropriate sensor coupled with a satellite affords a vehicle for the coverage, repeatability, and synopticity required for meaningful application of ocean color to oceanographic problems.

Observation from a satellite, of course, is inherently directed toward observing only the upper 10-100 meters, or less than 1% of the total volume of the ocean. However, this limitation is not as severe as it appears. This surface portion of the ocean is where most of the biological activity occurs and where man's activities typically take place.

The upper layer is also the part of the oceans where most dynamic changes occur with the effects of the winds and storms, the major addition and loss of heat, the presence of sea ice, and the effects of tidal systems. This upper layer also supports photosynthesis upon which the entire biological resource of the sea depends. It is also the zone where man acts on the sea by activities such as dredging, fishing, and contamination with chemical pollutants. This zone is within the range of ocean color measurements.

4.4.2 TECHNICAL DISCUSSION

4.4.2.1 Atmospheric Effects. Viewing the ocean from orbit must also take into account the atmosphere. While a full treatment is beyond the scope of this discussion, some of the important areas are noted. The light energy "upwelled" from the ocean is derived from the sun and must, in effect, take a two-way trip through the air and water column before reaching a possible observa-

tion satellite. After solar energy reaches the top of the atmosphere it is transmitted directly downward through the atmosphere, scattered, absorbed and reflected both directly and diffusely from the surface. It enters the water where it is scattered and absorbed, and part of it returns to the surface and re-enters the atmosphere before it reaches the measuring instrument.

Of the two major factors affecting the transmission of visible solar energy through the atmosphere, absorption is probably the less significant although ozone, oxygen, and water vapor are important absorbers in certain wavelengths.

Scattering is the more important and complex consideration regarding the measurement of ocean color from orbital altitudes. Scattering tends to have the greatest influence on the blue portion of the visible spectrum or that below 0.50 micrometers. Without treating the subject exhaustively, in the presence of air masses with high visibility, pure, dry air where molecular (Rayleigh) scattering predominates, corrections are usually not complex.

The introduction of aerosol particles in the atmosphere, with their distributions of various sizes, results in spectral extinction that is difficult to deal with. Aerosol particles generally emanate from sources on land, so the problem may have particular significance near the coasts. It appears, however, that over the open ocean the aerosol to be found consists mainly of sea-salt particles with a relatively simple distribution. The distribution of the larger particles over the ocean is relatively small compared to land areas as shown by Junge [2] in the following table:

Table 4.4-1

Model Particle Concentrations per cm^3 in Surface Air

(after Junge, 1963)

Radius,	< 0.01	0.01-0.032	0.032-0.10	0.10-0.32	0.32-1.0	1.0-3.2	> 3.2	Total
Continent	1600	6800	5800	940	29	0.94	0.029	15,169
Ocean	3	83	105	14	2	0.47	0.29	207

The effect of the atmosphere on the blue portion of the spectrum and the importance of this portion to ocean color analysis indicates that viewing angles should be kept to a minimum to reduce the effects of atmospheric scattering.

Clouds, of course, are an atmospheric phenomena which will have a significant effect on our ability to make ocean color measurements in that they usually completely obscure the surface to optical sensors. Accordingly, account must be made on the distribution of clouds over the ocean when determining the ocean color sampling techniques to be employed.

4.4.2.2 Ocean Effects. Light irradiating the sea surface undergoes reflection and refraction. The reflected portion is polarized so that the component parallel to the sea surface predominates in the reflected light and, at Brewster's angle, is virtually the only component present. This can be made use of to select either the reflected skylight or the backscattered sunlight upwelling through the water surface, depending on whether the desired information relates to the shape of the reflecting surface or to the optical properties of the bulk water. The refracted portion penetrates the sea and, in the absence of scattering, is eventually extinguished by absorption. In reality, the light is scattered by particles of all sizes, from molecules through the larger colloidal particles and up to large bubbles or, in shallow water, by the bottom. On the high seas, about 5% of the incident light is backscattered upward toward the sky. This is about equal to the skylight reflected at near-incident angles and several fold larger than the fraction of reflected light passing through a suitably oriented polarizing filter.

The backscattered light so recovered, having been subjected to absorption and spectral scattering along a path length that varies with the distribution of scatterers in the sea, is markedly different in color from the incident "white" light. In clearest ocean water, the effective path length is quite long and the upward scattered light is strongly blue, with a dominant wavelength of about 0.45 micrometers.

In coastal regions the water may contain many colored absorbers, both inside the bodies of transparent plankters, and as solutes of tannins, chromatins, carotenoids, chlorophyll, and many other "foreign" compounds. In addition, suspended particles of very fine mud scatter the light selectively and add to its color. As a result, the transparency of the water is much decreased, and the dominant wavelength shifts from the blue into the green portion of the spectrum.

The distinctive color of water is a familiar observation and leads to such names as the Black Sea, the Red Sea, the White Sea, the Azure Sea, and the Vermillion Sea. Although water color was used by the earliest navigators to locate familiar water masses and associated current systems, modern navigators depend on more "scientific" (i.e., less natural) methods. For the most part, oceanographers rely on the temperature and salinity of the water and more particularly on their correlation to identify water masses of different origin. Water color itself is used as a measure of biological activity both past and present.

In remote sensor reconnaissance of the ocean, temperature is the only parameter that currently serves as a discriminant of water masses. Thus it is easy to distinguish the Gulf Stream water from the adjacent slope water by its temperature contrast. But for more subtle differences, this will hardly suffice. Surface temperature is quickly altered by air temperature and by radiation, so that water masses having very different histories can have identical temperatures. As an alternative to the correlation of temperature and salinity, it is suggested that the correlation of temperature and color might serve to distinguish different water masses.

Ewing(3) shows an example of the spectral variation of the backscattered light from the ocean measured at a flight altitude of 500 ft. This is shown in Figure 4.4-1. To emphasize chromaticity as distinct from brightness, the spectra are presented in terms of their normalized trichromatic coefficients. (As usual, the blue coordinate is omitted.) The color of the ocean water is shown by its relation to the light reflected from a neutral gray card. The displacement of the color toward the green and yellow relative to the clear ocean water is also shown. The figure also shows the sites over which the spectra were obtained.

The spatial and temporal variations in ocean color are frequently very subtle. In order to adequately assess the bulk chemical and biological properties which are related to these color variations, it is necessary to discriminate these subtle differences. The range of variation of interest to oceanographers is indicated by the Forel scale which, as stated previously, has eleven color categories from blue to green. The expanded Forel-Ule scale which adds yellow and brown colors has twenty-two categories.

It is evident therefore that the sensor to measure ocean color must have high spectral resolution and measure over the entire visible range from about .4 to .7 micrometers. The exact number of channels or the band width of the channels for the measuring instrument has not been determined experimentally, but it has been suggested that spectral resolutions of from 0.01 to 0.02 micrometers are required and are consistent with the existing body of ship-based ocean color measurements. Some preliminary examples for the requirement are the significant data on ocean properties which are bound in narrow spectral regions, such as the strong absorption band of chlorophyll in ocean water, and the greater differentiation and detail in densities evident in identifying coastal effluents.
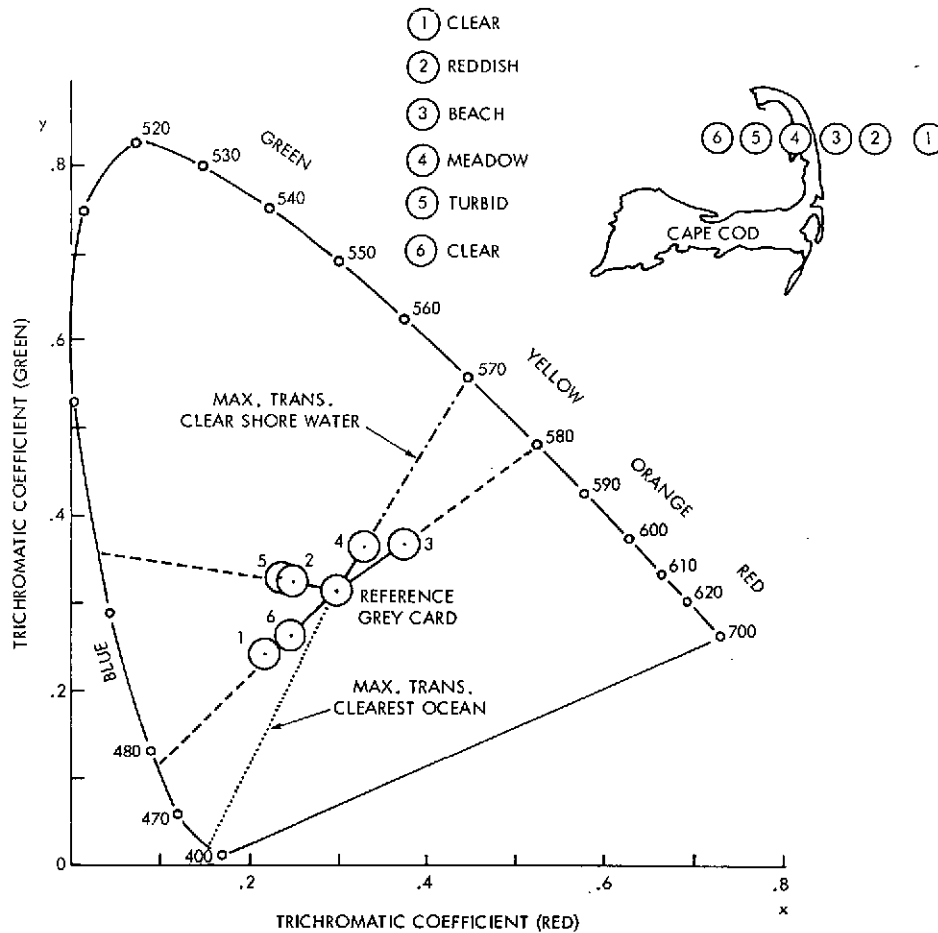
Figure 4.4-1. Chromaticity Diagram

Figure 4.4-2 (after Ewing [3]) shows a plot of data obtained by a water color spectrometer on low level aircraft flights off the coast of Southern California. This instrument, with a spectral resolution of .01 micrometers, shows features which could not be detected with an instrument of grosser resolution, i.e., the .515 micrometer absorption region on the algae curve. The high spectral resolution also shows detail which is important until research on use of water color spectrometer data reaches the point where it is known what data can be discarded as redundant or unimportant to water mass analysis.

Additional flight test to be conducted in the near future may furnish some quantitative data on the problem of selecting the optimum spectral resolution and required number of channels. During late July and August 1971, Goddard and Ames, in conjunction with SPOC and Scripps Institution of Oceanography will fly a filter wedge spectrometer designed by Dr. Warren Hovis of Goddard. The objective of the test is to obtain high altitude (50,000 feet) data at narrow spectral resolution (λ /$\Delta\lambda$) of about 100) over a spectral range of 0.4 to 2.4 micrometers. The data thus obtained will be correlated with surface measurements.

In addition, the Manned Spacecraft Center (MSC) expects to commence aircraft flight tests over the oceans of a Scanning Imaging Spectrometer (SIS) in late 1971. This instrument will have a range of 0.4 to 0.85 micrometers and a spectral resolution of .01 micrometers.
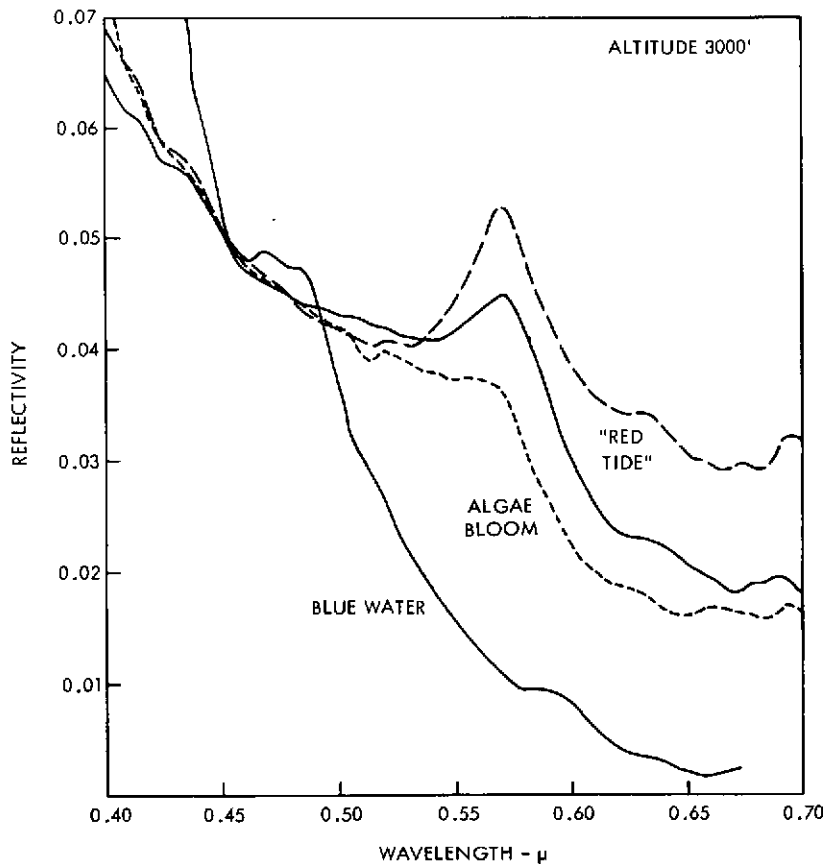
Figure 4.4-2. Spectral Reflectivity of Different Areas of Sea Water

4.4.2.3 Chlorophyll. The penetration of solar energy into the sea is fundamental to the eco-system since it controls the growth of primary plant producers and accordingly the behavior pattern of many marine animals. As stated previously the materials in the water result in differential scattering and absorption and alter the spectral composition of the light. Since chlorophyll affects the spectrum in a characteristic manner and since it is indicative of living matter, spectral measurements can be used as an index of the amount and distribution of phytoplankton.

High phytoplankton regions can support large populations of herbivores and onto successive links in the food chain to those which are of economic importance. Therefore, repeated mapping of chlorophyll on a world-wide scale could detect potentially productive areas and monitor relevant changes within those areas.

Nutrients which are added to the water generally sink below the surface. This fertilizer when brought to the upper layers in which light or solar energy penetrates coupled with other favorable factors results in blooms of phytoplankton or a growth of small plant life. The growth cycle lasts about 20 days. These nutrients are brought to the surface when conditions are favorable to drive away surface waters in areas (coastal) where replacement water must rise from the lower levels.

This upwelling condition can be intermittent and temporary depending on the character of the surface wind. Certain regions are identified where persistent surface winds and coastal configurations are such that large regions of upwelling are common and fairly large. These are shown in Figure 4.4-3. Even within these zones, however, conditions vary daily and seasonally, and the important plankton "blooms" depend on the nutrient source.

4-33
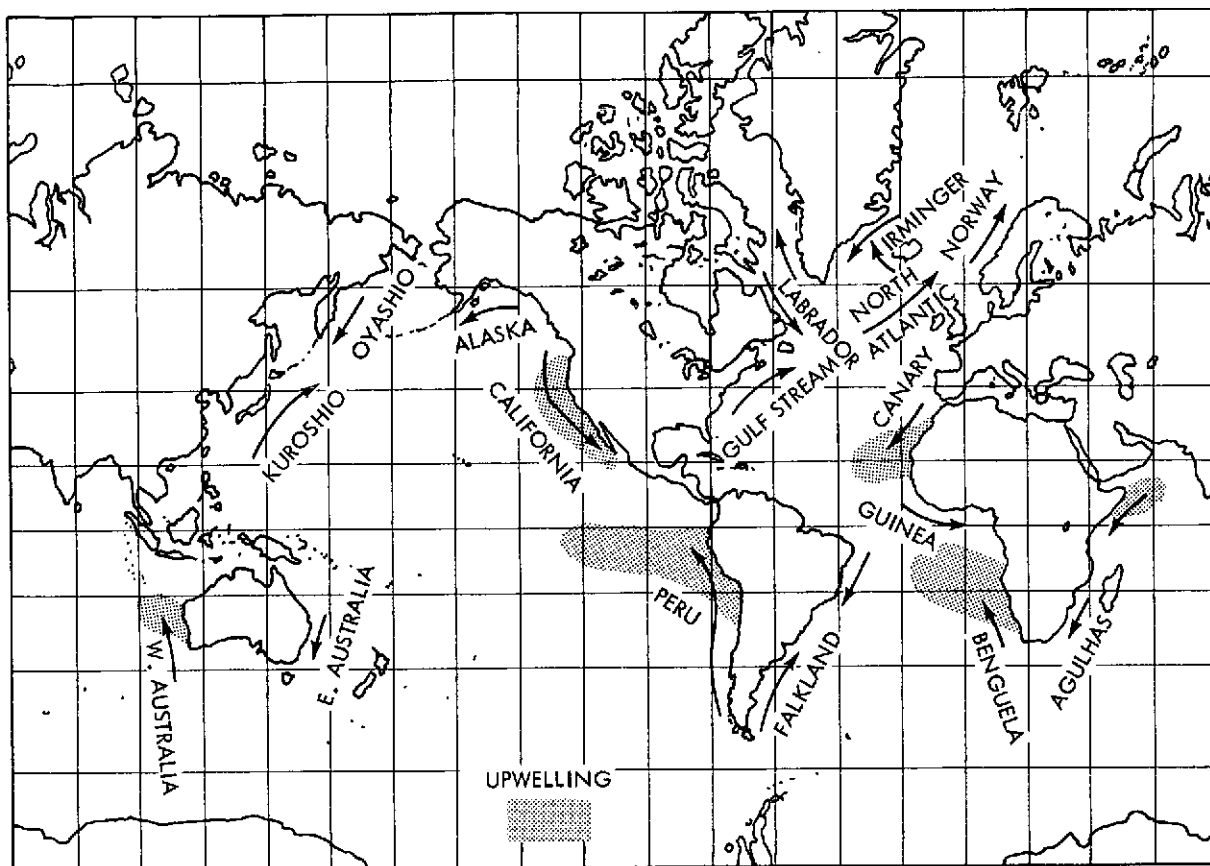
Figure 4.4-3. Major Ocean Surface Currents and Areas of Upwelling

Sun glitter occurs as result of a direct reflection of the sun from the ocean surface. While it is desirable to have a high sun angle, particularly to permit the maximum amount of energy into the sea and to provide time for "burn-off" of atmospheric haze, the closer to midday a visible region sensor is operated, the more likely a glitter pattern will occur in the field-of-view of the instrument, thus obliterating information about the bulk water properties. The preferred time to avoid haze and glitter might appear to be in the midafternoon, but in many regions there can be a convective build-up in the afternoon which may negate this advantage. It appears, all considered, that the preferred time would be some time before noon, or before the sun is at an angle which would significantly cause glitter to obscure color data.

Analyses of ocean color are best made with calm sea conditions, again to avoid glitter that might be reflected from waves, but also to minimize the amount of white water/foam that might be present. Such foam is generated by both breaking waves and wind and can be dealt with on a statistical basis, if necessary, by averaging observations over time. However, individual short samples of spectrometer type data should be avoided, or samples collected over relatively large spatial regions.

The development of remote sensors to study chlorophyll in the ocean takes on a different character than the sensors developed for chlorophyll measurement from plant material growing over terrain. Plants typically exhibit a high reflectance in the near infrared region (at wavelengths just beyond $0.7 \mu m$) where the influence of the absorption bands of chlorophyll, located in the visible part of the spectrum, rapidly decreases. Hence, healthy plants containing chlorophyll show a brilliant red in color infrared photography. The same technique when applied to chlorophyll in the ocean will detect surface chlorophyll and only the surface chlorophyll (the upper meter or so). The

detection of kelp beds and surface algae is an application of color infrared for the ocean areas. However, ocean plants more typically grow in the vertical column of water where photosynthesis occurs at depths on the order of tens of meters. There red light energy is readily absorbed by water and cannot be observed from these depths.

Chlorophyll has a strong absorption band in the blue region centered at about 0.44 micrometers and is about 0.04 micrometers wide. (There also appears to be a slight increase in the relative reflectance associated with chlorophyll as will be shown later.) It is this absorption by chlorophyll that is being utilized to develop an ocean color system to measure ocean plant crops.

Figure 4.4-4 shows the manner in which the percent of incident light changes as a function of chlorophyll concentration in the water and the wavelength of measurement. These data were acquired from an airborne spectrometer at about 325 meters altitude with an 0.005 micrometer spectral resolution and scanned in four seconds time from 0.40 to 0.65 micrometers. The very low chlorophyll concentration is typical of very sterile water (like the Sargasso Sea) where chlorophyll is less than 0.1 mg/m^3, the low chlorophyll condition is typical of coastal slope type water and is on the order of 0.3 mg/m^3 and the high chlorophyll concentration is undefined but less than about 3 mg/m^3. It can be seen that as chlorophyll concentration increases the water will tend to be less blue and more green. It is anticipated that an imaging ocean color spectrometer system will be capable of measuring chlorophyll on a quantitative basis with a logarithmetic scale. (i.e., 0.3, 0.3 to 0.6, 0.6 to 1.2, 1.2 to 2.4 mg/m^3 etc.) over the interval from about 0.3 to 10 mg/m^3, the region of most interest for chlorophyll measurement.

Clarke(4) et al. have made some spectral measurements over water with high chlorophyll content (about 3 mg/m^3, Georges Shoals), with low chlorophyll content (about 0.3 mg/m^3, north of the Gulf Stream) and with very low chlorophyll content (less than 0.1 mg/m^3, Sargasso Sea.) The data are shown in Figure 4.4-5. The values for the backscattered light from these areas have been calculated as percentages of the incident light. The curves display characteristic differences in shape. For the high chlorophyll water the backscattered light rose from values mostly about 2.2% of the incident light in the blue region of the spectrum, to about 2.5% in the green, and then dropped to about 0.3% in the red. For the low chlorophyll water the values were higher in the blue, dropped rapidly to much lower values in the green, and continued to drop in the red. For the very low chlorophyll water the backscattering was higher at all wavelengths shorter than 0.50 micrometers, reaching a maximum of 7% at 0.40 micrometers.

There are other factors which must be considered and assessed in measuring ocean color. These are in particular sun glitter and foam/white water.

4.4.2.4 Shoals. Within certain limits of water clarity and depth (about 20-30 meters) the effects of light reflected from the bottom can be used to estimate water depth. In the so called "optically deep" water, the only portion of the light that leaves the water is that component which has been scattered upward. The other components are absorbed. If the water is not "optically deep" and the light entering the water is reflected by a "bottom", then this light will be redirected upward and add to the emerging upward scattered light. The amount of emerging light is dependent upon the "optical thickness" of the water layer. If the assumption is made that the water layer is homogeneous and the bottom surface reflection is not spectrally dependent, then the spectral intensities of the emergent light can be compared and the optical depth of the water layer determined. In this technique one band is selected near the maximum transparency of sea water, i.e., 450-600 micrometers and the second band above or below this band.

4.4.3 SENSOR CHARACTERISTICS

4.4.3.1 Technical Description. The design of an instrument for characterizing ocean color with scanning mirror technology is based on the following parameters:

- Spacecraft altitude - 1000 km.

4-35

- Instantaneous field of view (IFOV) of the instrument - 2 km x 2 km.

- Ground velocity of the spacecraft - 6.36 km/sec.

- Twenty spectral bands of 0.015 μm bandwidth over the 0.4 to 0.7 μm spectral region.

- Scan angle - 38 degrees (±19 degrees from nadir).

- Width of swath on the ground - 400 n. miles (740 km)
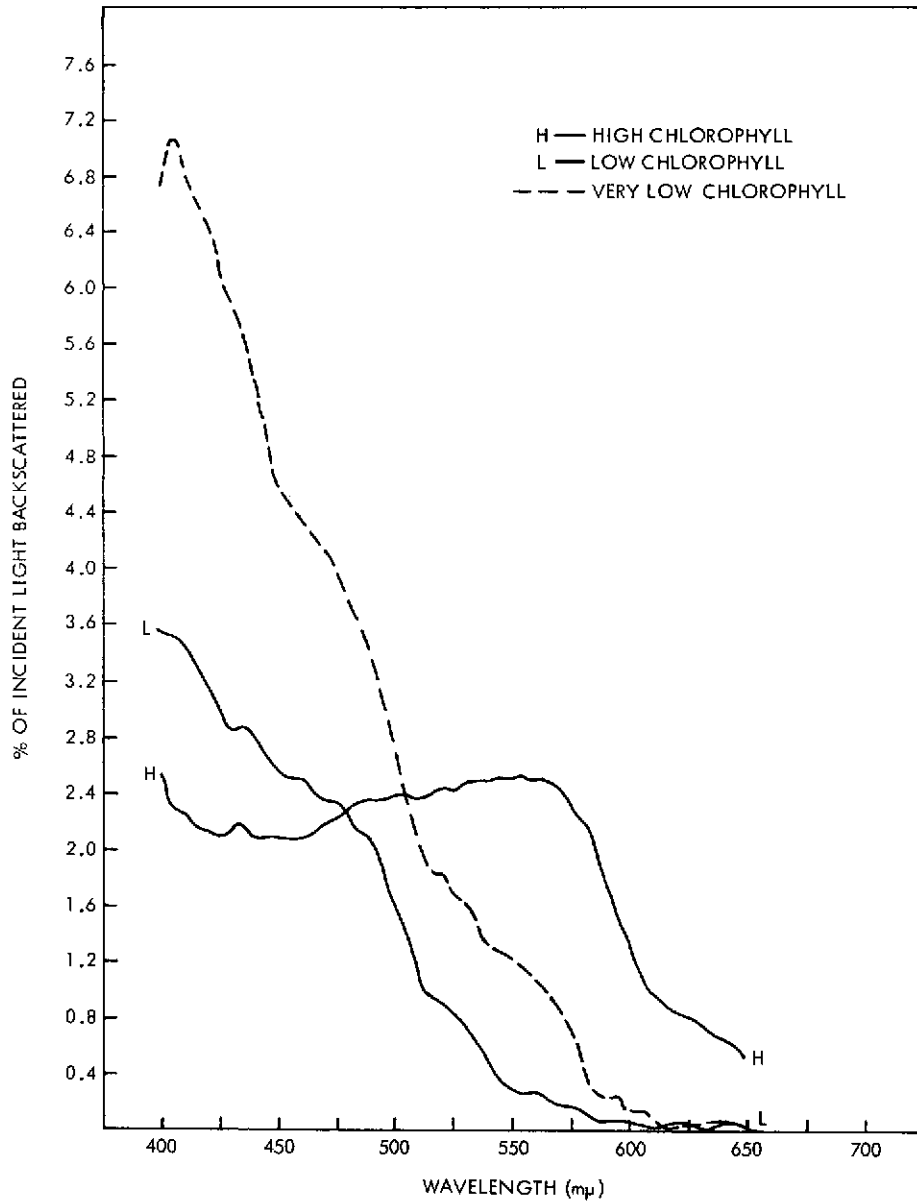
Figure 4.4-4. Percent of Incident Light Backscattered vs Wavelength as a Function of Chlorophyll Concentration in the Ocean
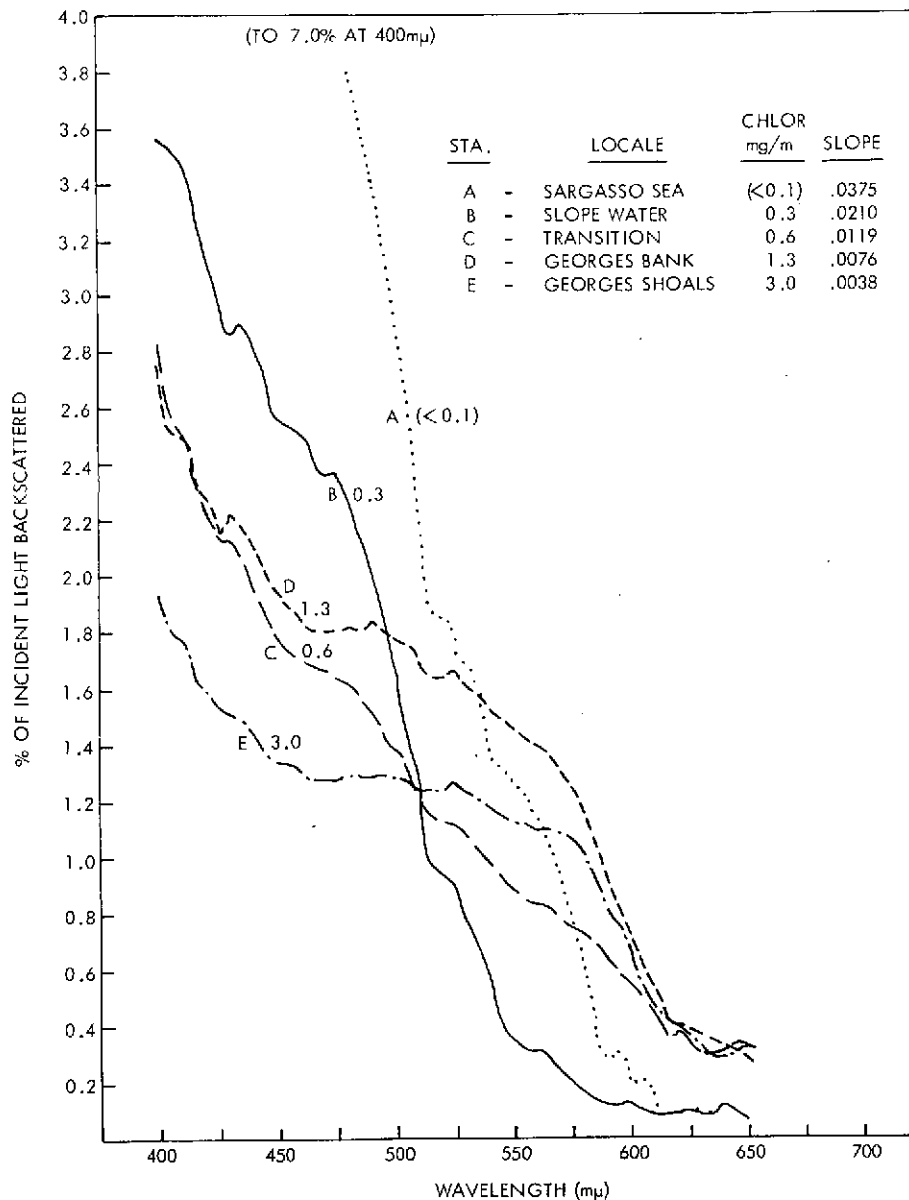
Figure 4.4-5. Percent of Incident Light Backscattered vs Wavelength as a Function of Chlorophyll Concentration in the Ocean

Scanning will be accomplished with a four-sided mirror. Four scans of the earth's surface will be made for each 360 degree rotation of the scan mirror assembly. Since one scan is required every 0.314 seconds (3.18 scans/second) to provide continuous coverage from scan to scan, the scan mirror assembly will have to rotate at one revolution every 1.26 seconds. The scan efficiency will be 0.278. The scanning is accomplished external to the imaging optics which means that the system is used on axis and a simple, all-reflective telescope will be satisfactory. The size of the primary mirror has been calculated for spectral bands centered at 0.54 μm and 0.46 μm. A mirror 7.6 cm in diameter is sufficient to provide a signal-to-noise ratio of 1 with a 0.1 percent scene reflectance at 0.46 μm. The same performance can be obtained with a 6.0 cm mirror at

0. 54 μm. If we assume that the larger mirror is used, we can obtain signal-to-noise ratios slightly higher than 1 at wavelengths longer than 0.46 μm and slightly less than 1 at wavelengths shorter than 0. 46 μm.

With a 12-inch focal length the field stop will be 0. 024 inch square to give the required IFOV of 2 km x 2 km. The input energy will be broken down into the required spectral bands by means of a grating. A collimating lens will be required in front of the grating and a re-imaging lens in back of the grating. A photomultiplier tube will be used to detect the signal in each spectral band. Fiber optics will be required to relay the energy from the focal plane of the re-imaging lens to the PMT's.

The estimated power required is 60 watts; the estimated weight is 45 pounds. These figures are for the scanner and do not include estimates for multiplexing and signal processing.

The active portion of the video will occur during 27.8 percent of the scan period. After sampling at a rate to provide two samples for each IFOV and digitizing to eight levels, the video rate will be approximately 1.6 megabits per second. With buffering in the information processing system, the data rate averages out to about 0.45 megabits/second. In addition to the active video, calibration will be required once each scan. This can be accomplished with a shutter and lamp arrangement similar to the internal calibration arrangement used with the MSS scanner for ERTS. A scan monitor system will also be required to provide a sync signal for reconstructing the data on the ground and for providing a start and stop for the video. Again, a technique similar to the one used on the MSS scanner should be satisfactory. The actual design of the scan monitor can be simplified considerably because the precision required for this instrument is significantly less than for the MSS.

4.4.3.2 Sensor Design. The size of the primary aperture was calculated for a change in surface reflectance of 0. 1 percent for 0.46 μm and 0.54 μm spectral bands. The signal-to-noise (peak signal to RSS noise) ratio in a PMT is

$$S/N = \frac{i_s}{\sqrt{4e\,i_t\,\Delta f}}$$

where e is the charge on an election and Δf is the noise bandwidth of the system. This equation is the basis for calculating the size of the primary aperture.

The signal (i_s) is considered to the the cathode current of the PMT generaged by the radiant power from the earth due to a change in surface reflectance of 0. 1 percent. The primary noise in the system is shot noise which is based on the cathode current resulting from the total radiant power from both the earth's surface and the atmospheric albedo (i_t).

$$i_s = SN_{\lambda s}\,\Omega A\,e_0$$

$$i_t = SN_{\lambda t}\,\Omega A\,e_0$$

where

S = responsivity of the PMT in amps/watt

$N_{\lambda s}$ = spectral radiance of the earth due to a change in reflectance of 0. 1 percent as seen from the satellite in watts/cm^2 ster.

$N_{\lambda t}$ = total spectral radiance as seen from the satellite.

Ω = solid angle subtended by the IFOV of the instrument in steradians.

A = area of the aperture of the primary mirror in cm^2.

e_0 = optical efficiency of the instrument.

Substituting for i_s and i_t in equation (1) and assuming that we can detect a signal with a S/N = 1 we can calculate the area of the primary aperture required:

$$A = \frac{4e N_{\lambda t} \Delta f}{S (N_{\lambda s})^2 \Omega e_0}$$

Using the following values:

e = 1.6 x 10^{-19} coulombs

$N_{\lambda t}$ = 1.49 x 10^{-4} watts/cm^2 ster (0.46 μm band)

Δf = 4.6 x 10^3 Hz

S = 125 x 10^{-3} amp/watt (0.46 μm band)

$N_{\lambda s}$ = 3.58 x 10^{-7} watts/cm^2 ster (0.46 μm band)

Ω = 4 x 10^{-6} steradians

e_0 = 0.2

we get a required area for the primary aperture of 34 cm^2. Allowing for an obscuration of 40 percent for the secondary mirror, this would require a primary 7.6 cm in diameter for the 0.46 μm band.

A similar calculation for the 0.54 μm band and using the following values:

$N_{\lambda t}$ = 9.66 x 10^{-5} watts/cm^2 ster

S = 95 x 10^{-3} amps/watt

$n_{\lambda s}$ = 3.9 x 10^{-7} watts/cm^2 ster

gives an area for the primary aperture of 25 cm^2 and a diameter of 6.0 cm.

$N_{\lambda s}$ is calculated by determining the total incident solar radiation over a 150 A band centered at the spectral band of interest. This is multiplied by cos 37 degrees and further reduced by the expected atmospheric losses. Since we are required to detect a surface reflectance as low as 0.1 percent, the total radiance of the surface (as seen from the satellite and assuming 100 percent surface reflectance) is multiplied by 0.001 and get the expected $N_{\lambda s}$.

The following parameters were used in the calculations:

Atmospheric, albedo

0.46 μm - 17 percent

0.54 μm - 13 percent

Scene reflectance

0.46 μm - 4.2 percent

0.54 μm - 2.2 percent

Extinction coefficient for air mass 1.

$$0.46 \mu m - 0.35$$

$$0.54 \mu m - 0.25$$

Based on these values for extinction coefficients, the atmospheric transmission for any air mass can be calculated from the following:

$$T = e^{-\tau m}$$

where T = atmospheric transmission

τ = extinction coefficient

m = air mass = sec θ where θ equals the solar zenith angle

We then have (for two passes through the atmosphere) a total air mass of 2.25 for a zenith angle of 37 degrees and the transmission for 0.46 μ m is 45.4 percent and for 0.54 μ m is 57.2 percent.

From the Engineering Standard for the Solar Constant, the solar spectral irradiance averaged over a small bandwidth centered at 0.46 μ m is 0.2066 watts/cm^2 - μ.

$$\frac{0.2066}{\pi} \cos 37 \text{ degrees } (0.015) = 7.9 \times 10^{-4} \text{ watts/cm}^2 \text{ ster}$$

Transmission from outside the atmosphere to the surface (air mass 1.25) and from the surface to the satellite (air mass 1) is 45.4 percent. The scene radiance as seen from the satellite for a reflectance change of 0.1 percent is then:

$$N_{\lambda s} = 7.9 \times 10^{-4} (.454) (.001) = 3.58 \times 10^{-7} \text{ watts/cm}^2 \text{ ster}$$

$N_{\lambda t}$ is made up of two components. The first is the atmospheric albedo and the second is the total reflected radiance of the surface as seen from the satellite.

$$N_\lambda \text{ albedo} = 7.9 \times 10^{-4} (.17) = 1.34 \times 10^{-4} \text{ watts/cm}^2 \text{ ster}$$

$$N_\lambda \text{ surface} = 7.9 \times 10^{-4} (.454) (.042) = 0.15 \times 10^{-4} \text{ watts/cm}^2 \text{ ster}$$

$$N_{\lambda t} = 1.34 \times 0.15 = 1.49 \times 10^{-4} \text{ watts/cm}^2 \text{ ster}$$

From the Engineering Standard for the Solar Constant the solar spectral irradiance averaged over a small bandwidth centered at 0.54 μ m is 0.1783 watts/cm$^2\mu$. Using appropriate values for albedo, surface reflection and atmospheric transmission the following radiance values are found for the 0.54 μ m band:

$$N_{\lambda s} = 3.9 \times 10^{-7} \text{ watts/cm}^2 \text{ ster}$$

$$N_{\lambda t} = 9.66 \times 10^{-5} \text{ watts/cm}^2 \text{ ster}$$

The noise bandwidth is determined from the following:

$$\Delta f = \frac{\alpha R K}{\Omega^{1/2} e_s 2}$$

where α = scan angle in radians = 0.873

R = scan rate in scans/second = 3.2

e_s = scan efficiency = 0.278

$\Omega^{\frac{1}{2}}$ = 0.002

K = factor to account for the filter passband and amplifier noise = 1.82

Δf = 4.6 x 10^3 Hz

4.4.4 SUMMARY

A preliminary design of an ocean color spectrophotometer is summarized in Table 4.4.2. The design develops the principal requirements on optics size and detector characteristics to achieve

Table 4.4-2

Oceanic Scanning Spectrophotometer

Design Parameters	
IFOV, km	2
Scan, deg	±19
Swath, nm (km)	400 (740)
Nodal crossing, LMT	0900, 1500
Revisit time, days	4
Spectral range (approx.)	
0.4 - 0.7 μm	Visible band
$\Delta\lambda$ = 0.015 μm	
No. of channels	To be determined
Sensor Characteristics	
Data rate, Mb/s	0.5
Power, watts	60 (25 average)
Weight, lb (kg)	45 (20)
Proj. Area, ft^2 (m^2)	3.7 (0.34)

the sensitivity required for measurement of the subtle changes of color of the sea. The number of channels into which the visible band (0.4 to 0.7μm) is divided is left open pending completion of a field investigation to be performed by GSFC in cooperation with SPOC, NOAA, and the Scripps Institution of Oceanography during the summer and fall of 1971. In general, it is considered that the number of channels required is not less than five (5) nor more than twenty (20).

The ocean color spectrophotometer is small enough to be considered for a SATS-class spacecraft, but for best interpretation of ocean color data in terms of ocean currents and nutrition, correlative data on sea surface temperature are required.

4.4.5 REFERENCES

1   Lepley, L. K., "Coastal Water Clarity from Space Photographs," Photogrammetric Engineering, Vol. 34, No. 7, July 1968.

2   Junge, C. E., 1963, "Air Chemistry and Radioactivity," New York, Academic Press.

3.   Ewing, G. C., The Color of the Ocean, Report of Conference, 5-6 Aug 1969, Woods Hole Oceanographic Institution, Cambridge, Mass.

4   Clarke, G. L., Ewing, G. C., Lorenzen, C. J., "Spectra of Backscattered Light from the Sea Obtained from Aircraft as a Measure of Chlorophyll Concentration," Science, Vol. 167, No. 3921, February 1970.

4.5 THEMATIC MAPPER

4.5.1 INTRODUCTION

The crop reporting and land-use system that has been developed by United States farmers and the Department of Agriculture has contributed to making the business of agriculture in the United States the most efficiently operated of its kind in the world. This system has been of value to the Government in establishing agricultural policy, and to individual farmers in the conduct of daily business. As the world enters a period of increasing population and potential food shortages, the necessity of applying new technology for the improvement of such information systems, in the United States and worldwide, becomes apparent.

As the world's population continues to grow, there is an accelerating shift to dense urban concentrations; man's urban, rural, and wildland environments deteriorate; and critical questions arise about the world's capacity to provide and distribute food.

Urbanization as a process in the United States, as well as in developing countries, is little understood; and its spread is so rapid that information available to local, state, and Federal Governments is neither accurate nor timely enough for effective management and planning.

Maps and statistical summaries and analyses are published two to ten years after data are collected. Small scale maps are neither uniform nor current.

Information that requires up-dating at frequent intervals (e. g. , snow-pack changes for predicting water yield, seasonal crop-condition reports, surveys of natural and man-made disasters, transportation studies, and urban-area changes) still, for the most part, has to be gathered by on-the-spot surveys by some combination of air photography and ground visits. These conventional methods are too costly for repeated coverage, and the information thus obtained cannot be analyzed in time for user applications.

Hydrology is concerned with the entire water cycle. Applied hydrology concerns all practical uses of terrestrial waters, notably for industrial, agricultural, and domestic purposes. Present engineering hydrology know-how could mitigate man's water problems almost anywhere, but at a prohibitive cost. The current level of understanding is considered to be grossly inadequate to meet many present and future complex problems of water planning and development in this country and throughout the world. For example, the number of lakes (greater than 200 km^2 surface area), the amounts of perennial or annual snow, world precipitation, evaporation, soil moisture, and other hydrologic components are not known with confidence.

For many years geologists have made use of aerial photography in their search for oil and minerals, and have become expert in its use. Space imagery is new and will first become available in a systematic way to geologists from ERTS-A in 1972. However, some Nimbus and Gemini photographs have been interpreted by geologists, and have indicated some very promising possibilities. In spite of less than optimum conditions of solar illumination, certain types of lineament structures on the earth often associated with mineralization could be identified. Much still remains to be done in relating remote sensing to classical geologic practice. Geology has many remote-sensing requirements in common with cartography, agriculture, and hydrology, although in general it needs lower-angle illumination to reveal geologic features in relief than in the case of the other disciplines.

The finite size of the world and the realization that if we are to maintain our environment indefinitely we must wisely manage our food, water, air, and other natural resource systems has become dramatically and starkly apparent. To accomplish this management requires near real-time knowledge of man's interaction with many of these factors. Satellites offer a broad coverage capability and a new perspective from which to make observations to aid in making resource management decisions. More intensive research in instrumentation and the

development of better sensors are needed to make greater use of satellites in collecting data for Earth Surveys. Development and improvement of multispectral imaging instruments is a basic requirement for the Earth Resources Program to detect a broad variety of earth spectral signatures. For many of the applications, a ground resolution of 200 feet or less is needed, which requires the sensor to have very fine angular resolution. One of the most challenging problems is the simultaneous attainment of very high resolution, good signal-to-noise ratio (S/N), and reasonably broad ground coverage for each of the well registered bands of interest.

Investigations of the spectral signatures and features associated with surface features of interest to the earth resource community are being conducted at various facilities. This work has shown that spectral reflectance and emittance observations provide a means of identification of minerals, crop and soil types, moisture stress in plants, vigor in vegetation and soil moisture conditions as well as a means of classification of land use.[1] The usefulness of measurements taken in the thermal bands for analysis of geologic features has long been established.[2]

4.5.2 SCIENTIFIC DISCUSSION

The identification of commodities of interest to the earth resources community by spectral analysis is possible because of the energy phenomena associated with the atomic and molecular structure of various species of plant life. These phenomena may be broadly defined by the following spectral regions: [3]

Visible	0.3 - 0.7 microns	Electronic transitions (atomic)
Near IR	0.7 - 1.3 microns	Photochemical reactions
	1.3 - 2.5 microns	Overtones of molecular vibration
IR	2.5 - 25 microns	Fundamental molecular vibration
	6.7 - 15 microns	Profile characterisitcs

A typical spectrometer plot of vegetation is shown in Figure 4.5-1.(4) Figure 4.5-2 illustrates the variance of this spectrum among five types of crops.

Seven bands have been suggested to provide the spectral information for agricultural commodities. (5) The instrument proposed employs these suggested bands as shown below.

Band Number	Wavelength (Micrometers)	Feature
1	.5 - .6	Green peak
2	.6 - .7	Chlorophyl absorption
3	.7 - .8	IR reflectance rise
4	.8 - 1.1	IR reflectance shoulder
5	1.55 - 1.75	Soil and Plant Particle size
6	2.08 - 2.35	Soil and plant water content
7	10.4 - 12.6	Radiance Temperature

These bands are also useful in the other areas previously mentioned.

The Multispectral Scanner (MSS) presently being built for ERTS A & B is a first step in the attempt to detect, locate, identify, map and measure Earth Resource phenomena from orbital altitudes. The Thematic Mapper for EOS has three main advantages over the MSS.

• Higher S/N for the same ground resolution (convertible to better spatial resolution for the same S/N).

• Additional spectral information (two bands between 1.55 - 2.35 micrometers).
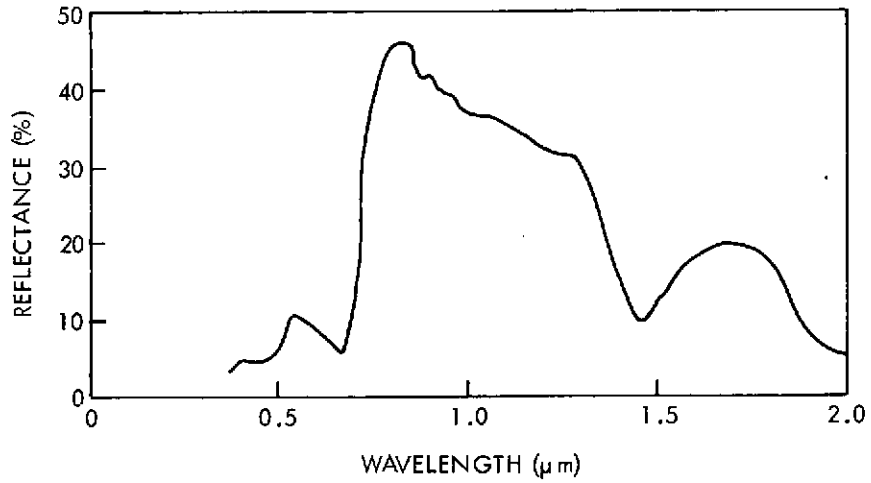
• Offset pointing capability.

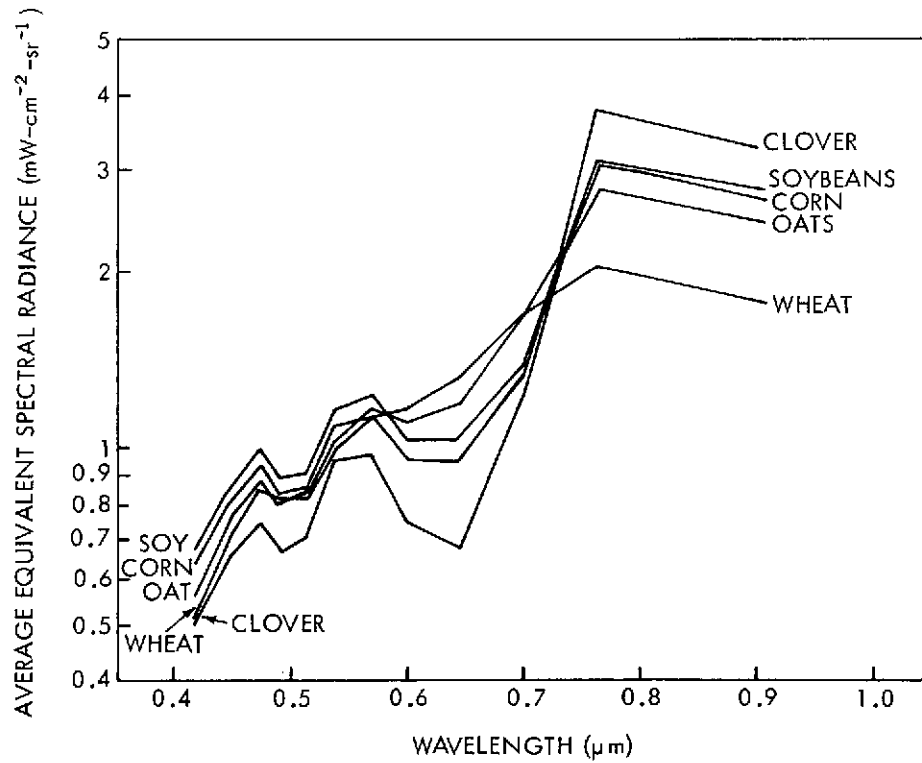Figure 4.5-1. Typical Spectral Response of Vegetation

Figure 4.5-2. Combined Signatures for Five Crops

Orbit contiguity such as is presently required for ERTS A & B will not necessarily be needed for many applications. Some experiments may require covering the same area instead of adjacent areas on consecutive days. This can be accomplished by the proposed offset pointing capability. The number of useful consecutive days of coverage, using offset pointing, depends primarily on the atmospheric effects of the "slant path" radiation. Three or four consecutive days per week should be practical for some applications. Another advantage of offset pointing is the ability, on command, to avoid clouded areas in favor of known clear areas within useful reach of the instrument.

The Thematic Mapper proposed for EOS is larger and heavier than the MSS. In order to achieve higher S/N and somewhat higher angular resolution, a 16-inch diameter telescope is employed. A primary task is to accommodate this large telescope with the necessary scanning mechanism. Also, three of the bands use detector arrays that require cooling. This will be accomplished by means of a radiant cooler capable of maintaining the two different types of detectors at their proper operating temperatures. Such a radiative cooler is presently under development.

4.5.3 INSTRUMENTATION

4.5.3.1 General Description. The Thematic Mapper is a line scan device that mechanically scans in a direction normal to the satellite velocity vector, assuming that the spacecraft is 3-axis stabilized. At an altitude of 1000 km the swath width is 185 km and the limiting ground resolution is approximately 33 m for the first six bands and 100 m for the seventh band. Such a swath is compatible with the film processing and data analysis equipment available in NASA and other earth observation data user agencies. The instantaneous field-of-view (IFOV) of each of the first six bands is 66 microradians and for the seventh band the IFOV is 200 microradians.

Four different types of detectors will be used to cover the seven spectral regions. They are shown in Table 4.5-1 together with their nominal operating temperature. Improved detectors for bands 5 and 6 that can operate at 240 K are presently under development.

Table 4.5-1

Spectral Bands, Detectors and Operating Temperatures

Band Number	Wavelength (Micrometers)	Detector Type	Operating Temp (K)
1	0.5 - 0.6	PMT	290
2	0.6 - 0.7	PMT	290
3	0.7 - 0.8	PMT	290
4	0.8 - 1.1	Si	290
5	1.55 - 1.75	InAs	120
6	2.08 - 2.35	InAs	120
7	10.4 - 12.6	HgCdTe	90

The detectors for the last three bands shown in Table 4.5-1 will be maintained at their proper operating temperatures by means of a radiant cooler. Such a dual temperature cooler is presently being developed by GSFC under contract with ITT. The dual patch temperatures under development will be approximately 90K and 120K for a base temperature of 300K and will be capable of maintaining a four element HgCdTe array on the 90K patch and two 7-element InAs arrays on the 120K patch. The cooler is being designed to operate at altitudes as low as 450 nautical miles. This Multi-Element Radiant Cooler task started during 1970 and a model of the cooler will be tested and delivered in 1971. [6]

Table 4.5-2 summarizes the anticipated performance of the instrument for an altitude of 1000km and a swath width of 185km. Such an instrument would have an average data rate of approximately 30 mb/s, a rate which is consistent with current S-band frequency assignments. It may be noted that halving the limiting resolution with the same swath width would quadruple the data rate.

Table 4.5-2

Thematic Mapper Anticipated Performance at 1000 km Altitude

Band No.	IFOV (Mrad)	IFOV (Feet)	(m)	Detectors Per Band	Limiting Resolution (Feet) (m)	Limiting Bandwidth (KHz/Band)
1-6	.066	200	(66)	9	100 (33)	360
7	.20	600	(200)	3	300 (100)	40

Band No.	Max. Scene Radiance (w/cm²/ster)	Low Freq S/N or (NEΔT)
1	27×10^{-4}	170
2	22×10^{-4}	130
3	17×10^{-4}	70
4	28×10^{-4}	200
5	4.3×10^{-4}	250
6	2.0×10^{-4}	200
7	20×10^{-4} (300K)	200 (0.4°C)

4.5.3.2 Substitution of a Blue Band For Band 6. Remote sensing in the blue region of ocean areas is desired by many members of the oceanographic community. An important application is the measurement of chlorophyll content. Ocean surface areas containing very low chlorophyll concentrations have a blue reflection several hundred percent higher than areas with high chlorophyll concentrations. Unfortunately, the atmospheric scattering of sunlight in this region is significant. Experimental data using high altitude aircraft will be taken to determine the effects of atmospheric scattering (particularly backscatter) on the ocean reflected sunlight. If warranted, a blue band can be used in place of the 2.1- 2.3 micrometer band. Substitution will have a significantly lower impact on the instrument than the addition of an eighth band.

As an example, a 0.44 - 0.48 micrometer channel could be added to the instrument. The performance in this channel will be determined by many parameters, among them the spectral bandwidth, target or scene reflectance and the magnitude of the backscatter component.

The ability to detect reflectance difference of nominally 1% (that is NEΔρ= .01) in adjacent scene areas has been identified as a goal for some oceanographic applications. For a scene reflectance of 3%, an anticipated backscatter component of 3×10^{-4} w/cm²/ster and the basic instrument characteristics defined earlier, an NEΔρ of 2% is obtained. By increasing the IFOV

to 0.2 m rad. and reducing the bandwidth appropriately, an NEΔρ of nominally 0.5% is obtained. Thus, it appears that the instrument design can be adapted to provide the desired performance at a sacrifice in ground resolution.

It should be recognized, however, that the blue channel is operating in a wavelength region where the instrument cannot distinguish between a change in ocean reflectance and a change in atmospheric transmission or a backscattered radiation change.

4.5.4 SYSTEM DISCUSSION

4.5.4.1 Optics. The design and fabrication of the optical system will be one of the major problems in sensor development. Alignment of the optics will be extremely critical and maintaining sharp focus in an orbital environment will require careful design.

The sensor will contain a catoptric (all reflecting) telescope with an aperture diameter of approximately 16 inches. A primary task is to accommodate the large telescope with the necessary scanning mechanism. One promising technique appears to be an image surface scanning system using eight catoptric probes mounted on a rotating wheel. The plane of the wheel is tilted with respect to the telescope optic axis, in order to keep size and weight to a minimum. The titled wheel configuration produces a conical scan and therefore the digital data will require rectification. The display system will be designed to be compatible with the curvilinear scan lines. An optical schematic of the image surface scanner is shown in Figure 4.5-3. The probe secondary and tertiary mirrors correct the aberrations of primary mirror.(7) A scan efficiency of 90% can be achieved with this type of system.
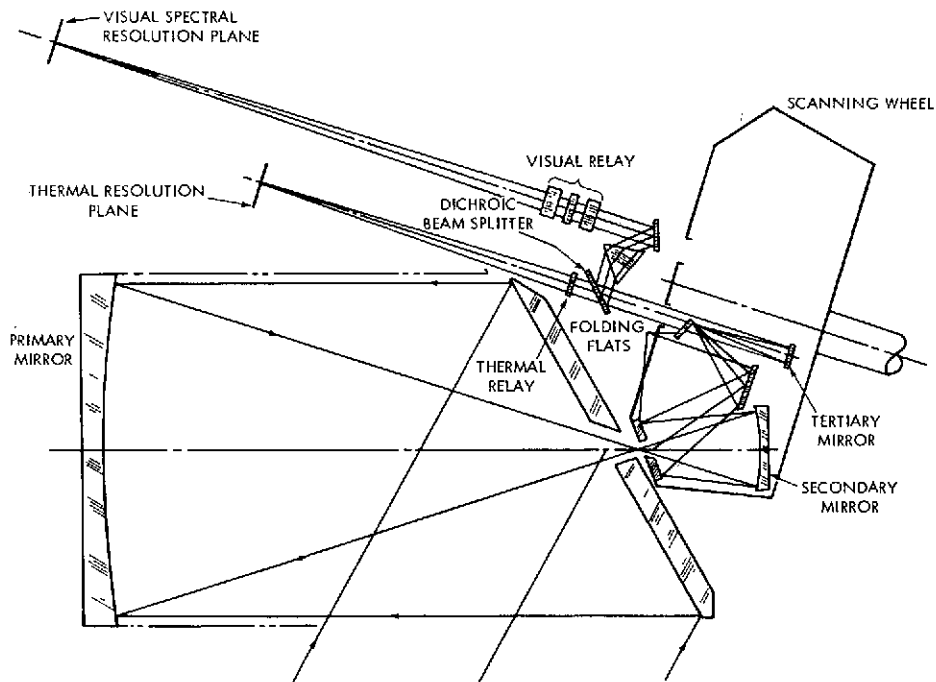

Figure 4.5-3. Optical Schematic of Catoptric Scanner and Spectrometers

Increasing the dimensions of the linear oscillating scan mirror system used on the nine inch aperture MSS (ERTS- A & B) to match a 16 inch telescope aperture does not appear to be practical. The anticipated weight of the larger rocking mirror mechanism is about 100 pounds and the scan efficiency is expected to decrease to 45% or lower, negating much of the advantage of the 16-inch telescope. By comparison the image surface scanner has greater growth potential; the collecting aperture can be further increased without introducing severe changes in the scanning mechanism.

Because the scanned field of view is only about 12°, the continuously rotating 45° object space scan mirror is far too inefficient to use. Increasing the number of mirror faces to obtain an adequate scan efficiency would result in a prohibitive increase in size and weight. Another object surface technique employs a single flat mirror that is rotated about an axis less than 45° with the normal to the flat mirror, producing a conical scan. While mechanically simple, such a nutating system would have a scan efficiency of about 30%, which is too low for our application.

Object surface scanners have a great advantage over the image surface scanners because they are "on-axis" systems and therefore do not suffer from the off-axis aberrations that are responsible for the complexity of the optical system of the image surface scanner. However, in order to compare favorably with image surface scanners in the domain of large, very high resolution, satellite borne scanners, they must have high scan efficiency without becoming overly heavy or complex. A competitive RFP for a breadboard model to develop the optimum scanning technique is in progress.

4.5.4.2 Offset Pointing. Offset pointing capability will require that the Thematic Mapper be gimbaled so that it can rotate about the spacecraft velocity vector (roll axis). The instrument will be free to rotate up to about $\pm 20°$ from its nominal position. The offset drive mechanism will have the capability of rotating the instrument in precise increments (about $5°$). This can be done by a dc torque motor coupled through a harmonic drive. Position readout of the offset angle could be monitored by a following potentiometer mounted to the harmonic drive. The position readout voltage would be proportional to the offset angle and would be telemetered to the ground station.

Another approach is to use a stepper motor to rotate the instrument. The angular position of the scanner is then determined by the number of steps the motor is driven from its nominal or zero reference position.

4.5.4.3 Calibration. Assurance that basic instrument requirements are met will be obtained by means of calibration and testing of appropriate overall and component characterisitics essential to the full understanding of the instrument operation. The measurements will include:

1. Signal-to-noise ratio over the expected range of scene radiance levels.
2. Relative spectral response
3. Band-to-band registration
4. IFOV
5. Modulation transfer function
6. Solar reflectance, with both real and simulated sun.
7. Scan jitter
8. Optical aberrations
9. Offset pointing

4.5.5 SUMMARY

A preliminary design of an advanced Thematic Mapper for the EOS Mission has been sufficiently advanced so that the principal design features and physical parameters of the sensor can be defined. These are listed in Table 4.5-3. None of the currently available Earth Observation

Table 4.5-3

Thematic Mapper

Design Parameters	
IFOV, km	66 (Channels 1-6)
	200 (Channel 7)
Scan, deg	±5
Swath, nm (km)	100 (185)
Nodal crossing, LMT	0900, 1500
Revisit time, days	17 (Less with pointing control)

Spectral Channels (Approx.)	
Channel wavelength, μm	Measurement
(1) 0.5 - 0.6	Green peak
(2) 0.6 - 0.7	Chlorophyl absorption
(3) 0.7 - 0.8	IR reflectance rise
(4) 0.8 - 1.11	IR reflectance shoulder
(5) 1.55 - 1.75	Soil and plant particle size
(6) 2.08 - 2.35	Soil and plant water content
(7) 10.4 - 12.6	Radiance temperature
Alternate channel (6)	
0.44 - 0.48	Coastal studies

Sensor Characteristics	
Data rate, mb/s	30
Power, watts	70
Weight, lb (kg)	265 (120)
Proj. area, ft^2 (m^2)	10 (0.93)

Spacecraft can accommodate the advanced Thematic Mapper, as presently conceived, from a size, weight, power, and data handling standpoint.

4.5.6 REFERENCES

1. Spectrum Identification Studies:

    a. Purdue University, Contract #12-14-100-8307 (20)
    b. University of Michigan, Contract #13-14-100-8923 (20)

2. An Approach to the Remote Detection of Earth Resources in sub-Arid Land, Jean Pouquest, NASA/GSFC Technical Bulletin #X-622-68-245, June 1968.

3. Target Studies: University of Michigan, Contract #AF 33-657-10974.

4. Investigations of Spectrum-Matching Techniques for Remote Sensing in Agriculture, University of Michigan, Contract #17-14-100-9503.

5. Conversation with Dr. Arch Park, NASA Hqs., (then at the Dept. of Agriculture), March 1968.

6. "Development and Fabrication of a Breadboard Dual Patch Multi-Element Radiant Cooler", 1969, Contract No. NAS 5-21132 with ITT.

7. Final Report for the Multispectral Point Scanner Study (Feb. 1969 to Dec. 1969). Contract No. NAS 5-11653 with Hycon.

4.6 PASSIVE MULTICHANNEL MICROWAVE RADIOMETER

4.6.1 INTRODUCTION

The primary objective of this passive microwave sensor system is to provide a facility to measure ocean energy transfer parameters such as sea surface temperatures, air-sea interactions (e.g., wind field and percentage foam cover), precipitation, and sea-air heat exchange from the measured percentage of open water in the polar regions together with cloud cover information from the Sea Surface Temperature Imaging Radiometer. Another important objective is to determine the appropriate local age of the ice canopy because of its importance in studying the dynamics of the canopy motion and because of its potential importance in determining feasible ice-breaker paths through the ice canopy. Ocean salinity was also considered as a possible parameter to be measured in this way, but evidence gathered to date indicates that any effects on the radiometric signal are so small (1) as to be almost always obscured by other interfering effects.

In order quantitatively to correct for microwave radiometric temperature variations caused by the atmospheric water content in the forms of vapor, cloud droplets, and rain droplets, these quantities must also be carefully measured. The particular choice of frequencies proposed here will be justified by a brief discussion of the microwave radiometric characteristics of the various effects.

4.6.2 TECHNICAL CONSIDERATIONS

4.6.2.1 Sea Surface Winds. In terms of microwave radiometric observables, surface winds manifest themselves in two ways, by roughing the sea surface and by generating foam. Under most circumstances, both increase the emissivity of the water (2-4). The roughness effect is quite weak in vertical polarization for angles in the neighborhood of 45°- 65° (5), hence separation from the foam effect should be possible when observing with a dual-polarized radiometer, since the foam effect is unpolarized.

4.6.2-2 Sea Surface Temperatures. The sensitivity of the microwave brightness temperature of sea water to its thermodynamic temperature when viewed at the nadir is rather weak, but shows a broad maximum near 6 gHz. At this frequency, change of 30K in the water temperature (over the range 273 - 303K) produces a 12K change in the microwave brightness temperature (100K to 112K). As can be seen in Figure 4.6-1, the peak is rather broad, with half-maximum points at 2 and 13.5 gHz. This effect can be enhanced appreciably by looking obliquely at the ocean surface using the vertically polarized component of the radiation. The aforementioned sensitivity increases from 12K to 16K at a zenith angle of 45°; at 60°, it increases further to 20K. The sensitivity of the horizontal polarization is correspondingly reduced to 7K at a zenith angle of 60°.

At frequencies near 20 gHz, the microwave brightness is practically independent of the thermodynamic temperature. At higher frequencies, the dependence actually reverses its sign, i.e., warmer water appears colder and vice versa.

4.6.2-3. Water Vapor. The center frequency of the water vapor line is 22.235 gHz but the line is broad enough so that its effect must be considered for all frequencies above approximately 10 gHz. The maximum sensitivity would be at the line center frequency, but, due to pressure broadening of the line at lower altitudes, this frequency would be much more sensitive to high altitude water vapor than to that at low altitudes. The sensitivity is more or less uniform throughout the lower troposphere at 21.5 gHz. By measuring at both frequencies, information can be obtained on the vertical profile of the water vapor in the atmosphere. For the purposes of this sensor system, however, the latter frequency will be chosen in order to provide a first-order atmospheric correction to the radiometer signals to provide improved surface information.

4.6.2-4. Nonraining Cloud Water. The absorption due to cloud water droplets is approximately proportional to the square of the frequency and directly to the water density, independent of the
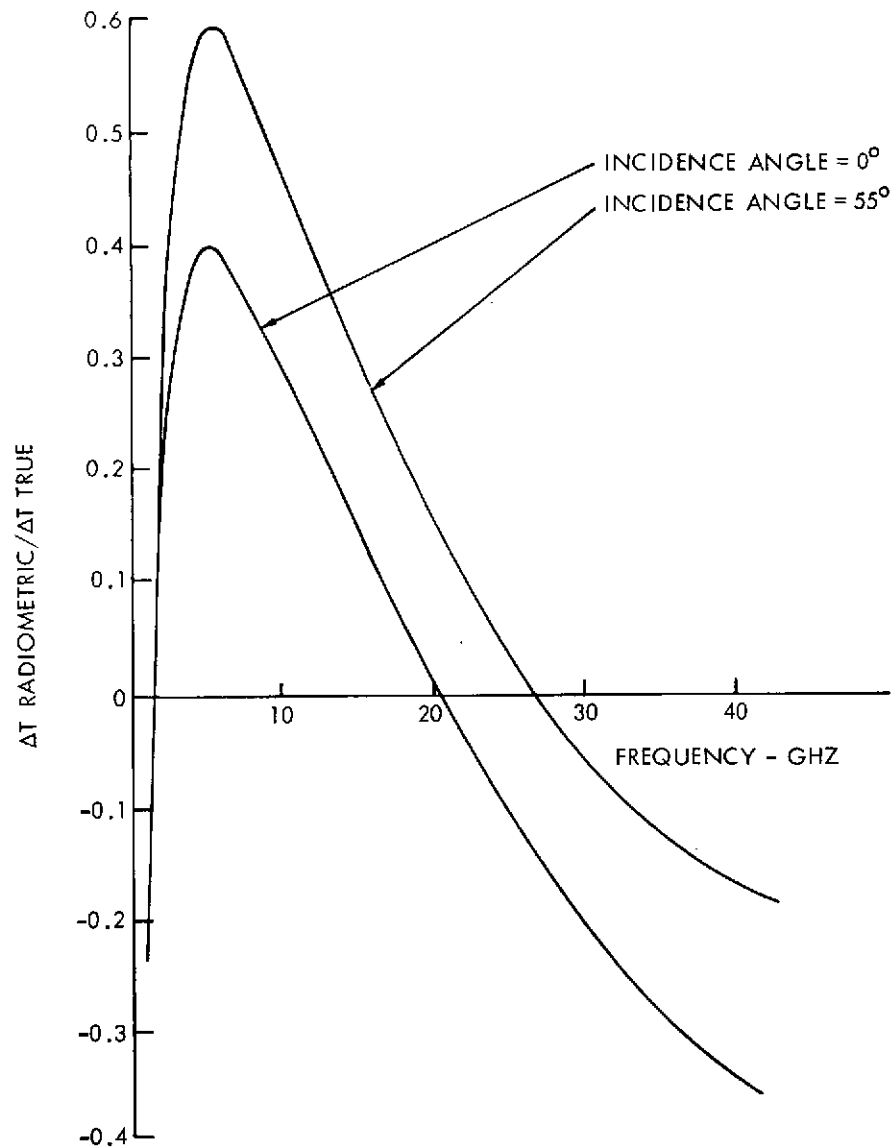
4-52

Figure 4.6-1. Radiometric Temperature Sensitivity for Calm Sea Water, Vertically Polarized Component. (Average Sensitivity in the true range of 273-303 K)

drop size distribution as long as all drops are much smaller than the wavelength. Since non-raining clouds contain few particles larger than 50 microns, this is satisfied for all frequencies below the 60 gHz oxygen band. 37 gHz was chosen to determine the amount of liquid water in the nonraining clouds taking into account the atmospheric window at that frequency and the additional usage in ice-mapping.

4.6.2-5. Rain Water. Since rain drops are much larger than the droplets found in nonraining clouds, i. e., the order of 1 mm, and since the index of refraction of water in the microwave region is the order of 10 (1), the drop size is comparable to the wavelength inside the drop. Thus the condition necessary for the quadratic dependence on frequency is no longer satisfied; the effect becomes one of even higher order (6). We can therefore separate the effects of raining and nonraining clouds. Because of their different frequency dependencies, these must be separately corrected for in order to get at the surface oceanographic parameters of interest.

4.6.2-6. Ice. The contrast between water and ice is quite large and only weakly frequency dependent. Considerations of resolution would dictate as high a frequency as possible for ice coverage measurements, taking into account that polynyas less than 1 km wide are also of importance to studies of ice dynamics and polar energy balance with the atmosphere. The 60 gHz oxygen band and clouds limit the highest practical frequency to about 37 gHz. At frequencies higher than 60 gHz, e.g. at the atmospheric window near 94 gHz, flyable low-noise radiometers are not yet available.

An effect which would interfere with ice coverage measurements but is of interest in its own right has been noted. Arctic ice seems to consist of two distinct types, one radiometrically warmer than the others (7). Visually, the two basic types appear to be related to multi-year, heavily hummocked ice and the first year ice which is newer and smoother. Up to 37 gHz, the radiometric temperature contrast between the two types of ice appears to be proportional to the microwave frequency. With this interference, old ice with much unresolved open water (smaller polynyas) would not be distinguishable from new ice, except for the following important characteristics. The emission from ice of either type is only weakly polarized, but that from open water is quite strongly polarized. Thus by measuring both polarizations, the two situations can be distinguished.

4.6.2-7. Soil Moisture. For soil moisture measurements, the lower frequencies and horizontal polarization would be the most sensitive, as has been demonstrated by Edgerton et al (8).

The brightness temperature changes, occurring as a result of soil moisture variation from 5 to 25% range from 80 to 120K in the horizontal component, depending on the frequency. The frequency effect is due to the frequency dependence of the dielectric constant of water, since the dielectric constant of the dry soil is roughly independent of frequency and is at least an order of magnitude smaller than the dielectric constant of water. The real part of the dielectric constant of water decreases from 75 at 5 gHz to 19 at 37 gHz (1). Because of the frequency dependence for the penetration depth of the radiation in the soil, the measurements at all frequencies could be used to obtain information on the moisture profile within the soil. A complicating feature for soil moisture measurements is the effect of soil temperature; an increase in microwave brightness temperature could be caused by either a decrease in soil moisture or an increase in soil temperature. The infrared temperature of the soil can be used to separate these effects, when weather permits. Otherwise, it may be possible to utilize the body of data obtained from the multichannel, dual polarization array for separating the effects of physical temperature and moisture content on the radiometric signature. Further field tests and operational flight experience will be required to confirm this hypothesis

4.6.3 CHANNEL SELECTION FOR OCEANOGRAPHIC STUDIES

In order satisfactorily to measure all of the oceanographic parameters of interest under most weather conditions to be encountered, it is preferable to make observations at five different

frequencies, all of them with dual polarization, as shown in Table 4.6-1. The reasoning behind these choices will be discussed.

Table 4.6-1

Microwave Channel Allocations for EOS

Frequency (gHz)	4.99		10.69		18.00		21.50		37.00	
Wavelength (cm)	6.01		2.81		1.67		1.40		0.81	
Polarization	V	H	V	H	V	H	V	H	V	H
Major Objectives	Sea temp.	Separation of surface and atmospheric effects	Separation of surface and atmospheric effects	Rain water in heavy rain	Separation of surface and atmospheric effects	Rain water in light rain	Separation of surface and atmospheric effects	Tropo. water vapor	Surface winds (through foam) sea ice/polynyas old ice/new ice	
Secondary Objective	← Soil moisture →								Total liquid water (non-raining clouds)	
Major Interferences	Heavy rain clouds, foam, and roughness		Foam and roughness				Clouds, foam and roughness		Heavy clouds	

The primary source of the sea water temperature data is the vertically polarized component of the 4.99 gHz frequency. The basic reason for this choice is the proximity to the peak sensitivity as shown in Figure 4.6-1 and that it is also in a radio astronomy band. Two of the major interferences are polarization-independent, i.e. the surface foam and heavy rain clouds, so the horizontally polarized component of the same frequency will be used to correct for these two particular effects. Ocean surface roughness, on the other hand, appears to have some dependence on polarization. Since it is also frequency dependent, the higher frequency channels will be used to obtain roughness data at frequencies where there is little or no effect of the physical temperature of the water. While the correction required for taking into account the effect of the varying water vapor concentrations at 4.99 gHz is not expected to be large by comparison with the foregoing effects, the correction is nevertheless important. Data from the 21.5 gHz channel will be utilized for this purpose.

Dual polarization has again been chosen to help distinguish between effects due to roughness, foam, and atmospheric absorption. The highest frequency channel (37 gHz) will not be used for this purpose since it is deemed too far removed from the 4.99 gHz channel to permit extraction of roughness data through the frequency dependence. The exact nature of the dependence referred to has yet to be determined. Heavy rainfall will also interfere with the determination of the temperature of the sea from the standpoint of contributing to the surface roughness; to some extent, it may be possible to correct for this interference by using data from the rain water channels. The range over which this will be possible remains to be determined.

The 37.0 gHz channel will be used to obtain data for the ocean surface wind speeds, inferred primarily from percentage foam cover. It is anticipated that determination of surface winds (greater than 7 meters/second) through the extent of foam coverage will be best in this highest frequency channel simply because the shorter wavelength should be better suited for observing thinner layers of foam than at 19.35 gHz, where such observations have been made by a mapping radiometer (2). Occurrence of heavy rainfall will render the 37 gHz channel useless for inferring winds; under such conditions, it may be possible to observe the surface at the longer wavelengths, but the effect of the raindrops on the surface may well obscure the determination of the percentage foam cover, anyway. Another important utilization of the 37 gHz channel is the determination of open water in the polar ice as well as ice age, as has been discussed earlier.

While water droplets have been listed as a major interference in obtaining the ocean surface parameters from the radiometric data, water vapor must also be taken properly into account. This is best done with a real-time measurement approach, with the channel on the side of the water vapor line to permit accurate water vapor correction under a wide variety of humidity conditions. Hence, the choice of the 21.5 gHz channel. If spacecraft constraints further limit this sensor to a four-channel radiometer, the water vapor corrections will have to be made by the less satisfactory technique of incorporating data from daily global profiles of water vapor and temperature obtained from operational satellite vertical sounders.

A three-channel approach has been chosen for the determination of the liquid water in the atmosphere, since this permits detection of water droplets over a wide range of water droplet sizes, in both raining and nonraining clouds. Another important advantage to this approach is that it permits the wavelength dependence of the water droplet signature to be utilized to unfold this particular feature from the rest of the interwoven data. Of necessity, the frequencies chosen for this purpose must be sufficiently removed from the water vapor line so as to reduce interference to a manageable level. 10.69 gHz (also a radio astronomy frequency) was chosen for its maximum sensitivity to water droplets found in heavy rainfall. In order adequately to determine the extent of water droplets in lighter rainfall, 18 gHz was chosen for its greater response to such droplets and yet reasonably small response to water vapor variations. 37 gHz was chosen to determine the amount of liquid water in the nonraining clouds taking into account the smaller droplet sizes involved and the atmospheric window at that frequency.

Dual polarization on all the channels has been specified in order to facilitate separation of surface and atmospheric effects since in general the former display polarization effects and the latter do not. It should be pointed out here that the dual polarization approach is obtainable with little impact on the antenna structure itself, the heaviest component in the system. It also should be emphasized that the dual polarization approach dictates that observations must be made at angles away from the nadir; the optimum zenith angle for this from other considerations would appear to be about 50°. Also, a conical scan, i.e. at a constant nadir angle, is dictated by the fact that microwave properties of surfaces are in general angle-dependent, with the exact dependence sufficiently variable from one sample to the next that correction for variation of scan angle would be impractical.

Finally, spatial resolution of 90 km on the surface would appear to be adequate for determination of all oceanographic parameters except the extent of polynyas in the polar ice canopies. In the latter case, the greatest resolution practically possible should be used. In the case of the water temperature channel at C-band, the antenna required for 90 km resolution is too large for the sizes of spacecraft being considered in this study. Since generally the sea temperatures are not expected to vary significantly over such distances, a 180 km resolution for that channel will provide useful ocean temperature data.

4.6.4 INSTRUMENT DESIGN

This section will describe in some detail a particular design concept for a multichannel microwave mapping radiometer, recognizing that changes in the spacecraft radiometry field may make different configurations more desirable. Some mention will be made also of some of the alternative configurations which seem like reasonable candidates for the near future. The concept to be described in detail here is based on presently available technology. It is reasonable to expect that when contracts for development of the flight radiometers will be released improved designs will be specified calling for reduced weight instruments with improved resolution.

As mentioned in the previous section, an important scientific constraint is the need for a conical scan pattern, i.e. the scanning beam must be kept at a constant angle with respect to the nadir. This may be done electrically by mounting a phased array vertically on the orbiting spacecraft, providing a fixed beam tilt in one dimension by adjusting the waveguide size, and scanning in the other dimension by varying the phase between the various stick elements of the array, as is the technique on the Nimbus-F ESMR. The EOS-A configuration will afford an opportunity of both an

improvement in the resolution to be available at 37 gHz on Nimbus F and a simultaneous multi-band view of the surface of the Earth, enabling a multiple purpose mission to be performed on an almost all-weather basis.

For the purpose of sizing the various arrays, all are assumed to be vertically mounted and conically scanning. The following equations were utilized:

$$Sin\,\beta = \frac{R + h}{R} Sin\,\theta \tag{1}$$

where θ is the angle from the nadir (constant scan angle), β is the angle from the zenith at the target, $R (=6370\ Km)$ is the Earth radius, and $H (=1000\ Km)$ is the altitude of the spacecraft.

The slant range is given by:

$$R' = \frac{Sin\,(\beta - \theta)}{Sin\,\theta}\,R \tag{2}$$

Assuming a cosine-squared array illumination for acceptable sidelobes, the width of the array is:

$$d\phi \simeq 1.5\,\frac{\lambda R'}{D_\phi} \tag{3}$$

The height of the array is:

$$d_\theta \simeq \frac{1.5\,\lambda R'}{D_\theta\,Sin\,\theta\,Cos\,\beta} = 3\,\frac{R + h}{R}\,\frac{\lambda R'}{D_\theta\,Sin\,2\beta} \tag{4}$$

Expressing (4) in terms of a single variable:

$$d_\theta \simeq \frac{3\lambda\,(R + h)}{D_\theta} \left\{ \frac{\left[\left(\frac{R + h}{R}\right)^2 - Sin^2\,\beta\right]^{1/2} - Cos\,\beta}{Sin\,2\beta} \right\} \tag{5}$$

In Equations (3) through (5), D_ϕ is the target element in the scan direction, ϕ is the azimuth angle of scan, D_θ is the target element in the direction normal to the scan, and λ is the wavelength. An additional assumption is that

$$D_\phi = D_\theta$$

The array then obtains the following shape factor:

$$\frac{d_\theta}{d_\phi} = 2\,\frac{R + h}{R\,Sin\,2\beta}$$

From the considerations in the previous section, the angle from the zenith at the target has been chosen as 55°, corresponding to an angle from the nadir of 45° at the spacecraft, according to equation (1). Table 4.6-1 illustrates one possible selection of multi-channel arrays that would satisfy the mission requirements. The philsophy was to obtain the highest possible resolution from a phased array constrained by the spacecraft configuration at 37 gHz for polar ice mapping, and to size everything else within spacecraft constraints in nearly integral multiples of the 37 gHz footprint size. The arrays would fit within the sensor bays as shown in Figure 4.6-2.
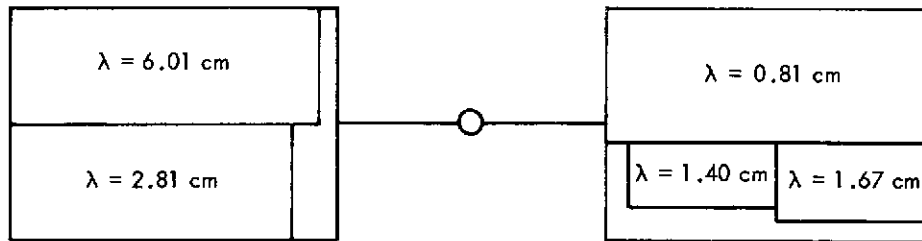

Figure 4.6-2.   Location of Radiometer Antennas within the
Sensor Bay Prior to Deployment

Deployment would be required if the sensor bays of the spacecraft are required to be in the horizontal plane for the other instruments on board. One possible means for accomplishing this is illustrated in Figure 4.6-3. Such a configuration would allow a generous amount of open area in the sensor bays for other experiments. Even in the stowed positions, ample room in the sensor bays is available for other experiments since the thickness of the arrays can be made less than 10 inches.

Within the constraints of the minimum spacecraft configuration, no further improvement in the spatial resolution of the 0.81 and 6.01 cm channels is possible without adding the complication of folding phased arrays or furlable reflector antennas. Such possibilities should not be dismissed lightly, but will not be discussed further here other than to mention that appropriate investigation of these concepts is being undertaken under the AAFE program. If additional weight and power could be assigned to this experiment, spatial resolution of the remaining channels could be improved within the minimum spacecraft configuration by allowing a relatively simple double deployment system, keeping the size of any single array within the bounds of the sensor bay before deployment. Under these conditions, an additional water vapor channel for improved real-time atmospheric corrections would be desirable.

Significant improvement in the spatial resolution of all channels could be realized in the nominal configuration of the spacecraft, utilizing also double deployment, as follows: 12.5 km at 0.81 cm; 50 km at 1.40, 1.67, and 2.81 cm; and 100 km at 6.01 cm.

Still another possibility that should receive further consideration is that of rotating the entire sensor bay so as to obviate the need for electronic scanning. The antenna could be mounted horizontally for this purpose, with the additional advantage that the conical tilt angle could be changed for the purposes of obtaining emissivity vs angle information from the viewed surfaces. The primary advantage in this arrangement would be the larger available values of the scan angle, ϕ, obtained in this manner; electronic scanning is limited to angles less than 35° on either side of the track in the dual polarized mode due to the appearance of grating lobes at larger angles.

The weights and powers shown in Table 4.6-2 were obtained by scaling from the design weights and powers of the Nimbus-F ESMR. Antenna and structure weights were taken as proportional to the array area, and weight of the electronics was considered to be almost constant, except
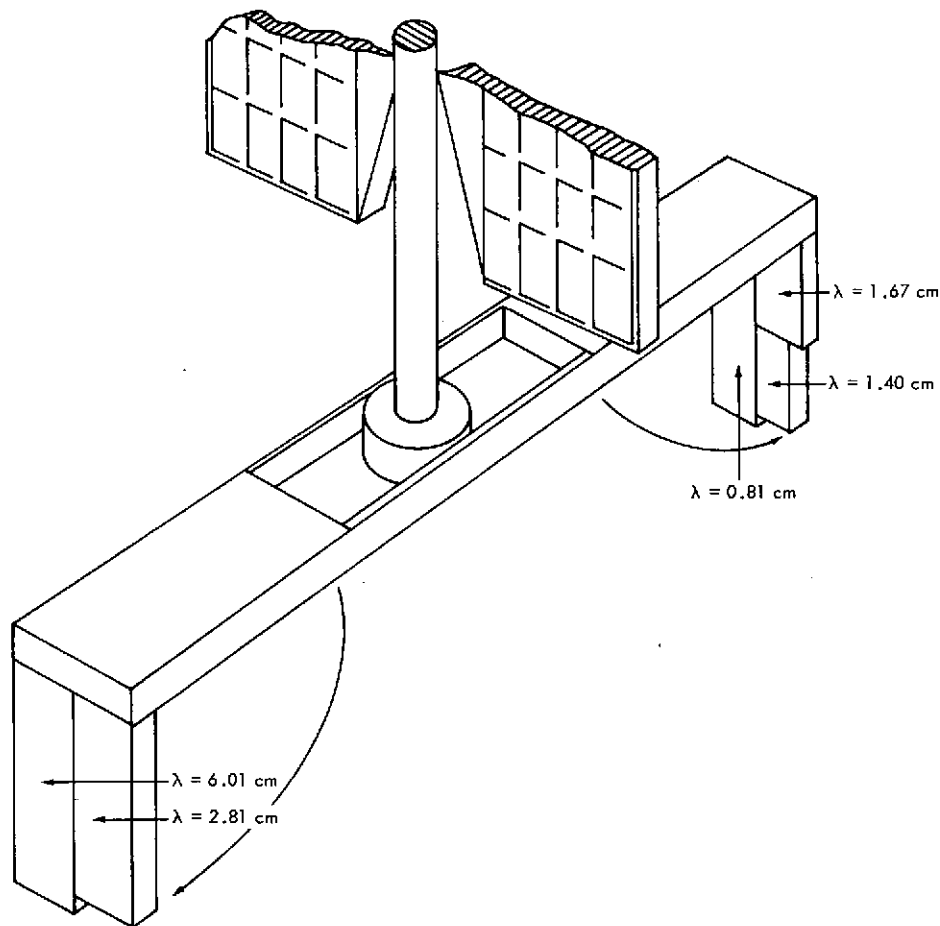
Figure 4.6-3. Antennas in Deployed Position

for the 6.01 cm channel where some weight was added to take into account the larger sizes of the waveguide and RF switches. Since a goodly portion of the required power for such radiometers goes into the phase shifters for the electronically scanned array, half the power used for the Nimbus-F ESMR was scaled according to array area, and the other half was added to this for the total power for a given array.

4.6.5 SUMMARY

Passive microwave radiometry offers the potential of nearly all-weather studies of a number of parameters of importance to oceanography and to an understanding of the energy exchange at the air-sea interface. Multichannel measurements are required to separate the various factors which contribute to the microwave signature of the earth surface and atmosphere. The microwave sensory system (Table 4.6.-3), as compared to a number of other earth observation sensors, is an order of magnitude larger in size, weight, and power consumption. Such a system cannot be accommodated on any of the current (ERTS/Nimbus) or proposed (SATA) R and D spacecraft. Size considerations, coupled with the desirability of correlative data from the infrared and visible portions of the spectrum, lead clearly to the requirement for a new spacecraft design.

Table 4.6-2

Physical Characteristics of the EOS Microwave Radiometers

Frequency gHz	Wavelength cm	Target Diameter km	Antenna Width m	Antenna Height m	Antenna Area sq. m	Weight lb	Power watts
37.00	0.81	22	0.86	2.12	1.70	128	95
21.50	1.40	88	0.37	0.92	0.35	55	40
18.00	1.67	88	0.44	1.10	0.50	68	50
10.69	2.81	88	0.75	1.84	1.30	107	80
4.99	6.01	183	0.77	2.02	1.60	155	90
				Totals	5.45	513	355

Table 4.6-3

Passive Multichannel Microwave Radiometer

Design Parameters	
Scan	Conical, half angle-45°
Polarization	Dual
Swath, nm (km)	730 (1350)
Nodal Crossing, LMT	0900, 1200, 1500
Rivisit time, days	1+

Channels (preliminary)

Freq. (GHz)	(cm)	Ant. Length (m)	IFOV (km)	Purpose	
4.99	6.01	2.02	183	Sea Sfc. Temp.	Soil Moisture
10.69	2.81	1.84	88	Heavy Rain	Soil Moisture
18.0	1.67	1.10	88	Light Rain	Soil Moisture
21.5	1.40	0.92	88	Water Vapor	Soil Moisture
37.0	0.81	2.12	22	Sea Ice	Total Liquid
				Surface Winds (Roughness, Foam)	Water

Sensor Characteristics	
Data rate, mb/s	0.01
Power, watts	355
Weight, lb. (kg)	513 (233)
Projected Area ft², (m²)	58 (5.5)

4.6.6 REFERENCES

1. J. A. Lane and J. A. Saxton, "Dielectric dispersion in pure polar liquids at very high radio-frequencies," Proc. Roy. Soc. A 214, 400 - 545 (1952).

2. W. Nordberg, et. al., "Measurements of microwave emission from a foam covered, wind driven sea," J. Atmos. Sci. 28, 429-435 (April 1971)

3. G. F. Williams, Jr., "Microwave measurements of bubbles and foam," to be published in IEEE Geosciences Elec. (October 1971)

4. J. P. Hollinger, "Passive microwave measurements of sea surface roughness," to be published in IEEE Geosciences Elec. (July 1971)

5. J. P. Hollinger, "Passive microwave measurements of the sea surface," J. Geo. Res. 75, 5209 (1970).

6. N. E. Gaut and E. C. Reifenstein, III, "Interaction model of microwave energy and atmospheric variables," Final Report, Contract NAS 8-26275 (February 1971)

7. W. Nordberg, et. al., "Aircraft measurements of microwave emission from Arctic Sea ice," to be published in Remote Sensing of the Environment. Also, data from the Arctic flights of the NASA Convair 990 in March 1971.

8. A. T. Edgerton, et. al., "Microwave emission characteristics of natural materials and the environment," Final Report No. 9016R-8 for contract No. N00014-70C-0351 (February 1971).

4.7 UPPER ATMOSPHERIC SOUNDER

4.7.1 INTRODUCTION

The upper stratosphere and mesosphere (i.e., the region between about 30 km and 90 km) have been largely neglected in satellite remote sensing applications because quite logically of efforts to consider first the lower atmosphere immediately around us with its obvious importance to daily weather. But the entire atmosphere is one, and there is increasing evidence that it is a highly correlated medium. Results from rocket observations have produced some sketchy, though important, inferences of interactions between the stratosphere and mesosphere in such areas as radiative exchange, large-scale horizontal eddies, gravity waves, tidal oscillations, etc. [1].

Recent rocket flights reported by Theon and Smith indicate that at high latitudes a strong correlation exists between upper air temperature variations and the upward propagation of gravity waves from the troposphere [2]. Also, Wallace and Kousky [3] have found evidence from an analysis of radiosonde data of downward propagating Kelvin-like waves in the tropical stratosphere accompanied by temperature fluctuations of 3-5K. This type of wave produces an upward flux of westerly momentum which may be large enough to account for the westerly accelerations associated with the quasi-biennial oscillation. Smith, Katchen, and Theon (4) have described dramatic temperature changes of more than 30K occurring within several hours in the winter temperature structure of the upper mesosphere, observed with rocket grenade soundings at Point Barrow, Alaska. Figure 4.7-1 shows their results from six such soundings on the night of 31 January-1 Febuary 1967.
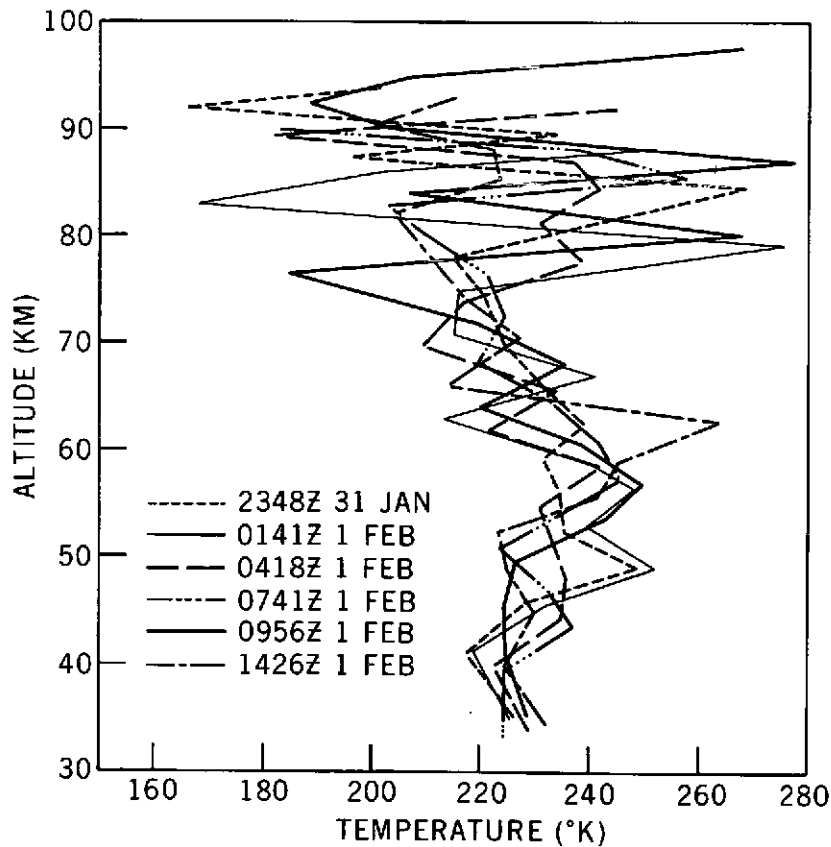

Figure 4.7-1. Winter Temperature Structure at a High Latitude Station
(Pt. Barrow, Alaska - Jan.-Feb., 1967)

Investigations of the composition of the upper air will increase our understanding of atmospheric processes, such as dynamics and photochemistry. For example, recent investigations of the ozone content of the atmosphere, inferred from Nimbus 3 spectra in the 9.6μm ozone absorption band, indicate a high correlation between ozone in the upper air and tropospheric weather systems [5]. The sensing of ozone profiles on a global scale and to higher altitudes will be of increased importance as similar studies progress. The measurement of airglow and scattering in the ultraviolet, visible, and near infrared can reveal information regarding the constituents of the high atmosphere and the atomic and molecular transitions resulting in the observed emissions. The spatial and temporal monitoring of water vapor in the upper atmosphere would be applicable to studies of transport mechanisms such as the possibility that large quantities of water vapor are injected into the stratosphere by cumulus towers, especially in the tropics. Similarly, the detection and monitoring of other trace constituents such as the oxides of nitrogen, sulfur dioxide, methane and ammonia would be applicable to studies of transport mechanisms as well as having obvious implications with respect to Enviromental Quality and atmospheric pollution (see Section 4.8 below).

4.7.2 SENSOR OPTIONS

4.7.2.1 Advance Limb Radiance Inversion Radiometer. A promising technique for vertically sounding temperature and composition in the stratosphere and mesosphere is the limb scanning to be employed by the Limb Radiance Inversion Radiometer (LRIR) to be flown on Nimbus-F in 1974. That experiment, scanning the atmospheric limb in four spectral intervals and in only one direction from the spacecraft, will make the following vertical profile measurements:

Temperature, ± 6K, 2 km vertical resolution,
15 km to 70 km.

Water Vapor, ± 2 PPM, 5 km vertical resolution
15 km to 42 km.

Ozone, ± 0.001 cm NTP/km, 2 km vertical resolution,
15 km to 50 km.

Measurements of the same atmospheric volume will be made in a minimum time interval of a half-day. Characteristics of the instrument are the following:

Size: radiometer, 1.1 ft^3
cooler, 1.8 ft^3

Weight: radiometer, 28.0 lb.
cooler, 28 lb.

Power: radiometer, 36 watts continuous
cooler, solid cryogen

Data rate: 3,920 bits per second

View: 50° out of orbit plane and 31° towards horizon, with 5° vertical scan field for radiometer.

Spectral radiances:
9.4 - 10μm (O_3)

14.0 - 16.3μm (CO_2)

14.5 - 16.7μm (CO_2)

20 - 40 μm (H_2O vapor)

It appears entirely feasible to modify the LRIR concept for advance applications on EOS in the following respects:

- View in several azimuthal directions on either side of the spacecraft, thus yielding improved temporal resolution (e.g., view the same atmospheric volume within 2 to 4 hours, or 1 to 2 orbits)

- Improved accuracy (Temp. $\pm$ 1K; Water Vapor $\pm$ 0.5 PPM; ozone $\pm$ 0.0007 cmNTP/km)

- Improved vertical resolution (Temp. 1 km; Water Vapor 2 km; ozone 1 km)

- Additional channels for sensing other trace constituents

- Radiative or Vuilleumier Cycle cooling

4.7.2.2 Microwave Sounder. Another promising technique for vertically sounding the temperature structure of the atmopshere involves the inversion of radiances of upwelling thermal microwave emission. Studies of an Advanced Applications Flight Experiment entitled "Microwave Temperature Sounding of the Mesosphere and Upper Stratosphere" are now being carried out by M.I.T. That instrument is designed to obtain temperature profiles for the altitude region 15-80 km at nadir for contiguous zones ~100 miles wide and ~200 miles long. Characteristics of the instrument are the following:

Size: 0.56 ft^3

Wieght: 25 lbs.

Power: 25 watts

Data rate: 50 bits per second

View: nadir viewing

Spectral channels: 4 in 60 GHz oxygen absorption band, corresponding to weighting function peaking near 70, 50, 40 and 18 km.

4.7.3 SUMMARY

The upper atmosphere sounding, as outlined requires a sensor of modest weight and power. (Table 4.7-1) Like the Nimbus-F sensor, it also could be accommodated on an ERTS Nimbus class spacecraft. For data interpretation, the limb radiance technique requires that knowledge of spacecraft rates be known with an accuracy of 2.8×10^{-4} degrees/sec which implies a rate gyro reference of the type considered for EOS, thus it would benefit from flight on the EOS series.

4.7.4 REFERENCES

1.   Nordberg, W., 1969: Interactions Between the Upper and Lower Atmosphere, pp. 53-74 in Annals of the IQSY, Volume 5, Solar-Terrestrial Physics: Terrestrial Aspects. MIT Press

2.   Theon, J.S. and W.S. Smith, 1970: Seasonal Transitions in the Thermal Structure of the Mesosphere at High Latitudes. J. Atmos. Sci., 27, 173-176

3.   Wallace, John M and V. E. Kousky, 1968: Observational Evidence of Kelvin Waves in the Tropical Stratosphere. J. Atmos. Sci., 25, 900-907.

4. Smith, W. S., L. B. Katchen, and J. S. Theon, 1968: Grenade Experiments in a Program of Synoptic Meteorological Measurements, pp. 170-175 in Meteorological Investigations of the Upper Atmosphere, Vol. 9, No. 31, ed. R. S. Quiroz, 231 pp. Am. Meteor Soc., Boston, Mass.

5. Prabhakard, C., V. V. Salomonson, B. J. Conrath, J. Steranka, and L. J. Allison, 1971: Nimbus 3 Satellite Observations of Ozone Associated with the Easterly Jet Stream over India During the 1969 Summer Monsoon. (Accepted for publication in the J. Atmos. Sci.)

Table 4.7-1

Upper Atmospheric Sounder

Design Parameters			
Global coverage	Daily		
Nodal crossing, LMT	0900, 1200, 1500		
Pointing	Self contained		
Sampling interval	108 minutes, twice (or more) daily		
Measurements		Altitude	Vertical
Parameter	Precision	Range	Resolution
Temperature	$\pm 1°C$	15-70 km	1 km
Water Vapor	$\pm 15\%$	15-50 km	2 km
Ozone	$\pm 5\%$	15-60 km	1 km
Sensor Characteristics[1]			
Data rate, Mb/s	< 0.01		
Power, watts	27		
Weight, lb (kg)	56 (25)		
Proj. Area, ft^2 (m^2)	1.3 (0.12)		

1- Based on Limb Radiance Inversion Radiometer

4.8 ATMOSPHERIC POLLUTION SENSOR

4.8.1 INTRODUCTION

One of the clearest signs of the deleterious effect of man on his environment is air pollution. Smog in our large cities, reaching levels causing discomfort to humans - and occasionally even endangering life, is becoming a familiar byproduct of our civilization. Carbon monoxide (CO) is spewed forth from millions of internal combustion engines and certain industrial processes at the rate of 220 million tons per year. The long lifetime and toxic nature of this gas makes it one of the most important pollutants. But the CO concentration in the atmosphere has not increased at the rate it should from simple considerations of production rates. On the other hand the sink mechanisms removing CO from the atmosphere are not well understood and their locations are unknown. It is now thought that a removal process occurs in the stratosphere. It is important to begin monitoring the concentration of CO globally in order to study possible sinks in the stratosphere and more funamentally to monitor possible changes as an indication that the capacity of the environment to remove CO is being exceeded. It is estimated that in 1967 some 13.4 billion metric tons of carbon dioxide (CO_2) were released from fossil fuel combustion and that emissions in 1980 will be 26 billion metric tons for the world as a whole. CO_2 has been steadily increasing in the atmosphere at 0.2 percent per year since 1958. An 18 percent increase resulting from fossil fuel combustion to the year 2000 (from 320 ppm to 379 ppm) is projected. Theories and speculations of the global effects of pollution have included assertions that the buildup of CO_2 might warm up the planet and cause the polar ice to melt, thus raising the sea level several hundred feet and submerging coastal cities. On the other hand there have been warnings that particles emitted into the air from industrial, energy, and transportation processes might prevent some sunlight from reaching the Earth's surface, thus lowering global temperature and beginning a new ice age. (1, 2) The atmosphere also acquires from natural and man-made sources a number of variable trace gases such as sulfur dioxide (SO_2), oxides of nitrogen, and water vapor. Particles can result from photochemical reactions between trace gases such as SO_2, NH_3 (ammonia), and O_3 (ozone) or atomic O. Such reactions are strongly influenced by humidity or the presence of cloud droplets. The question of large quantities of H_2O being deposited into the stratosphere by a fleet of supersonic transports (SST's) and of the consequent photochemical effects with possible ultraviolet radiation reaching the ground has been much in the news recently in connection with debates over the future of the American SST program.

We simply don't know enough now to resolve many of the questions concerning the future effects of atmospheric pollutants. But it is clear that we must begin monitoring certain of the important pollutants on a continuing basis in order to establish a baseline from which detection of change can be ascertained and upon which our knowledge of the effects of these pollutants can grow. In this regard the Williamstown Report (1) states the following (p. 17):

> "We recommend that the following program of action be initiated as soon as possible:
>
> a. Begin now to monitor the lower stratosphere for water vapor, cloudiness, oxides of nitrogen and sulfur, hydrocarbons, and particles (including the latter's composition and size distribution)."

The Williamstown Report also states the following regarding CO (p. 211);

> "Whether or not the steady-state concentration is increasing, determinations are needed of the effect of increased emission on the regions where CO is removed. If, as seems likely, a significant fraction of the carbon monoxide is being transported into the ozone layer of the stratosphere, the increase in the importance of the CO-OH reaction could be influencing the overall ozone reaction mechanism in the stratosphere."

4.8.2 SENSOR OPTIONS

4.8.2.1 Remote Gas Filter Correlation Analyzer. One possible instrument for monitoring global air pollution is a Remote Gas Filter Correlation (RGFC) Analyzer whose characteristics are currently being investigated by General Dynamics Convair Division under an AAFE Contract entitled "Development of Satellite Experiments to Monitor Global Air Pollution." Previously General Dynamics had concluded in a study for NASA entitled "Study of Air Pollution Detection by Remote Sensors" that the gas filter correlation approach had strong advantages. (The results of this study are given in Contractor Report CR-1380 dated July 1969.) The RGFC Analyzer employs an optical correlation technique, using gas filters to selectively measure the change in infrared radiation due to specific pollutants. Three modes of sensing are being investigated. The first two are for tropospheric measurements, i.e., observing the (1) infrared emission and (2) near-infrared reflected solar radiation from the Earth-atmosphere system. The third, (3) observing the sun's radiance in occultation, is for stratospheric measurements.

It is believed that concentrations as low as 0.001 ppm and as high as 350 ppm of the atmospheric pollutants CO, CO2, SO_2, NO, NO_2, NH_3, and CH_4 can be measured by this technique. CO to the required accuracy has already been detected by this technique from an airplane at 10,000 feet.

Characteristics of the instrument are the following:

Size: 0.5 ft^3

Weight: 30 lbs

Power: 7 watts mean; 10 watts max.

Data Rate: 400 bits per second

IFOV: $5° \times 5°$

View: nadir viewing

Spectral region: 2 to 20μ m

4.8.2.2 Carbon Monoxide Pollution Experiment. Another possible instrument for monitoring pollution is a correlation interferometer designed by Barringer Research Limited and being fabricated by the General Electric Company under an AAFE contract entitled "Carbon Monoxide Pollution Experiment (COPE) for Earth Oriented Applications Satellites." The COPE is directed toward the solution of two problems of global concern: (1) the potential CO buildup in our environment and (2) the possible contribution of CO to the CO_2 greenhouse effect.

The characteristics of the correlation interferometer are the following:

Size: 0.4 ft^3

Weight: 30 lbs

Power: 12 watts average, 24.5 watts max.

Data Rate: 400 bits per second

View: $2° \times 2°$, downward; and $0.1° \times 0.1°$ limb viewing

Spectral resolution

Spectral radiances: Within the 2.3 μm CO absorption band which extends from 2.32 μm to 2.37 μm.

CO_2 absorption bands at 2.01 and 2.06 μm

4.8.2.3 High Speed Interferometric Spectrometer. Another relevant AAFE investigation, conducted by the Jet Propulsion Laboratory, is entitled "Global Survey of Atmospheric Trace Constituents and Pollutants." The purpose of this investigation is to utilize a modified laboratory high speed interferometer in remote field tests to demonstrate the ability of the instrument to identify atmospheric pollutants without constant adjustment. Paralleling the initial field tests, the Principal Investigator proposes to design and fabricate an engineering model of the interferometer. This engineering model would be tested remotely in the field and then used in aircraft and/or balloon flights if the feasibility of such flights is demonstrated.

The proposed characteristics of the engineering model of the High Speed Fourier Interferometric Spectrometer are the following:

Size: Instrument 4.0 ft^3

Electronics 4.0 ft^3

Weight: 80 lbs

Power: 60 watts

Data Rate: 20,000 bits per second

View: 1.25° X 1.25° downward

Spectral Resolution: 0.12 cm^{-1}

Spectral Range: 2000 – 8000 cm^{-1}

4.8.3 SUMMARY

Sensing of atmospheric pollution from satellites is a new application never before attempted. However, in view of the possible consequences of unbridled pollution, it is important to develop remote pollution sensing techniques as soon as possible. A promising development is the Remote Gas Filter Correlation (RGFC) Analyzer whose characteristics are summarized in Table 4.8.1.

This instrument is of modest weight and power. It could be accommodated as the single sensor on a SATS class spacecraft, for an initial test. It is important to note, however, that for optimum data reduction, a knowledge of the atmospheric temperature profile and of the cloud cover is necessary. Beginning in 1972, the NOAA operational satellite will provide both types of data on a continuing basis. Hence, these data, in addition to worldwide radiosonde data, could be obtained for use in developing techniques for analyzing the RGFC Analyzer data on a global basis. However, the subsequent flight of the instrument on EOS, with correlative cloud cover and upper atmospheric sounder data available, would permit the sensing of pollutant concentration to higher accuracies and spatial resolutions.

Table 4.8-1

Atmospheric Pollution Sensor

Design Parameters	
IFOV, deg	5×5
Pointing	Nadir
Nodal crossing, LMT	0900, 1200, 1500
Spectral Range, μm	2-20
Modes	Reflected sunlight Thermal emission Direct sunlight (occultation)
Possible gases to be monitored	CO, CO_2 SO_2 NO, N_2O, NO_2 NH_3 CH_4
Sensor Characteristics	
Data rate, Mb/s	< 0.01
Power, watts	10
Weight, lb (kg)	30 (14)
Proj. Area, ft^2 (m^2)	0.7 (0.06)

4.8.4   REFERENCES

1. SCEP Work Groups, 1970: Man's Impact on the Global Environment. Report of the Study of Critical Environmental Problems (SCEP), sponsored by MIT, and held at Williamstown, Mass. in July 1970. MIT Press, Cambridge, Mass. 319 pp.

2. Rasool, S.I. and S.H. Schneider, 1971: Atmospheric Carbon Dioxide and Aerosols: Effects of Large Increases on Global Climate. Science, 173 (3992), 138-141 (9 July).

4.9 FUTURE SENSORS

4.9.1 INTRODUCTION

Several other classes of sensors were considered for the initial EOS payloads but were not specified explicitly for a variety of reasons, such as: additional research required to demonstrate the feasibility of a new instrument or measurement technique; important drawbacks exist although the measurement technique has been demonstrated; experience with data from forthcoming missions is needed before specifying improved instrumentation; or the instrument is highly specialized, but is proven in space applications, is small, light, and low in power and data requirements, and could reasonably be expected to be accommodated on any spacecraft configuration. Perhaps the most likely candidate for future EOS payloads, radar is, because of its general interest, treated in some depth in section 4.10.

4.9.2 TYPES OF MEASUREMENTS AND SENSORS

4.9.2.1 Polarization Measurements. Many types of instruments have been flown and are being developed for flight on meteorological and Earth resources satellites to obtain measurements in four dimensions, i.e., the (1) spatial and (2) temporal variations of the (3) intensity of radiation emerging from the top of the atmosphere in (4) different parts of the spectrum, ranging from ultraviolet to centimeter wavelengths. A fifth dimension in remote sensing, scarcely touched with respect to Earth Observations satellites to date, is the polarization of the emerging radiation. The use of polarization measurements more completely characterizes the radiation field and, hence, gives additional information concerning the nature of the scene being viewed. Coulson, Bouricius, and Gray [1] and Coulson [2] investigated the optical reflection properties of natural surfaces and found that there is a strong dependence of both the intensity and degree of polarization of the reflected radiation on the physical state of the surface (e.g., its moisture content), as well as on the angle of incidence of the radiation, the azimuth and elevation angles at which the surface is viewed, and the wavelength of the radiation. The possibility of determining the turbidity of the atmosphere and of inferring such parameters as atmospheric aerosol content, concentration, and distribution from visible radiation polarization measurements has been discussed by Sekera [3] and Hariharan [4] , reporting on research performed under NASA Grant NGR 05-007-041. An engineering model of a Visible Radiation Polarization Experiment has been constructed by General Electric under subcontract to UCLA (Principal Investigator: Professor Z. Sekera). UCLA is responsible for the development under an Advanced Applications Flight Experiments (AAFE) contract (see AAFE Program below). Recent research with polarization measurements in the visible suggests their application to the measurement of soil moisture [5] . The measurement of soil moisture was identified by the Joint Organizing Committee (JOC) of the Global Atmospheric Research Program (GARP) as a required measurement of the amount of water available for evaporation to increase the realism of the numerical forecast models. Aircraft flights of a polarimeter to investigate its ability to remotely sense a soil moisture parameter as well as turbidity and cloud particle size distributions are planned in the fall of 1971 under RTOP (Research Technology Objective and Plan) 160-44-53, "Remote Sensing Techniques for Atmospheric Structure and Surface Conditions Relevant to Meteorology." The results of these flights may well indicate a polarization experiment for a future satellite mission for the measurement of soil moisture, as well as possibly a polarization experiment to sense atmospheric turbidity and/or cloud particle size distributions.

4.9.2.2 LIDAR Measurements. LIght Detection and Ranging (LIDAR) is an optical 'radar' technique employing Light Amplification by Stimulated Emission of Radiation (laser) energy. Lidar is a generic, rather than a specific, technique and thus can be applied in a variety of forms to a wide range of research and operational problems. Research applications have largely been confined to ground-and-aircraft based systems to date and have included the investigation of dust in the high atmosphere; studies of air motion and turbulence revealed by cirrus and other clouds; boundary layer phenomena, as shown by variations in turbidity in the mixing layer; turbulence

and diffusion processes using suitable indicators; and investigations of the effects of cirrus and other particulate layers on the measurement of radiation in and through the Earth's atmosphere. The use of lidar in remote probing of the atmosphere has recently been reviewed by Collis [6].

Ground-based lidar systems are capable of probing the atmosphere up to 100 km. However, progress to date on developing a satellite lidar system has been limited by at least the following two primary reasons. (1) Compared to a ground-based system sensing the 30-km altitude, the lidar return from a satellite for an equivalent resolution depth would be down by a factor of 100. However, because of the greater effect of increased atmospheric density over the further $1/R^2$ diminution, the satellite signal in a 300-km orbit from the 1-km level would be below the ground-based 30-km signal by only a factor of 4.5. (2) A second severe limitation has been the very poor efficiency of solid-state lasers. Present methods of pumping imply large weight penalties for the power supply, e.g., a 400-km grid point density requirement with one pulse per grid point would need about the equivalent of 100 watts of continuous power [7].

Thus, it would appear that at the present time, a satellite borne lidar system is not in contention. However, with continuing research in this field, the situation may change dramatically in the near future.

4.9.2.3 <u>Sunglitter Measurements</u>. It has been shown by Cox and Munk [8, 9] that the surface of the ocean may be differentiated into small, mirrorlike, planar surfaces that have individual characteristic slopes. They found that, to a first approximation, the distribution of the slopes of these small elemental surfaces is Gaussian and that the variance varies linearly with the horizontal components of the surface wind speed. Thus, the possibility exists of remotely sensing the glitter pattern of reflected sunlight and, from it, inferring the surface wind speed and direction. Investigations of such applications have been made by Strong and McClain [10] and Strong and Ruff [11] for near-Earth satellites, and by Levanon [12] for geostationary satellites. A drawback of a sunglitter measuring system on a near-Earth satellite is the limited spatial coverage, constrained by the relatively narrow glitter swath (approximately paralleling the orbital track) and further constrained by the obscuration of the glitter by clouds whenever they occur. However, valuable correlations could be made in conjunction with measurements from all weather microwave sensors.

4.9.2.4 <u>Cameras</u>. Cameras of various configurations have flown on all meteorological satellites to date, a three-channel Return Beam Vidicon camera is scheduled to fly on ERTS-A and B, and a six-band Multispectral Photographic Facility (S-190) using 70 mm film will fly on Skylab. The future flight use of advanced camera systems is indicated, particularly after some experience has been gained with the ERTS and Skylab camera data.

4.9.2.5 <u>Auxiliary Space Science Measurements</u>. In one sense all near-Earth satellites operate within the confines of the upper atmosphere and therefore are affected by its density of charged and uncharged particles and by the perturbations of the gravitational and magnetic fields found within it. In the past, research meteorological satellites have carried "space science" experiments - usually of low weight, volume, power, and data characteristics - essentially on a non-interference basis, and it is expected that EOS will play a similar role.

As we look to the coming decade, it appears probable that there will be increased human activity at high altitudes and in space. Supersonic transports (SSTs) will probably fly in stratospheric airlanes, and a space shuttle will probably be developed to place unmanned satellites (like EOS) into orbit and, subsequently, to orbit modules of a permanent space station and service the space station with men and supplies. While it is possible in principle to design high altitude air and space flight vehicles to cope with all foreseeable environmental extremes, it is not always feasible to do so in terms of economic factors, mission objectives, and required system performance. Thus, there is a need to learn more about those aspects of the space environment that may adversely affect men and equipment in space.

For example, the Space Disturbance Forecast Center (SDFC) of NOAA (located in Boulder, Colorado) has indicated a need to make research observations of solar protons in the range 100 Kev-to-2 Gev concurrently with measurements of solar protons having energies up to 60 Mev now made routinely on NOAA operational satellites. Also, the SDFC has indicated a need to make measurements to the total energy deposited into the upper atmosphere by means of electrons and protons from the radiation belts having low energies in the range 1 Kev to 500 Kev.

The purpose of these measurements is to investigate energy exchange processes across the upper atmospheric boundary and to develop models and techniques for forecasting dangerous conditions for high altitude manned flight as the era of supersonic transports and manned space stations approaches.

In the aforementioned examples, the SDFC has indicated an interest in proposing these specialized experiments in the role of the traditional Principal Investigator. The development and flight of small, simple experiments of this type can be included on a non-interference basis on the EOS satellites.

The discussion above of future sensors is extremely limited. Many other sensors are being and will undoubtedly continue to be developed by the broad scientific community throughout Government, the Universities, and Industry. The Advanced Applications Flight Experiments program described below, is one mechanism for developing these new sensors.

4.9.3   ADVANCED APPLICATIONS FLIGHT EXPERIMENTS (AAFE) PROGRAM

The Advanced Applications Flight Experiments (AAFE) program is intended to develop an effective inventory of space application experiments from which future missions and flight experiments for approved flights may be selected. Past experience has shown that when specific flight opportunities arise, the time left for general solicitation is frequently inadequate. In the AAFE program, emphasis is placed on the early solution of technical problems, permitting engineering development without commitment to a definite flight mission. The AAFE program, which has been in effect for two years, is progressing to the point where engineering models of new instruments will soon be tested in the laboratory as well as in the field, on balloons, and on aircraft. After evaluation of their performance, the most promising experiments will become candidates for space in the time frame immediately. following the Nimbus, ERTS, and Skylab series of missions. Thus, the AAFE program is of direct relevance to the concept of an Earth Observatory Satellite.

A summary of the 29 experiments under development in the AAFE program, 11 of which are FY 70 starts and 18 of which are FY 71 starts, is shown in Attachment C. It is expected that an additional group of FY-72 starts will be selected in the next few months from the proposals received in April 1971.

4.9.4   REFERENCES

1. Coulson, K.L., G.M. Bouricius, and E.L. Gray, 1965: Optical Reflection Properties of Natural Surfaces. J. Geophys. Res., 70, 4601-4611.

2. Coulson, K.L., 1968: Effect of Surface Reflection on the Angular and Spectral Distribution of Skylight. J. Atmos Sci. 25, 759-770.

3. Sekera, Z. 1967: Determination of Atmospheric Parameters from Measurement of Polarization of Upward Radiation by Satellite or Space Probe. ICARUS, 6, 348-359.

4. Hariharan, T.A., 1969: Polarization of Reflected Solar Radiation Over Land, Sea, and Cloud Surfaces. Pure and Applied Geophysics, 75, (IV), 222-229.

5. COSPAR Working Group 6, 1971: The Feasibility of the First GARP Global Experiment (FGGE) and the Criticality of Initiating Systems Planning. Report to the JOC (and Annex K thereto: Possibilities of Observing Soil Moisture from Spacecraft as Required for FGGE)

6. Collis, R.T.H., 1969: LIDAR, pp 147-171 in Atmospheric Exploration by Remote Probes, Vol. 2; Proceedings of the Scientific Meetings of the Panel on Remote Atmospheric Probing. National Academy of Sciences - National Research Council, 698 pp.

7. Panel on Remote Atmospheric Probing, 1969: Atmospheric Exploration by Remote Probes, Vol. 1; Summary and Recommendations. Final report to the Committee on Atmospheric Sciences, National Academy of Sciences - National Research Council, 61 pp.

8. Cox, C. and W. Munk, 1954: Measurement of the Roughness of the Sea Surface from Photographs of the Sun's Glitter, J. Opt. Soc. Am., 44, 838-850.

9. Cox, C. and W. Munk, 1956: Slopes of the Sea Surface Deduced from Photographs of Sun Glitter. Bull, Scripps Inst. Oceanography, 6 (9), 401-488.

10. Strong, Alan E. and E. Paul McClain, 1969: Sea-State Measurements from Satellites. Mariners Weather Log, 13 (5), 205.

11. Strong, Alan E. and Irwin S. Ruff, 1970: Utilizing Satellite Observed Solar Reflections from the Sea Surface as an Indicator of Surface Wind Speeds. Remote Sensing of Environment, 1, 181-185.

12. Levanon, N., 1968: Determination of the Sea Surface Slopes Distribution and Wind Velocity Using Sun Glitter Viewed from a Synchronous Satellite, pp 1-15 in Meteorological Satellite Instrumentation and Data Processing, Final Scientific Report on Contract NASw-65, Dept of Meteorology, The University of Wisconsin, 179 pp.

4.10 RADAR IN EARTH RESOURCES STUDIES

4.10.1 INTRODUCTION

In the visible and near infrared regions of the spectrum, sensors operating as imagery systems depend on solar illumination and are, therefore, in this sense, bistatic "active" systems. However, occultation by cloud cover, precipitation, gaseous absorption and emissions may either bias these sensors' outputs or render them inoperative by reducing or eliminating the signal source.

Active radar systems, carrying their own signal sources - the continuously transmitted (C.W.) monofrequency signal or the pulsed signal - can be operated monostatically or bistatically. Aircraft (Military) radar systems generally exemplify the first mode while ground-based mortar and ballistic missile detection systems employ the latter mode. As analytical instruments, bistatic radar systems have been employed for data gathering of planetary bodies - Earth, Moon, Mars, Venus-ice fields, and the NASA Echo - II Communications Satellite. The active system, therefore, if the wavelength is so chosen as to utilize the natural windows of the microwave spectrum (1 to 0.01 meter), becomes essentially independent of weather states, ionospheric and tropospheric anomalous propagation and of solar illumination levels and eclipses. "Corrections" for radiometer "noise-like" signals are based upon the extraction of "noise-power equivalent" emissions of a radiometric target from which are subtracted the "noise-power equivalent" signal from a reference standard at known temperature T_r. This is the well-known Dicke-switched differential radiometer system. A radar, however, operates at maximum efficiency as a coherent system - i.e., the radar emitted signal pulse, upon reflection from the target, is correlated against a delayed portion of the emitted signal. Any perturbation of the intervening ionosphere or troposphere or signal jitter is translated into a "noise factor" which is incoherent with the correlated signal. Hence, a coherent, active radar system operating with a readily achievable 10db or better signal to noise ratio is far less susceptible to noise errors than is the radiometer noise measuring system. In fact, the radiometer system reads a total "temperature": $T_{BR} = (T_{B1} + T_{B2} + T_{B3}) = E_t$ where the emissivity E_t is attributable not only to the target area under consideration, but has contributions of E_{t1}, E_{t2}, as self emission and attenuation from every constituent layer between the target surface and the radiometer antenna system. Hence, the radiometer's greatest problem is to somehow measure and sort out the emissivities in situ, or to compute these correction factors. Furthermore, since the radiometer signal is of "noise" quality, no correlation techniques can be applied to the measured noise data so as to enhance the signal or to apply power spectrum analyses. Correlation is possible in a radar system which measures a reflection coefficient σ_0 where σ_0 is defined as the differential backscattering cross section and is utilized as a normalized signal level from a characteristic target per unit area of that target as a function of polarization, angle of incidence, and target character determined by the complex dielectric constant. All those characteristics affect the radiometer emissivity measurements - including thermometeric temperature insofar as it affects the real or imaginary constituents of the complex dielectric constant (ϵ^*). The reflection σ_0 is related to the material emissivity by $\sigma_0 = 1 - \epsilon^*$, actually $\epsilon + r + \alpha = 1$ where r is the reflection coefficient and the attenuation α is $<< 1$ and may be utilized as a link between the two instruments. A further, important characteristic of the active radar system is the depth of penetration into the target materials as functions of frequency, complex dielectric constant, polarizaton and wavelength. The active radar, therefore, dependent on these parameters, can penetrate (particularly dry soils where the real part of $\epsilon^* = 4$) to a depth of 1 to 3 wavelengths.

4.10.2 APPLICATIONS AND TECHNIQUES OF RADAR

Extensive aircraft and ground site radar plots of σ_0 for earth, soil, ice fields, oceans, and high resolution ($<< 100$ feet) data have been plotted. From these, conversions to emissivity and predictions of the radiometric, apparent blackbody T_{BR} temperatures can be derived and compared with actual radiometeric observations. Such static data, cannot be extended to dynamic conditions for water bodies where wind driven waves are developed. Statistically derived σ_0 data, for wind speeds, characteristic wave heights and surface conditions,

including foam, have been verified by active radar on aircraft flights; furthermore, as a special case of a nadir-looking radar mode, height-finding altimetry is possible to the extent that short pulse (nanosecond) radar with data analysis of the backscattered, distorted pulse can determine altitude (from 500Km altitudes) to within 1-3 meters and the sea surface (sea state) characteristics from which wind speeds may be determined.

4.10.2.1 Real Aperture Radar and Radiometer System.

The radar system, with an antenna as a "real aperture" provides a resolution element of $\beta_{\theta,\phi} = k \dfrac{\lambda}{L_{\theta,\phi}}$ radians — if resolution is defined as the angular beamwidth β at 3db points below the peak antenna gain axis at θ (O). Radiometer systems sharing the same antenna with the radar achieve the same resolution or may choose to integrate all energy within the main beam contained within the first nulls of the radiation envelope For a beam of cross sectional dimensions of $\beta_{\theta,\phi}$ at 3db points $k_1 = 1.45$ radians, while for $\beta_{\theta,\phi}$ between nulls, $k_2 = 2.0$ radians. Both antenna system efficiency factors are n = 0.67 and side lobes are acceptably suppressed to 32 db below the maximum antenna gain figure. λ is the wavelength and $L_{\theta,\phi}$ is the dimension in the θ and ϕ planes, respectively.

The radar system as well as the radiometer, can share the same polarization control inherent in the design of the real aperture antenna. Where electronically steerable antennas have beam steering under ferrite control, nanosecond pulse length systems may be constrained by the finite rise time of the ferrites; however, ferrite developments offer improved response times in the near future and synthetic aperture systems do not, at present, utilize electronically scanned beams. In the future, the combination of an electronically scanned antenna system, for a transverse swath coverage of 300 km (θ_0 variable between 75° and 55°) and programmed pulse duration τ, would yield large swath coverage and high resolution (ΔW, ΔA) capabilities for global coverage.

A most important quality of the radar system "real aperture" antenna application is that the two volumetric beam dimensions are controlled by the θ, ϕ plane aperture dimensions. Unlike the radiometer, the range dimension control of the radar is utilized to cut off in time the area extent of illumination by control of the pulse duration time τ and the interval between pulses. Figure 4.10-1 indicates that a beam, at aspect angle ϕ_0 illuminates a region projected on the surface
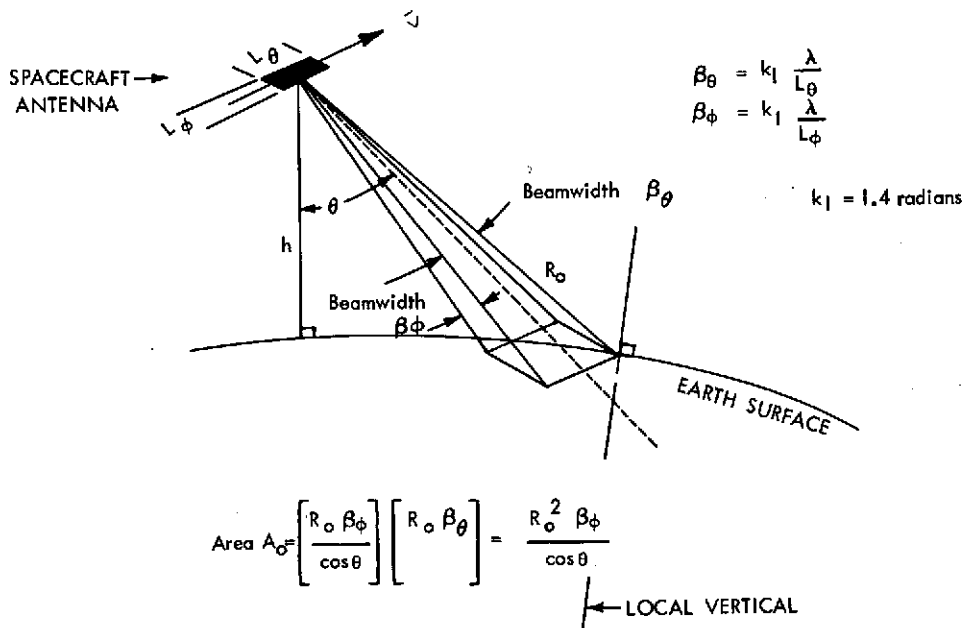

Figure 4.10-1. Real Aperture Antenna

(land, ocean) $A_0 = \dfrac{R_0^2 \beta_\theta \beta_\phi}{\cos \theta_0}$ which could serve to define the radar backscatter area or $\sigma_0 = \dfrac{\sigma}{A_0}$ or for a radiometer as the illuminated Area Ao. Since the radiometer has no time/area gating function, all energy contributions during the radiometer detector integration period of 20-100 milliseconds will determine the radiometeric input. The radar, with control of pulse duration time, can almost arbitrarily confine the area of illumination to the first Fresnel Zone and exclude contributions in time/range area by cutting off the illumination (transmitter power) by the pulse gating. As seen in the diagram, Figure 4.10-2, a pulse of duration τ is intercepted by the earth/
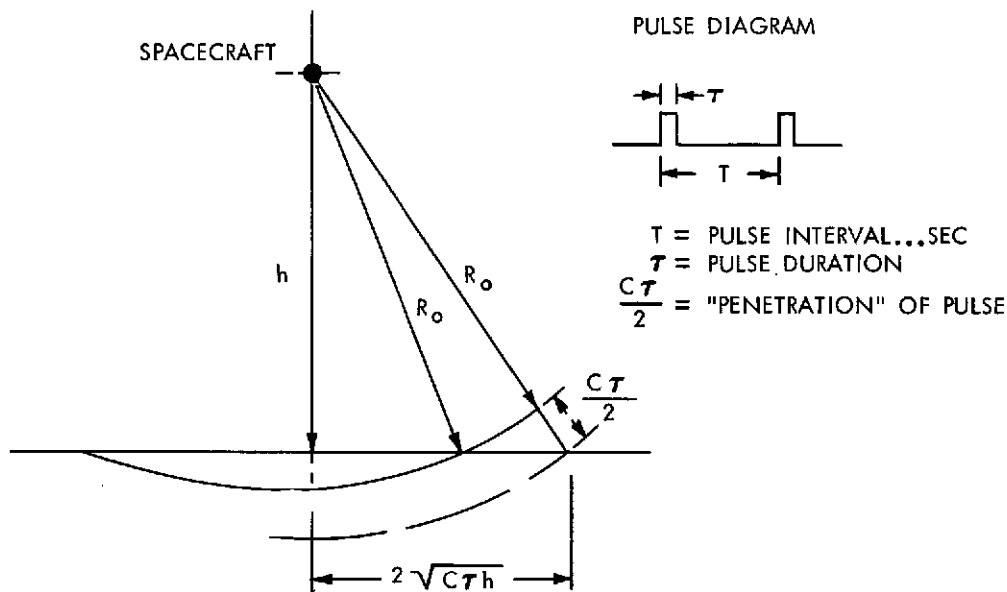
Figure 4.10-2.   Interception Of the Radar Beam by Earth/Water Surface

water surface and continues to spread; during the interval between incidence and the outer portion of the antenna beam (3db points) the pulse duration τ controls the spread of energy, within

an annular radius $q = 2\sqrt{c\tau h}$ where c is the velocity of propagation, τ =pulse duration and

h=the altitude. Another control parameter is the fact that the radiometer integration period is tens of milliseconds in order to achieve an acceptable temperature discrimination of

$\Delta T_B = \dfrac{2(T_e + T_a)}{\sqrt{Bt}} = 1^\circ K,$ where B is the detector bandwidth and t is its integration

time and T_e and T_a are the noise power equivalent temperatures of the radiometer input signal and system temperature at the antenna. The radar, however, is computed to provide a single pulse sensitivity, so that even for 10-100 nanosecond pulse durations, the backscatter value σ_0 is sufficient to characterize the observed target area. Thus, for dynamic conditions of turbulent seas, meterological turbulence and rain, the radar provides analytical samples at nanosecond intervals. If many such pulse intervals were recorded for the same target area, signal averaging would tend to significantly improve the statistical data description.

4.10.2.2 Synthetic Aperture Radar System. A further extension of radar parameters is the two dimensional control of the azimuth, along-track resolution and the cross-track resolution of the "synthetic aperture antenna"-radar system. As shown in Figure 4.10-3, the analogy of a point source (omnidirectional response) antenna moving along a flight path, with velocity $\overline{V}$ and direction indicated, may collect signal returns from a point target Q. The amplitude of the collected signal at positions Q_1, Q_2, . . . Qn is determined by the radar return characteristic σ_0 of the target as functions of λ , incident angle θ_0 , polarization, sea state, salinity, and soil moisture (for a generalized target). The change in amplitude versus ΔR in range is considered small for total flight path lengths $L \ll (R + \Delta R)$. L may be in the order of 1-10 meters compared with R $\geq$

4-76

500 Km. The phase changes, however, are determined by the factor $\phi_n = \frac{2\pi}{\lambda}(\Delta R_n)$. Over a flight path of dimension L, the phase angle continuously changes and must be recorded at intervals corresponding to the sampling of amplitudes $(A_1 \ldots A_n)$ along the effective "synthetic" aperture equivalent to path length L. The production of an "image" in this system is, therefore, based upon the collection of amplitude and phase history of signals collected along a synthesized antenna composed of an arbitrarily small aperture to avoid illumination biasing of the target area Q. The elemental antenna is moved along a path of dimension L along the track of velocity vector V of the spacecraft or aircraft. After recording of the amplitude and phase history, these data are then matched against a reference oscillator as a coherent detection scheme as so to reconstruct a real image with phase errors $\phi_1, \phi_2 \ldots \phi_n$ corrected for maximum gain and resolution for a real aperture equivalent of length L. Although a real aperture (resolution $\beta = k\frac{\lambda}{L}$) may be diffraction limited as a function of λ , the synthetic aperture system is theoretically unlimited, with a resolution, ΔA along track, of $\frac{L}{2}$ but in practice reduced to $\Delta A = L$. The resolution ΔA

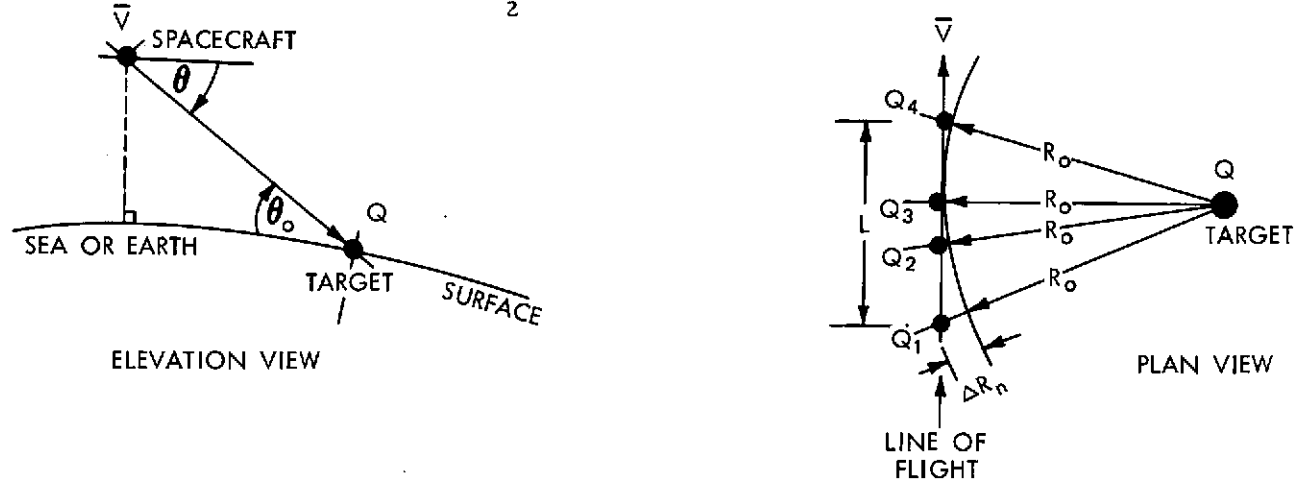ELEVATION VIEW   PLAN VIEW

LINE OF
FLIGHT

Figure 4.10-3.   Synthetic Aperture Development

is independent of altitude. See Figure 4.10-4. The key to the coherent radar detection and signal processing is the presence and stability of the reference local oscillator which provides the phase reference for the transmitter pulse initiation time, the range-gating function and the coherent reference for the received pulse correlation and processing to obtain the processed data for each resolution cell of dimension L. The oscillator stability is 10^{-14} short-term with long term drift either controlled or corrected and is within the state-of-the-art as manifested by such equipment now flying on aircraft. The "synthetic aperture" antenna system, is free of the diffraction effects of the real aperture. The choice of swath width (W) (transverse to flight direction), resolution ΔA (along flight path), pulse duraction time τ , and pulse interval are interrelated. The procedures for choice of parameters and determination of the average power consumption for a system which might be applicable to EOS future systems are described in Figure 4.10-5. It should be emphasized that for 500-1000 km altitudes and resolution elements of 10 meters by 30 meters (cross track) that average power consumption is approximately 1 K.W. and includes the recording of signal amplitude and phases on 35 mm photographic film or video tape records with a video bandwidth requirement of 6 MHz. No further processing is contemplated on board the spacecraft. Data transmission from the analog recording converted to digitized data and r. f. carrier modulation would require a 30-35 MHz r. f. band occupancy for transmission to ground terminals directly or via a Tracking and Data Relay Satellite System. At the ground processing station the digital data could be reconverted to continuous-strip photographic-quality images.

A A = ALONG TRACK (AZIMUTH) RESOLUTION
A W = CROSS TRACK RESOLUTION
θ = DEPRESSION ANGLE
θ_0 = ASPECT ANGLE AT TARGET AREA

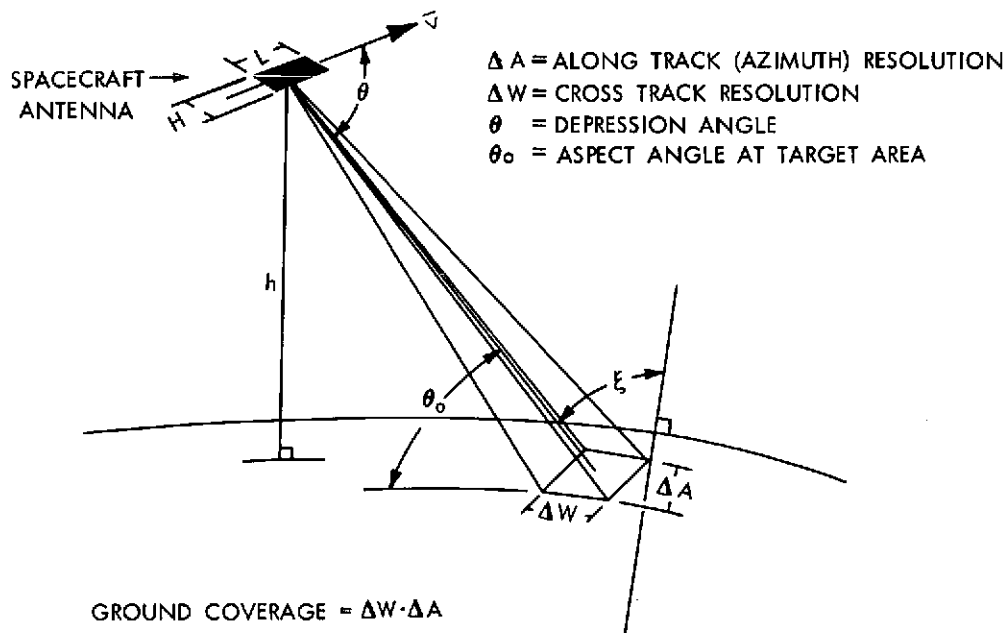GROUND COVERAGE = $\Delta W \cdot \Delta A$

Figure 4.10-4. Synthetic Aperture Antenna

4.10.2.3 Choice of Resolution Elements. The initial design parameter of the synthetic aperture radar system is the choice of resolution elements ΔA (along track) and ΔW (across track). The average power required for the radar is proportional to $\frac{1}{\Delta W \cos^2 \theta_0}$, so that the initial choices of θ_0 would critically determine the average power required for a ground target area $\cdot \Delta W \cdot A = \Delta W \cdot L$. In fact, for detection of oil on sea surfaces, a high aspect angle $\theta_0 \approx 75^0$ is recommended, whereas for general sea state measurements $\theta_0 \approx 55^0$; further, for analytic data of σ_0 versus hydrological, ice, and crop data θ_0 should vary between 90^0 (nadir) and 10^0 (lower limit toward grazing.) The nadir look is ideal for radar calibration, highest resolution capability (minimum beam spread), and for sea height-altimetry mode and sea state measurements. It may be desirable to incorporate a tiltable antenna system, in transverse dimensions, to permit a variable θ_0 aspect angle to satisfy these diverse requirements. Concurrently, the ΔW target area dimension may be chosen so that $\Delta W = \Delta L$(a square resolution element), however, for values of $\Delta W = \Delta L = 10$ meters, the average power required would be several kilowatts. A compromise resolution element, particularly suited to agricultural crop species identification (on a statistical sample basis) would be the $\Delta A = 10$ meters and $\Delta W = 30$ meters. This is suggested by (Ref. 1) the fact that as a sampling area increases the number of detectable species is increased exponentially (to upper and lower asymptotic bounds). The $\Delta A = 10$ meters resolution element is sufficiently small to be useful for ice targets, to delineate ice-clear paths, hydrological surveys and land faults and general topographical features. For sea state and large areas of homogeneous nature the ground resolution may be increased to kilometer dimensions and the swath dimensions in tens of kilometers. As seen in Figure 4.10-6, the choice of angle θ_0 and the surface roughness characteristics vary over wide ranges, for example, the sea coupled to wind-generated waves has a normalized backscatter return (nomalized to normal incidence $\xi = 90^0$) that varies from 0 to + 10db for moderate wind velocities and varies between -15db to +5 db for the same wind velocities but angle of incidence change of 15^0. For larger angles of incidence, $\xi > 30^0$, σ_0 drops to -15db. The radar system must be designed for a 40db (10^4 ratio of signal power) excursion for such dynamic conditions, and consequently the transmitter average power, (Pav.) is directly affected. The radiometer system generally provides for a dynamic signal excursion of 15db, and for emissivity ranges of less than 10db. The radar dynamic range is generally set to provide for low incident angles $\xi_c = 75^0$ and rough surfaces both of which yield values of σ_0

Specify

1. Azumith Resolution — ΔA — meters
2. Orbit Altitude — h — kilometers
3. Aspect Angle — θ_0 — degrees
4. Frequency — f — (GHz)
5. Receiver Noise Figure — $\overline{NF}$ — $^\circ K$
6. Cross Track Resolution — ΔW — meters
7. Antenna Length — L — meters
8. Pulse Repetition Rate — PRF — pulses per second
9. Swath Width — W — meters
10. Antenna Height — H — meters
11. Atmospheric Losses — La — $\left(\frac{1}{power\ ratio}\right)$
12. System Losses — Ls — $\left(\frac{1}{power\ ratio}\right)$
13. Backscattering Coefficient — σ_0 — (power ratio)
14. Pulse Length — τ — seconds
15. Average Power Radiated — Pav — watts
16. Average Input Power — P_{in} — watts

● $PRF = \dfrac{130 \times 10^3}{(1 + h/6379)^{3/2}}$ pulses per second

● Swath Width $W = \dfrac{0.6\ c}{\overline{PRF}\cos\theta_0}$ c = velocity of propagation

● $H = \dfrac{h}{wf\ sin^2\theta_0}$ antenna height

Figure 4.10-5   Synthetic Aperture Antenna Choice of Parameters

(normalized) = -40db because of low values of reflectivity, multiple, rough scattering (diffuse scattering), and shadowing of rough surfaces. It is this latter characteristic of the radar reflectivity mode, together with the depolarization effects, which provide the analytical basis for

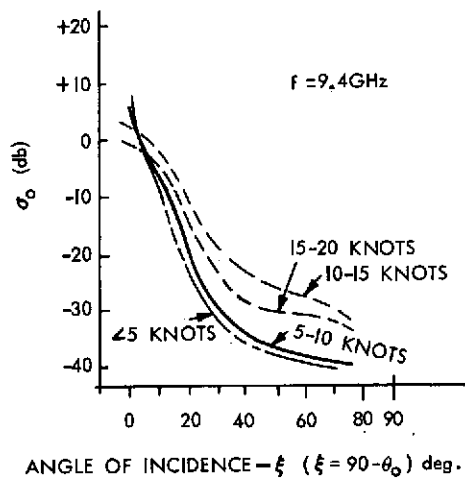ANGLE OF INCIDENCE — ξ ($\xi = 90-\theta_0$) deg.

Figure 4.10-6.   Radar Backscatter (Sea and Wind Velocity)

determination of sea surface state on a topographic feature plot when the resolution element is in the order of tens of meters. Where a blanket of foam is present on the sea surface, the ratio of foam coverage to total area, for resolution elements of 10-50 km, is generally less than 30%; hence, a high resolution element of 1 km or less, would provide a "beam filling" capacity for best analysis of foam contribution. The target area assessment of foam and spray effects is linearly related to the ratio of foam area to no-foam area. Again, according to the Rayleigh criterion of selecting an operating wavelength which is either $\lambda/4$ for maximum signal return, or $\lambda/2$ for penetration of the foam/spray layer, the evaluation of foam cover can be treated as an impedance discontinuity.

4.10.3 SYNTHETIC APERTURE SYSTEM DESIGN

Example: (Frequency=10 GHz) As indicated in Figure 4.10-5 the specified input parameters azimuth resolution ΔA, altitude h, aspect angle θ. , frequency f, and receiver noise figure NF are selected. The antenna length $L = \Delta A$, and the pulse repetition rate PRF, swath with W and antenna dimension H are determined from equations in Figure 4.10-5. For this example $\Delta A =$ 10 meters. The average radiated Power required is of the form:

$$Pav = K f \overline{NF} \left(\frac{Lv}{\sigma_0}\right)\left(\frac{h}{v}\right)\left(\Delta w \cos^2\theta_0\right)^{-1/2} \text{watts}$$

The quantity $K = .0254, f(GHz)$ - assumed to be 10GHz, NF is determined from state of the art to' be 3.5db (2.24 power ratio) for an uncooled parametric amplifier and 0.3db for a cooled para- meteric amplifier. The atmospheric loss figure La is less than 1db (1.26 power) except for severe thunderstorm activities. The reflection coefficient of the ocean surface, (Ref. 2) Figure 4.10-6 shows an average cross section as a function of angle of incidence ($\xi = 90^0 - \theta_0$) and wind speeds 0-20 knots coupled to the ocean surface. For an aspect angle $\theta_0 = 75^0$, $\sigma_0 = -17db = 0.063$ power ratio. The ratio of altitude of the radar system to the ground track velocity for a circular orbit is given by $\frac{h}{v} = \frac{h}{4.275 (1 + h/r_0)^{3/2}}$ where h and r_0 (the earth radius) are in the same units of measurement. For 556 km, $\frac{h}{V} = 80$, and for 926 km, $\frac{h}{V} = 140$. $\Delta W = 30$ meters is selected as a parameter.

The average transmitted power required is 136 watts for altitude of 555.6 km; the transmitter, however, has an assumed efficiency of 0.30; the total input power is now construed to include transmitter efficiency and receiver electronics, therefore, the total power required is:

P total = (Pav (3.33) + 75) watts

In this example P total = 136 (3.33) + 75 = 528 watts for the side looking synthetic aperture radar with the summarized characteristics for sea state and including oil slick observations: Resolu- tion area: $\Delta A = 10m$, $\Delta W = 30m$, f=10GHz, $\theta_0 = 75^0$, $\sigma_0 = -17$ db (moderate rough sea). Antenna dimensions 10 meter length X 0.1 meter. Additional operating parameters such as pulse duration time $\tau = 2 \Delta W \cos\theta_0$ nanoseconds and radar system bandwidth are: pulse duration (W=300 meters) = 52 nanoseconds and a bandwidth of 20 MHz.

In parametric form, a plot of cross track resolution (ΔW) for an in-track assumed resolution of 10 meters is shown in Figure 4.10-7 as a function of altitude h and total input power, for frequency f = 10 GHz and other parameters as cited.

The mechanical dimensions and weights for the example system are:

Antenna: 10 meters X 0.1 meter (folded antenna)
Weight: 61.5 kilograms

Transmitter/Receiver - 64 kilograms
Pointing accuracy: 0.02 mradian (10 meter resolution)
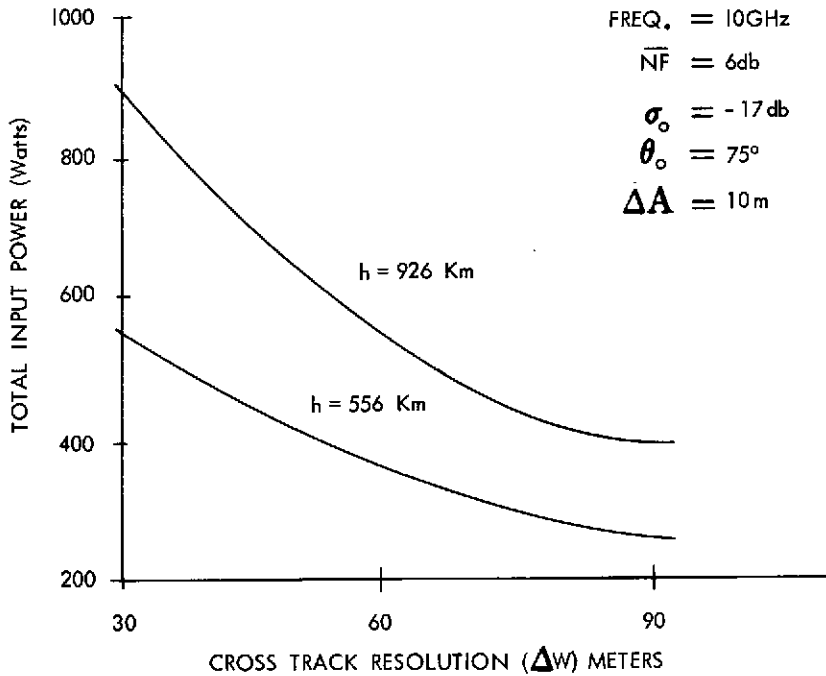Data Transmission Bandwidth - 30 to 35 MHz

Figure 4.10-7.   Synthetic Aperture Radar

4.10.4   SUMMARY AND CONCLUSIONS

The "synthetic aperture" (active) radar system is within the state-of-the art of technical develop-
ment. In conjunction with appropriate wavelengths it can function as an all-weather, night and
day analytical sensor for the Earth Observatory Satellite System. The choice of variables is
sufficiently great to provide for resolution elements as small as (1 meter)^2 independent of space-
craft/aircraft altitudes. The power requirements are in the order of kilowatts; however, the most
significant improvements in transmitter efficiency (better than the nominal 30% today) and receiver
noise figures, would linearly reduce such power requirements.

4.10.5   REFERENCES

1   Cain, S.A., 1938, "The Species Area Curve", American Midland Naturalist, 19:513-581

2   Grant and Yaplee "Backscattering from Land and Water", proceedings IRE, July 1957.

4.11 ACRONYMS AND ABBREVIATIONS

SCMR	Surface Composition Mapping Radiometer
NOAA	National Oceanic and Atmospheric Administration
VHRR	Very High Resolution Radiometer
IFOV	Instantaneous Field of View
K	Kelvin
μ m	micrometers
mr	milliradians
NE$\Delta\rho$	Noise Equivalent Radiance Difference
Hg Cd Te	Mercury-Cadmium-Telluride
SSTIR	Sea Surface Temperature Imaging Radiometer
SATS	Small Applications Technology Satellite
n.m.	nautical miles
GARP	Global Atmospheric Research Program
WWW	World Weather Watch
WMO	World Meteorological Organization
D*	Specific Detectivity
MSC	Manned Spacecraft Center
SIS	Scanning Imaging Spectrometer
PMT	Photomultiplier Tube
ERTS	Earth Resources Technology Satellite
SPOC	Spacecraft Oceanography Project (U.S. Navy)
In As	Indium Arsenide
ESMR	Electrically Scanned Microwave Radiometer
AAFE	Advanced Applications Flight Experiments
LRIR	Limb Radiance Inversion Radiometer
RGFC	Remote Gas Filter Correlation Analyzer
COPE	Carbon Monoxide Pollution Experiment

RTOP   Research and Technology Operating Plan

LIDAR   Light Detection and Ranging

SECTION 5

MISSION PROFILE AND PAYLOAD SELECTION

SECTION

MISSION PROFILE AND PAYLOAD SELECTION

SECTION 5

MISSION PROFILE AND PAYLOAD SELECTION

5.1 STUDY APPROACH

A major element of the present study has been a series of trade-off analyses involving payloads and spacecraft. The payloads considered are illustrative in that they represent sensor groupings which meet in varying degree the data needs of the earth observatory disciplines as presently understood, as well as the probable course of sensor evolution. The requirements which these payloads place on the space platform have been developed, and the scale of the space platform is considered in the light of current and future launch vehicle capability. The results of these analyses provide a basis for program definition, not only for EOS A and B but also for follow-on spacecraft. A payload selection was also made for the ERTS/Nimbus spacecraft to permit evaluation of a program based on a continued use of this spacecraft system.

In the course of the trade-off analyses, the full set of seven key sensors described in Section 4 was considered as a combined payload for a single spacecraft. To further evaluate the relationship between spacecraft and launch vehicle capability, payloads were developed for a new EOS spacecraft design which utilizes the full capability of the Delta launch vehicle with an 8-foot diameter shroud (Delta 2910). For such a spacecraft two launches are required to meet all mission goals. In order to illustrate a mission for the late 1970's two payload selections were made which indicate that the probable course of sensor development will require a growth in the EOS design to approximately double the power and weight, and would make good use of the capabilities of the Space Shuttle System.

5.2 MISSION PROFILE

The instruments for remote sensing and the measurements that each can make have been shown in Section 4 to have considerable value individually. However, measurements taken at the same time and place by several sensors, can be expected to combine synergistically to yield a greater result than the sum of the measurements taken separately. Table 5.2-1 is a "Mission Matrix" which has been included to illustrate this point. Specific measurement parameters are grouped under the four Earth Observation Discipline Areas. The three symbols, P, S, and C, denote a level of correspondence between data and the goals of the EOS Disciplines.

- ● P   identifies a primary measurement of a given parameter

- ● S   identifies a sensor providing supporting data which (although its nature is of primary importance to a given parameter) is considered to be secondary because of a shortcoming in one or more characteristics, (e.g. spatial or spectral resolution may be somewhat less than optimum).

- ● C   identifies a sensor making measurements essentially of correlative importance with respect to other primary or supporting measurements.

The matrix illustrates the interdisciplinary aspect of the data, a key consideration in planning for the EOS Mission.

- ● Each facility sensor, while serving a primary purpose, provides correlative data for other disciplinary areas.

- ● Each disciplinary area is supported by more than one sensor.

Table 5.2-1

EOS Mission Matrix[1]

	S.S. Temp. I. Rad.	Cl. Physics Rad.	Oceanic S. Spectro.	Thematic Map.	P.M. Microwave Rad.	U.S. Sounder	A. Pollution
OCEAN SURVEY							
Sea Surface Temperature	P		C	C	P		
Sea Surface Roughness	C				P		
Sea Surface Composition (Color)	C		P				
Sea Surface Phase (Ice ve. Liquid)	C				P		
Sea Surface Pollution	C		P	C			
Cloud Cover Survey	P				C		
Precipitation Survey	C	P			P		
Radiation Budget Over the Oceans	P				C		
Shoal and Coastal Mapping[2]	C		C	P			
Sea Surface Currents[3]	C		C	C			
Sea Surface Geopotential Figure[4]	C		C				
ENVIRONMENTAL QUALITY							
Atmospheric Pollution	C					C	P
Sea Surface Pollution	C		P				
TERRESTRIAL SURVEY							
— Agriculture and Forestry							
Terrain Mapping	C			P			
Soil Moisture	C			C	S		
Snow/Ice Survey	C			P	S		
Atmospheric Pollution	C						P
— Geology and Mineral Resources							
Earth Surface Composition	C			P			
Soil Moisture	C			C	S		
— Geography, Cartography, and Cultural Res.							
Terrain Mapping	C			P			
Soil Moisture	C			C	S		
Snow/Ice Survey	C			P	S		
Atmospheric Pollution	C						P
— Hydrology and Water Resources							
Terrain Mapping	C			P			
Soil Moisture	C			C	S		
Snow/Ice Survey	C			P	S		
METEOROLOGY							
Sea Surface Temperature	P		C	C	P		
Sea Surface Winds (Inferred fm. Roughness)	C				P		
Sea Surface Phase (Ice vs. Liquid)	C				P		
Cloud Cover Survey	P	P			C		
Precipitation Survey	C	P			P		
Cloud Composition (Ice vs. Liquid Water)	C	P			C		
Cloud Thickness	C	P					
Cloud Density of Condensed Water	C	P			C		
Cloud Drop Size Parameter	C	P			C		
Cloud Top Pressure Level	C	P					
Upper Atmospheric Temperature	C					P	
Upper Atmospheric Composition[5]	C					P	
Soil Moisture (Garp-Scale)	C			C	P		
Snow-Ice Survey	C			C	P		
Radiation Budget	P	C					
Atmospheric Pollution	C						P

NOTES:

1. Visible and infrared imagery produced from the 0.754μ m and 11μ m data of the Cloud Physics Radiometer is considered to be generally of correlative value for all other types of measurements.

2. It is possible to replace one of the channels of the Thematic Mapper with a blue (0.44-0.48 μm) channel for purposes of shoal and coastal mapping. However, to achieve an NE$\Delta\rho$ (noise equivalent reflectance difference) of 0.25% with a spatial resolution corresponding to a target size equal to the IFOV (instantaneous field of view), results in a degraded spatial resolution of about 600 meters.

3. The capability of collecting data from floating platforms (e.g., buoys) of known location and, additionally, of determining the sequential positions of free-floating platforms is considered to be an important application of space technology to ocean surveys. However, because of plans to provide continuing facilities making these capabilities available on the polar orbiting (TIROS N) and geostationary (SMS/GOES) operational environmental satellites, such systems are assumed to be available and, therefore, are not explicitly specified for the EOS missions.

4. The making of altimetric measurements of the sea surface geopotential figure is considered to be an important application of space technology to ocean surveys. An altimeter on Skylab will make initial measurements of this type, but a very limited time totalling only about 45 minutes will be available for this experiment. Optimum measurements of this type to attain accuracies within centimeters require a dynamically quiet spacecraft with satellite-to-satellite tracking and corner reflectors. High quality altimetric measurements are being planned as part of the Earth Physics Program, beginning with a proposed GEOS-C (Geodetic Satellite) experiment in 1973-74, followed by a SATS (Small Applications Technology Satellite) mission one or two years later. Therefore, altimetric measurements of the ocean surface are assumed to be available concurrently and are not explicitly specified for the EOS missions.

5. Upper atmospheric measurements of composition may also have a direct application to Environmental Quality. For example the report of the Study of Critical Environmental Problems recommends that before large-scale operation of SST's begins, a program be initiated "to monitor the lower stratosphere for water vapor, cloudiness, oxides of nitrogen and sulfur, hydrocarbons, and particles." Some of the sounders being considered do have the capability of monitoring stratospheric water vapor content (and ozone) and may have the capability of monitoring other of the aforementioned gases as well.

Because of this interdisciplinary aspect of the mission there is a natural temptation to consider all sensors for a single launch. Payload and payload support characteristics pertinent to the definition of a spacecraft and launch vehicle for such a single mission are given in Table 5.2-2. Since total spacecraft weight ordinarily ranges between 3 and 5 times the payload weight it is evident that such a mission would exceed the 2400 - 2600 lb total launch capability of the Delta 2910.

Utilizing the Titan launch vehicle capability and the spacecraft designs developed later in this report, a payload weight of 2500 lb, with 1200 watts available, could launch such a full payload and would permit a spacecraft with a margin of 1370 lb and 700 watts allocatable to sensors developed by principal investigators. This margin would be adequate for a Radar system or might be utilized to develop new instruments of other kinds. The Space Shuttle would of course provide a similar capability. This launch capability is not currently planned for WTR in the mid-seventies (see Section 8), hence other alternatives have been examined.

Table 5.2-2

Single Mission Profile and Sensor Characteristics

	Wt. (lb)	Power (watts)	Area (ft^2)	Data (Mb/s)	Cooler	Comments
Oceanic Scanning Spectrophotometer	45	60 (25 ave)	3.7	0.5	no	20 channels (0.4 to 0.7 IFOV 2 km, ± 20° scan angle
Sea Surface Temperature Imaging Radiometer	45	30	1.3	0.33	yes	5 channels (0.5 to 11.5 μm) IFOV 2 km, ±5° scan angle
Cloud Physics Radiometer	70	40	1.9	0.22	yes	5 channels (0.75 to 2.125 μm) IFOV 2.5 km, ±5° scan angle
Thematic Mapper	265	(70 ave)	1.0	30	yes	7 channels, visible and IR
Thematic Mapping Support	205	155	—	—	—	Estimate includes precision attitude control system and 2-70 Mb/s tape recorders.
Upper Atmospheric Sounder	56	27	1.3	0.01	yes	Advanced 2-horizon LRIR
Atmospheric Pollution Sensor	30	10	1.3	0.01	yes	FOV 5° x 5°
Passive Multichannel Microwave Radiometer	513	355 (143 ave)	65	0.01	no	5 channels dual polarization conical scan
Totals	1129	500	84	31.8		

5.3 ERTS/NIMBUS PAYLOAD SELECTION

The ERTS/Nimbus spacecraft can support payloads up to 500 lb. Making use of this payload capability, an attractive mission with sensors drawn from both the EOS study and the on-going ERTS program is feasible. The new sensors are the Oceanic Scanning Spectrophotometer and the Sea Surface Temperature Imagery Radiometer. In addition, the thematic mapping mission of ERTS could be continued with the five channel Multispectral Scanner (MSS), and with a single Return Beam Vidicon (RBV) camera. Table 5.3-1 lists the payload characteristics of these four instruments.

Table 5.3-1

Candidate ERTS/Nimbus Payload

Discipline/Sensor	Weight (lb)	Power (w)	Notes
Oceanography			
Oceanic Scanning Spectrophotometer	45	60 (25 ave)	5 - 20 channels IFOV 2 km $\pm19^\circ$ Scan angle
Sea Surface Temperature Imaging Radiometer	45	30	5 channels IFOV 2 km $\pm51^\circ$ scan angle
Thematic Mapping			
Multispectral Scanner	120	20	5 channels IFOV 86μrad
RBV	75	10	1 camera FOV 100 n.m. x 100 n.m.
Tape recorders	160	30	2 - 15 Mb/s
Margin	55	45	
Total	500	160	

It is possible that the Multispectral Scanner could be changed to the extent of spectrally shifting some of the channels based upon continuing research being carried out in the NASA ART/SRT programs and in other government and non-government activities, thereby investigating optimum center wavelengths and spectral bandpasses for various remote sensing applications. Data from the MSS and RBV are of primary value for terrestrial survey purposes (see Table 5.2-1). Testing in orbit of the Sea Surface Temperature Imaging Radiometer and of the Ocean Scanning Spectro-photometer would afford valuable opportunity to assess the performance of these instruments and the analysis techniques utilizing their data for oceanic purposes.

However, it is emphasized that a comprehensive survey of the oceans from a satellite requires microwave sensors in addition to visible and infrared sensors. The inability of the ERTS/Nimbus spacecraft to carry the multichannel microwave sensors makes this spacecraft unsuitable for such a comprehensive survey. It is clear that a larger spacecraft is needed to meet this objective.

While the combined payload selected for the ERTS/Nimbus would provide some coverage in oceanography it must be viewed as an interim measure.

5.4 EOS A AND B

Constraining the design of the EOS spacecraft to the expected launch capabilities of the Delta vehicle in 1976 resulted in the necessity of considering two separate payload combinations. Since the combined launch vehicle-payload concept studied by Lockheed for the Unified Nimbus Observatory (UNO), Appendix B, would result in roughly the same in-orbit payload, it is not considered separately here.

Two separate launches permit development and flight test of all the key sensors identified in this study. As shown in Table 5.4-1, each payload could include basic sensors of value to global oceanography and meteorology. EOS A would stress oceanography and meterology but would also include a set of multiple frequency, conical, scan ESMR's. These would provide information regarding sea ice, surface winds (foam), cloud droplets, water vapor, and soil moisture. In EOS B, this set of ESMR's would not be flown. Instead, EOS B would carry an advanced Thematic Mapper, and associated equipments, to provide more coverage in terrain resources and coastal oceanography.

Table 5.4-1

Candidate EOS A and B Payload

	EOS-A			EOS-B		
	Oceanography/Meteorology			Terrain Survey/Oceanography		
	Wt. (lb.)	Power (watts)	Description Orbit Adjust Not Required	Wt. (lb.)	Power (watts)	Description Orbit Adjust Required[1]
Oceanic Scanning Spectrophotometer	45	60 (25 ave)	20 Channels (0.4 to 0.7μm) IFOV 2km, 19° scan angle	45	60 (25 ave)	Same
Sea Surface Temperature Imaging Radiometer	45	30	5 Channels (0.5 to 11.5μm) IFOV 2km, 51° scan angle	45	30	Same
Cloud Physics Radiometer	70	40	5 Channels (0.75 to 2.125μm) IFOV 2.5km, 51° scan angle	--	--	None
Thematic Mapper	--	--	none	265	140 (40 ave)	7 Channels, 66μ rad resh
				70	(40 ave)	Wide Band Video Tape Rec. 30 min. record time (30 mb/sec.
				50	50	Precision Altitude Determination System.
Upper Atmospheric Sounder	56	40		50	40	
Atmospheric Pollution Sensor	30	10	FOV 5° x 5°	--	--	None
Passive Multichannel Microwave Radiometer	513	355 (105 ave)	freq. res. (gHz) (km) 4.99 183 10.69 88 18.0 88 21.5 88 37.0 22			None
Other	11	--	--	115	25	To be selected

1 Orbit adjust estimates included as part of spacecraft

Besides broadening the total coverage, use of two EOS spacecraft permits rather efficient utilization of spacecraft system capabilities. Thus EOS A for global oceanography and meteorology, does not require orbit adjust which results in an increase in payload capability. Another effective payload increase results from the elimination of precision attitude determination. Attitude determination to an accuracy of 0.1 degrees is quite adequate for EOS A. The data rates associated with payload of EOS A (1.2 mb/sec) are much less than EOS B (30 Mb/sec) and so recording and transmitting requirements for EOS A are more easily met.

5.5 EOS C AND EOS D

The candidate payloads proposed for EOS A and EOS B are based on the state-of-the-art developments which could be available for flight in 1976. Future sensor developments covered in Sections 4.9 and 4.10 could, in the next few years, progress to the point where larger, more capable spacecraft are required. Payload selection for EOS C and EOS D will be made in 1974 - 1975 for flight in the late 1970's. Two candidate payloads, Table 5.5-1, have been selected to illustrate the possible course of program evolution. Payload I is essentially the four earth resource facility-type sensors listed in Table 5.2-2, thus it accomplishes in one flight many of the objectives of EOS A and EOS B. In contrast to EOS A and EOS B there is an appreciable reserve capacity for accommodating other sensors developed by principal investigators. The margin of 280 lb (127 kg) is based on an assumed total payload weight of 1200 lb (545 kg). The spacecraft structure described in Section 7.2 will support such a payload. The upper limit is probably somewhat higher, being fixed by the available launch vehicle capability.

Payload II illustrates an approach to thematic mapping which employs both Synthetic Aperture Radar and the Thematic Mapper included on EOS B. For the first flight test of synthetic aperture Radar, the correlative data in the visible and infrared imagery of the Thematic Mapper is required. The weight margin of 405 lb (180 kg) could be allocated to principal investigators. Some of it could be allocated to obtaining higher resolution in the visible and infrared if such a requirement develops for the late 1970's.

The impact of high resolution on the data system is evident. Data rates in excess of 65 Mb/s require a bandwidth beyond the current or projected capability of S-band at the NASA ground stations. These higher data rates have led to consideration of a K-band data system described in Sections 7.5 and 7.9. For the same reason the EOS C and EOS D spacecraft also have the capability of precisely orienting a 4-foot antenna for K-band communication to a Tracking and Data Relay Satellite (TDRS). Transmission of data rates up to 100 mb/sec to a TDRS is quite feasible from the EOS spacecraft, assuming an 8 to 10 foot dish on the TDRS. The same computer and computer program utilized in precision attitude control the Thematic Mapper can be used for open loop-orientation of this antenna to an accuracy of better than 0.1 degrees. Or the computer can be used for initial acquisition of the TDRS with a switchover to an auto-track system. If and when a TDRS system becomes available, this capability can be utilized to reduce or eliminate the wide band tape recorder requirements as well as to provide real time, worldwide thematic mapping coverage. In a similar fashion, K-band transmission of 100 mv/sec data to EOS ground stations is feasible, utilizing a rather small (1-1/2 ft) oriented antenna. In fact, transmission of these data rates to a local ground station is practical since a ground antenna of 15 feet or less in diameter is sufficient.

Table 5.5-1

Illustrative Payloads for EOS C and D

Sensor	Payload I			Payload II			
	Wt. (lb)	Power (w)	Data Mb/s	Wt. (lb)	Power (w)	Data Mb/s	
Oceanic Scanning Spectrophotometer	45	60 25ave	0.5				
Sea Surface Temperature Imaging Radiometer	45	30	0.33				
Thematic Mapper	265	70ave	30.	265	70	30	7 channel, 66 μrad
	150	105		150	105		Wide Band Tape Recorders
	100	100		100	100		Precision Attitude Control System
Passive Multichannel Microwave Radiometer	515	140	0.01				
Synthetic Aperture Radar				280	780 300ave	35	IFOV 30 μrad
Other	280	180*		405	75*		
Total	1200	650	30.8	1200	650	65	

*Beginning of life

SECTION 6

ORBIT ANALYSIS

SECTION 6

ORBIT ANALYSIS

PRECEDING PAGE BLANK NOT FILMED

ILLUSTRATIONS

TABLES

SECTION 6
ORBIT ANALYSIS

6.1 INTRODUCTION

Instruments for gathering earth resource data from space place stringent requirements on the orbit selection. These requirements will control such factors as the ground-trace pattern, frequency of earth coverage, solar-illumination angle, duration of pass time, and mission longevity. This section describes the factors governing selection of orbits for EOS A and EOS B as a basis for EOS orbit selection in future missions after sensor characteristics have been defined.

The orbits for earth-resources missions should be nearly circular in order to keep a uniform distance between the earth's surface and the spacecraft instruments which are generally optical. Uniformity in distance from lens to object standardizes optical characteristics and aids interpretation of visual data. A constant angle of illumination at a given spacecraft latitude can also assist visual interpretations. To achieve this circular orbit requires an orbital plane that rotates about the earth at the same angular rate as the mean angular velocity of the earth about the sun known as a sun-synchronous orbit. Paragraphs 6.6 and 6.7 describe the selection of the value for the solar-illumination angle and its influence on the launch window.

Another requirement for the orbit is repeatability of its ground-trace over selected areas of the earth after a predetermined number of days, so that repeating the traces may furnish a predictable pattern of coverage and permit direct comparison of similar data taken at regular intervals.

6.2 ORBITAL CONSIDERATIONS

6.2.1 SUN-SYNCHRONOUS ORBITS

The obate spheroid shape of the earth produces forces that perturb a spacecraft orbit. Resolving these forces into surface components, those components normal to the orbital plane provide the torque which results in the angular velocity:

$$Wo = 10 \ (R_e/R)^{7/2} \cos i \qquad (1)$$

where

Wo = rotational rate of the orbital plane in degrees per day

R_e = equatorial radius of earth = 3442 n.m.

R = mean distance of satellite from earth's center (for a circular orbit, this is the radius of the orbit)

i = angle of inclination of orbital plane with equator

To make the orbit sun-synchronous, the rotational rate of the orbit must equal the mean rotational rate of the earth about the sun (360 degrees per year, or Wo = 0.98561 degrees/ day). Substituting this value into (1) yields the relationship between the orbit radius and inclination angle. Figure 6.1-1 is a plot of this relationship. For moderately low-earth orbits at the most probable orbital altitudes, the orbit-inclination angle i is not sensitive to changes in orbital altitude. For the entire range of orbital altitudes considered, the near-polar orbit is considered desirable because such an orbit will extend satellite earth coverage beyond the ±80-degree latitudes.
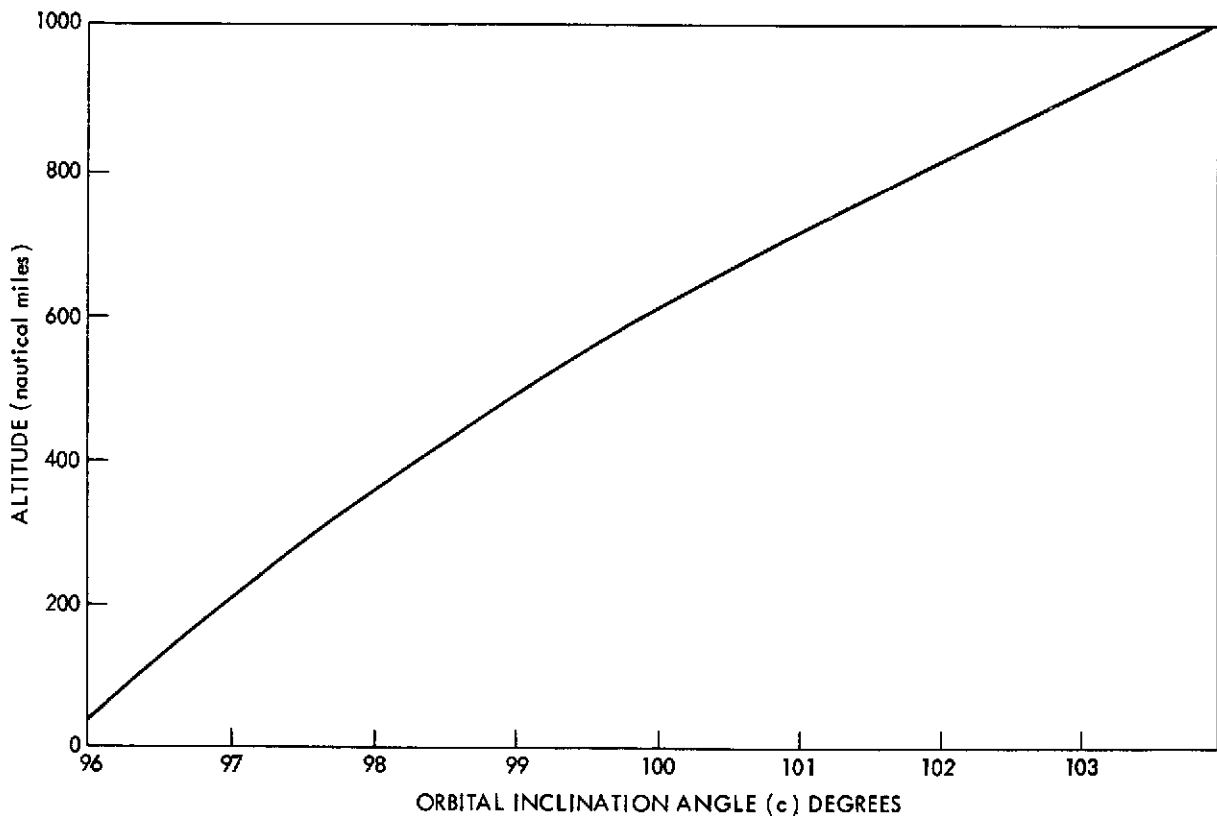
Figure 6.1-1. Sun Synchronous Orbit Relationship Altitude Versus Inclination Angle

6.2.2 ORBITAL ALTITUDE

In setting up a circular sun-synchronous orbit with repeat ground trace, the only free variable is the orbital altitude, which governs not only the frequency of earth-surface coverage but also the pattern of coverage.

However, selection of an orbital altitude must consider both the need for fine resolution of data (which indicates low orbital altitudes) and the fact that a low altitude reduces communications time between satellite and ground station (station pass time), increases atmospheric air drag (a threat to mission longevity), and can reduce scan width of the payload's optics until it needs excessive time to achieve global coverage.

The simplest type of circular and repetitive orbit that can satisfy the requirement is one that repeats itself daily; therefore, the orbital period must be such that there is an integral number of orbits per day. Let

$$N = \text{number of orbits per day,}$$

then, for a circular orbit, the orbital altitude that uniquely requires a given N is given by

$$\frac{1440}{N} = 2\pi\sqrt{\left(\frac{Re + h}{K}\right)^3} \qquad (2)$$

Table 6.2-1 shown the values of h for various values of N.

TABLE 6.2-1

ALTITUDE FOR VARIOUS VALUES OF N

N	h(nm)	h(km)
10	1472.27	2728.12
11	1169.75	2167.55
12	909.86	1685.97
13	683.74	1266.97
14	484.88	898.48
15	308.37	571.41
16	150.44	278.77
17	8.16	15.12

Most earth-resources missions will have orbits whose periods will be very close to integral multiples of a day. Therefore, altitudes in Table 6.2-1 represent specific altitudes possible for earth-resources missions. The only suitable orbits are those for N = 13, 14, and 15 because the air drag would be excessive in orbits for N = 16 and 17, and payload instrument resolution would be unsatisfactory for orbits of N=12 or less.

6.2.3 ORBITAL DRAG

The investigation[2] by Fuchs and Strafella of the ERTS orbit considered five sources of orbital perturbation: drag, high-order tesseral coefficients, solar-radiation pressure, lunar potential, and solar potential.

Effects of the latter three on orbits typical of the ERTS and EOS missions were found negligible. Certain high-order tesseral coefficients have resonance effects that produce dispersions in longitude; however, these resonance effects were considered beyond the scope of this report.

The most significant influence was that of air drag. Reference (2) gives the change in semimajor axis with respect to time as

$$\frac{da}{dt} = -\frac{2B\rho V^3 a^2}{K}$$

(3)

where

a	=	semimajor axis (r for a circular orbit)
t	=	time
B	=	ballistic coefficient $= \frac{1}{2} C_D \frac{A}{M}$
C_D	=	drag coefficient = 2.4
A	=	projected frontal area
M	=	mass of satellite
V	=	velocity of the satellite
K	=	gravitational constant

these missions envision circular orbits only, the semi major axis may be expressed as

$$a = \frac{K}{V^2}$$

Substitution in (3) yields

$$\frac{da}{dt} = -\frac{2B\rho K}{V}$$

(3a)

Three discrete bands of altitude, largely governed by the value of N, will yield repetitive coverage cycles. Table 6.2-2 shows appropriate values for each orbit.

TABLE 6.2-2

ORBITS PARAMETERS FOR VARIOUS VALUES OF N

N	h(n.m.)	a(n.m.)	$V(^{n.m.}/sec)$	$-2^K/V(n.m.^2/sec)$
13	683.742	4125.400	3.90010	32178.92208
14	484.878	3926.536	3.99764	31393.77583
15	308.678	3750.345	4.09047	30681.31877

Spacecraft and atmospheric parameters must be specified in order to compute the effect of air drag. Table 6.2-3 lists representative spacecraft parameters with corresponding ERTS values.

TABLE 6.2-3

REPRESENTATIVE SPACECRAFT VALUES

S/C Wt (lb)	S/C Area (ft^2)	$B^{(1)}$
2500	190	2.93
3800	275	2.79
7500	575	2.95
1980 [2]	72.0	1.40

(1) Based on a drag coefficient of 2.4
(2) Presently estimated ERTS values

Table 6.2-3 shows that the probable range of the ballistic coefficient is from 1.0 to 3.0.

Atmospheric density for corresponding altitudes was obtained from a number of sources but primarily from Reference 2. For a given altitude, Table 6.2-4 lists the corresponding density in metric and English units.

TABLE 6.2-4

ATMOSPHERIC DENSITIES

N	Altitude (n.m.)	Altitude (km.)	ρ (kg/m^3)	$\rho(Slugs/ft^3)$
13	684	1285	$3.8x10^{-16}$	$5.306x10^{-19}$
14	485	899	$4.863x10^{-15}$	$6.790x10^{-18}$
15	308	573	$6.20x10^{-14}$	$8.657x10^{-17}$

Assuming a range of B from 1.0 to 3.0 in increments of 0.5, we can compute the change in semimajor axis for a 20 day repeat cycle by using equation (3a).

$$\Delta a = -B\rho \, \frac{2K}{V} \, x \, (6080.27)^2 \, x \, \Delta T,$$

where $T = 17.28x10^5$ seconds per 20 days repeat cycle.

TABLE 6.2-5

Reduction in Semimajor Axis (ft) for 20 Day Period

N \ B	1.0	1.5	2.0	2.5	3.0
13	-1.09	-1.64	-2.18	-2.72	-3.27
14	-13.62	-20.43	-27.24	-34.05	-40.86
15	-169.67	-254.50	-339.34	-424.17	-509.00

From the values given in the Table 6.2-5, it can be seen that the reduction in semi-major axis for N = 13, 14, and 15 differ by orders of magnitude. It should be recalled that N is the number of orbits per day. From analyses not yet described, the maximum tolerance allowable in the semimajor axis is 283 ft. If the change in semimajor axis exceeds this amount, an orbit maintenance operational procedure is required. Therefore one can recognize that, if an orbital altitude of 308 n.m. were selected (M = 15), the orbital maintenance operational procedures could be required from every 11 days (B = 3.0) to every 33 days (B = 1.0). If the ballistic coefficient were approximately 1.4 (as indicated for ERTS), an orbit maintenance operational procedure could be required for each 20 day repeat cycle.

Apart from the additional burden imposed on operations by the constant need for orbit maintenance, additional on-board propellant would be required to supply the impulsive force necessary for orbit maintenance. If one considers a 3800-lb spacecraft at a 308-n.m. altitude orbit and with a ballistic coefficient of

2.79, one can compute the additional weight of on-board propellant to maintain the orbit for a year duration.

$$\Delta a \text{ (due to air drag)} = -473 \text{ ft/20 day repeat cycle.}$$

The orbit in-plane correction necessary is

$$\Delta V = \frac{Vc}{2a} \Delta a \ , \tag{4}$$

so that:

$$\Delta V = 0.24 \text{ ft/sec.}$$

For a 3800 lb satellite, the impulse required is

$$FT = M_\Delta V = \frac{3800}{32.12} \times 0.24 = 28.4 \text{ lb. sec.} \tag{5}$$

For normal ambient conditions (pressure and temperature), hydrazine has a specific impulse of 220 seconds. Assuming 80% nozzle efficiency, the weight of on-board propellant expended per orbit maintenance precedure is:

$$\Delta W = \frac{28.4}{220 \times .8} = 0.16 \text{ lbs.}$$

Since this is on a 20-day repeat cycle, it would have to be repeated approximately 18 times. Therefore, the total weight of additional propellant required will be approximately 3.0 lb.

Because of the need for constant orbit maintenance procedures, even though substantial extra propellant is not require, low altitude orbits (N = 15) should not be considered for earth resource missions except when payload requirements dictate such need.

For orbits with a value of N = 14, the in-plane orbit adjust problem is much less severe. The worst-case situation (B = 3.0) would require an in-plane orbit adjustment every half-year; ERTS, for which (B = 1.40), should not require an in-plane orbit adjustment for a full year.

When N = 13 or lower, air drag has little or no effect on reducing the semimajor axis.

6.2.4 GROUND-STATION PASS TIME

The time required for a satellite and a ground station to communicate with each other is a constantly recurring problem, especially in low-altitude orbits. There is no easy answer for the question: What is the minimum acceptable station pass time? The time required to "lock" in the S/C signal; the need, type and validation required for commands; the type, speed of transmission and quantity of telemetry data are some of the factors that need be considered.

Figure 6.2-1 shows a ground station at any point "P" on the surface of the earth. Let the Z axis of a coordinate system intersect the point "P" and pass through the center of the earth. The line-of-sight of the ground station is a right circular cone symmetrical about the Z axis with the vertex at P. The half-angle of the cone is m. The equation of the surface of the cone, referred to an orthogonal coordinate system with the origin at P, is:

$$x^2 + y^2 - m^2 z^2 = 0 \tag{6}$$

The equation of the cone referred to the geocentric coordinate system is

$$x^2 + y^2 - m^2 (Z - Re)^2 = 0. \tag{6a}$$

Assume that the cone intersects a sphere whose radius equals that of an earth resources satellite circular orbit; the intersection is a circle contained in a plane parallel to the x - y coordinate planes and at a height Z above the xy plane.

The equation of the sphere is given by

$$x^2 + y^2 + z^2 = R^2. \tag{7}$$

Equating (6a) to (7) and solving for Z yields

$$Z = \left(\frac{\tan m}{\tan m - \tan \phi'}\right) Re \tag{8}$$

where ϕ' is the half-angle of the cone generated by lines passing through the origin and through the circle of intersection. This angle ϕ' represents the limiting angle above which a satellite contained in an orbital plane (at an angle greater than ϕ' with the xz plane) does not pass in line of sight of the ground station. Solving for this angle ϕ' and relating to z yields the results shown in Table 6.2-6 for the three cases of N under consideration.
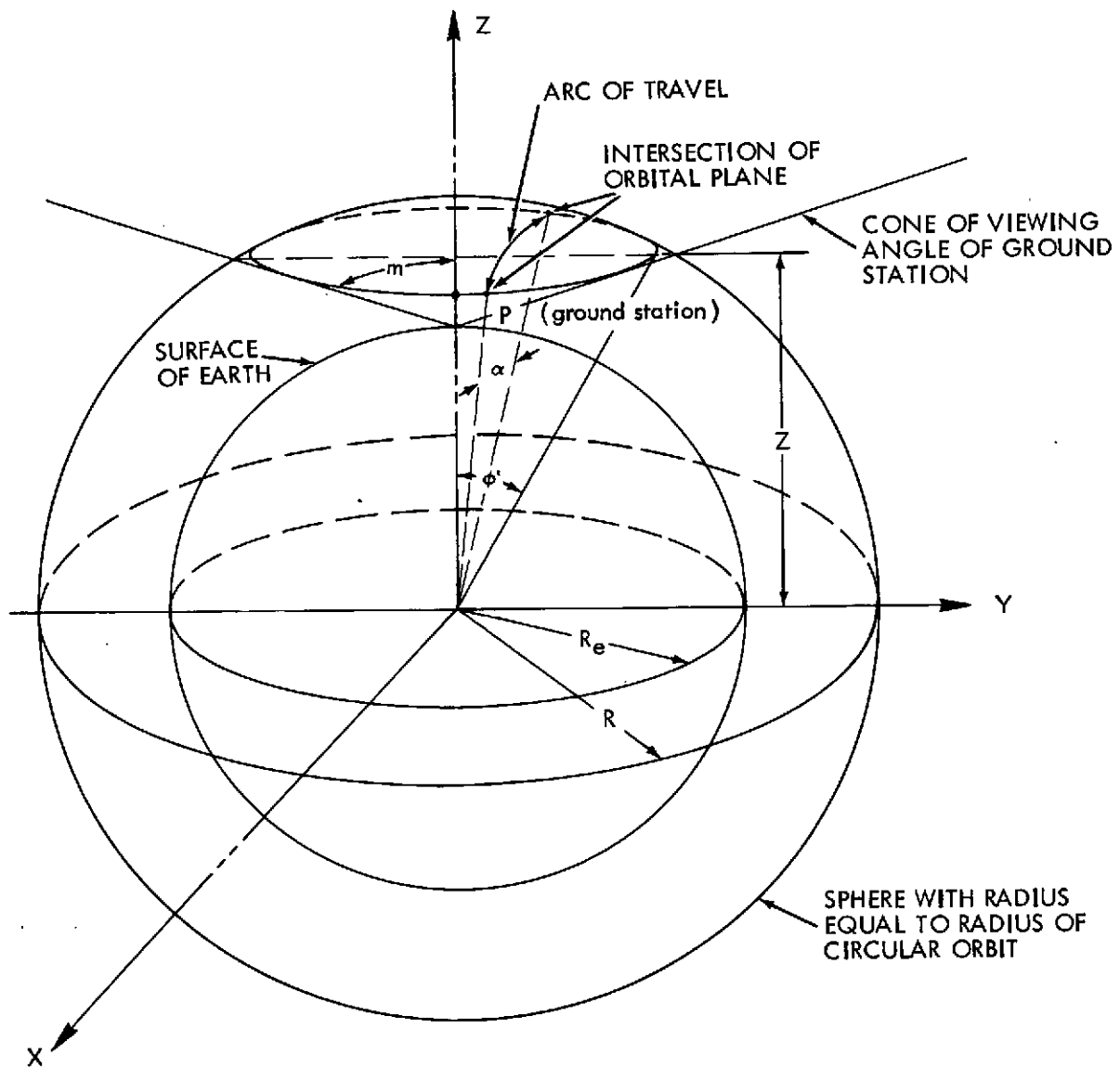
Figure 6.2-1. Geometry of Analysis of Ground Station Pass Time

TABLE 6.2-6

Results for N Under Consideration

N	R (n.m.)	ϕ'(degrees)	Z (n.m.)
13	4125.4	29.1	3604.8
14	3926.5	24.4	3575.5
15	3750.3	19.3	3539.7

Having established the height of the plane of intersection of the viewing cone of the ground station with the sphere containing possible EOS orbits, it now becomes necessary to determine the angle of arc generated by the orbital plane passing thru this circle of intersection. The angle starts when the satellite enters the circle and ends when it leaves the circle. The parameter is the angle ϕ that the orbit plane makes with the XZ plane. The equation of a plane parallel to the x coordinate and at an angle ϕ with the XZ plane is given by:

$$\sin\phi \; y + \cos\phi \; z = 0$$

The vector contained in this plane and in the yz plane is given by:

$$\vec{A} = R (\sin\phi \; \hat{j} + \cos\phi \hat{K})$$

The vector contained in this plane and in the circle of intersection is given by

$$\vec{B} = R \left(\sqrt{\frac{1-Z^2}{R^2 \cos^2\phi}} \; \hat{i} + \frac{\tan\phi Z}{R} \; \hat{j} + \frac{Z}{R} \hat{K} \right)$$

The cosine of the angle of these two vectors is given by the dot product. Solving for the cosine of the angle, we get

$$\cos\alpha \; \pm \frac{ZR}{\cos\phi}. \tag{9}$$

Determining the angle α, it is a relatively easy matter to compute the time of passage of a satellite through the 2 α angular distance. Figure 6.2-2 is a plot of the results in the cases considered (for N = 13, 14, 15).

N (orbits/day) | **ALTITUDE (n.m.)**
13 | 683.7
14 | 484.9
15 | 308.37

ASSUMPTIONS

1 - VIEWING ANGLE OF GROUND SITE IS 5° ABOVE HORIZONTAL
2 - CIRCULAR ORBIT

GROUND STATION

N = 13

N = 14

N = 15

TIME FOR STATION PASS - MINUTES

ϕ = ANGLE ORBITAL PLANE MAKES WITH LOCAL VERTICAL THROUGH GROUND STATION
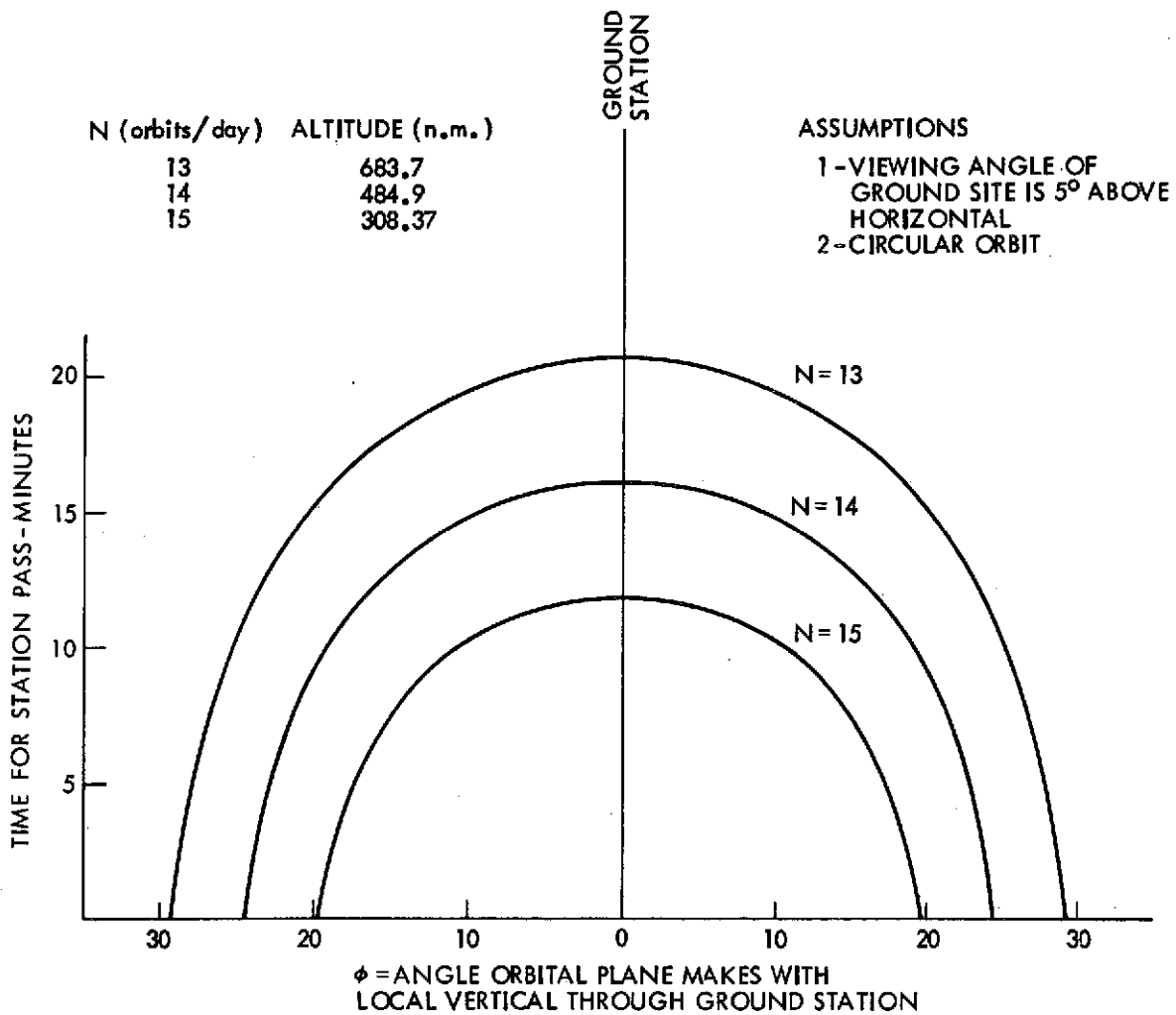
Figure 6.2-2. Station Pass time–Orbit Plane Intercept Relationship for Various Altitudes

6.2.5 ORBITAL PERIOD

We can assume that the period of the circular orbit will be substantially smaller than the period of the rotation of earth and that the axes of revolution of the earth and orbit will be perpendicular or near perpendicular to each other. In this case, the angle that the earth turns while the spacecraft completes one orbital revolution is

$$\theta_e = \omega_e T. \tag{10}$$

As the process continues, there will be some integer value of revolutions such that the earth will have turned through the angle $n\theta_\epsilon$ which will have the closest proximity to one complete revolution of the earth or 360 degrees. The resultant phase angle can be expressed as

$$\alpha = n\theta_e - 360 = \overset{+}{\underset{-}{}} (nT\omega_e - 360) \tag{11}$$

where:

$n\theta_e > 360$, the sign is positive and there is a westward drift of the orbit.

$n\theta_e = 360, \alpha = 0$ and there is no phase difference.

$n\theta_e < 360$, the sign is negative and there is an eastward drift of the orbit.

To obtain complete earth coverage in M days, the required incremental angle to be covered per day is given by

$$\gamma = \frac{\omega_e T}{M} \tag{12}$$

This should be equated to the phase angle (α) or, for the general case, some integer multiple (c) of α,

$$\pm (nT\omega_e - 360) = \frac{cT\omega_e}{M} \tag{13}$$

Recalling $\omega_e = 0.25$ degrees/second and solving for T, we get

$$T = \frac{1440}{n \mp \dfrac{c}{M}} \tag{14}$$

We can immediately recognize that

$$N = n \mp \frac{c}{M} \tag{15}$$

Examining (15), for the case where c = 0, N = n and we recognize the case previously discussed to obtain orbital altitude as a function of N orbits/day. Equation 14 precisely determines the orbital period required. When the minus sign is used, drift rate is westward, and conversely eastward when positive. Although no restrictions have been placed on c and M other than they be integers, subsequent analyses will show that c will be normally small compared to M and that the value of N is

6-18

predominately influenced by and is in close proximity to n. Hence the statement previously made concerning validity of assuming descrete altitudes is verified.

6.3 GROUND TRACE CONSIDERATIONS

6.3.1 SWATH WIDTH

One factor that must be considered is swath width which is directly related to the number of days required to achieve global coverage. We recall the required incremental angle to be covered per day as given by (12).

$$\gamma = \frac{\omega_e T}{M} = \frac{T}{4M}$$

The swath width equivalent to this angle is

$$S = 2 R_e \sin \frac{\gamma}{2}$$

Since $\frac{\gamma}{2}$ will be small

$$\sin \frac{\gamma}{2} \approx \frac{\gamma}{2} \text{ (radians)},$$

and

$$S = \frac{\pi R_e T}{720 M} \cdot \tag{16}$$

By substituting (14) into (16), we obtain

$$S = \frac{2\pi R_e}{Mn \mp c} \cdot \tag{17}$$

The interesting relation is thus established that the required swath width to obtain complete global coverage is determined by the circumference of the earth divided by the number of orbits in the repeat global coverage cycle. Referring to equation (17), since n is largely determined by the orbital altitude, required swath width thus is largely determined by M (days required to obtain global coverage). Again we note that the influence of c in orbital height and swath width considerations is relative minor.

The required swath width (presuming contiguous coverage) is determined by instrument payload consideration. For the ERTS MSS, the scan width is 100 n.m. Since an overlap of 10% between adjacent scans was desired, a 90 n.m. orbital swath width was prescribed. A possible upper limit of 200 n.m. for scan width seems probable. Figure 6.3-1 shows values of S computed as a function of

$$(N = n \mp \frac{c}{M})$$

for various values of M. Since the value of N has been shown to be restricted between 13 and 15 and for a given range of swath widths from 80 n.m. to 200 n.m., the range of permissible values of M (days to complete global coverage) will range from 8 to 20.
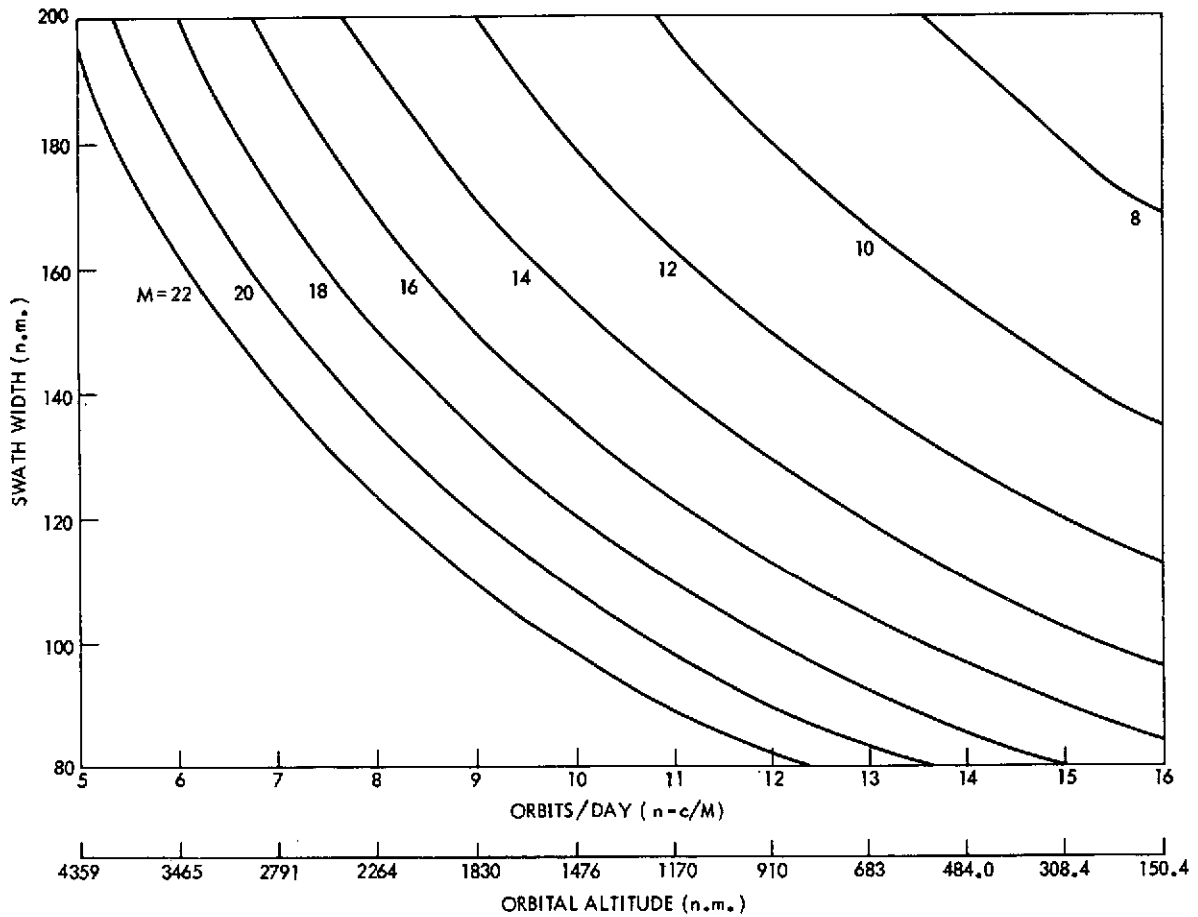
Figure 6.3-1. Swath Width Relationship to N (Orbits/Day) for Various Values of M

6.3.2 EARTH COVERAGE PATTERN

From (13) we recall that the integer c established the size relationship of the phase angle$(\alpha)$to the incremental angle (γ). When c = 0, there is no phase angle (α) and every orbit is repetitive in its ground trace.

To illustrate the cases where c has integer values other than zero, we choose the case where M = 9 for purely illustrative reasons. It should be recalled that M is the number of days to achieve global coverage. The value of 9 was chosen because it is large enough to illustrate sufficient cases of the ratio $\pm$ c/M to completely explain the influence of C on the earth coverage patterns but small enough so that excessive cases need not be considered.

When c = $\pm$ 1, then the phase angle α would be exactly equal to the incremental angle γ and global coverage would be obtained by successive adjacent incremental orbits. For negative values, drift is westward; for positive values, drift is eastward. This is graphically shown in Figure 6.3-2.

When c = $\pm$ 2, the phase angle is twice the incremental angle and on interesting multiple path orbital coverage is established. The first four days of orbit sweep the earth with the second five days of orbit repeating the sweep but filling in the gaps left by the first sweep.

This can be seen in Figure 6.3-2. Complete global coverage is obtained but the possibility of any large area of "real estate" on the earth left unobserved for relatively long periods of time is substantially reduced. This might be of interest in many missions.

When c = 3, an interesting phenomena occurs in the pattern. Recalling that M = 9, the ratio

$$\frac{c}{M} = \frac{3}{9} = \frac{1}{3}$$

In effect, M is equal to 3 (3 days to obtain a global coverage) and c is equal to 1 (adjacent coverage pattern) as shown in Figure 6.3-2. As the 9 days planned for coverage presumably sized the swath width, this would leave large areas of the earth unobserved by the satellite. Unless there are specific reasons for this type of coverage pattern, it would normally be considered undesirable. Therefore, it can be stated that the value of c should not be a number factorable into M because this would degrade the orbital coverage pattern.

When c = 4, a multiple-path orbital coverage pattern also results as shown in Figure 6.3.2.
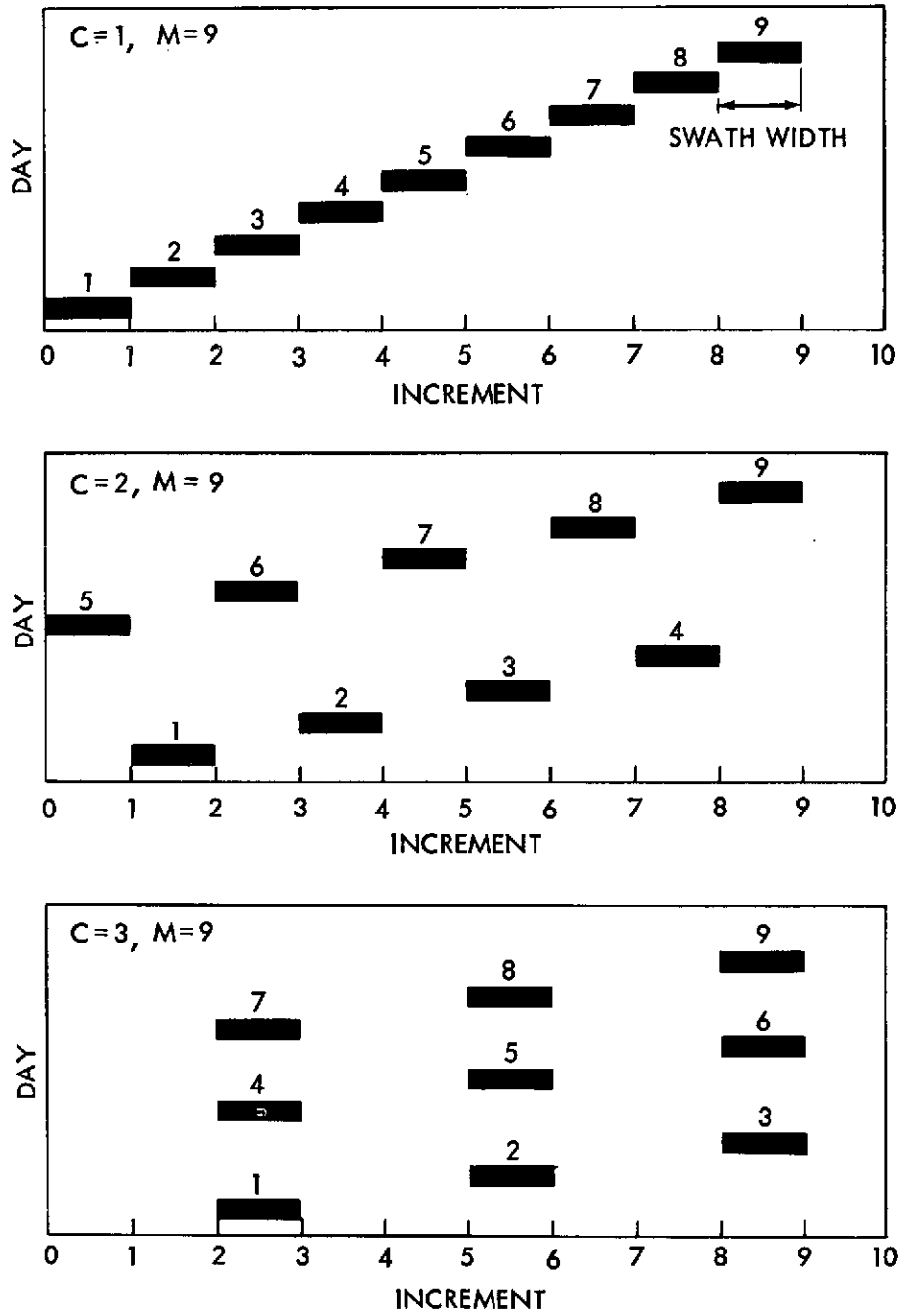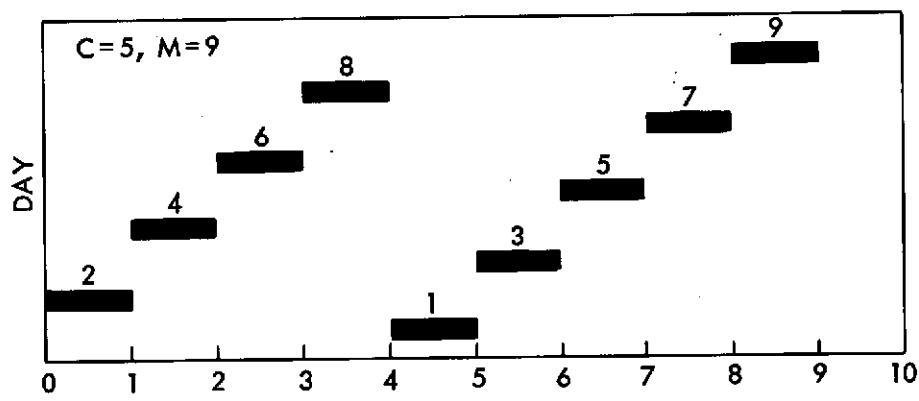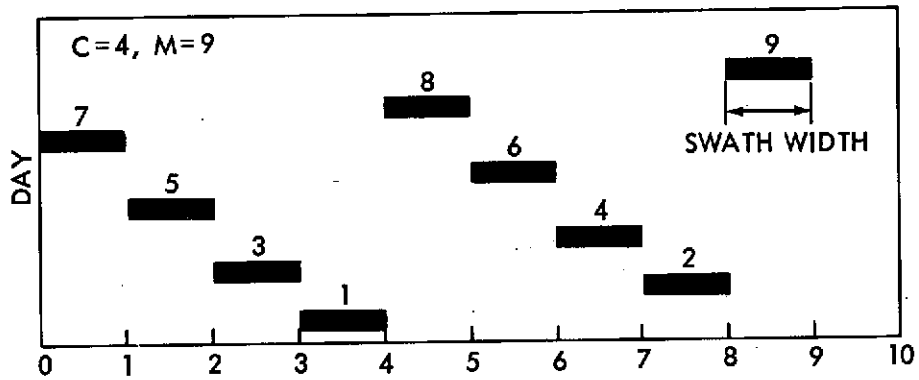
Figure 6.3-2.   Pattern of Orbital Coverage
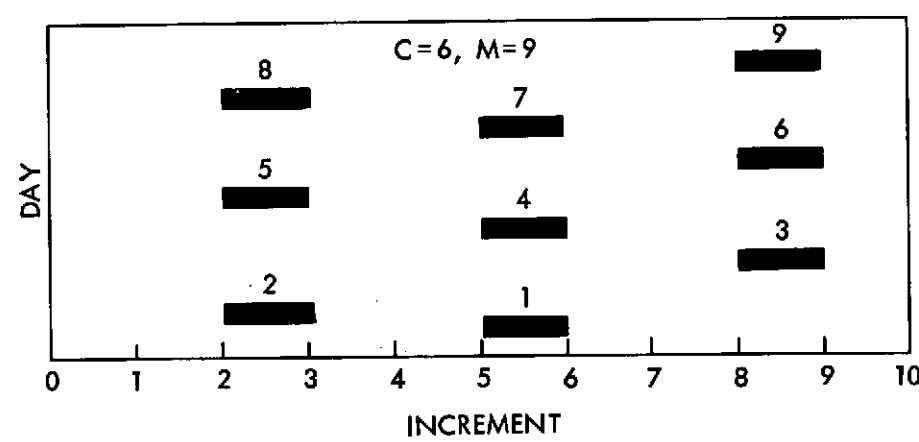
Figure 6.3-2. Pattern of Orbital Coverage (continued)

When c = 5, a multiple path orbital coverage pattern results which is similar to the case where c = 4 but with the direction reversed. If we recall the expression for orbits/day as

$$n \mp \frac{C}{M},$$

it can be seen from the example under consideration that

$$14 - 5/9 = 13 + 4/9.$$

The sense of direction of drift is thus reversed from westward to eastward when the ratio c/M becomes greater than one half.

Selecting the value of integer c will therefore determine the type of coverage pattern, the degree of global coverage, and the sense of direction of global coverage.

6.4 ORBIT SELECTION

Information is now available to select an orbit required for a given earth-resources mission in general and the EOS missions in particular.

In the payload proposed for the EOS mission, two instruments control orbit selection for EOS:

Instrument	Scan [1] Width (n.m.)	Operating [2] Altitude (km)
Oceanic-scanning spectrophotometer	400	1000 (539 n.m.)
Thematic mapper	100	1000 (539 n.m.)

(1) All other instruments either have horizon-to-horizon scan widths or the scan-width concept is not applicable.

(2) It is assumed that all other payload instruments are also designed to operate at this altitude.

From the above list, two values for orbit selection are quickly determined:

(a) Table 6.2-1 shows that the orbital frequency (n) must be in the vicinity of 14 orbits/day to best satisfy the orbital altitude requirements of 1000 km (539 n.m.).

(b) A multiple-path ground trace pattern will most efficiently use the two different scan widths where c = 4.

As noted earlier, where c = 4, the chronologically sequential ground trace would be four swath widths apart to accommodate the oceanic-scanning spectrophotometer, whereas the physically adjacent ground traces (1 swath width) would accommodate the thematic mapper for most efficient use of both instruments. The spectrophotometer would achieve complete earth coverage in one fourth the time it takes the thematic mapper to achieve the same.

The thematic mapper, with a smaller scan width, becomes the instrument that governs the number of days required to achieve complete earth coverage. The 100-n.m. scan width requires a 10 percent sidelap in adjacent ground traces which results in a 90-n.m. swath width requirement. Equation 17 shows a requirement of approximately 240 orbits to achieve complete global coverage, assuming a 90 n.m. swath width. Solving for M (given that n = 14 and c = ±4) produces two solutions:

Where c = -4, M = 17.4 days.

Where c = +4, M = 16.8 days.

Because M must be an integer, 17 days will satisfy both cases. The orbital frequency is thus reduced to two cases:

$$\text{Case I:} N = 14 - \frac{4}{17} = 13 \ 13/17 \text{ orbits/day}$$

$$\text{Case II:} N = 14 + \frac{4}{17} = 14 \ 4/17 \text{ orbits/day}$$

Specific orbital considerations are recomputed for the two cases:

Case	Scan Width (n.m.)	Period (n.m.)	Orbital Altitude (n.m.)
I	92.4	104.613	529.1
II	89.4	101.159	441.2

Although case I does not quite satisfy the 10 percent sidelap requirement, it is not seriously compromised and the orbital altitude is much closer to the required value than in case II. For these reasons, case 1 was selected as the EOS orbit.

With the orbital altitude determined, the angle of inclination (i) of the orbital plane to obtain sun-synchronism was computed to be 99.36 degrees. Figure 6.4-1 is a plot of swath patterns for the EOS orbit.
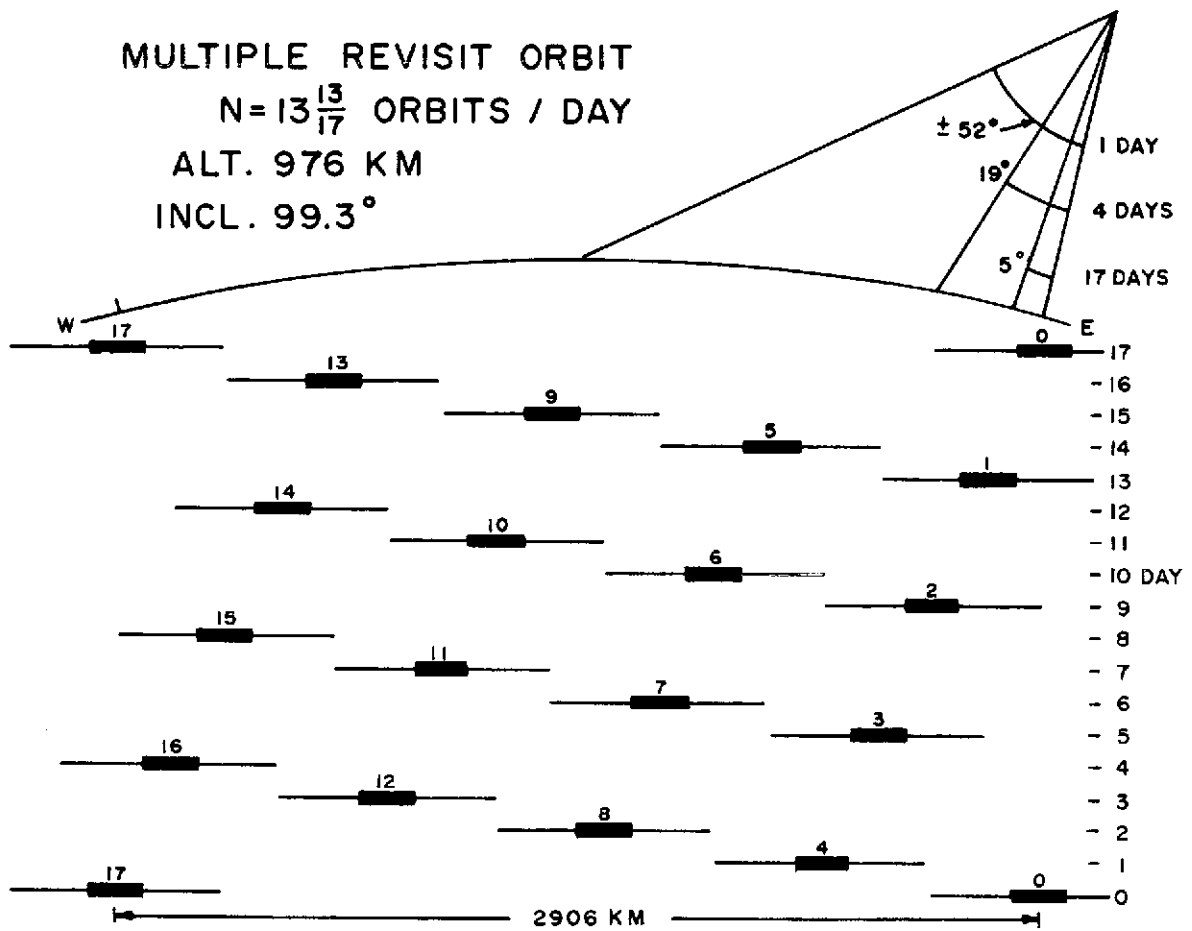
Figure 6.4-1.   EOS Swath Patterns

6.5 ORBITAL PRECISION REQUIREMENTS

Precision in orbital period is the maximum tolerance in orbital period required
to prevent more than an ± x-percent sidelap in swath width in initial and final
orbit after a repeat cycle of M days.

The number of orbits per repeat cycle is

$$\Sigma = Mn \pm c .$$ (18)

Equation 17 gives the swath width as

$$S = \frac{2\pi R_e}{\Sigma} .$$

Maximum tolerance in swath width is defined as

$$xS = \frac{2\pi R_e x}{\Sigma} .$$

The angle of rotation of the earth equivalent to this tolerance in swath width in degrees is

$$\Delta\theta = \frac{xS}{R_e} \cdot \frac{180}{\pi} = \frac{\pm 360 x}{\Sigma} .$$

Since ω_e = 1/4 degrees/minute

$$\Delta T = \pm \frac{1440 x}{\Sigma} = \frac{xT}{M} .$$

As this is the cumulative tolerance of Σ orbits, the tolerance per orbital period is given by

$$dT = \frac{xT}{M^2 \left(n \pm \frac{c}{M}\right)}$$ (19)

Relating this to changes in the semimajor axis, we have for the orbital period

$$T = 2\pi \sqrt{\frac{a^3}{K}} .$$

Differentiating with respect to time yields

$$dt = \frac{3}{2} \frac{T}{a} da .$$

Rearranging and substituting in (19) yields

$$da = \pm \frac{2}{3M^2} \frac{(R_e + h) x}{\left(n \pm \frac{c}{M}\right)} \tag{20}$$

Equation (20) defines the permissible tolerance in semimajor axis in terms of orbital coverage parameters, altitude, and allowable percent of sidelap. The orbital altitude (h) is not independent, but depends upon the values of all the orbital coverage parameters. However, it is predominantly influenced by N. Table 6.2-1 shows this relationship.

To provide an illustrative example, we may select values from Figure 6.3-1 to provide a worst case situation. Such values are given below.

$$n = 14$$

$$M = 20$$

$$C = 1$$

$$h = 484.878 \text{ n.m.}$$

$$x = 0.1$$

Substituting these values in (20) and solving for da, produces

$$da \pm 283.21 \text{ ft}$$

For this worst case condition, the semimajor axis (radius for a circular orbit) must be kept to a tolerance of ± 283 ft in order to prevent excessive sidelap at the end of 20 days.

This value of ± 283 ft change in semimajor axis appeared in the discussion on atmospheric drag, which concluded that an orbit with N equal to 15 orbits/day was unsatisfactory from an atmospheric drag standpoint.

6.6 SOLAR ILLUMINATION ANGLE

A sun-synchronous orbit is one that maintains a constant angle β between the mean sun and the orbit plane of the spacecraft. Sun-synchronous orbits have the desirable property of minimizing variations in η throughout the year for a point at a given latitude. Angle η is the angle between the sun and the local vertical at the subsatellite point.

Variations of angle n at a given latitude arise because of ellipticity of the earth's orbit about the sun and the angle of the axis of rotation of the earth with ecliptic plane. The value of η for points at different latitudes as the spacecraft proceeds along its orbit will of course differ substantially.

Knowledge of angle η (the solar-illumination angle) is important in predicting the illumination intensity for picture-taking purposes and for analyzing shadows in the resulting pictures. Specification of this solar illumination angle has been the subject of much discussion between two classes of users, photo interpreters and radiometric interpreters. The photo interpreters, who analyze surface and terrain characteristics and depend on shadows to aid them in their studies, desire large solar illumination angles; large enough to cast long shadows, but not large enough to reduce illumination intensity below a usable level. On the other hand, users who depend upon radiometric energy or on spectral signatures reflected or radiated from the ground want very small solar-illumination angles or high noon conditions. Obviously, high noon conditions make more radiometric energy available for measurement, and this produces better data.

Discussions conducted as part of the ERTS program reached a compromise on the solar-illumination angle: at 50°N latitude, with the sun at vernal equinox, the sun shall be no lower than 30 degrees above the local horizontal. Since η is the complement of the angle above the local horizon, solar-illumination angle should be no greater than 60 degrees under the same conditions. The latitude chosen, 50° N, is the northern boundary of the continental United States.

Figure 6.6-1 shows the geometry of the solar-illumination angle measurement. Given the orbital inclination angle (i), the latitude angle (L) and the sun-illumination angle η , the following equation will serve to compute the angle of the argument of nodes:

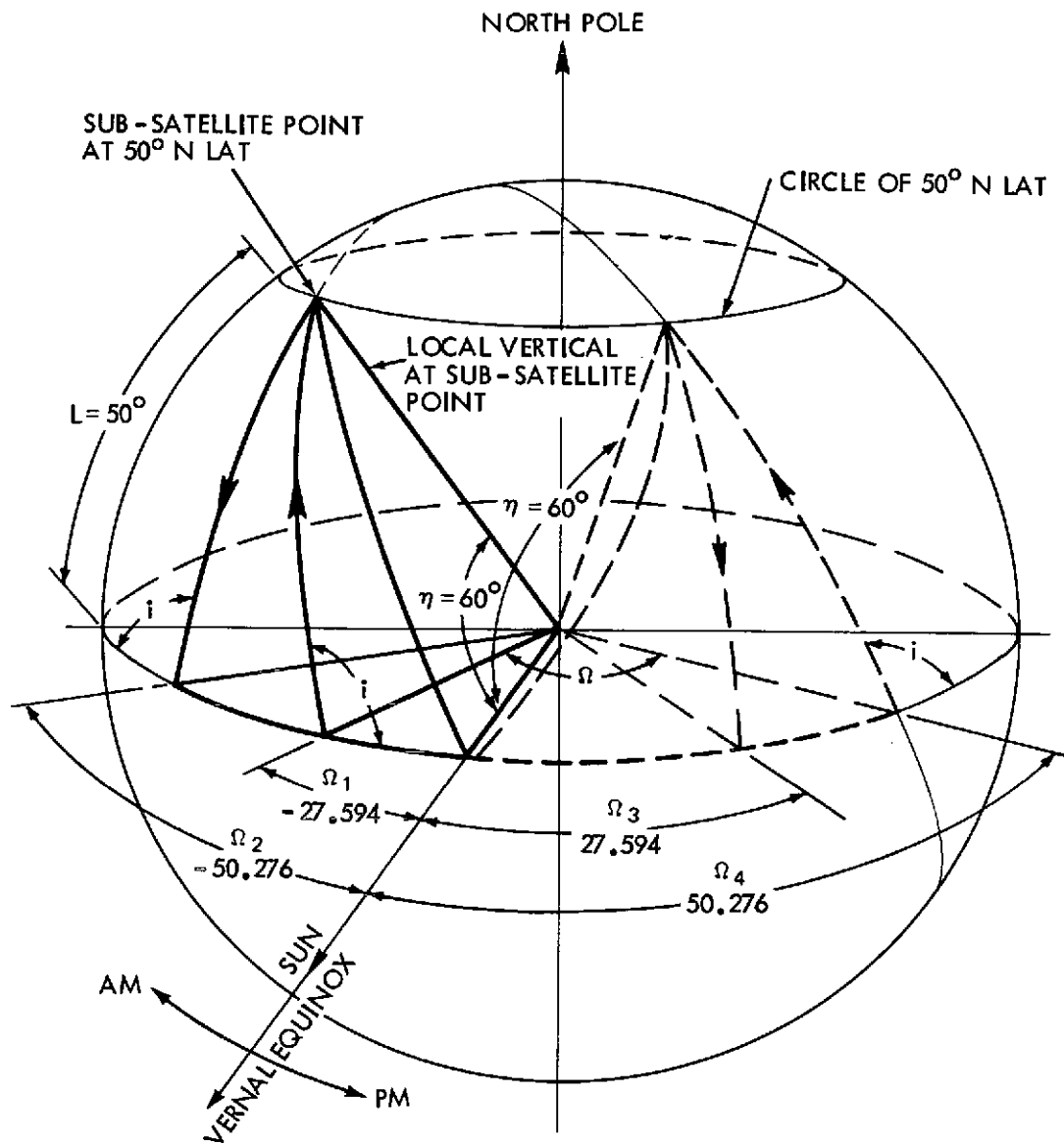$$\Omega = \sin^{-1}\left[- \tan L \, \text{ctn} \, i\right] - \cos^{-1}\left[\frac{\cos \eta}{\cos L}\right] \tag{21}$$

Figure 6.6-1. Geometry of Solar Illumination Requirement

For the 13 $\frac{13}{17}$ sun-synchronous orbit under consideration, i = 99.36°. The sun-illumination angle requirement yields L = 50° and η = 60°. Substituting these values produces Ω = $\sin^{-1}$ (.19665) - $\cos^{-1}$ (.77786), from which

$$\Omega_o = \begin{Bmatrix} 11.341° \\ 168.659° \end{Bmatrix} - \begin{Bmatrix} 38.935° \\ 321.065° \end{Bmatrix} \tag{22}$$

6-30

Four possible orbits have an argument of the angle of ascending node that will satisfy the sun–illumination angle requirement. Four solutions are given in Table 6.6-1.

Table 6.6.1
Candidate EOS Launch Windows

Case	Ω	Local Time	Node Condition
1	-152.406°	1:50 P.M°	Descending
2	-27.594	10:10 A.°M?	Ascending
3	+50.276	3:21 P.M.	Ascending
4	+129.724	8:39 A.M.	Descending

Figure 6.6-1 shows the geometry of the four possible solutions. Paired cases 1-2 and 3-4 are symmetrical to each other about the equinox. Use of available and typical solar–ephemeris data makes it possible to compute and plot the sun–illumination angle (η) as a function of days after vernal equinox.

Figures 6.6-2 and 6.6-3 are typical plots for an approximate EOS orbit for the southern hemisphere and northern hemisphere respectively. Using the 50 degree latitude criterion will provide satisfactory illumination in the northern hemisphere from vernal to autumnal equinox, and in the southern hemisphere from autumnal to vernal equinox. Between ±30 degree latitudes, the illumination should be satisfactory all the year.

6.7 LAUNCH WINDOW CONSIDERATIONS

Four possible orbits will satisfy the solor–illumination angle requirement; the four are actually 2 pairs of summetrical orbits about local noon. One pair of symmetrical orbits is 10:10 a.m. ascending and 1:50 p.m. descending; the other pair is 8:39 a.m. descending and 3:21 p.m. ascending. The local time at nodal crossing is the only parameter which can be controlled to satisfy the solar illumination angle requirements of earth observation missions in sun–synchronous orbits. When considered for a range of latitudes the four possible orbits are seen to represent two characteristics sets.

Computing and plotting the sun–illumination angle η as a function of latitude of the subsatellite point for a given day (spring equinox) as shown in Figure 6.7-1 shows that the (am ascending, pm descending) pair of orbits has a wider variation in angle of illumination for the day than the other pair of orbits.
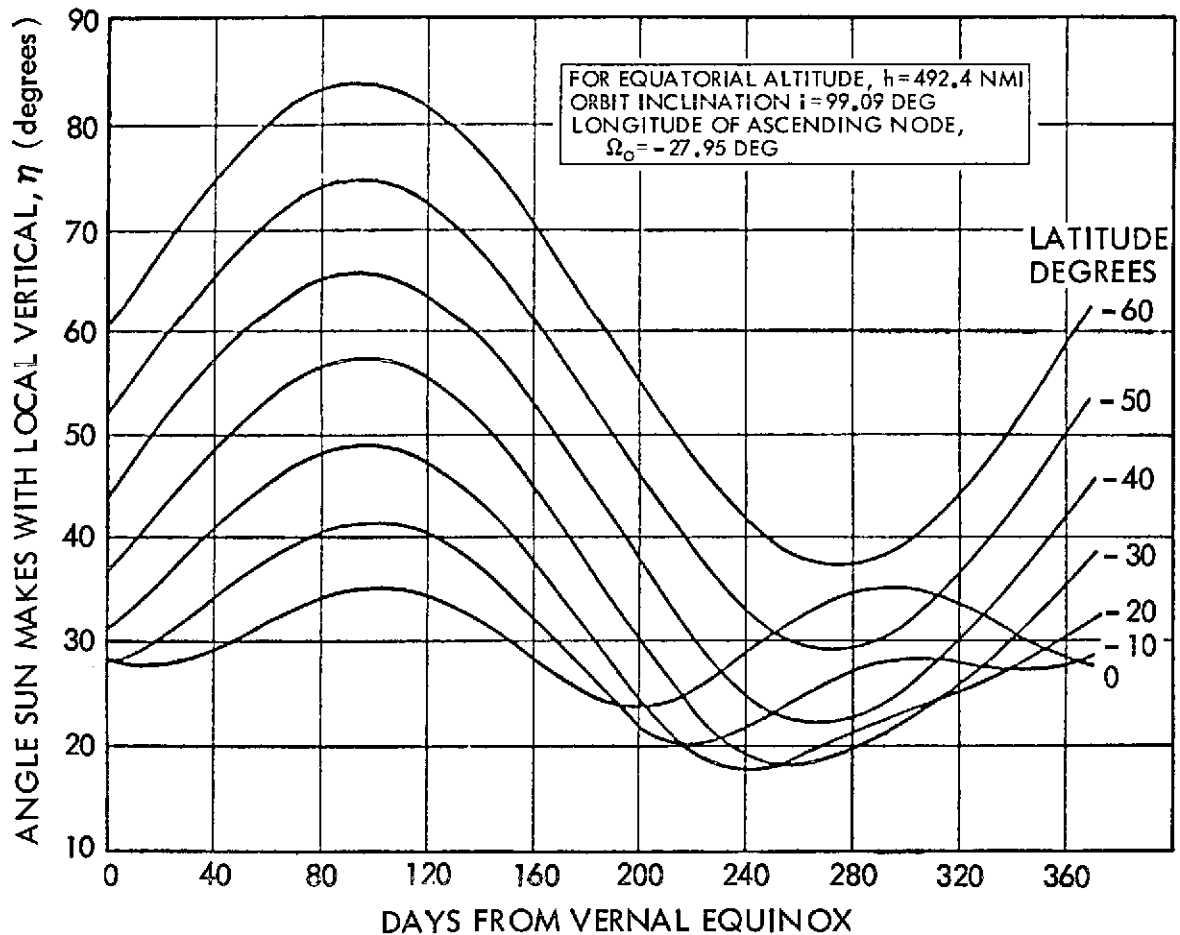
Figure 6.6-2.   Sun Illumination Angle (η) for Several
Latitudes in the Southern Hemisphere

The same situation exists for other days selected (autumn equinox and the two solstices). However, the (am descending, pm ascending) launch windows have other characteristics that have caused the am-descending window to be chosen by ERTS as its launch window and thus should also be selected by EOS.

Solar-illumination angles for (am descending, pm ascending) launch windows are more constant than those of the other set and this is the characteristic that governs the choice of launch windows.

The morning launch was considered preferable to the afternoon launch because an RCA study[3] on cloud cover indicated a higher probability of convective cloud cover in the afternoon than in the relatively cooler morning.
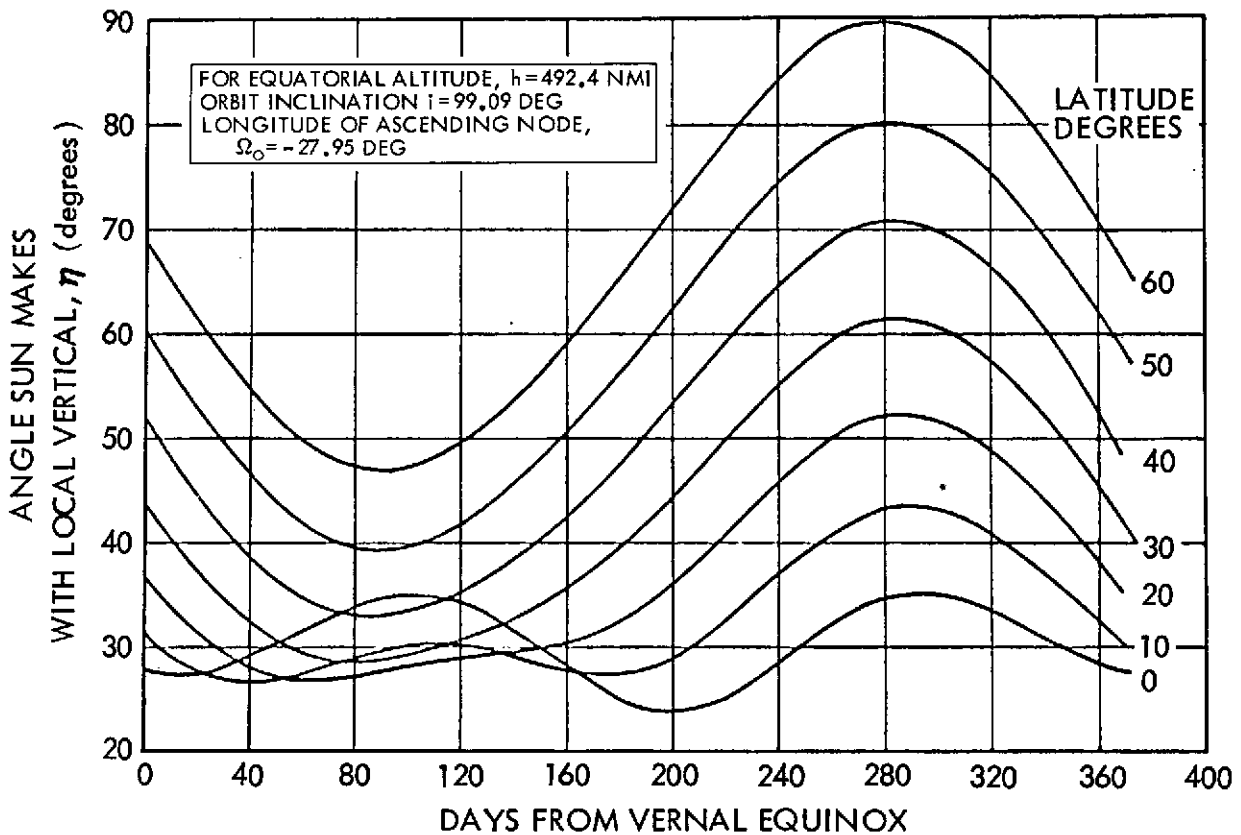
Figure 6.6-3. Sun Illumination Angle (η) for Several
Latitudes in the Northern Hemisphere

6.8 SUMMARY

A circular orbit with a repetitive ground-trace characteristic is essential to earth-observation satellite (EOS) missions. This, in general, constrains selection of orbital altitude to regions about three specific altitudes of interest: 571, 898, and 1267 km (308, 485, and 684 nm). The low-altitude orbit (571 km), which would encounter relatively high air drag with corresponding operational problems and reduced mission longevity, is undesirable   The high-altitude orbit (1267 km) would reduce sensor resolution to undesirable values. An orbital altitude at about 898 km appears most useful for EOS missions; this altitude in turn constrains the orbital frequency to approximately 14 revolutions/day.

The sun-synchronous requirement results in a near-polar orbit compatible with the requirement for near-full-earth coverage. The inclination angle of the orbital
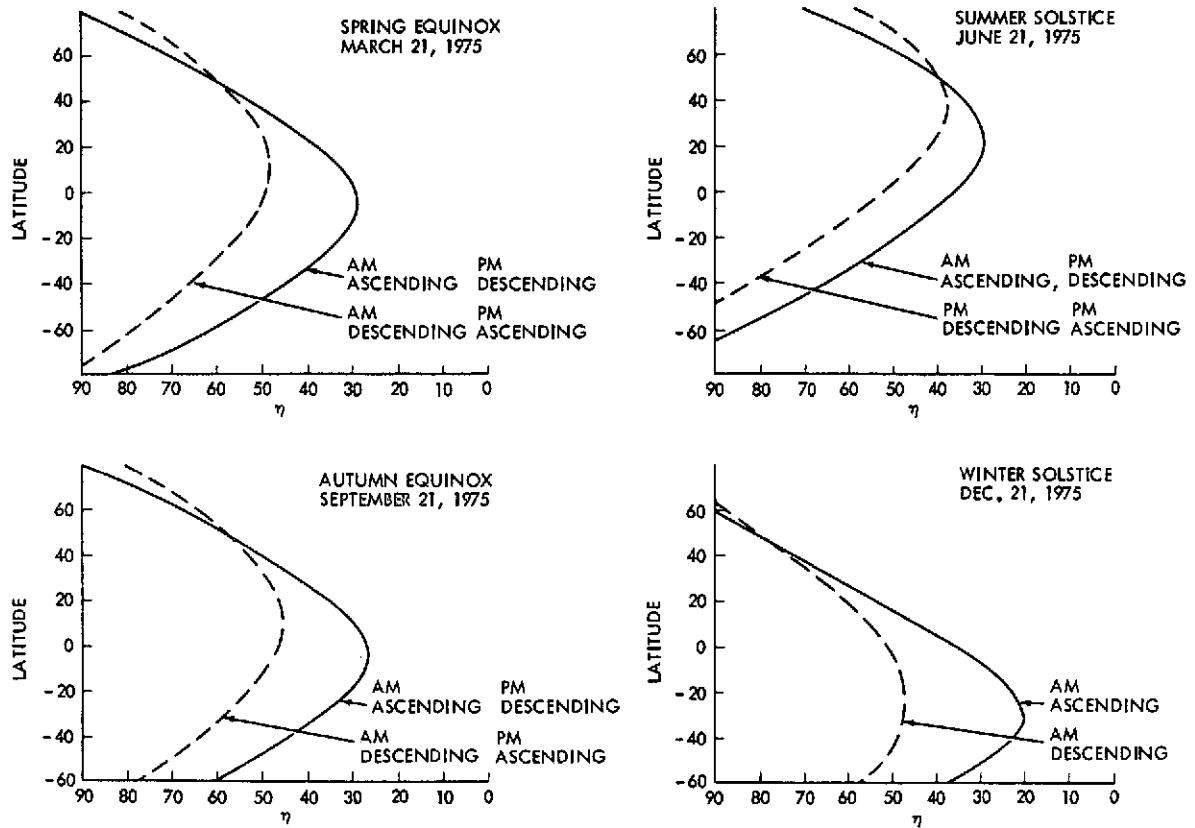
Figure 6.7-1. Variation of Sun Illumination Angle " η "
With Latitude for four Seasons

plane, approximately 99 degrees, is relatively unaffected by the orbital altitudes under consideration.

The following significant relationship exists:

$$N = n \mp \frac{c}{M}$$

Where

N = orbital frequency (orbits/day)

n = orbital frequency to the nearest integer (as noted, 14 for EOS)

c = integer which determine ground-trace pattern (negative indicated westward progression; positive indicates eastward progression)

M = days required to obtain full earth coverage

Payload considerations previously discussed led to selection of the orbital frequency for the EOS missions as

$$N = 14 - \frac{4}{17} = 13 \frac{13}{17} \text{ orbits/day}$$

Parameter for the circular orbit are therefore:

Period = 104.6   minutes

Altitude = 529   n.m.   (979.9km)

6.9 LIST OF SYMBOLS

η = solar-illumination angle (degrees): the angle between the local vertical at a subsatellite point and the sun

W_o = rotational rate of the orbital plane in degrees/day

R_e = equatorial radius of the earth

c = integer (related to orbital patterns)

R = mean distance of satellite from earth's center (for circular orbit, equal to radius of orbit)

i = angle of inclination of orbital plane with equator

N = number of orbits per day

h = orbital altitude

K   =   gravitutional constant

a   =   semimajor axis

t   =   time

B   =   ballistic coefficient = $1/2\ C_D\ A/M$

C_D =   drag coefficient

A   =   projected area of satellite

M   =   mass of satellite

n   =   integer number of orbits

T   =   orbital period (minutes)

ω_e =   angular rotation of the earth relative to the orbital plane = 0.25 degrees/minute

M   =   days required for global coverage

θ_e =   angle that earth turns during one orbital period

Σ =   Number of orbits per repeat cycle

L   =   Angle of Latitude

6.10 REFERENCES

1.   Berman, A.I. The Physical Principles of Astronautics
       John Wiley & Sons, 1st ed., 209

2.   Fuchs, A.J. and R.A. Stratella ERTS Orbit Selection
       Analysis   GSFC X-832-70-144, April 1970

3.   RCA interdepartmental correspondence, Gurk to Smith, September 13, 1967
       Probability of a Clear Sky

SECTION 7

SPACECRAFT

ILLUSTRATIONS

TABLES

7.1 INTRODUCTION AND SUMMARY

This section summarizes the conclusions of the EOS spacecraft design studies.
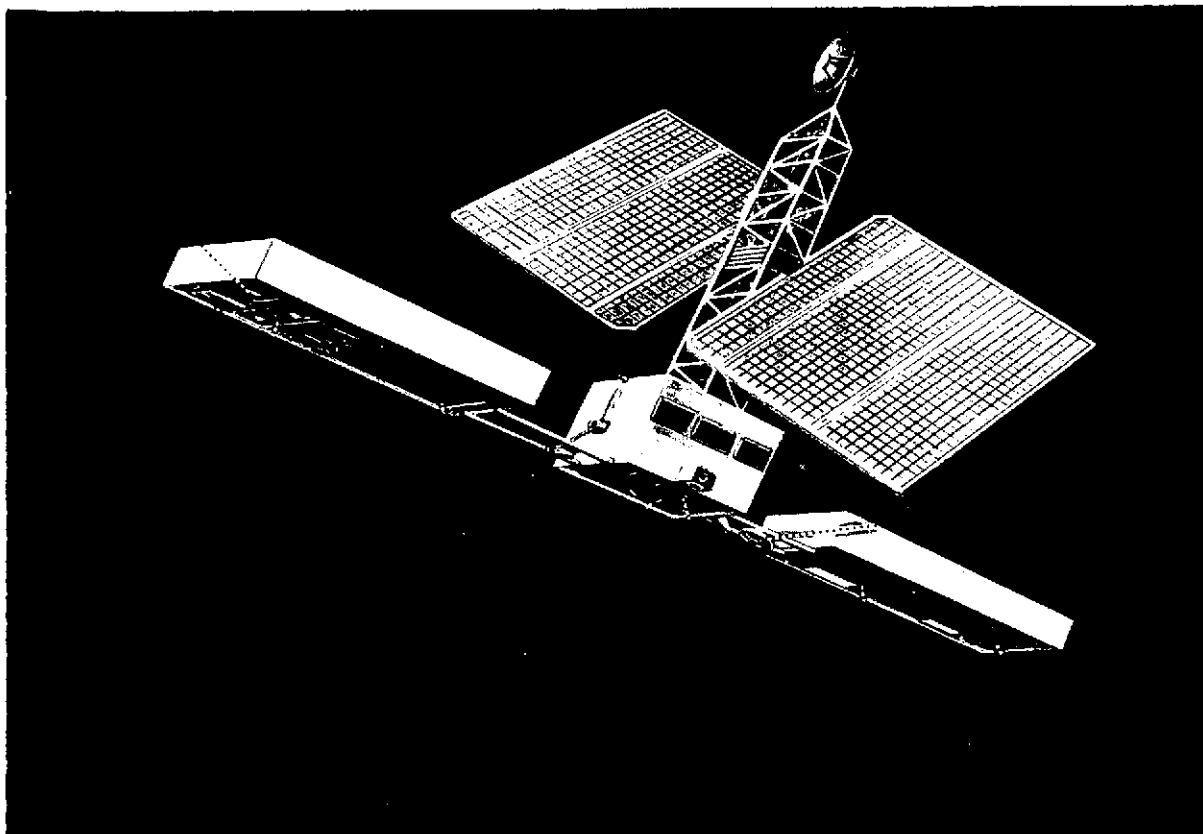
Figure 7.1- 1. EOS Baseline Spacecraft

The baseline spacecraft structure, shown in Figure 7.1-1, consists of a central body and two deployable sensor bays. A rigid tower atop the central body supports the attitude control, propulsion, power system and solar arrays. The two instrument bays are folded during launch in a back-to-back arrangement against the tower. This basic design was chosen from a large number of candidate approaches as the best compromise between the constraints imposed by launch vehicle shrouds and the on-orbit missions that the spacecraft must fulfill.

The primary features that the design approach displays are:

- A large ratio of earth viewing area to spacecraft weight (approximately 0.04 ft^2/lb).
- Efficient utilization of the Delta Launch Vehicle volume/envelope.
- Three axis stabilization by proven techniques for relating terrain data to geographic coordinates (an accuracy of about 100 meters without landmarks can be provided).
- Ability to operate in all likely EOS orbits.
- Compatibility with the Shuttle operational capability when available.
- Modularity in design to facilitate subsystems checkouts and integration and to provide flexibility in choice of sensors.

7-9

7.1.1 STRUCTURE

The baseline structure for both the EOS A and B and EOS C and D spacecrafts consists of a central body, two deployable sensor bays, and a tower atop the central body. Both spacecraft are designed to conform to the Delta shroud having an inside diameter of 86 inches.

The tower is a rigid structural assembly which is used to house and support the solar array rotating mechanism and the attitude control system. For the EOS C and D spacecraft it will also support the data relay antenna. In the stowed configuration the sensor bays are latched to the tower. The mechanism for deploying each sensor bay in orbit consists of a motor driven lead screw (with redundant motor drive) and a deployment arm which produces 90 degree rotation of the bay about a horizontal shaft at the bottom edge of the central body. The mechanism is designed for zero backlash and to be self-locking in the deployed confgguration. The bay and associated deployment mechanism are each integral units that can be readily assembled to the central body making replacement of an entire sensor bay possible with little difficulty.

The oriented solar arrays are folded against the tower in the stowed or launch configuration. They are attached to either the sensor bays or tower. Once in orbit they are deployed via a system utilizing stored energy in the form of a spring and motor damping to control the opening rate. The paddle deployment angle is preset prior to launch in accordance with the chosen orbit hour angle to provide perpendicular alignment between the sun's rays and the solar paddle surface.

In the deployed configuration, the spacecraft appendages (bays and solar paddles) are designed to have natural frequencies greater than 1 Hz to minimize interaction with the spacecraft control system. In the launch configuration, along the thrust axis, the lowest natural frequency is 89 Hz for the EOS A and B spacecraft and 57 Hz for the EOS C and D spacecraft, which meet the requirements of both the Delta and the Titan launch vehicles.

The summary of the power and weight budgets for the various EOS spacecraft, we well as the balance available for payloads, is given in Table 7.1-1. All power figures refer to orbital average values.

7.1.2 POWER

The power system is a direct energy transfer system that utilizes oriented solar arrays for power/generation and NiCd batteries for storage. A regulated bus voltage of +28 V ±2% is maintained by the combination of shunt, boost battery discharge, and individual battery charge regulators. The regulators are standby redundant except for the battery charge regulators where an individual failure is not catastrophic. All electronics can be packaged in a single Power Control Unit to facilitate power system checkout and integration with the spacecraft.

The power system is designed to operate at the nominal level for two years, in any likely EOS orbit, with three year operation possible at degraded performance levels. Thus, the NiCd battery capacity for a given power mission is sized to limit depth of discharge to 25% or less. Similarly, the solar array capacity is oversized at beginning of life so that rated power system output is available after two years of operation in the maximum altitude EOS orbit.

7.1.3 COMMAND AND DATA HANDLING

All of the EOS command and data processing can be handled by four basic subsystems. These are: (1) a command system similar to that on the ERTS/Nimbus; (2) a Versatile Information Processor (VIP) for low data rates (including housekeeping); (3) a Manipulated Information Rate Processor (MIRP) for medium data rate sensors (12.5 kb/sec maximum) and; (4) a Multi-megabit Operation Multiplexer System (MOMS) for high data rate sensors. (100 mb/sec maximum). The command system will utilize the S-band for the r-f link. It will provide a total of 512

Table 7.1-1

Approximate EOS Power and Weight Budgets

	EOS A and B		EOS C and D	
	Power (Watts)	Weight (Lbs)	Power (Watts)	Weight (Lbs)
SPACECRAFT				
Structure	---	675	---	865
Power	---	325	---	500
Data Handling	85	180	105	210
Communications	35	70	65	150
Attitude Control	65	315	65	325
Orbit Adjust	---	120	---	160
Thermal	15	85	15	110
Harness	---	180	---	270
Spacecraft Totals	200	1950	250	259
PAYLOAD	250	650	500	1210
TOTALS	450	2600	750	3800

commands of which 127 can be stored commands. The VIP system, for low rate sensors and housekeeping, has an output rate adjustable up to 12.5 kb/sec. Both analog and digital data can be accommodated. The total spacecraft sampling requirements can be fixed prior to orbit or can be changed in orbit via command by a reloadable memory. Real-time data is transmitted over a low power VHF link while recorded data (32 to 1 playback) is multiplexed with the real-time MIRP data for transmission to ground over an S-band link.

The MIRP system will be used to sample and format medium data rate sensors. It will be capable of sampling rates appropriate for each sensor so that sampling rates can be matched to sensor output characteristics. The total MIRP output bit rate will be approximately 1.2 mb/sec. A 32-track tape recorder (24 to 1 playback) is used for one orbit storage with transmission to ground over an S-band link.

The MOMS will be used on EOS only when a high rate sensor is flown such as the Thematic Mapper planned for EOS B. The Thematic Mapper produces a bit rate between 30 and 80 mb/sec depending on the scan efficiency and instrument resolution. A video tape recorder with 1-1 playback will provide up to 30 minutes of storage of 30 mb/sec data. Transmission of real-time and/or recorded MOMS data to ground will be over an S-band link.

EOS C and D missions may include a Sensor, requiring a 100 mb/sec data rate which is within the MOMS capability. The aforementioned video tape recorder can be adapted to handle the increased rate with less storage time (e.g. 15 minutes at 60 mb/sec or 10 minutes at 90 mb/sec). Both real and recorded data would require transmission links at higher than S-band frequencies. K-band would permit spectral bandwidths of 100-200 mHz and is recommended for this application.

7.1.4 COMMUNICATIONS

In terms of the information capacity that must be provided, the major communication function to be performed by the EOS spacecraft is transmission of the observational data to ground stations. Since the complement of instruments to be flown on each EOS is different, the communication requirements for each EOS is also different. However, the three communication systems proposed for EOS - A will also be common to all of the spacecraft. These three are: (1) a VHF beacon, telemetry and low data rate system, (2) an S-band real-time data, ranging and command system and (3) a S-band stored data transmission system. The VHF system will permit the more-or-less usual function required during launch; it will serve as an acquistion aid for the large ground station antennas; and it will serve as a beacon for the Minitrack network. The VHF transmitter can be modulated by the VIP telemetry system output. The S-band real-time data system will be modulated by a multiplexer which combines the outputs of the VIP recorder, the VIP real-time VIP output and the real-time MIRP output. The S-band stored data transmission system will be used to transmit the output of the full orbit recording of the MIRP data. The MIRP data is recorded at a rate of 1.2 mb/sec and played back 24 times faster when the spacecraft is over a ground station. Therefore, the S-band stored data system will have a 30 mb/sec transmission capacity.

The Thematic Mapper on EOS B will require an additional S-band transmission link, This link will transmit the MOMS output data either directly or after recoding with a maximum rate of 30 mb/sec. The projected characteristics of the Thematic Mapper of advanced design for EOS C and D will require a 100 mb/sec or higher transmission link. A 22 gHz K-band system is proposed that could operate directly with a ground station or a synchronous data relay satellite. A steerable half meter parabolic antenna will permit transmission of a 100 mb/sec channel to any ground antenna equivalent to a 1.8 ,eter parabolic dish. When a Data Relay Satellite Systems (DRSS) is available the 100 mb/sec data can be transmitted to the DRSS via an additional oriented 1.3 meter antenna mounted on top of the tower. In any of these cases, a 30 mb/sec S-Band channel will be retained for the tape recorder playback mode of medium rate data to ground.

7.1.5 ATTITUDE CONTROL

The Attitude Control System (ACS) performs the following functions.

- Acquistion of the desired earth-pointing orientation from any initial attitude, with initial rates of a few degrees per second.
- Spacecraft attitude stabilization with respect to a local vertical-orbital reference to a mean accuracy of about 0.5 degree (bias) in each axis with attitude perturbations of 0.2 degree rms and rate excursions limited to + 0.005 degree per second.
- Medium accuracy attitude determination to about $\overline{0}.1$ degree via ground processing of ACS sensor and torquer data.
- Solar array orientation.

Analysis of the payload sensor requirements indicates that the ACS must provide good rate stability (about 0.01 degree per second) and precise nnowledge of spacecraft attitude (about 0.1 degree for coarse resolution sensors and about 0.001 - 0.005 degree for the Thematic Mapper). Precise attitude knowledge is not needed in real-time. The simplest way of meeting these requirements is to control the spacecraft to about one-half degree. Ground processing of ACS sensor and torquer data for after-the-fact attitude determination will yield 0.1 degree accuracy. To meet the 0.005 degree requirement of the Thematic Mapper, an additional group of sensors called the Stellar Inertial Measurement System (see next section) can be flown on the spacecraft.

The ACS is a three-axis reaction-wheel/cold gas control system and the basic design concept is similar to that of this ERTS/Nimbus type of control system. Rate gyros and sun sensors activate cold gas jets via dead band and hysteresis logic circuits for initial capture; the jets are also used for wheel desaturation and for coarse attitude control. Sun sensors orient the solar

paddles via single axis drives. The outputs of horizon sensors and rate gyros are processed to provide error signals to three, 2 phase, 400 Hz reaction wheels with their inverters gated by pulse modulators.

The essential differences between the proposed ACS and the present ERTS Nimbus design are:

- Use of three rate gyros instead of two to provide better rate damping and also more precise attitude information.
- Use of more precise rate gyros that are presently available.
- Use of more precise horizon sensors that are now available or are being developed.
- Use of redesigned control loops to take advantage of the increased sensor accuracy.

Medium accuracy attitude determination is done via ground computers using telemetered sensor and torquer data. All the know bias and error sources can be modeled and fairly good accuracy (0.1 degree) may be obtained in this after-the-fact smoothing and interpolation of data with much less effort than is necessary for real-time estimation.

7.1.6 PRECISION ATTITUDE DETERMINATION

For EOS flights containing the Thematic Mapper, it is necessary to relate the sensor data to geographic coordinates to an accuracy of about 100 meters. Landmark techniques using identifiable ground truth points within the sensor field of view can be used to provide the best achievable accuracy. The precision attitude determination scheme as an alternate or supplement, attractive because of significantly lower computational load. In this method, the inertical attitude of the sensor is continuously measured via a precision 3-axis gyro and star sensor combination. The star sensor serves the purpose of correcting the gyro drift errors. The telemetered inertial attitude information (about 0.002 degree) is combined with accurate orbit ephemeris data (30-100 meters) in ground processing to yield after-the-fact geographical referencing to an accuracy of better than 110 meters rms.

The basic Precision Attitude Determination System can be expanded on future EOS flights to provide closed loop precision attitude control of selected sensors. This involves the addition of a computer aboard the spacecraft to perform precision attitude estimation in real-time. The resultant earth-oriented attitude information used to orient the individual sensors via precision servo drives to local vertical, to a desired offset from vertical, or to and commanded latitude and longgitude within view. A pointing accuracy better than 0.01 degrees (175 meters) appears to be feasible. The same precision attitude control system could also be used to orient the planned antenna atop the tower of the EOS C and D spacecrafts communication to a Data Relay Satellite. Any required accuracy in this application of up to 0.1 degrees can be readily met

Both precision attitude determination and precision attitude control will require the initial use of landmarks for the removal of bias errors associated with various misalignments (associated with the payload sensors, gyros and star sensors). This may delay the achievement of final accuracy for several days after injection into orbit, but this is of little consequence in a two year or longer mission.

7.1.7 ORBIT

An orbital altitude of about 980 km has been determined to be best suited to the EOS missions. The repetitive ground-trace pattern and field-of-view-overlap selected on the basis of the imagery systems to be flown led to the selection of other important orbital parameters. The orbit plane inclination angle will be about 99 degrees. The orbit period will be 104.6 minutes and the number of orbits per day will be 13 $13/17$.

On EOS flights containing high resolution Thematic Mappers (e.g. EOS B), orbit adjust capability is required to obtain the desired synchronized repetition cycle for the satellite

subtrack. For this reason, the orbit adjust system is designed as a separate module to permit its easy inclusion when required.

The orbit adjust system is sized to correct for initial vehicle injection errors and to maintain the required orbit for any EOS mission for a period of three years. The worst case total velocity increment required to accomplish this is estimated to be 200 ft/sec. This yields total required impulses of 15,500 lb. sec. for EOS B and 23,000 lb. sec. for EOS C and D.

A blowdown hyxrazine system using Shell 405 catalyst type thrusters is planned. Each thruster is sized for a nominal 5 pound force output and is capable of producing a minimum impulse of 0.15 lb-sec. Actual thrust will vary from about 6 pounds at the beginning of life to 3 pounds near the end. Extended firing at the end will produce the required impulse magnitude.

7.1.8 THERMAL CONTROL

Thermal control of the EOS spacecraft will be accomplished with a system of fixed and louvered radiator areas, heat pipes, multilayer insulation, and thermal control coatings. The thermal analysis performed showed that there are no basic problems in maintaining the proper temperature environment in the central body and in the sensor bays for the spacecraft sizes and mission under consideration. The controlled temperature environment is 25 ± 10 C throughout the spacecraft except for the batteries located in the central body. The ambient temperature of the batteries will be controlled to $20^\circ \pm 10^\circ C$ to extend battery life.

A study of various cooling methods has limited the choice to the following:

- Passive-radiator Cooler
- Solid Cryogenic Cooler
- Vuilleumier Refrigeration System

The passive-radiator cooler, though feasible, is rather complex with questionable reliability. A solid-cryogenic cooler using argon would weigh about 70 lbs. for a two year mission, and could present integration difficulties. The Vuillerimier regrigeration system is attractive in its flexibility and controllability, but because of its high thermal power requirement (70-100 watts) an isotope heat source may be necessary. Noting that a cooler has not to date accomplished these requirements on a NASA spacecraft, it is recommended that further study be done before selecting the sensor cooler for EOS.

7.2 STRUCTURE AND MECHANICAL SYSTEMS

7.2.1 INTRODUCTION

Conceptual design of a spacecraft is a many-fold iterative process. At the outset, major factors such as available or projected launch vehicles and shrouds establish gross bounds on certain parameters such as total weight that can be placed into specific orbits. Judicious choice of mission goals then permits rough estimates of the portion of weight in orbit that must be devoted to the basic spacecraft structure and service functions such as attitude control and communications. With estimates in hand of the weight, volume and electrical power available for payload, specific instrument complements or mission profiles can be generated which modify, refine or further define the characteristics that the spacecraft must possess and from this another level of design detail can progress.

The spacecraft design summarized in this section as a "baseline" design reflects not only the above mentioned factors, but also many other more subtle considerations necessary to arrive at and define the basic requirements of the EOS spacecraft. It also serves to establish the feasibility of translating these requirements into flight hardware. As such, it provides a basis on which a more detailed study can proceed.

7.2.2 SPECIFIC REQUIREMENTS

Table 7.2-1 lists the major specific requirements directly affecting the spacecraft design. Following is a brief explanation of the items listed in table 7.2-1.

Both the EOS A and B and EOS C and D configurations were sized to fit into a Delta shroud with an 86" inside diameter. The EOS A and B are launchable by a Delta. However, it is not certain at present whether the launch capability of the Delta will be increased enough by the time an EOS C and D version is ready. In any event a Titan (or possibly the Shuttle) would certainly be satisfactory. One of the basic design constraints on both the EOS A and B and C and D versions is that the transition to the EOS C and D could be accomplished by only an increase in the length of the sensor bays. This accounts for the identical values of items 1, 11, 13, and 14 in table 7.2-1.

The EOS program as presently conceived could span a decade or more of spacecraft launches and thereby overlap with the Shuttle program. A Shuttle launch would make possible spacecraft retrieval which places a requirement on the spacecraft to have the capability of launch and retrieval. Two major mechanical and structural impacts on the spacecraft are that a docking cone can be included and that the sensor bays be retractable. Retractability is not deemed necessary for the solar paddles at this time due to the complexity of an unlatching mechanism. Further, degradation of solar cells in space over long periods of time makes the value of their recovery questionable. However, if solar cell roll-up arrays become operational, retractability will be more attractive.

After many iterations of possible sensor payloads to be flown, four potential EOS missions were identified, each having a particular assortment of sensors. They are the EOS A, EOS B, EOS C, and EOS D. An earth viewing area of 100 square feet satisfies the EOS A and B requirements and 145 square feet is satisfactory for the EOS C and D version. Each of these viewing areas includes 25 square feet of the central body.

The Thematic Mapper sensor requires cooling of at least one channel down to $90^{\circ}K$. This required location of a radiant cooler in one sensor bay which would view dark space and not see any part of the spacecraft or earth. Due to the large paddle area and its rotation about the pitch axis (with a 45° offset due to the 9:00 orbit) the angles of view are quite limited. A detailed discussion is presented in section 7.8.

Table 7.2-1

EOS Spacecraft Design Requirements

	EOS A&B	EOS C&D
1. Shroud I. D. (inches)	86	86
2. Docking Cone	Yes	Yes
3. Earth View Area (Ft^2)	100	145
4. Solar Paddle Area (Ft^2)	128	216
5. Radiant Coolers	Yes	Yes
6. Solar Array Drive and Angle Preset Mechanism	Yes	Yes
7. Data Relay Antenna Dia. (Ft.)	--	4
8. Deployable Parabolic Antenna Dia. (Ft.)	--	1.5
9. 8" Antennas (Quantity)	3	3
10. Retractable Sensor Bay Mechanisms	Yes	Yes
11. Central Body Volume (Ft^3)	100	100
12. Attitude Control	Yes	Yes
13. Maximum Sensor Bay Depth (In.)	21	21
14. Sensor Bay Width (Ft.)	5	5
15. Sensor Bay Length (Ft.)	7.5	12
16. S/C Weight (lb)	2500	3800
17. Sensor Weight (lb)	550	1100
18. S/C Ave. Regulated Power (Watts)	450	750

Based upon the sensors selected (Section 4.0), the average regulated power was established resulting in the solar cell paddle area and battery size required. Section 7.3 describes the basis for selection of the power system such as battery depth of discharge, solar cell degradation, etc. For the EOS A and B, 128 square feet of solar cell area is required and for the EOS C and D, 216 square feet is required. An RTG power system was not chosen for the many reasons discussed in Appendix E.

One of the design requirements of the EOS spacecraft is that it must be able to function in an orbit hour angle ranging from 0900 to 1500. To maintain peak solar cell output for these requirements necessitated a solar array drive and an angle preset mechanism to maintain perpendicularity between the solar array surface and the sun.

The EOS C and D spacecraft includes a data relay antenna located at the upper end of the central tower and a deployable antenna mounted between the struts of one sensor bay. These additions do not seriously affect the spacecraft design, however, the data relay antenna does necessitate lengthening the delta shroud. This too is not a major design change since the delta shroud does not exist at present.

On certain missions the requirements for a precision attitude determination system put stringent constraints on the amount of backlash, or unpredictable displacement of sensor bays, while in the deployed position. As a result a method by which all pivot joints could be preloaded to prevent backlash is proposed and the design details are contained in Appendix D.

7.2.3 DESCRIPTION

Based on the specific requirements for both an EOS A and B and the EOS C and D spacecraft the baseline spacecraft was determined. It consists of a central body, two deployable sensor bays and two bi-fold solar array paddles having their motor drive mechanisms mounted in the central tower.

It should be mentioned here that there are alternate spacecraft designs which offer particular advantages in certain areas and are discussed in Appendix C. However, the three body baseline design presented in this section represents a considered compromise among all the conditions that have to be satisfied (e.g. sensor volume, earth viewing area, cooler fields of view, solar array shadowing, thermal designs, thruster locations, etc.) Presently, the EOS A and B is launchable by a Delta and the EOS C and D by Titan. With these vehicles the minimum launch lateral and thrust fundamental frequencies were established for each spacecraft, Table 7.2-2. These frequencies were used to size both spacecraft in order to preclude dynamic coupling between the spacecraft and launch vehicles. All calculations are based on the spacecraft being hard mounted to the vehicle at the separation plane. In addition the desired orbital natural frequencies shown in Table 7.2-2 were met. Where necessary, an inertial load for the deploying or deployed mechanism is assumed. The sensor bays have been designed to deploy in a 1 g field with the spacecraft on its side and each bay supported through its center of gravity. This should limit the maximum loading on the pivot points to 0.125 g. Thus, the pivot points affected

were designed to this gravity loading. Calculated spacecraft frequencies based on the structural design presented herein are shown in Table 7.2-2 and compare favorably with those required. The structural weight breakdown associated with the calculated spacecraft frequencies is shown in Table 7.2-3.

Both spacecrafts were sized for the Delta shroud (86 inches I. D.). The length of the shroud is variable and as such can be optimized for each spacecraft configuration. Under present planning, the Delta can only launch the EOS A and B spacecrafts with the EOS C and D spacecraft launchable by a Titan. However, it is conceivable that some future Delta would have the capability of launching the EOS C and D. Thus, making the latter compatible with the Delta shroud may eliminate the need for future design changes. Other than the larger solar paddle areas of the EOS C and D the only major structural change over the EOS A and B design is that the length of each sensor bay is increased from 7 1/2 feet to 12 feet.

7.2.3.1 <u>EOS A and B Spacecraft</u>. The EOS A and B spacecraft (Figures 7.2-1 and 7.2-2) consists of a central body with 25 ft^2 of earth viewing area and two sensor bays each with 37.5 ft^2 of earth viewing area. Each sensor bay is attached to the central body by two deployment arms and are locked into the deployed position by the drive mechanism. A welded tubular tower is attached to the central body and is used for securing the sensor bays during launch and for the attachment of the solar arrays to two array drives located in the central portion of the tower. The arrays contain 64.0 ft^2 of solar cell area and are attached to the sensor bays in the stowed position. This configuration can be stowed on a Delta booster with an 86 inch inside diameter fairing. In the normal sequence of deployment, the solar arrays are unlatched from the sensor bays and deploy first. The sensor bays are then deployed firing explosive bolts to separate the bays from the tower. A ball screw then deploys the bays. An improvement on this scheme may be to latch the solar arrays to the tower, rather than the bays, so that deployment of solar arrays and sensor bays could occur in any sequence without interference.

a. Deployment Mechanism. The deployment mechanism (Figure 7.2-3) for each bay consists of a single ball screw jack mounted on the vertical center line of an outer surface of the central body, whose normal is along the velocity vector. Redundant motors drive the screw jack through a stroke of 19.5 inches. As the ball screw fitting travels the length of the screw it is supported to the outer surface of the central body by a track, Section A-A, to prevent bending in the screw. The ball screw is connected to the sensor bay by a deployment arm. Bearings in all parts of the drive assembly will be suitably preloaded to eliminate backlash and end play. A typical method of preloading all pivot joints is shown in Appendix D. The use of duplexed bearing assemblies is a reliable technique by which all radial and axial play can be removed through preloading of bearing pairs. Also, preloading of the lead screw or ball screw arrangement should be incorporated to obtain zero backlash.

b. Solar Array. The solar array as illustrated in Figure 7.2-4 consists of two 1 inch thick honeycomb panels with widths of 25 and 50 inches by 132 inches long. The 25 inch wide panel is attached to the solar array drive mechanism mounted in the tower, with a yoke type hinge fitting and hinge pins. Honeycomb material is sandwiched between aluminum skins and internal primary load carrying box beams. Aluminum channel sections are fitted on all sides of each panel. Restraint hinge and motor mount fittings are added where required in the edge members of each panel and then bonded. The panels are joined by four hinge fittings each. The outer hinges have a single torsion spring for deployment while the inner hinges contain two each. One of these hinges on each panel also has a deployment motor and a full deployment lock (details C, H and section K-K of Figure 7.2-4). Shear fittings have been added to the panels in such a manner as to remove forces in the X-X axis when in the stowed position.

When in the stowed position the panels are folded flat and parallel to the X-X axis surface of the tower. Six restraint links attached to the sensor bays connect to the restraint fittings on the outer solar array panels.

Table 7.2-2

EOS Spacecraft Natural Frequencies

		Frequency (Hertz)			
		Thrust Axis		Lateral Axis	
Spacecraft	Configuration	Calculated	Required	Calculated	Required
EOS A&B	Launch	89	40	35	25
	Orbit S.A.[1] / S.B.[2]	1.0 / 4.7	1	--	--
EOS C&D	Launch	57	15	10.6	10
	Orbit S.A. / S.B.	1.0 / 1.6	1	--	--

[1].S.A. = Solar Array
[2].S.B. = Sensor Bay

Table 7.2-3

EOS Structural Weight Tabulation (Lbs.)

	EOS A&B	EOS C&D
Tower	130	130
Sensor Bay Deployment Mechanism	145	145
Sensor Bays	180	350
Central Body	190	190
Miscellaneous (Estimated)	30	50
Total	675	865
Percent of Total Weight	27	23
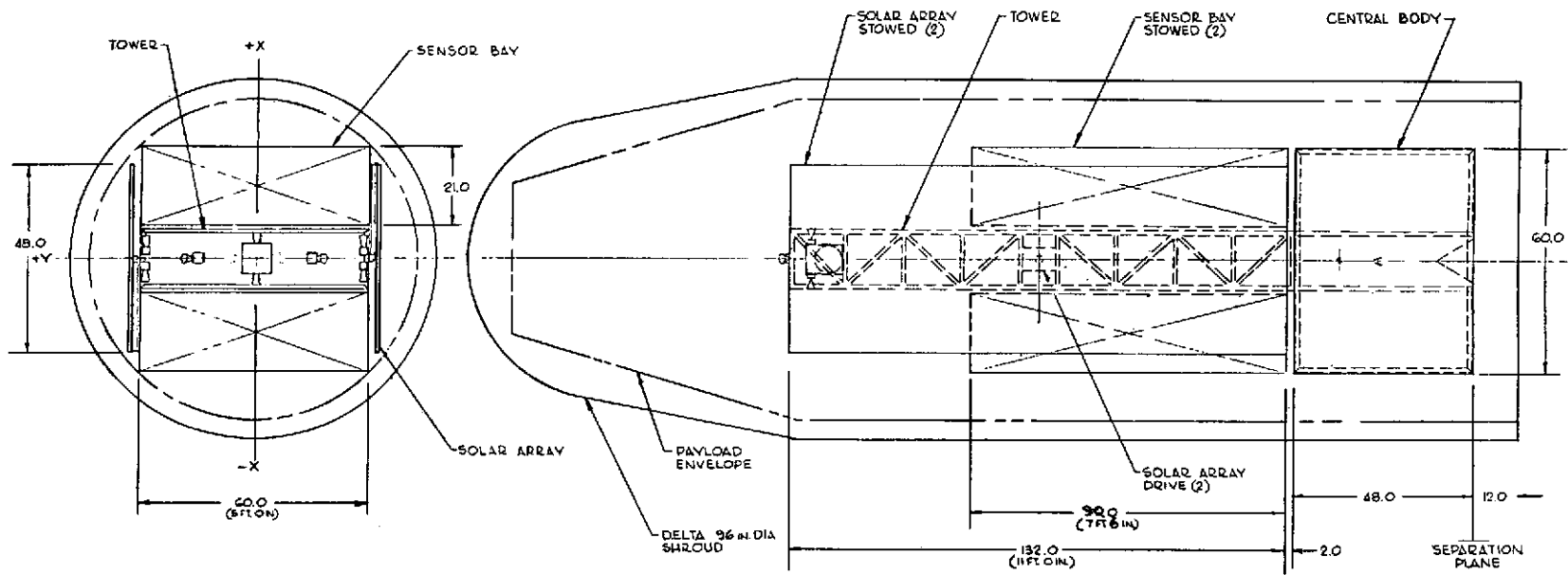
Figure 7.2-1.   EOS A and B Spacecraft (Stowed)

JET LOCATIONS (SEE FIG 12)

164.0
(13 FT. 8 IN.)

16.0

TOWER

8 IN. DIA ANTENNA (3)

DEPLOYMENT MOTOR

SOLAR ARRAY
DRIVE (2)

SOLAR ARRAY - DEPLOYED
64 FT² EACH ARRAY - TOTAL 128 FT²
(SEE FIG. 8)

PHASED ARRAY
ANTENNA

EQUIPT. INSTALL.
(SEE FIG 11)

12 IN DIA
DOCKING CONE

LOUVERS
(SEE FIG 13)

VIEW ON BOTTOM OF CENTR. BODY
VIEW A-A

CENTRAL BODY 25 FT²
EARTH VIEWING AREA
(SEE FIG 9)

SENSOR BAY (2) 37.5 FT² EACH
EARTH VIEWING AREA
(SEE FIG. 10)

DEPLOY. MECH. (SEE FIG 5)

A

A

+X ◄— ◄—X

+Z

TOTAL EARTH VIEWING
AREA 97.5 FT.²

Figure 7.2-2.   EOS A and B Spacecraft (Deployed)
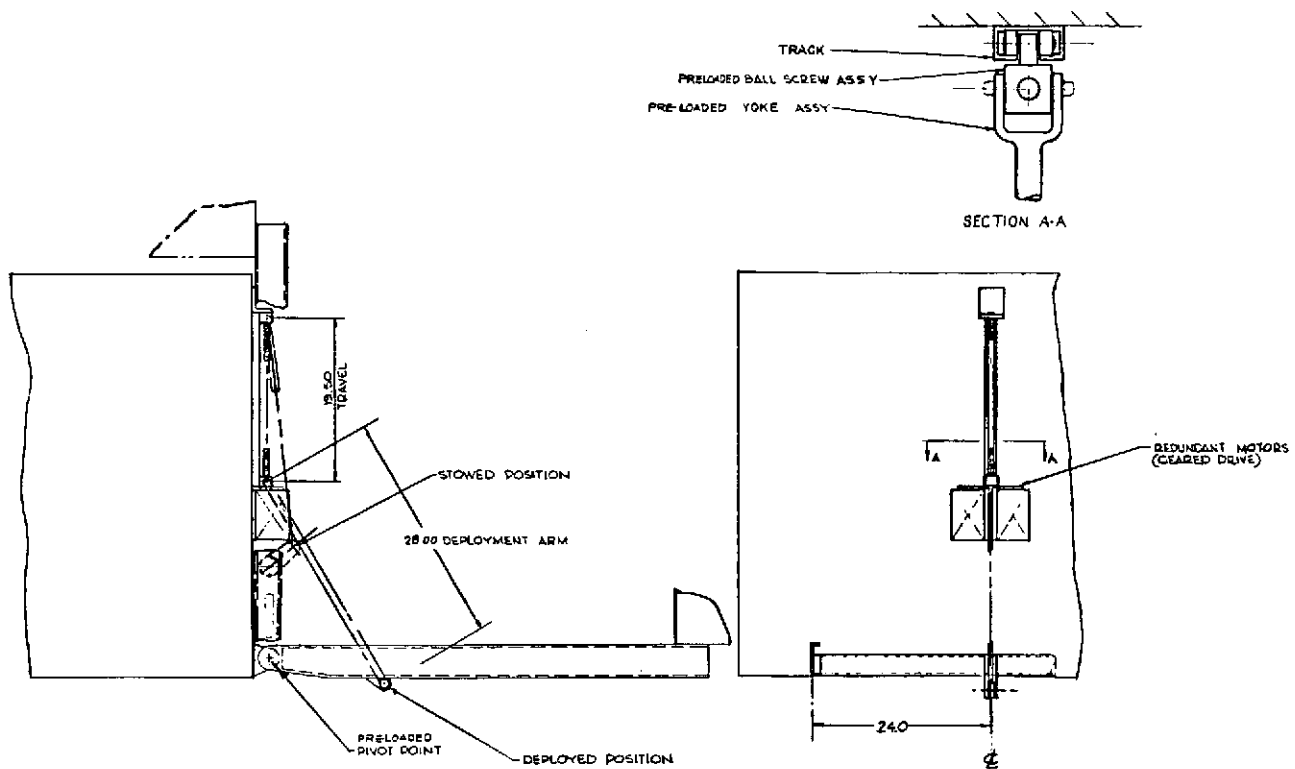
Figure 7.2-3. EOS Sensor Bay Deployment Mechanism

Deployment of the array is accomplished by releasing the six restraint links and applying power to the deployment motors. Deployment is controlled by the gearing of the motors which accomplishes two functions. They act as a brake controlling the rate and position of each panel to prevent interference with adjacent components during deployment and also assure complete deployment and locking in the extended position. Additional locking mechanisms are discussed in Appendix D.

c. Central Body and Tower. The tower (Figure 7.2-5) is a welded tubular type structure with a cross section of 16 x 60 inches and 134 inches long. Life fitting locations are supplied on the upper end of the structure and machined fittings on the lower end for attachment to the center body. Attachment fittings for the sensor bays are also incorporated.

The center body (Figure 7.2-5) is 60 x 60 inches square and 48 inches high, is fabricated from extruded aluminum structure with aluminum outer skins, and is fitted with a honeycomb center shelf with integral heat pipes. Shear webs run from the upper surface to the center shelf to distribute the shear loads. A docking cone is also supplied in the lower surface of the center body. Four removable panels on the X-X surfaces are provided for installation or removal of equipment.

The equipment housing (Figure 7.2-6) in the central body is mounted on the upper surface of the -Y outer skin and the shelf as shown. Four access panels are provided in the X-X outer skin panels for installation and removal of equipment. There is considerable additional mounting area and volume available for future growth when required. Two 16.5 inch diameter orbit adjust tanks for the hydrazine propellant are shown mounted in the central body.

The control jet geometry required for attitude control and orbit adjust is shown in Figure 7.2-7. The geometry is such as to prevent impingement of the plume on the deployed surfaces of the solar arrays and sensor bays when activated. The attitude control jets are located at the
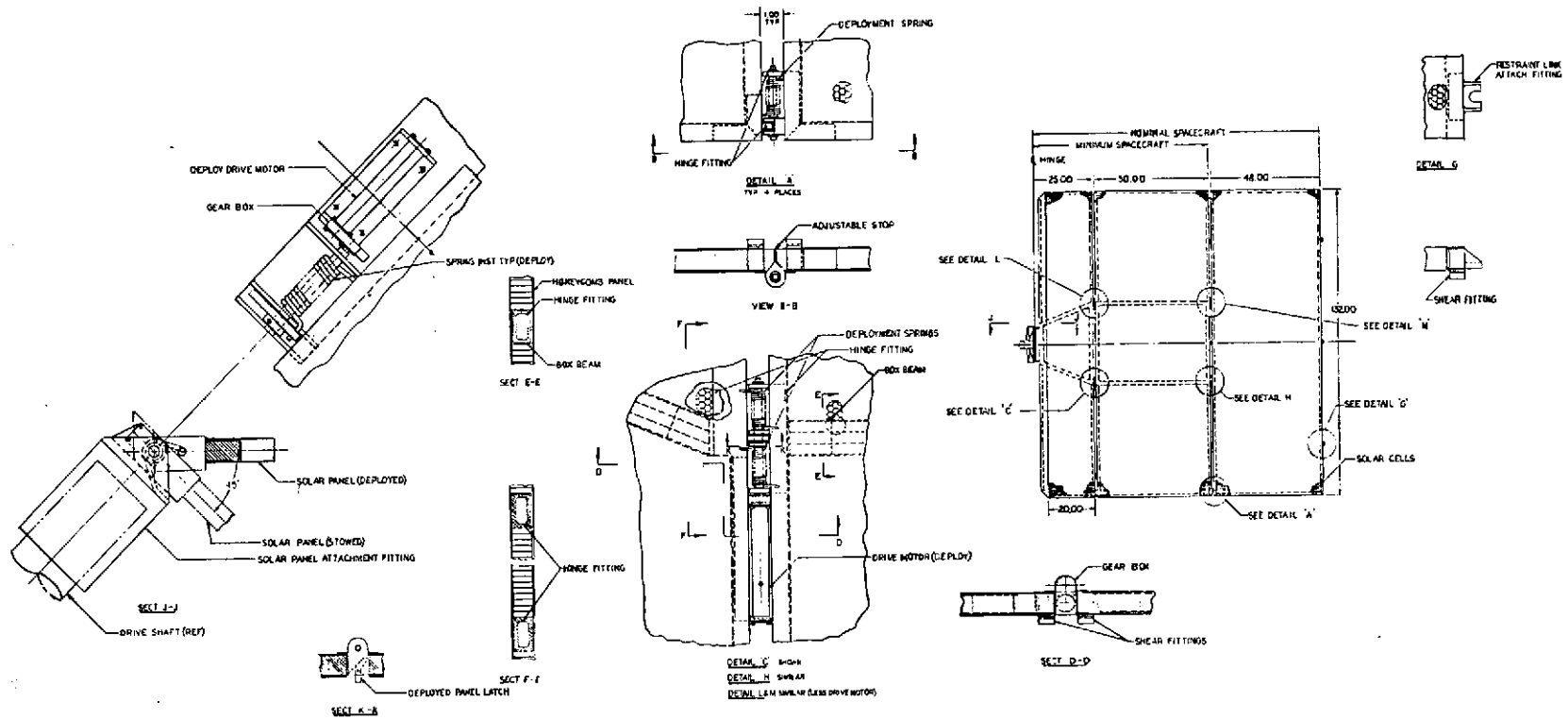
Figure 7.2-4.   EOS Solar Panel

SECTION E-E

HEAT PIPE
HONEYCOMB PANEL

HEAT PIPE
OUTER SKIN

SECTION D-D

HEAT PIPES ALTERNATELY BEND UP OR DOWN

SECTION C-C

A

SECTION A-A

REMOVABLE LIFTING HOOKS

SHEAR WEB

HONEYCOMB SHELF

DETAIL-B

SHEAR WEB

600

120 DIA DOCKING CONE

MACHINED FITTING (2)

DETAIL 'B'

Figure 7.2-5.   EOS Central Body and Tower

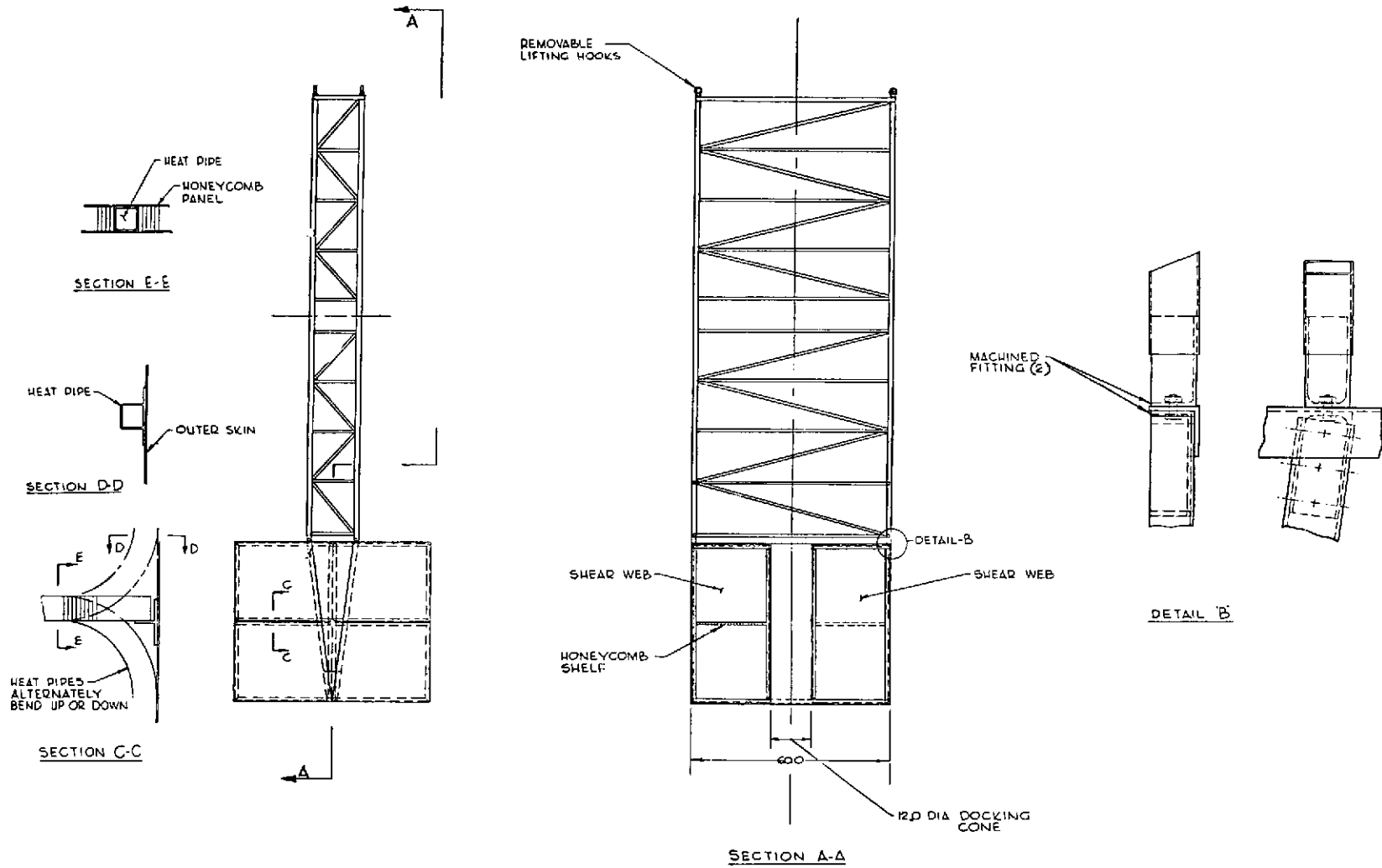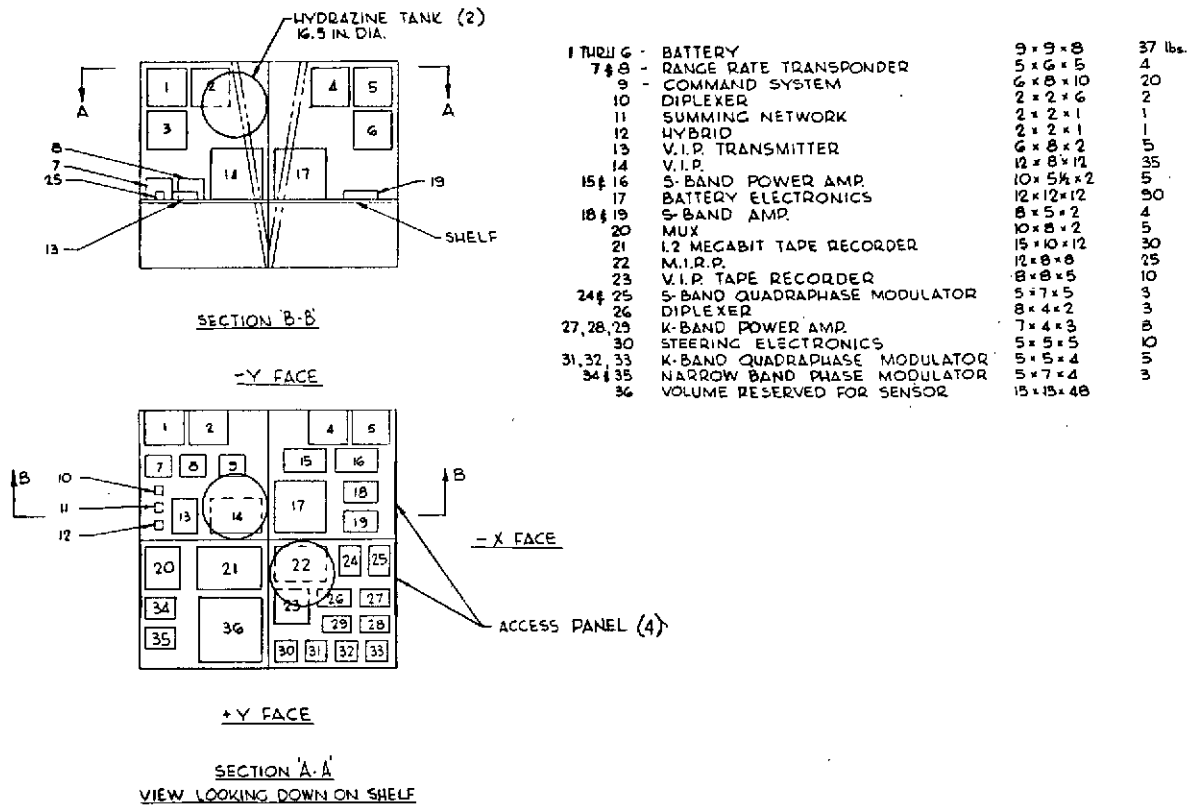|			
1 THRU 6	BATTERY	9 × 9 × 8	37 lbs.
7 & 8	RANGE RATE TRANSPONDER	5 × 6 × 5	4
9	COMMAND SYSTEM	6 × 8 × 10	20
10	DIPLEXER	2 × 2 × 6	2
11	SUMMING NETWORK	2 × 2 × 1	1
12	HYBRID	2 × 2 × 1	1
13	V.I.P. TRANSMITTER	6 × 8 × 2	5
14	V.I.P.	12 × 8 × 12	35
15 & 16	S-BAND POWER AMP.	10 × 5½ × 2	5
17	BATTERY ELECTRONICS	12 × 12 × 12	90
18 & 19	S-BAND AMP.	8 × 5 × 2	4
20	MUX	10 × 8 × 2	5
21	1.2 MEGABIT TAPE RECORDER	15 × 10 × 12	30
22	M.I.R.P.	12 × 8 × 8	25
23	V.I.P. TAPE RECORDER	8 × 7 × 5	10
24 & 25	S-BAND QUADRAPHASE MODULATOR	5 × 7 × 5	3
26	DIPLEXER	8 × 4 × 2	3
27, 28, 29	K-BAND POWER AMP.	7 × 4 × 3	8
30	STEERING ELECTRONICS	5 × 5 × 5	10
31, 32, 33	K-BAND QUADRAPHASE MODULATOR	5 × 5 × 4	5
34 & 35	NARROW BAND PHASE MODULATOR	5 × 7 × 4	3
36	VOLUME RESERVED FOR SENSOR	15 × 15 × 48	

Figure 7.2-6. EOS Equipment Layout in Central Body

top portion of the tower such that an area of approximately 2 1/2 feet by 16 inches is left vacant for possible use by a precision attitude determination system.

The attitude control propulsion system is configured so that the entire system can be handled as a unit. The propulsion system for orbit adjust is configured so that the entire system can be omitted for a mission that does not require precise control of the orbit swathing characteristics.

d. Sensor Bays. The sensor bays are utilized to house a variety of sensors and associated components As discussed previously, there will be an A, B, C, and D spacecraft. This is necessary because of the large number of possible payloads that are available and as such they all cannot fly on one spacecraft.

Basically the bays have been designed to be removable from the deployment structure as an integral module. For design purposes a worst case payload was chosen, from a structural point of view, to determine if a reasonable structural arrangement was possible. This payload consisted of several fixed sensors located at the outer portion of the bay and a rotating radiometer mounted on the inner portion. Figure 7.2-8, is the resulting structural configuration. The sensor bay is formed by two 90 inch long channel shaped longerons 5.5 inches deep, separated by channels at 3 places to a width of 60 inches. In the areas of the microwave radiometer diagonal channel construction is used to add lateral stiffness to the longerons, the tie-in points being stabilized with gussets. The equipment shelf is 1 inch honeycomb construction tied to surrounding channels with angles. The deployment arms are 48 inch long channels separated by a perpendicular channel which holds the arms 48 inches apart. Mounted to this channel is a bracket to which the operating mechanism is bolted. Diagonally mounted removable angles are inserted between the two arms to add the lateral stiffness required. These angles are removable to allow access to central

7-25
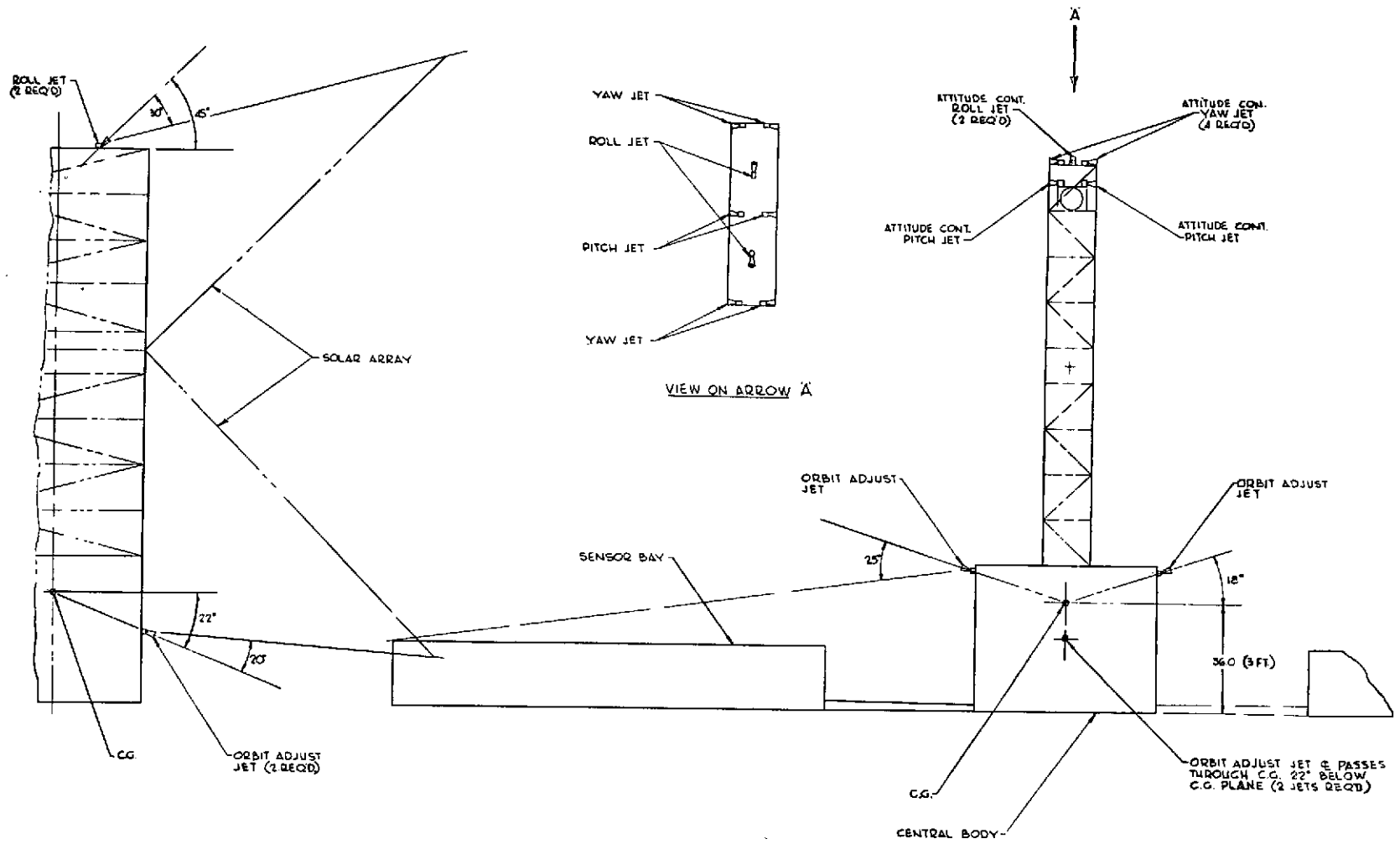
Figure 7.2-7. EOS Control Jet Geometry

SECT A-A

HONEYCOMB EQUIPMENT SHELF

PIVOT POINT

CLEARENCE PATH
MICROWAVE RADIOMETER REF

48.00

90.00

21.50

18.00

SENSOR BAY DISCONNECT
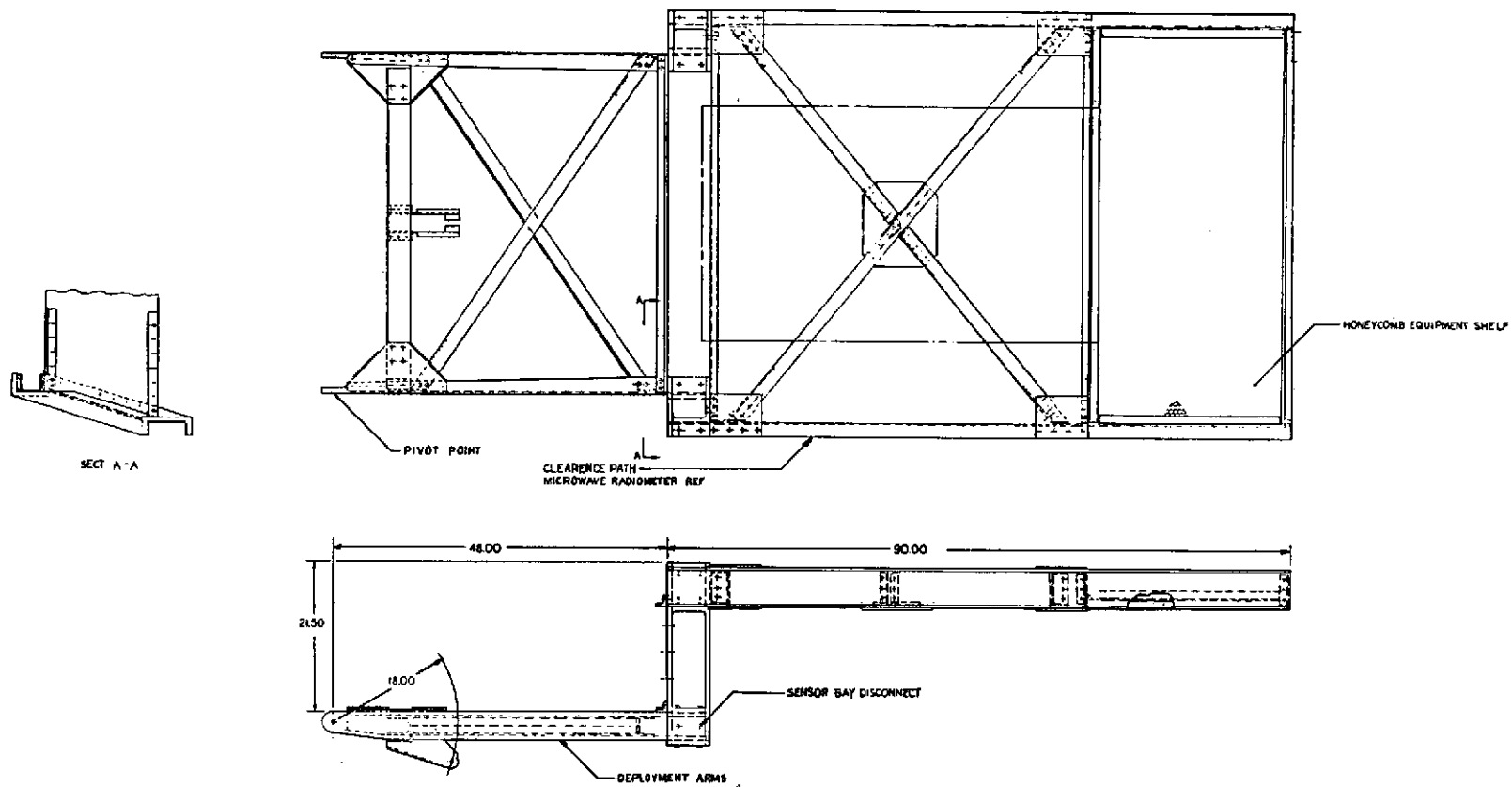
DEPLOYMENT ARMS

Figure 7.2-8.   EOS Sensor Bay Structure
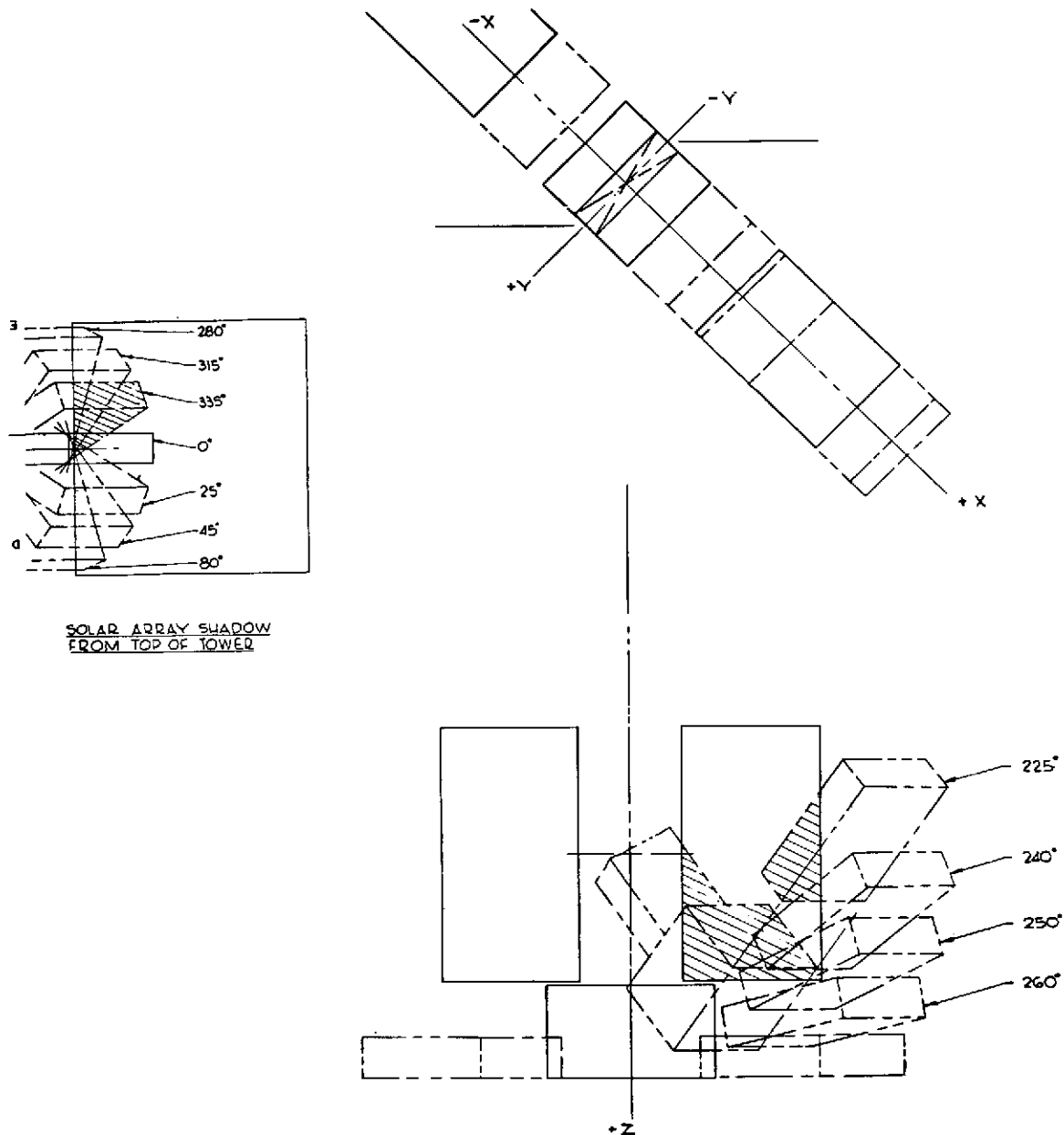
Figure 7.2-9. EOS A and B Solar Array Shadow Study

body access doors, when the equipment bay is in the stowed position. Machined "I" type fittings are used to connect the deployment arms and the sensor bay which are also tied together with a webb and two angles. The joint between the machined "I" fittings and the deployment arms is used as a disconnect point.

The sensor bay deployment arms are hinged to the central body at two places. When stowed in the vertical position the sensor bay is attached to the tower with several pyrotechnic release bolts. Energizing the pyrotechnic holding devices releases the sensor bay from the tower for deployment Supplying power to the ball screw jack will drive the sensor bay to the stowed positions when required.

e. Solar Array Shadowing. One of the factors directly affecting the solar cell area and the quantity of batteries required for a given mission is the amount of shadowing occuring during the sunlit portion of the orbit. The affect of shadowing is that the amount of power derived from the cells is reduced from what would be available with full illumination. Normally, the amount of power lost is greater than the shadowed paddle area due to the fact that the cells are interconnected. A typical array has a number of cells connected in series forming a network or pattern such that if one cell is shadowed the entire string of cells becomes electrically open thus not supplying power. Therefore, the actual loss is more than just the loss of the one cell.

There are techniques however, where through the use of sophisticated circuitry the loss of power approaches the individual cells shadowed. Therefore, that part of the paddle and battery design, Section 7.3, affected by shadowing was based on the average solar array area shadowed during the sunlit portion of the orbit.

The following method was used to determine the amount of solar paddle shadowing. Figure 7.2-9 depicts the orbital motion of the EOS A and B spacecraft with the projected shadow areas of the sensor bay, central body and tower on one solar paddle. To conserve space this motion is displayed by maintaining a fixed paddle pitch axis and rotating the spacecraft about this axis. In order to plot the shadowed area an arbitrary angular reference system was established with 0° being the equatorial location of the spacecraft in a 9 o'clock orbit.

Figure 7.2-10 is a plot of the total effective solar array area in percent for each 10° incremental rotation of the spacecraft about its pitch axis during the sunlit portion of the orbit. As can be seen from this figure the total average area shadowed is only 5.95 percent.

It should be noted here that the EOS one paddle design described in Appendix C would eliminate the shadowing problem.

7.2.3.2 EOS C and D Spacecraft. This concept (Figures 7.2-11 and 7.2-12 is similar in design to the EOS A and B spacecraft. The same tower, central body and deployment arms are used. The purpose of this concept is to enable the spacecraft to grow considerably with a minimum additional redesign. Two new sensor bays each with 60 ft^2 of earth viewing area, obtained by increasing the length to 12 feet, are substituted for the 37.5 ft2 sensor bays. On this configuration an 18.0 inch diameter earth viewing parabolic antenna and a 48 inch DRS antenna are utilized. The solar arrays are increased in size to 108 ft^2 each by the addition of another panel to each array. This configuration is shown in an 86.0 inch inside diameter Delta fairing. The deployed configuration is shown in Figure 7.2-12. The solar paddles, shown in Figure 7.2-12, consist of 3 panels with widths of 25, 50 and 48 inches by 132 inches long. Construction of the panels and their mounting to the tower are similar to that on the EOS A and B spacecraft.

The percentage of the solar array shadowed was determined utilizing the same techniques as employed in the EOS A and B shadowing study. Figure 7.2-13 shows the orbital motion of the EOS C and D spacecraft with the projected shadow areas of the sensor bay, tower, central body and the additional DRS antenna at the upper end of the tower. Figure 7.2-14 is a plot of the total effective solar array area in percent for each 10° incremental rotation of the spacecraft about its pitch axis during the sunlit portion of the orbit. As can be seen from this figure the total average area shadowed is only 7.24 percent.

The possible requirement to increase the average regulated power to 1600 watts on a future EOS C and D would require approximately twice the solar paddle area. If conventional bi-fold paddles are used a Titan shroud would have to be used instead of the Delta because of the restricted design space inside the Delta shroud. A possible exception to this would be if the roll out solar arrays proved feasible.

Figure 7.2-10   Total Effective Solar Array Area of EOS A and B Spacecraft - vs. - Orbit Position
(0° at the Equatorial Decending Node)

Figure 7.2-11.   EOS C and D Spacecraft (Stowed)

7-30

ANTENNA

100.0

JET (SEE FIG. 12)

TOWER

SOLAR ARRAY
DRIVE (2)

DEPLOYMENT MOTORS

8 IN. DIA. ANTENNA (3)

SOLAR ARRAY – DEPLOYED
108 FT^2 EACH ARRAY – TOTAL 216 FT^2
(SEE FIG. 8)

EQUIPT. INSTAL.
(SEE FIG. 11)

DOCKING
CONE

LOUVERS
(SEE FIG. 13)

VIEW ON BOTTOM OF CENTR. BODY
VIEW A-A

DEPLOY MECH.
(SEE FIG. 5)

CENTRAL BODY 25 FT^2
EARTH VIEWING AREA
(SEE FIG. 9)

SENSOR BAY (2) 60 FT^2 EACH
EARTH VIEWING AREA
(SEE FIG. 10)

224.0
(18 FT. 8 IN.)

A

A

+X

-X

18 IN. DIA. ANTENNA

+Z

Figure 7.2-12.   EOS C and D Spacecraft (Deployed)

Figure 7.2-13. EOS C and D Solar Array Shadow Study
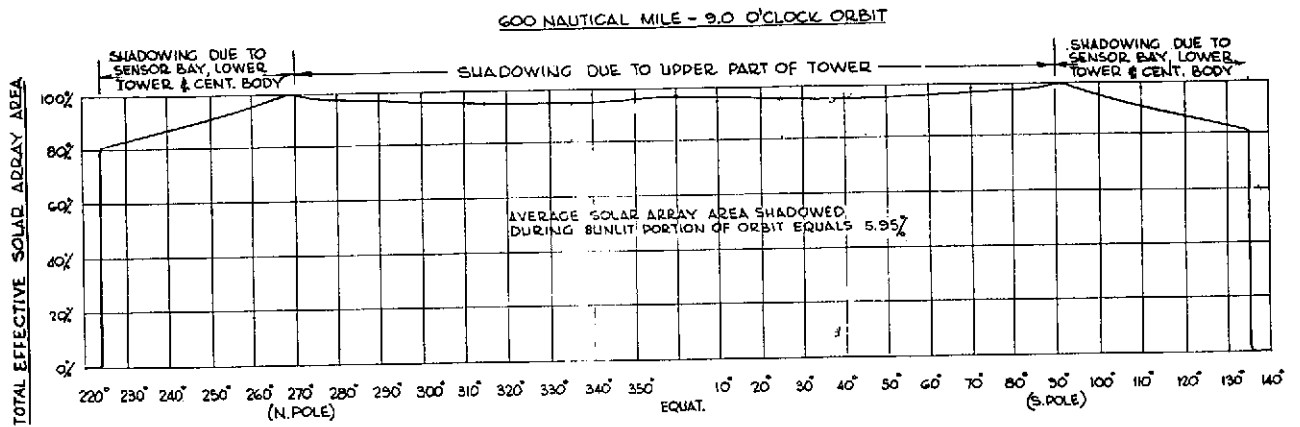
Figure 7.2-14. Total Effective Solar Array Area of EOS C and D Spacecraft - vs. - Orbit Position (0° at Equatorial Decending Node)
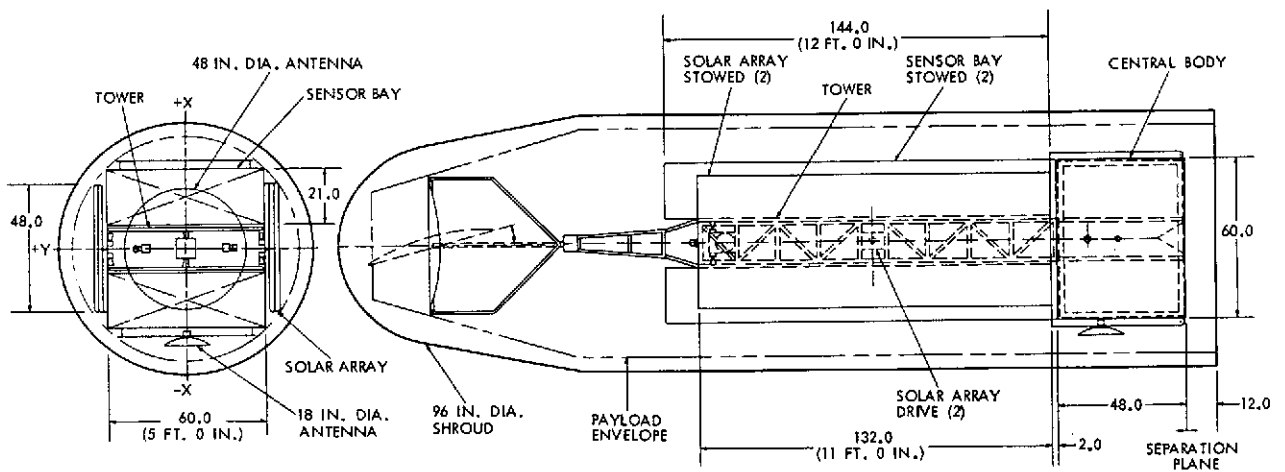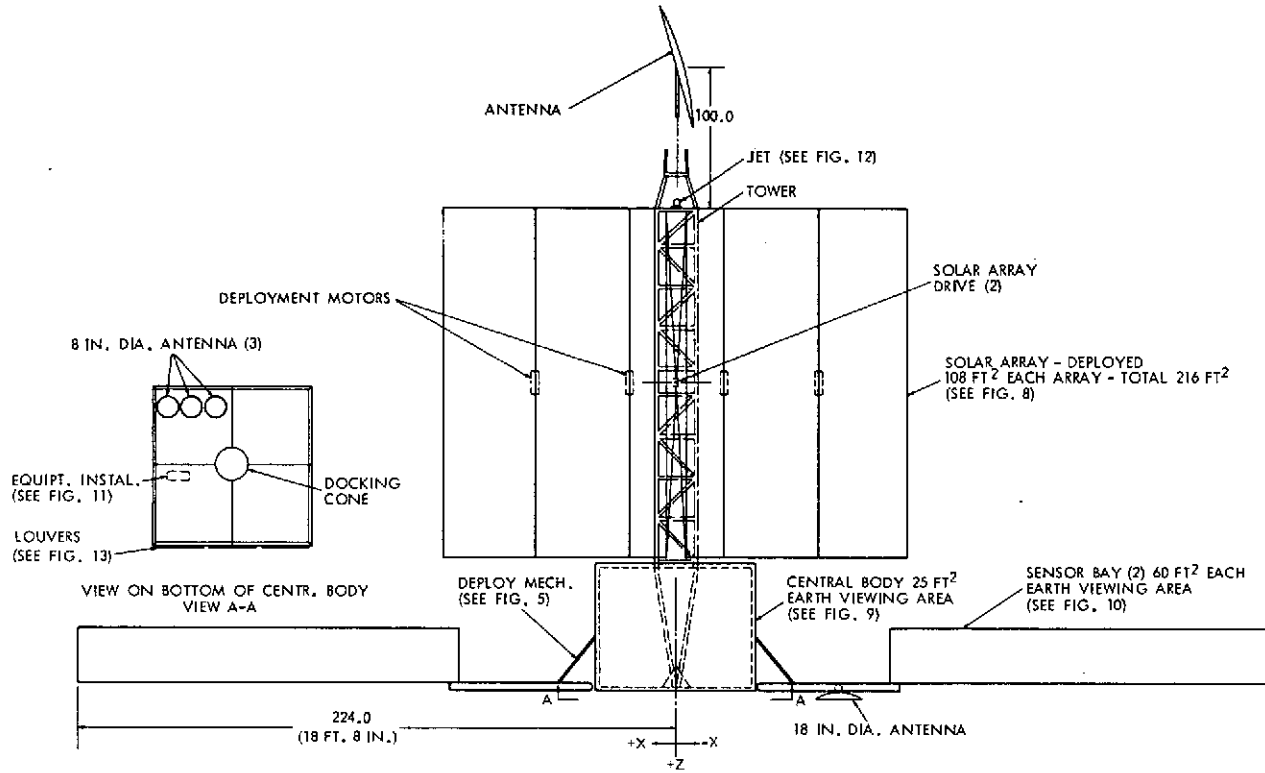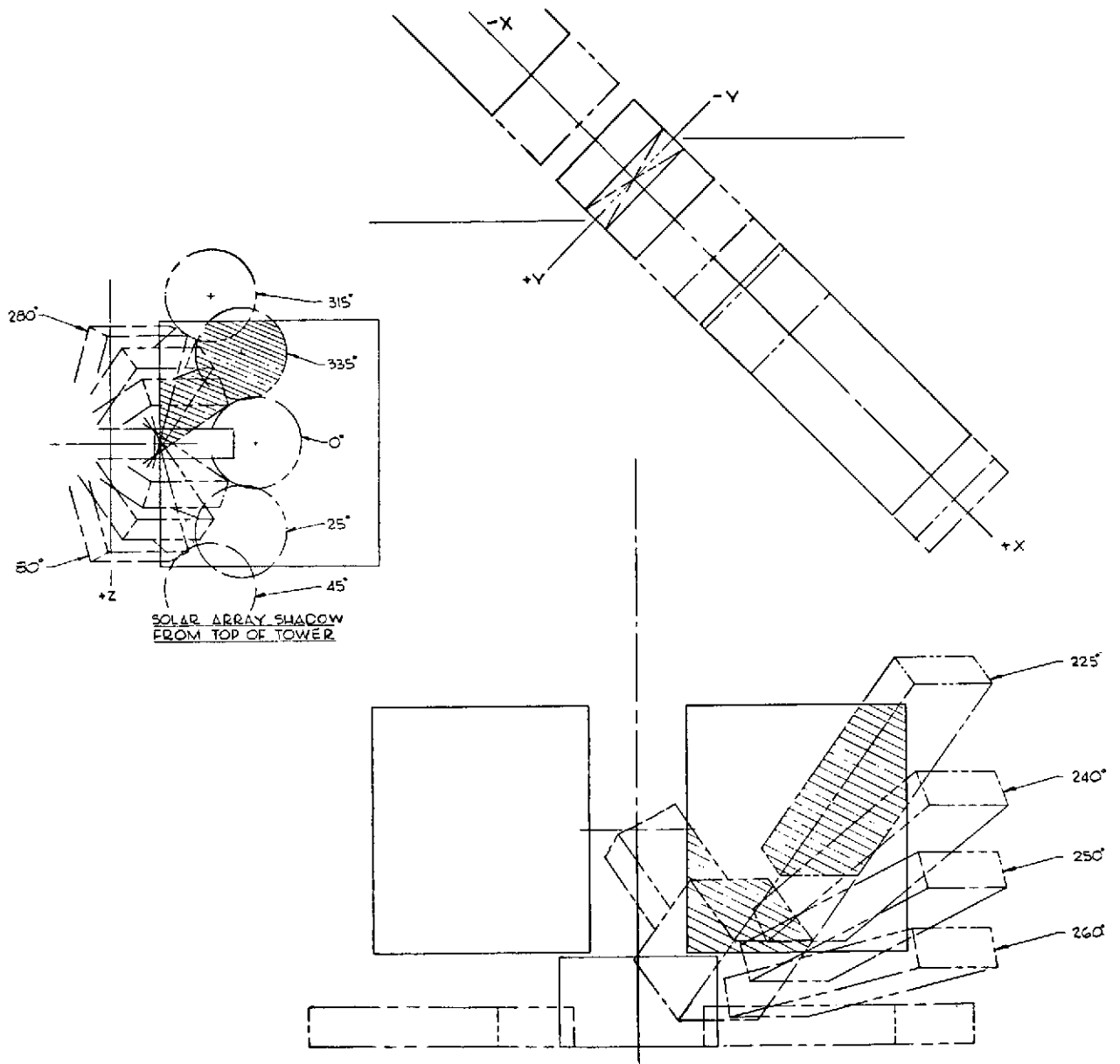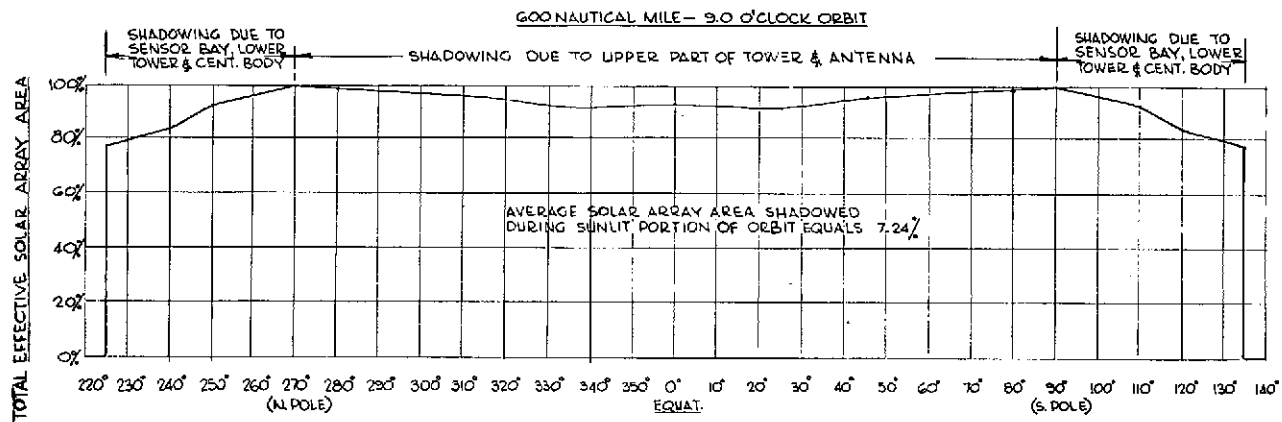
7.3 POWER SYSTEM

7.3.1 INTRODUCTION

The solar array battery and nuclear power system configurations were studied for their application to the EOS mission requirements. The power levels studied were 450 watts for EOS A and EOS B, 750 watts for EOS C and D, and a maximum power of 1600 watts for a possible maximum payload mission. The maximum power level would require a larger shroud, such as the Titan shroud, to accommodate the larger solar array. A summary of the power budget for the proposed EOS missions is shown in Table 7.3-1. All power figures refer to orbital average.

Table 7.3-1

EOS Power Budgets

Subsystem	EOS A, B Watts	EOS C and D Watts	Maximum Power Mission (Watts)
Data Handling	85	105	170
Communications	35	65	110
Attitude Control	65	65	90
Thermal	15	15	30
Payload	250	500	1200
Total	450	750	1600

Mission lifetime requirements were specified to be two years minimum and three years with degraded load capability. Orbit altitudes ranged from 400 to 600 nautical miles, and orbit hour angle from 9:00 a.m. to 3:00 p.m. The regulated bus voltage was selected as +28V ± 2% consistent with silicon transistor technology and the availability of a more efficient S-Band transmitter operating at +28V. In addition, an increase in system efficiency results due to lower I^2R losses with a 28V system.

Nuclear system design approaches are discussed in detail in Appendix E. Much of the background technical information was supplied by the Atomic Energy Commission. The Conclusions regarding the applicability of a nuclear power supply for EOS resulted from this study.

Nuclear options considered were the Multi-Hundred Watt (MHW) Radioisotope Thermoelectric Generator for the EOS A, B missions, with batteries included to meet peak power requirements. For the maximum power supply design, two concepts considered were the Zirconium Hydride (ZrHx) reactor system with static Thermoelectric (T/E) conversion and a Radioisotope Brayton Cycle system.

The RTG option was scaled upward in power level and the reactor option was scaled downward to meet the requirements of the EOS C and D systems. Scaling inefficiencies became apparent in the case of the RTG due to system complexity, cost and configuration cumbersomeness. In the reactor system, specific power and efficiency decreased because of the inconsistency between the design and the application criteria. A major reconfiguration of the spacecraft would be required to utilize the reactor power system.

7-35

The nuclear systems proposed can be catagorized as new technology in that they represent products of ongoing development programs. Therefore it is important to realize that although some sub-system components are technologically mature, the systems themselves have not been demonstrated. For example, in the systems considered, performance, weight and lifetime are postulated on the successful development of one or more components such as a high temperature (> 1200°C) isotope fuel capsule for the MHW, stable lead telluride tubular converters for the reactor system, or dependable gas bearings for the high speed rotating Brayton system. In each instance the component is a critical one and derated performance results in a large penalty or an impractical system. In spite of the many application studies for all the above systems there is much uncertainty in lifetimes, weights and efficiencies. Extrapolations from any of these analytical studies to the EOS application involves a high degree of risk . In addition the weight and cost of the nuclear system, as compared to a solar array/battery system is unfavorable, as shown by Table 7.3-2. It does not appear that a nuclear power system would offer any substantive advantage over solar power systems for the EOS missions and is therefore not recommended for further consideration at this time.

Table 7.3-2

Solar and Nuclear Systems

Power (Watts)	Development Cost[1] (M)			System Cost[2] (M)			Weight (lb)		
	450	750	1600	450	750	1600	450	750	1600
Solar Approach	1.3	1.9	3.6	1.3	1.9	3.6	340	530	1090
MHW-RTG[3]	30	30	30	9.3	16.1	32	425	635	1515
Reactor Tye[3]	--	74	74	--	20	20	--	635	1445
Isotope Cycle Brayton[3]	--	--	130	--	--	25	--	--	2624

[1]Including system integration costs.
[2]Based upon NASA reimbursed costs to the AEC for additional SNAP 27 units as follows: Fuel Cost, $13,000/watt electrical; $725,000/unit (75 watt each); Total reimbursable cost to AEC for 3 units (75 watts each) was $5.1 M.
[3]No firm foundation is available to determine accuracy of these cost values. See discussion in Appendix E.

The recommended power system for all EOS designs is an oriented solar array/battery system that utilizes direct energy transfer (DET). The highlights of the studies leading to the recommended solar array system are given in the remainder of this section. Details can be found in Appendix F.

7.3.2 SYSTEM CONFIGURATION

Two solar array/battery systems were considered for fulfilling the EOS requirement of a regulated bus. These are a series regulated system (similar to Nimbus or Tiros) and a shunt-boost system (similar to IMP-I and ATS-F). The latter is called a direct energy transfer (DET) system.

Figure 7.3-1 shows the essential features of the two configurations. In the series system, solar array power during the day and battery power at night is delivered to the load through an in-line bucking regulator, with a typical efficiency of 90%. Battery charge power is controlled through a series charge regulator. A shunt regulator prevents the unregulated bus from rising to excessive voltages when the solar array is lightly loaded.

SERIES REGULATED SYSTEM

SHUNT-BOOST REGULATED SYSTEM
(direct energy transfer system)
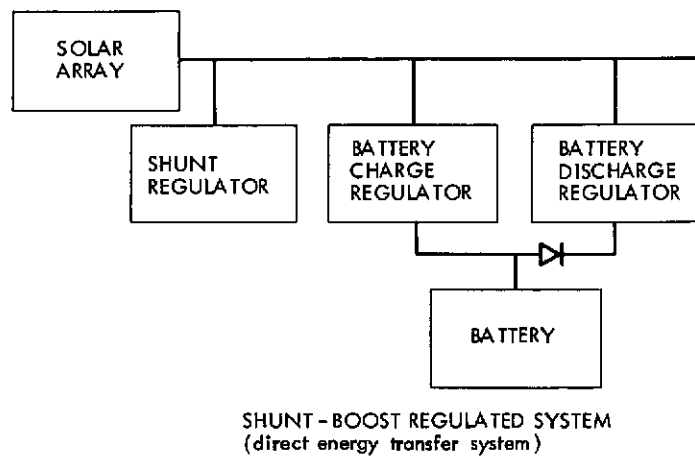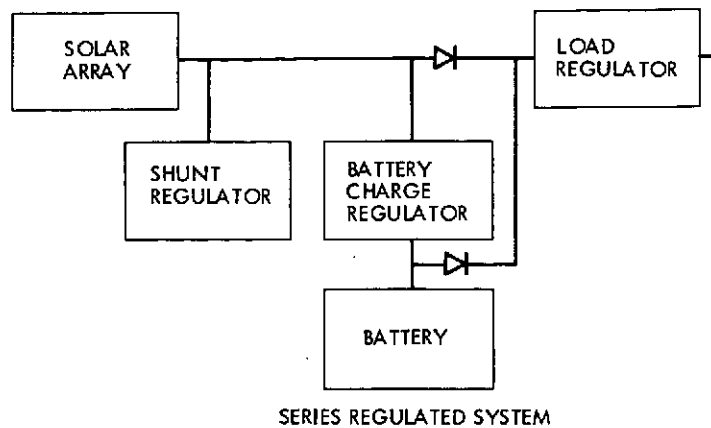
Figure 7.3-1.   Comparison of Series and Shunt-Boost Regulated Systems

The DET system has the same number of major components, but they are arranged differently. During satellite night, the power flow in both configurations is similar; i.e. from the battery through an in-line regulator. However, in the DET system the power is boosted up to the regulated voltage whereas the series system usually reduces the input power down to the regulated voltage. During satellite day, the regulated bus is maintained by shunting any solar array power in excess of the load power with the battery charge regulator and/or the shunt regulator. Therefore, regulated solar array power is delivered to the loads without passing through an in-line device with the attendant loss of efficiency.

At 500 n.m. altitude and high noon circular orbit, the ratio of required solar array power for a DET to that for a series configuration (all other considerations being equal) is 0.925. Thus, the DET system is recommended because of the lower solar array power it requires.

A somewhat more detailed description of the DET system follows. Referring to Figure 7.3-2 the central control unit monitors the regulated bus and activates the particular electronic unit necessary to maintain regulation. For example, during satellite night, the control unit, sensing a falling bus voltage, turns on the boost battery discharge regulator. During sunlight, as the solar array begins to augment the battery power, the discharge regulator will begin to turn off. When the solar array can fully supply the load power, the discharge regulator is turned completely off and the buck battery charge regulator is turned on. The control unit keeps the shunt regulator turned off until the battery has been fully charged or until the maximum allowable charge rate has
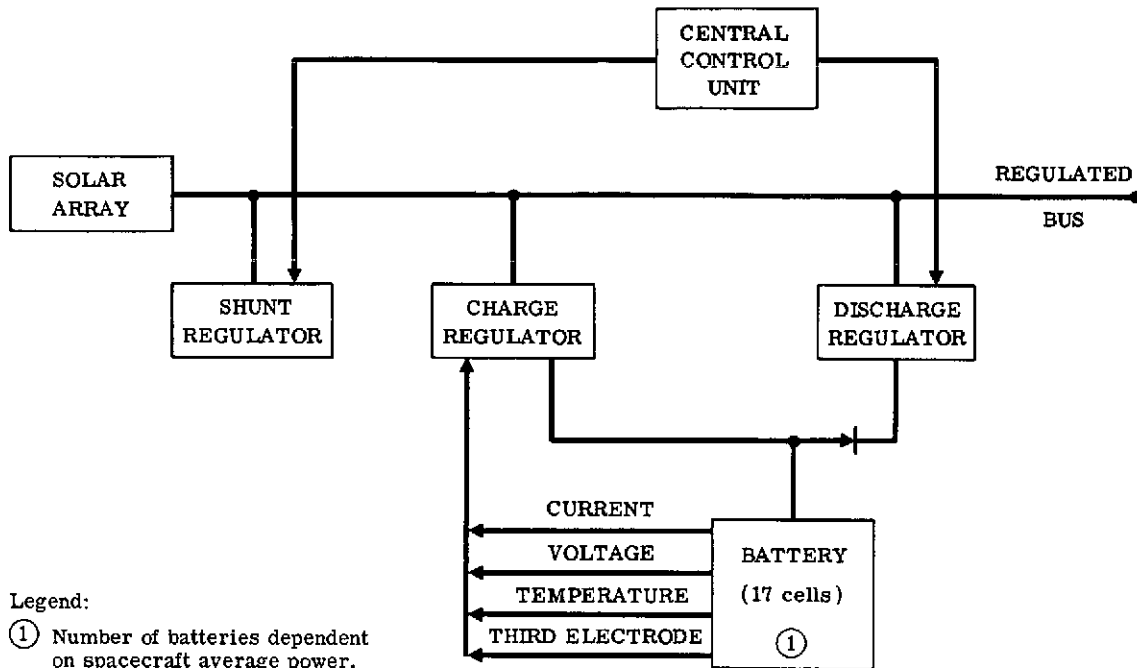
Figure 7.3-2. Recommended EOS Power System (Direct Energy Transfer)

been reached. Each of these latter two conditions implies an excess of useable solar array power and the regulated bus voltage will begin to rise when they occur. The control unit senses the rising voltage and turns on the shunt regulator sufficiently to maintain regulation within proper limits.

All critical electronics are fully redundant. In the event of a unit failure, the appropriate electronics are automatically switched upon receipt of signals from the failure detection circuitry. Simultaneously, all non-essential spacecraft loads are turned off in an attempt to remove the fault and to conserve battery power.

Table 7.3-3 shows the fault conditions that activate the failure detection circuitry. Each function is time delayed to negate transient effects and can be overridden by ground command.

Table 7.3-3
FAULT CONDITIONS

1.	Regulated bus overvoltage
2.	Regulated bus undervoltage
3.	Battery undervoltage
4.	Simultaneous discharge regulator current and charge regulator current
5.	Simultaneous discharge regulator current and shunt regulator current
6.	Simultaneous charge regulator and shunt regulator current (prior to current limit or fuel charge)

7-38

7.3.3 SOLAR ARRAY

Several EOS orbits and power levels have been considered in the solar array design. In particular, 400, 500, and 600 nautical mile, sun-synchronous orbits were studied at hour angles of 9:00 a.m. and high noon. Power levels were specified to be 450, 750, and 1600 watts of average regulated power with 100 percent peak overloading for the EOS A and B, EOS C and D and maximum power missions respectively.

The solar array was taken to be sun-oriented, similar to the Nimbus ERTS arrangement. This does not rule out fixed arrays as a possibility for EOS. Trade-off considerations of fixed vs. oriented arrays should be studied during Phase B. The oriented design selected as the baseline is based on proven techniques and is compatible with the rest of the spacecraft design presented in this chapter. Large lightweight fixed arrays, such as the roll-up arrays proposed by various manufacturers, require more study to establish their feasibility, reliability, and compatibility with the overall EOS spacecraft design. For example, the interaction between large flexible arrays and the spacecraft control system would have to be established and shown to be non-injurious to the arrays and to control system performance. Detailed calculations in the oriented solar array study are given in Appendix F. The key points of this study are the following:

The required solar array power varies linearly with the average load power and the ratio of satellite eclipse time to satellite sun time. Thus, a 400 nautical mile high noon orbit requires more solar array power than a 600 nautical mile high noon orbit. Similarly, a 600 nautical mile high noon orbit requires more solar array power than a 600 nautical mile, 9:00 a.m. orbit.

However, some factors run contrary to this trend when sizing the Beginning Of Life (BOL) solar array capacity. For one, the solar array degradation with time is much more pronounced at 600 nautical miles than at 400 nautical miles. Secondly, the shadowing of the solar array in a 9:00 a.m. orbit may offset the effect of increased time in daylight when compared to a high noon orbit of the same altitude.

The net effect of lifetime and altitude on required BOL solar array power, for high noon orbits, is shown in Figure 7.3.-3. The curves are normalized with respect to average load power, so that they apply equally well to the 450w, 750w, and 1600w average power systems. It is evident that the 600 nautical mile orbit imposes the severest requirement on BOL solar array power. For a two year mission, the required BOL solar array power is 2.36 times the average load power.

If the solar array power capability were designed to satisfy the 600 nautical, high noon orbit, then there would theoretically be some reserve capacity in a 600 nautical mile, 9:00 a.m. orbit. Calculations show that this theoretical reserve capacity would range from about 9 percent at the summer solstice to 18 percent at the winter solstice. However, shadowing studies for the baseline spacecraft configuration indicate an 8 to 10 percent loss in average solar array power in a 9:00 a.m. (or 3:00 p.m.) orbit due to shadowing of one solar paddle by parts of the spacecraft. Thus, the solar array design for the 600 nautical mile high noon orbit would closely match the solar array power required in the 9:00 a.m. and 3:00 p.m. 600 nautical mile orbits as well.

In summary, an oriented solar array power capacity equal to 2.36 times the average required load power would satisfy all EOS orbits from 400 to 600 nautical miles at orbit hour angles from 9:00 a.m. to 3:00 p.m. for two years. Beyond two years there would be a deficiency for a 600 nautical mile orbit, in the solar array power to support the same average load, as shown by Figure 7.3-3. This would necessitate a reduction in the average load power after two years for this orbit. Interestingly enough though, this solar array sizing would support the same average load over a three year period in the case of a 500 nautical mile orbit, again as shown by Figure 7.3-3.

Taking into account various solar array design factors such as packing factor, operating temperature, etc., the solar array output at BOL is estimated to be about 9.34 watts per square foot. This output, combined with the solar array design goal for EOS of 2.36 watts per watt of average load power,
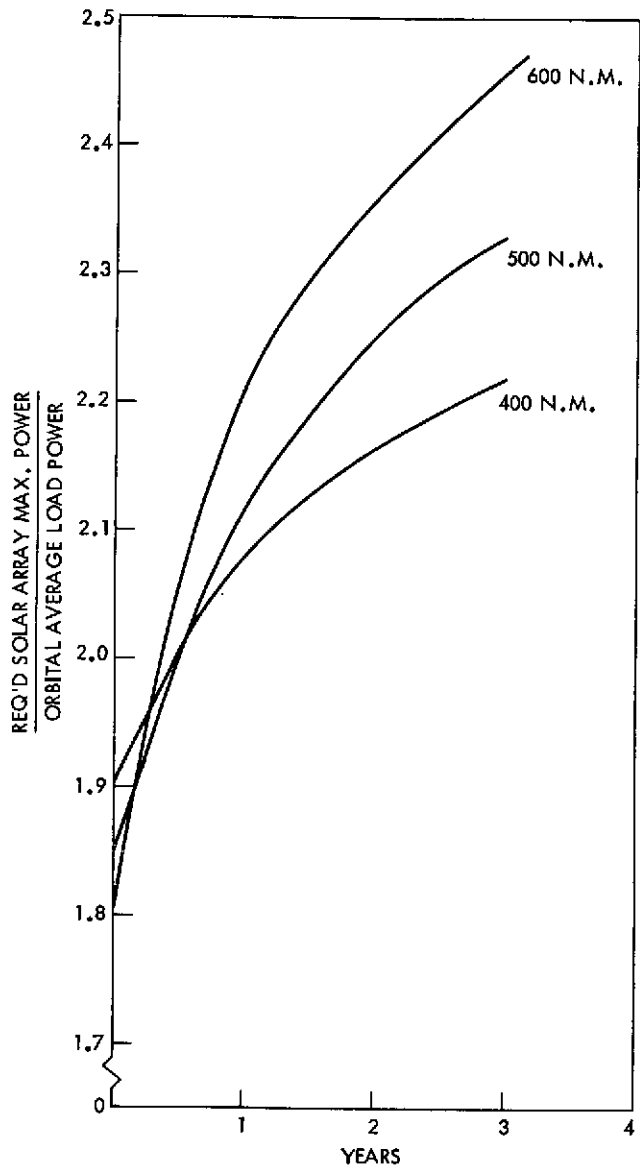
Figure 7.3-3.   Solar Array Maximum Power vs Lifetime

enables the determination of array area for the various sizes of EOS power systems under consideration.   Weight estimates can also be formed based on typical lightweight arrays which weigh approximately 1.0 pounds per square foot (including wiring and deployment mechanisms). Solar array power, size, and weight for the various missions are summarized in Table 7.3-4 in which an extra 5 percent margin has been included.

7.3.4 BATTERY

High charge and discharge rates coupled with extended lifetime requirements dictate the use of nickel cadmium N_iCd batteries for EOS. A_gCd and AgZn batteries are impractical because they do not possess the aforementioned requirements.

Table 7.3-4

Solar Array Summary Beginning of Life (BOL)

Avg Load Power (W)	Solar-Array Power (BOL) (W)	Solar-Array Size (ft^2)	Solar-Array Weight (lb)
450	1120	120	120
750	1860	200	200
1600	3960	425	425

Table 7.3-5 shows the number of nightime cycles that EOS will experience at the three altitudes of 400, 500 and 600 n. m.

Table 7.3-5

EOS Battery Cycles

ALTITUDE (n. m.)	400	500	600
CYCLES (2 yr)	10,548	10,150	9,776
CYCLES (3 yr)	15,822	15,325	14,664

Tests at NAD Crane and GSFC have shown NiCd cycle life in excess of 12,000 cycles at 25 percent Depth Of Discharge (DOD) at 25°C for charge and discharge rates similar to those that will be experienced on EOS. There are 20 cells currently undergoing testing in excess of 20,000 cycles. To date one cell has failed, after 5,000 cycles, to deliver the required ampere-hours. Since 12,000 cycles more than meets the EOS requirement of two year lifetime, this nominal depth of discharge appears to be a reasonable choice. Further data and analysis relating to this choice can be found in Appendix F.

In the following paragraphs relating to battery sizing, 25 percent DOD is treated as a maximum allowable DOD. Thus, utilizing an integral number of standard ampere-hour batteries, the actual DOD will generally be less than 25 percent. This then provides an additional safety factor with regard to battery life. Table 7.3-6 shows the required ampere hour capacities for 25 percent DOD for the EOS A and B, EOS C and D and maximum power missions at any of the EOS altitudes.

Table 7.3-6

Required Ampere Hour Capacity

POWER (W)	450	750	1600
CAPACITY	66	111	236

The required number of various standard batteries, their total weight, and the resultant depth of discharge is shown in Table 7.3-7. This table assumes 17 series cells per string which is derived by limiting the maximum cell voltage to 1.53 volts and by maintaining the string voltage low enough to permit regulation to +28 volts by the DET system.

Table 7.3-7

Number of Batteries Required For 25 Percent

Maximum Depth of Discharge (DOD)"

Battery Size (Amp-h)	450 w Avg. Load			750 w Avg. Load			1600 w Avg. Load		
	No.	Wt (lb)	DOD%	No.	Wt (lb)	DOD%	No.	Wt (lb)	DOD%
15	4	122	24	7	213	23	14	427	25
20	3	126	24	5	210	24	10	419	25
50	2	212	16	2	211	24	5	525	21
100	1	209	16	1	209	24	3	627	17

The selection of the batteries for each mission is governed by several factors. One is the desirability of avoiding an excessive number of batteries since this adds to the cost. Another is the need to avoid an overly large capacity battery for a given mission since this can result in a DOD much below 25 percent with a consequent increase in battery system weight. Another factor is the desirability of using the same battery size on the EOS A and B and EOS C and D missions. The growth from EOS A, B to EOS C and D battery system can then be implemented by simply adding a few more of the same type battery.

Taking these factors into account, the recommended battery system for the EOS A and B missions are three 20 amp-hr batteries. For the EOS C and D missions, five 20 amp-hr batteries are required. As seen from Table 7.3-7, this results in a 24 percent DOD which allows a small margin over a two year lifetime. For the maximum power mission, five 50 amp-hr. batteries are appropriate, resulting in a 21 percent DOD.

7.3.5 ELECTRONICS

The recommended Direct Energy Transfer (DET) system utilizes a shunt regulator together with buck-charge and boost-discharge battery regulators, all of which are controlled by a central control unit. The shunt regulator and boost-discharge battery regulator are each standby redundant and automatically switched upon failure. Only one battery charger is provided for each battery since failure of one battery/charger combination will only degrade load capability.

The shunt regulator maintains bus voltage, when solar array power is in excess of needs, by shunting the excess through power resistors. These resistors should be mounted at or external to the spacecraft skin, for thermal dissipation purposes. Each buck battery charger utilizes a pulse width modulation (PWM) design that is non-dissipative although a simpler dissipative design is possible at reduced efficiency (82% vs 90% for the PWM design). For the baseline system, the PWM design is recommended. The battery discharge regulator utilizes a boost autotransformer design to maintain a +28V ± 2% bus for an input voltage between 17 and 26 volts.

Since a 100 percent power overload capability is considered desirable at this time, all of the regulators are sized for 900, 1500, and 3200 watts for the EOS A and B, EOS C and D and maximum power missions respectively. If these peak overloads do not materialize upon more detailed examination, then of course the size and weight of these regulators can be reduced.

The Central Control Unit (CCU) determines the mode of operation of the system. The essential feature of the CCU is that deadbands must be provided over the range of regulation to separate the operating ranges of the shunt, buck, and boost regulators. This separation insures that the

solar array is used to its maximum efficiency, and that simultaneous operation of two electronic units is avoided when not essential.

The CCU, charge and discharge regulators, telemetry and failure detection/protection circuitry could all be packaged in a single unit designated as the Power Control Unit (PCU). This packaging scheme is in line with the modular design goal for EOS. It would allow checkout of all power system electronics at one time and would facilitate integration into the spacecraft via a single mechanical interface. Table 7.3-8 shows the estimated electronics weight for the three power profiles under consideration.

Table 7.3-8

Power System Electronic Weight

AVG LOAD POWER (W)	450	750	1600
WEIGHT (lb)	54	90	192

7.3.6 SUMMARY

The recommended power system for EOS utilizes oriented solar arrays, a direct energy transfer system, and NiCd batteries to provide a +28V ± 2% regulated bus. The average regulated power is 450, 750, and 1600 watts for the EOS A and B, Eos C and D and maximum power profiles under consideration.

The regulators are sized to handle a 100 percent peak overload. All of the regulators are standby redundant except the batter chargers where an individual failure is not catastrophic. The batteries are sized to limit depth of discharge to 25 percent or less which is consistent with a minimum of two years life. Three year life may be possible with the same system with degraded performance.

The sizes and weights of the various power system components for each mission profile, as well as the weight totals, are given in Table 7.3-9.

Table 7.3-9

Solar Power System Weights

ITEM	450 w SYSTEM		750 w SYSTEM		1600 w SYSTEM	
	SIZE	Weight (lb)	SIZE	Weight (lb)	SIZE	Weight (lb)
Solar Array	120 ft^2	120	200 ft^2	200	425 ft^2	425
NiCd Batteries	3-20 amps (24% DOD)	126	5-20 amps (24% DOD)	210	5-50 amps (21% DOD)	525
Electronics (DET System)		54		90		1 92
Total Weight		3 00		500		1142

Note that the solar array weight does not include the weight of the solar array drive (~ 20 lbs.) which, by custom, is included in control system estimates.

Each system is capable of supplying its rated average load power for a minimum of two years in any EOS orbit from 400 to 600 nautical at any hour angle between 9:00 a.m. and 3:00 p.m. At altitudes lower than 600 nautical miles, there is added margin in the power system which can be converted to longer life and/or increased daylight loads.

7.4 COMMAND & DATA HANDLING SYSTEMS

7.4.1 INTRODUCTION

The data handling requirements for the several EOS missions are separable into three data rate ranges.

a. Low-rate data (less than 12.5 kb/s). This includes all housekeeping telemetry and any low data rate experiments such as the Passive Multichannel Microwave Radiometer.
b. Medium rate data (0.1 to 2 mb/s). The Ocean Scanning Spectrophotometer, Sea Surface Temperature Imaging and Cloud Physics Radiometer would be included in this category.
c. High rate data (30 mb/s and greater). The Thematic Mapper is in this category.

For EOS A, only the first two of the above data rates will be utilized. The Passive Multichannel Microwave Radiometer and spacecraft housekeeping have low data rate requirements of less than 8 kb/s. All other EOS A sensors are in the medium rate category. For EOS B a high data rate requirement would exist for the Thematic Mapper. This sensor's resolution of 66 meters would result in a 30 mb/s output rate.

For future EOS missions, the data rates associated with the low and medium rate sensors would not significantly change over present requirements. However, because of possible increased resolution requirements for thematic mapping or the addition of other high data rate sensors such as radar, the high data rate requirement could increase to 100 mb/sec.

The three distinct data rate categories (with separate utilization requirements for each category, i.e. full orbit storage for medium rate and partial orbit storage for full rate) led to the conclusion that a separate data handling system for each category would provide the most efficient and flexible approach to implement EOS requirements. Moreover, by designing separate systems, different logic circuitry could be employed with different power dissipation requirements for each system. This would result in a more efficient power budget for the total system requirements. Power utilization becomes extremely important because of the high power circuitry required for the high data rate system. Yet another reason for the choice of separate data handling systems is that full advantage can be taken of existing Nimbus/ERTS designs and past experience.

In the development of system concepts to handle the above types of data, flexibility was taken to be of primary importance. This flexibility will provide for accommodation of various sensor compliments and for future growth in capacity for various EOS missions.

The three data handling systems proposed to meet EOS data handling requirements are shown in Figure 7.4-1. The Versatile Information Processor System (VIP) would process the data from the low data rate sensors and spacecraft housekeeping telemetry (from 1 to 12.5 kb/sec), the Manipulated Information Rate Processor (MIRP) would process the data from medium data rate sensors (up to approximately 2 mb/sec) and the Multi-megabit Operation Multiplexer System (MOMS) would process the data from the high rate sensors (30 mb/sec and up).

The proposed VIP system is based on an existing concept whereas the MIRP & MOMS are new concepts. Through the use of reprogrammable memory, the VIP low rate data handling system will provide a high degree of sampling and formatting flexibility-this flexibility being achieved without design or wiring changes. The VIP system proposed would be similar in concept, but not in hardware implementation, to the low rate data handling system flown successfully on Nimbus IV (also to be flown on advanced Nimbus & ERTS satellites). The VIP has proved to be reliable and adaptable to various mission requirements and can be used efficiently for various EOS payload configurations.

The MIRP medium rate data handling system will sample sensors during their active scans at full required rates and then buffer and use the sensors' back scan time to output the buffered

TABLE 7.4-1

DATA HANDLING SYSTEM PARAMETERS

Versatile Information Processor (VIP)		
Centralized, redundant	-	1170 cu. in., 7.5 watts, 37 lbs.
Remote, redundant	-	1000 cu. in., 7 watts 34 lbs.
VHF transmitter	-	80 cu. in., 3.5 watts, 4 lbs.
VIP tape recorder	-	280 cu. in., 7 to 11 watts, 10 lbs.
Manipulated Information Rate Processor (MIRP)		
Redundant, w/o buffers	-	500 cu. in., 7 watts, 14 lbs.
Buffers	-	250 cu. in., 9 watts, 9 lbs.
1.2 megabit tape recorder	-	800 cu. in., 30 watts, 30 lbs.
Multi-megabit Operation Multiplexer System (MOMS)		
Redundant, w/o buffer	-	1000 cu. in., 70 watts, 50 lbs.
2.0 megabit buffer	-	700 cu. in., 16 watts, 25 lbs.
30 megabit tape recorder	-	3000 cu. in., 70 watts-record, 120 watts-playback- (17 watts average), 80 lbs
Command System		
Command clock	-	480 cu. in., 15 watts, 20 lbs.

samples. This will reduce average sampling bandwidth requirements and enable data rates compatable with the packing density capability of tape recorders being developed.

The MOMS high rate data handling system will, like the MIRP, reduce output bandwidth requirements by selective sampling and smoothing.

Although possible use of an on-board computer for the data handling systems is not now being recommended, there are many potential uses for such a computer that should be investigated in a detailed trade-off study in Phase B. The section which follows later titled "On-Board data Processing on EOS" examines potential computer usage on EOS.

A summary of basic parameters of the proposed data handling system is given in Table 7.4-1.

7.4.2 DATA HANDLING SYSTEMS

7.4.2.1 Versatile Information Processor VIP. The Versatile Information Processor (VIP) that will be used to format all analog and digital low rate sensor and housekeeping inputs is shown in Figure 7.4-2 and is described in greater detail in Appendix G. The VIP offers considerable flexibility in the sampling and formatting of inputs. This flexibility is achieved through the use of a reprogrammable memory without wiring changes to the system. The VIP is modular in construction and its capacity can be easily expanded or decreased for different mission requirements. For example, on Nimbus IV, 575 analog gates were contained in the VIP analog multiplexer module. The analog capacity can be doubled to 1150 analog gates by adding a second multiplexer module. If, however, the present capacity is excessive for a particular mission, a smaller multiplexer module containing fewer input gates could be substituted.

The VIP's output rate is variable between 1 and 12.5 kb/sec (100 to 1250 samples/sec). Analog, single-bit digital, and serial-digital data can be handled by the VIP. Without hardware changes, any input can be sampled at a multitude of rates. The total spacecraft sampling requirements can be changed by programming accomplished through a reloadable memory.

On EOS A and B, the Passive Multichannel Microwave Radiometer, in addition to all of the spacecraft housekeeping telemetry, will use the VIP. The formatted VIP output will be recorded on a single track, narrow band tape recorder (similar to the one being utilized on ERTS) and played back at a 24 to 1 speedup ratio and then transmitted over the S-band transmission link. Real-time VIP data will be transmitted over a low power VHF transmission link. In addition to providing a low power, real-time VIP only mode which will utilize existing ground equipments, VHF transmission is required for S-band signal acquisition at Stadan sites.

The VIP output will also be formatted into the MIRP data stream to be transmitted over the S-band link in real or stored time. The VIP output will be sent directly over the S-band link (either directly or after storage) when the MIRP is turned off. The Phase B study should consider the need for the various S-band VIP modes of operation when the complement of sensors is better defined.

For futher Phase B consideration, the possibility of storing part of the VIP data for VHF data (24 kb/s playback rate) could be transmitted over the VHF link. This 1 kb/s rate is sufficient for all the housekeeping information.

A two track tape recorder could store the total VIP output on the track for transmission over the S-band link and could store the 1 kb/s VIP housekeeping telemetry on the second track for VHF transmission.

7.4.2.2 Manipulated Information Rate Processor (MIRP). The Manipulated Information Rate Processor (MIRP) which will be used to sample and format the medium rate data is shown in Figure 7.4-3 and is described in greater detail in Appendix G. The MIRP will use memory loaded instructions to develop control signals to generate multiple sampling rates tailored to each sensor output characteristic and thereby reduce the average rate and bandwidth requirements. Sensor data will be sampled by the MIRP in analog or digital form.

Three sensors presently specified, the Oceanic Imaging Spectrophotometer (OIS), the Cloud Physics Radiometer and the Sea Surface Temperature Imaging Radiometer Will utilize the MIRP. During the sensor's earth scans, sensor channels will be sampled and placed in a smoothing buffer to be outputted during the full 360 degree sensor scan. Selective sampling and smoothing will provide a more than 3 to 1 reduction in output bit rate.

The OIS outputs 20 channels at 2 km resolution over a $\pm$ 25 scan. At 28 percent scan efficiency, using 2 samples per IFOV element, 8 bits per sample, and 10 percent allowance for synchronization and calibration, the total bit rate would be 1.76×10^6 bit/sec. A buffer for a full scan would need 140,000 bits. This is the maximum size that would be required since it is possible to read out and store simultaneously so that only a portion of the scan need be stored. Using a 140,000 bit buffer would result in a reduced output bit rate of 496 kb/sec.

The Cloud Physics Radiometer outputs 5 channels at 2.5 km resolution over a + 51 degree scan angle; the Sea Surface Temperature Imaging Radiometer outputs 5 channels at 2 km resolution over a + 51 degree scan. At 28 percent scan efficiency, using 2 samples per IFOV element, 10 bits per sample, and 10 percent synchronization allowance, the total bit rate would be 1.83×10^6 bits/sec. Full buffering would require a 159,700 bit buffer and would average the output bit rate to 506 kb/sec. The random access buffers required by the MIRP are within the present memory state-of-the-art. Using unipolar, 2 mil plated wire the MIRP memories would require 9 watts, and occupy 250 cu. in. and weigh 9 lbs. Thus, with buffering the total output bit rate for the above sensors would be approximately 1.2 megabits/sec. Additional experiments under consideration which may use the MIRP should not effect the output bit rate significantly.

To achieve 10 bit accuracy, analog to digital conversion should be accomplished within sensors that require such accuracy. The converted digital data can then be formatted and multiplexed into the MIRP output bit stream.
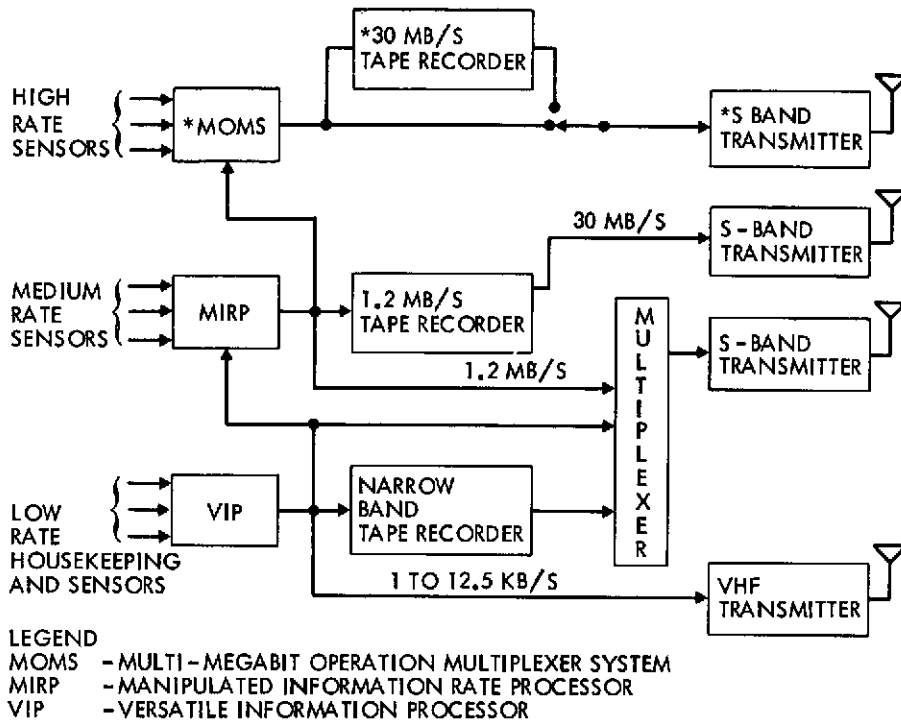
Figure 7.4-1. Basic EOS Data Handling System for EOS A and B
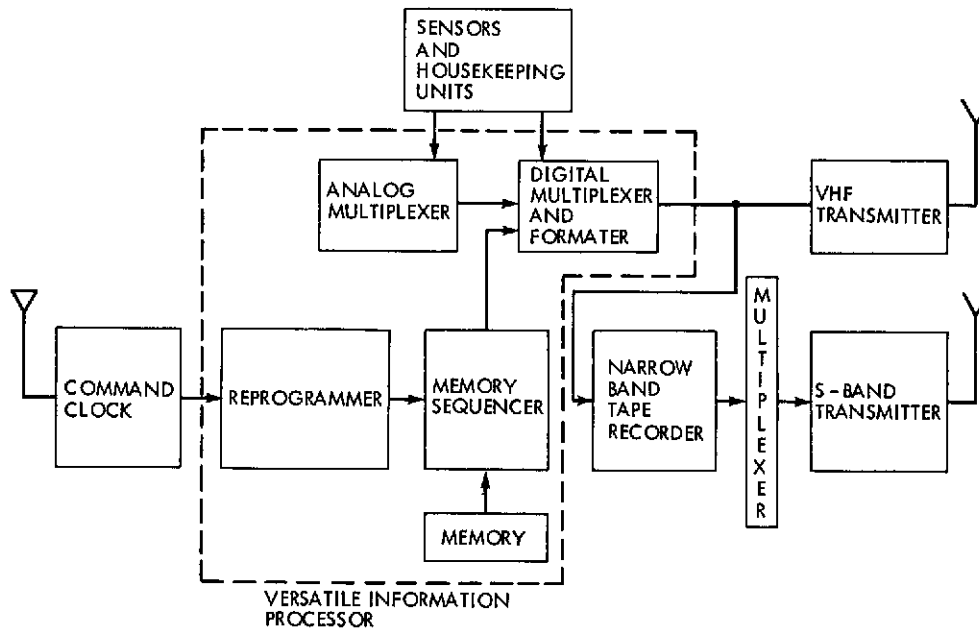(Redundancy Cross Strapping not Shown)

Figure 7.4-2. Versatile Information Processor (VIP)

7-48

MANIPULATED INFORMATION RATE PROCESSOR
(MIRP)

SENSOR A — CONFIGURATION SELECTOR — MULTIPLEXER — ANALOG TO DIGITAL CONVERTER — BUFFER — OUTPUT CONTROL SEQUENCER — MULTIPLEXER — S-BAND TRANSMITTER

DATA REDUCT PROCESSOR — OUTPUT CONTROL SEQUENCER — 1.2 MB/S TAPE RECORDER

SENSOR B

SPACECRAFT COMMAND

SAMPLE SCYC GENERATE   SAMPLE SCYC GENERATE   INPUT TIMING CONTROL

INITILIZE A
INITIALIZE B — CYCLE SELECTOR

VIP (real time)   VIP (play back)
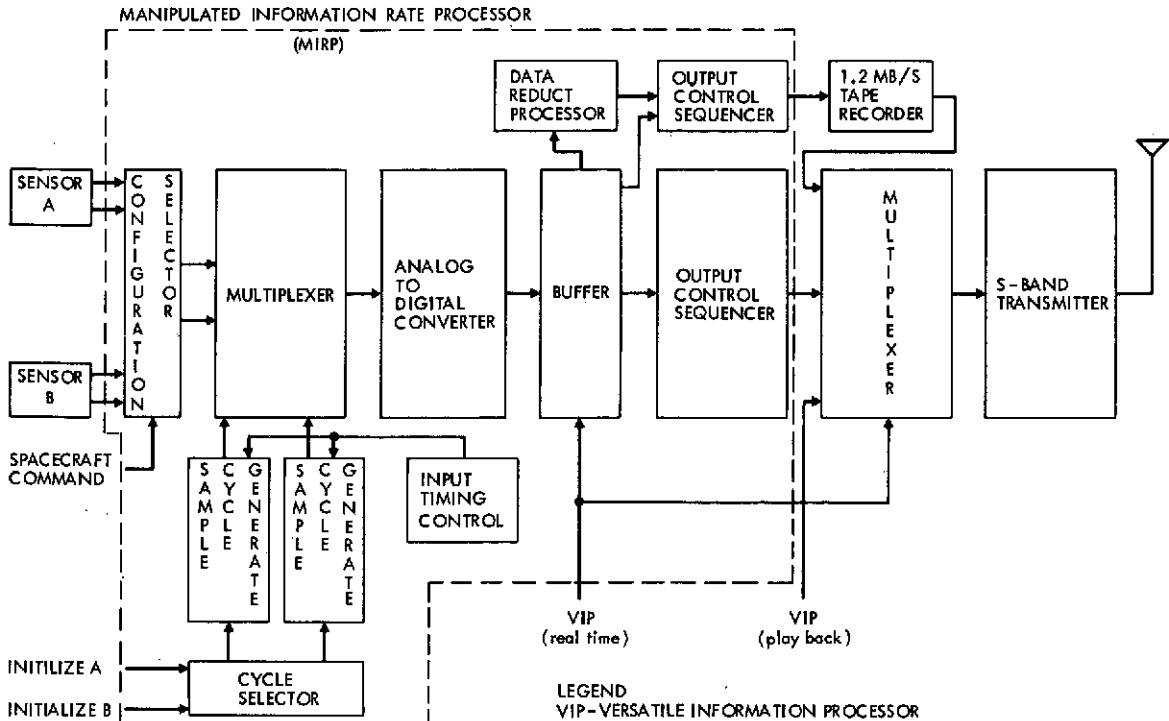
LEGEND
VIP—VERSATILE INFORMATION PROCESSOR

Figure 7.4-3.   Manipulated Information Rate Processor (MIRP)

Since the MIRP sensors require either 8 bit accuracy or 10 bit accuracy, from a total system consideration it may be more efficient to design the MIRP with a variable word length formatting capability.

A reel-to-reel digital recorder will be used to record the 1.2 mb/s serial data. The data stream will be longitudinally recorded on parallel tracks. Co-planar reels with sufficient tape for 110 minutes of recording will operate at a tape speed selected commensurate with long life operation. A record to playback ratio of 24 to 1 will enable data dump in no longer than five minutes. The tape recorder is expected to weigh about 30 pounds, occupy a volume of 800 cubic inches, and dissipate 30 watts of power.

Since the MIRP tape recorder will have a full orbit storage capacity, it is feasible, by the addition of one more tracks, to use this tape recorder for VIP storage in place of the aforementioned VIP narrow band tape recorder. The Phase B study should evaluate the trade-offs in using the 1.2 mb/s tape recorder for VIP as well as MIRP storage.

The real time and stored MIRP outputs, along with the VIP stored and real-time outputs, would be multiplexed for transmission over the S-band link as shown in Figure 7.4-1. Because of the asynchronous nature of the bit streams and because of the bit interleaving and bit gaps that would result, time division multiplexing is not recommended. Frequency division multiplexing is proposed for the MIRP S-band link.

7.4.2.3 Multi-megabit Operation Multiplexer System (MOMS). The high resolution Thematic Mapper on EOS B requires a new data handling concept-the Multi-megabit Operation Multiplexer System (MOMS). The MOMS would use a separate Multiplexer module for each high rate sensor under control of the Format Control unit. (Figure 7.4-4.) The Multiplexer module would contain input gating and the analog-to-digital converters. By hardwiring the formatting unit, timing pulses will be sent to the Multiplexer modules to control the sampling times. The converted digital data would be sent back to the formatting unit to be outputted into a serial bit stream.
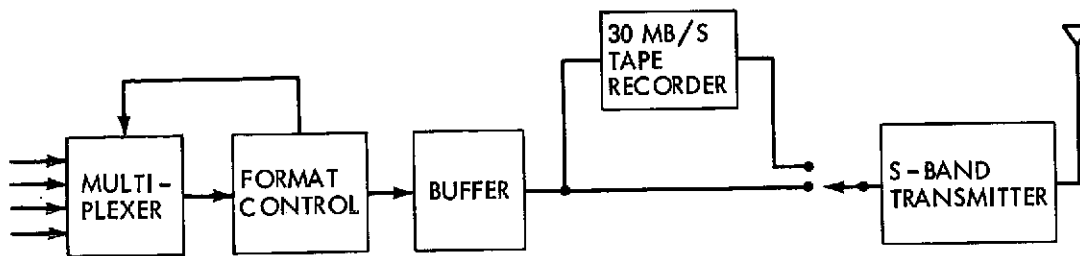
Figure 7.4-4. Multi-Megabit Operation Multiplexer System (MOMS)

Separate modules for multiplexing and control will allow different sources to be used with the MOMS by simple modification to the Format Control unit.

The Thematic Mapper has not yet been developed sufficiently to determine its scan efficiency. It is estimated that the scan efficiency will be between 30 and 80 percent and calculations regarding the sensor data requirements were made for both efficiency extremes. The present approach to Thematic Mapping calls for 6 bands with 9 detectors each having 66 meters resolution along with another band of 9 detectors having 200 meters resolution. Quantizing of the bands will average 7 bits/sample. Assuming 2 samples per IFOV element, the resulting output bit rate would be 80×10^6 bits/sec at 30% efficiency and 30×10^6 bits/sec at 80% efficiency.

At efficiencies of 80 percent or greater the 30 MHz S-band data link could be utilized; however at lower scan efficiencies the S-band link would not be adequate. Several approaches to decrease MOMS output bit rates to be compatable with the S-band link were considered. The first would make use of a circulating smoothing buffer which would accept data at full rates during the active portion of the scan and shift out at a slower rate during the following scan interval. Using this approach the smoothed output bit rate would be reduced to 24×10^6 bits/sec for the case of 30% scan efficiency.

The cost for using this buffer, however, is considerable. A buffer size of 2.11×10^6 bits would be required. Such a buffer appears to be feasible. It is estimated that a 2×10^6 bit memory of the type required, using unipolar 2 mil plated wire, would require 16 watts, occupy 700 cu. in. and weigh 25 lbs. It is again noted that the effect of a low scan efficiency instrument results in direct and considerable cost to the MOMS and to its transmission link.

A second approach to decreasing data rates would be to reduce the sampling from 2 to 1.4 samples per IFOV element. This would make inclusion of smoothing buffers more attractive, especially if high scan efficiencies are not obtainable. At 30% percent scan efficiency for example, the output bit rate would be smoothed from 53×10^6 bits/sec to 16×10^6 bits/sec using a 1.48×10^6 bit buffer.

A future Thematic Mapper may provide 40 meters resolution. At this value, and assuming 2 samples per IFOV element the resulting output bit rate will be 230×10^6 bits/sec at 30 percent efficiency and 86.5×10^6 bits/sec at 80 percent efficiency. Using a smoothing buffer would average the bit rate to 69×10^6 bits/sec. Buffer sizes of 3.4×10^6 bits and 0.48×10^6 bits at 30 percent and 80 percent scan efficiencies respectively would be required. Preceding comments about buffer feasibility would be even more applicable.

If a smoothing buffer is utilized for the MOMS, an appropriate buffer failure mode of operation would be incorporated into the MOMS design. In this mode of operation, a smaller number of preselected detectors whose data rate could be handled over the MOMS S-band link without

buffering would be multiplexed into the output bit stream. Additional circuitry would be required for the MOMS in the buffer failure mode; however, this circuitry would only be powered in the event of buffer failure.

The MOMS tape recorder will contain electronic buffers for compensation of skew and jitter caused by tape motion irregularities. It will also employ error control coding to overcome short dropouts to achieve a bit error rate of 1×10^6.

Serial data entering the recorder will be fanned into approximately 100 tracks across the tape width. At a tape speed of approximately 20 inches per second, each track will contain 15 kilobits per inch which in a double density code infers a magnetic flux reversal pattern of 15 thousand per inch (the equivalent of 7.5 thousand bits per inch of biphase data).

The recorder, packaged as two units, will occupy volumes of 2600 and 400 cubic inches each and weigh a total of 80 pounds. An average power per orbit (based on 10 minutes of record at 70 watts and 10 minutes of playback at 120 watts) will be approximately 17 watts for the 110 minute orbit.

The data will recorded on two inch tape on a tape transport modified for longitudinal recording from the ERTS - MSS/RBV transverse quadraplex recorder. Longitudinal was selected as opposed to transverse recording with its extremely high head-to-tape pressure and speed, to exploit the low head and tape wear rates accompanying the longitudinal process and from which reliability and long life derive. Additionally, to further enchance life, the recorder reels will be coplanar to allow the tape to circumvent the elevation change imposed by coaxial reel machines where tape guidance becomes complex and the mechanical stresses in the tape may become unavoidably excessive.

Four thousand feet of tape will be used to store 6×10^{10} bits recorded at 30 megabits/second for 30 minutes. The tape drive and tensioning will be accomplished without capstans and will utilize servo-controlled, brushless DC reel motors. Thus different tape speeds can easily be implemented to adapt to different mission requirements.

7.4.3 SYSTEM HARDWARE CONFIGURATION

The multiplexing, formatting and buffering circuitry associated with the MOMS and MIRP systems should be located in the immediate proximity of the sensors with analog outputs utilizing these systems. Processing near the source is necessary due to the quantization accuracy required and due to noise and signal perturbations resulting from the spacecraft environment and long harnesses. Spacecraft considerations may necessitate that the MOMS and MIRP tape recorders and transmitters be located up to 35 feet from their respective multiplexers. No problem is anticipated in routing the serialized multiplexer digital outputs to the tape recorder and transmitters if shielded coax pairs are used for the spacecraft harness.

With regard to the spacecraft configuration of the VIP, an attractive option exists. The VIP hardware can be designed with remote multiplexing modules to form a decentralized VIP processor as opposed to the present centralization approach. The decentralized processor, with distributed multiplexer input gating for each sensor would result in a significant reduction in the number of ' harness wires required. See Figure 7.4-5.

The remote multiplexing module would be a low power unit capable of multiplexing up to 32 inputs of several combinations of analog and digital signals and would transmit this multiplexed data back to a central control core for conversion and formatting. Five interconnect wires are required between each remote module and the central control core: one control line which provides for both channel address information and power strobing, one Pulse Amplitude Modulation data return line, two power lines, and one power return line.

The Phase B study should investigate trade off involved in utilizing remote modules for VIP system. If it is not feasible to locate the MOM & MIRP near their data handling systems, remote modules for these systems should also be considered.
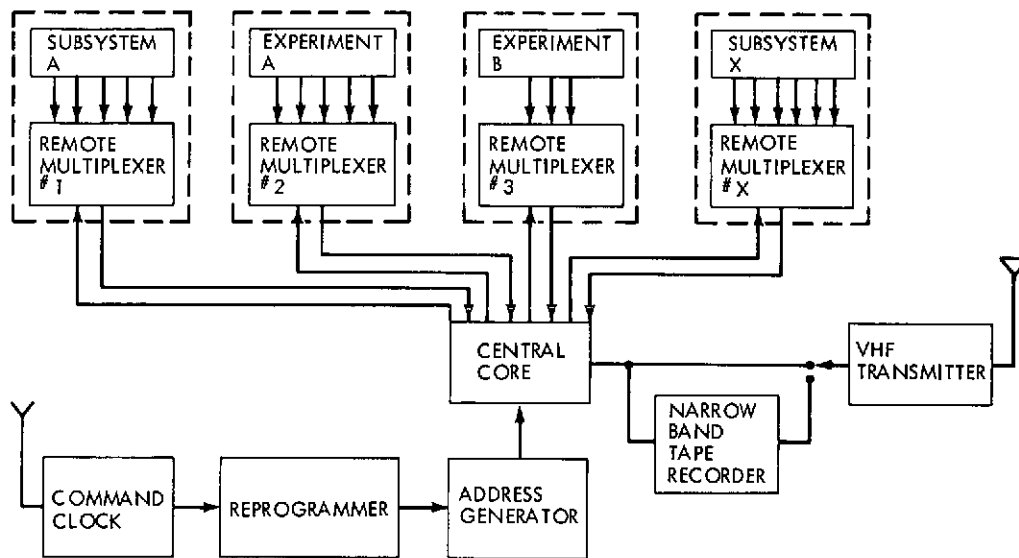
Figure 7.4-5. Versatile Information Processor (VIP) With Remote Multiplexing Modules

7.4.4 EOS ON-BOARD DATA PROCESSING

There are many areas where on-board data processing may be beneficial. By utilizing a small multiple purpose computer on a time shared basis, significant flexibility would result in utilizing spacecraft systems. In addition, less complex sensors and lower sensor data rates could be obtained.

The computer could be valuable in efficiently handling some EOS pointing control requirements. The computer could program antenna pointing to either a Data Relay Satellite or to a direct readout ground station.

The computer could be used for special processing to handle unique read-out requirements of international users.

The computer, in conjunction with the precision pointing system could provide correctional information, such as needed to null out gyro drift errors. Also adaptive filtering, depending on activity of control system parameters could be accomplished by computer control. A further related task would be to anticipate spacecraft disturbances such as would result from antenna pointing and apply control system compensation to the disturbances.

An on-board computer could be used directly or indirectly to enable more efficient sensor design resulting in decreased bandwidth requirements. The computer in conjunction with a low resolution, "look ahead" sensor (5 mile resolution, 60 second look-ahead) could analyze the sensor's data to optimize offset-pointing and data sampling of the high resolution terrain survey sensors. Data from the look-ahead sensor would enable the computer to program high resolution sensor sampling for clouds, shore lines, etc. This could result in lower average data rates and less costly ground processing.

In general, if selection or sampling criteria for a sensor can be established, then the computer could make decisions to control sampling.

Other potential uses of an on-board computer include: adaptive or emergency responses to spacecraft anomalies; optimizing charge current of batteries or programming of solar arrays; providing gridding information for sensor data; smoothing short bursts of MOMS data to send over the MIRP data link; and augmenting spacecraft command memory, VIP memory and memory sequencer.

Instead of developing a highly specialized computer for the EOS mission, a more general purpose spacecraft computer would be proposed. The computer would be of advance type now under development, similar to the computer previously flown on OAO. The physical characteristics for this non-redundant computer are estimated to be:

Size	700 cubic inches
Weight	40 pounds
Power	15 watts

7.4.5 COMMAND SYSTEM

The command system for EOS must accept commands from the ground via the S-band link for control of all subsystems and experiments, provide accurate time reference for all data, and provide stable frequencies (1.6 MHz and less) for use by subsystems and experiments on the spacecraft. The command-clock system concept used on Nimbus IV and ERTS A and B could be utilized for EOS.

Coded commands with a selected addresses are received by the command receiver, demodulated, parity checked, and executed in real-time by one of two real-time command modules. Coded commands with time will be transferred through a real-time command module to command memory for futher execution. Unencoded commands will be received demodulated, and executed in real-time.

The command system will provide a total of 512 commands. Up to 127 commands can be stored for execution at a later time. These 127 stored commands can be any of the total 512 commands. The stored commands can be executed at prescribed delay times up to 18 hours and can be repeated at intervals from 2 seconds up to 9 hours by appropriate message formatting. Both current pulse commands for relay commanding and voltage pulse commands for logic circuitry commanding would be required.

For timing and control the command system would provide several coherent frequencies with experimenter and spacecraft subsystems developing from those provided any additional frequencies required. Also, a simple time code with error checking would be available.

The command system will also provide digital outputs to be used in programming of the VIP and MIRP systems. Digital command words will also be provided for other systems as required.

7.5 COMMUNICATION SYSTEMS

7.5.1 INTRODUCTION

This section describes the proposed communciation systems and their interfaces with the Command and Data Handling Systems (Section 7.4) on the spacecraft and the Tracking and Data Acquisition Systems (Section 9) on the ground. The major communication requirement in terms of information capacity is imposed by the need to transmit the observatory data to ground stations. However, orbital tracking, house-keeping telemetry and command functions must also be provided for. Selection of communication system parameters such as frequency, modulation type, and tracking system is covered in Section 9 with the emphasis on using available ground support systems. Consistent with Section 5, three distinct communication systems will be blocked out for the three spacecraft; EOS A, and EOS B and the proposed growth satellites EOS C and D.

7.5.2 EOS A COMMUNICATION SYSTEM

The communication system on EOS A, Figure 7.5-1, consists of three subsystems: the S-Band playback data system; the S-band real time data, ranging and command system; and the VHF low data rate and housekeeping system. Redundancy and normal cross-strapping are not shown in Figure 7.5-1
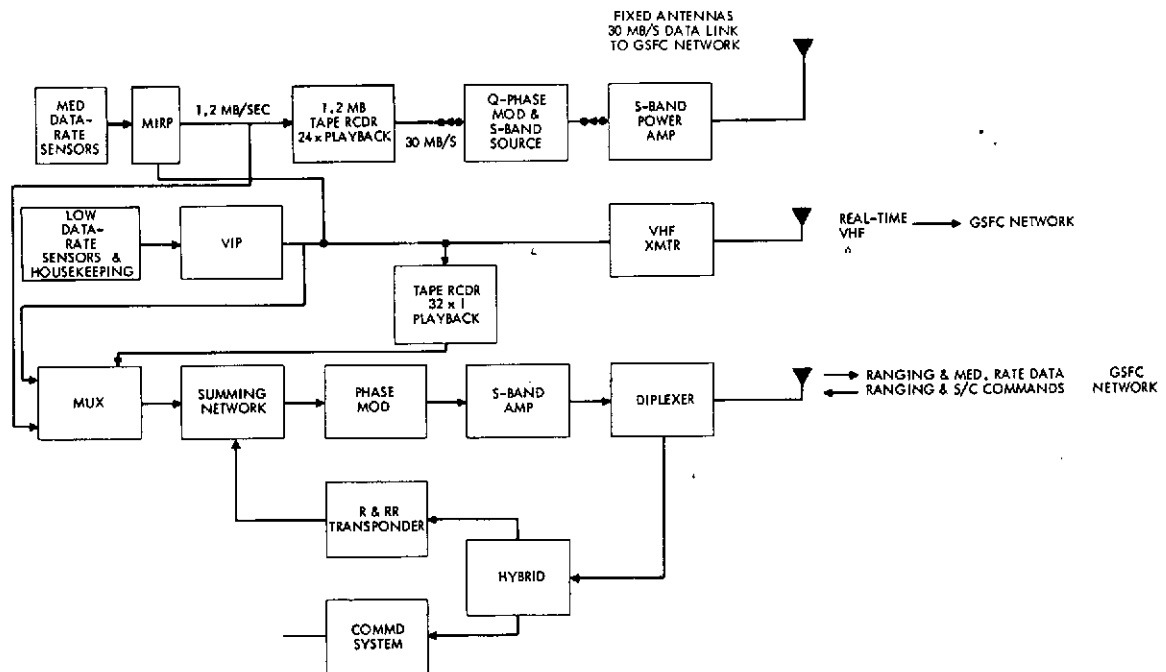

Figure 7.5-1 EOS A Communications System

The rationale for the proposed system is given below and the following paragraphs include functional descriptions of each block in Figure 7.5-1. The information from the medium data rate sensors is required over large ocean areas and therefore at least one complete orbit must be recorded and played back over the S-Band playback data link. A playback at 24 times the record speed would result in a data rate of 30 mb/s and a playback time of approximately 4 minutes which is consistent with available ground capabilities and station visibility for the proposed orbit. Any NASA station listed in Section 9 could presently support this data link with the addition of an EOS unique demodulator and a wide-band tape recorder. The S-Band data, ranging and command link is required for three reasons, (1) to transmit the medium rate data when the tape recorder is in the playback mode, (2) to establish an orbital determination system compatible with all NASA range

PRECEDING PAGE BLANK NOT FILMED

and range-rate systems, and (3) to establish a command system compatible with all NASA stations. Justification for the VHF link is, (1) a VHF link is required for S-Band acquisition at some NASA stations, (2) an omni-directional antenna is valuable for orbit and altitude determination during the launch and early orbit phase of a mission, and (3) it allows minitrack to be used as a back-up orbital determination system during the life of the mission.

7.5.2.1 Quadriphase Modulator and S-Band Source. The input to this unit would be the 30 mb/s data from the digital tape recorder described in Section 7.4.2.2. This unit would contain the S-Band source and the circuitry required to quadriphase modulate this source. The output would be a low-power modulated S-Band signal.

7.5.2.2 S-Band Power Amplifier. The function of this unit is to amplify the output of the quadriphase modulator to a level consistent with mission requirements. The link analysis (Table 9.2-1) indicates a minimum S/C transmitter power of +33.1 dbm. (2 watts), but this calculation is based on an ideal system and does not include system degradation caused by departure from an ideal system in the spacecraft and the ground system. Careful design can reduce the system losses to less than 3 db. Therefore a power amplifier with an output power of +40 dbm. (10 watts) is recommended to provide a margin of about 4 db. Development trends will determine if a solid state amplifier or a T.W.T. will be used. Although TWT's have exhibited excellent reliability in space in the past and continue to improve, it is expected that S-Band transistor amplifiers will overtake TWT's prior to the design of the EOS.

7.5.2.3 S-Band Antennas. The fixed S-Band antennas proposed will have +4db gain at normal acquisition angles. The proposed antenna has been developed for ERTS and is readily available.

7.5.2.4 Multiplexer (Mux) Summing Network and Phase Modulator. The function of the MUX is to multiplex the output of the real time MIRP data, the real time VIP data and the VIP tape recorder playback data into a format suitable for summing with the range and range-rate transponder output. The function of the summing network and phase modulator is straight forward and is proposed to be identical to the ERTS USB system, thus eliminating the need for hardware development.

7.5.2.5 S-Band Amplifier. This unit amplifies the output of the phase modulator to a power level of approximately 5 watts as indicated by the link discussion in Section 9.2.4. S-Band transistor amplifier, with power levels exceeding this requirement, will be used by other NASA projects (Nimbus F, 8 watts) prior to EOS and development costs should be minimal.

7.5.3 EOS B COMMUNICATION SYSTEM

The addition of the Thematic Mapper and its associated 30 mb/s data rate will require an additional communication link on EOS B. Figure 7.5-2 is a block diagram of the EOS B communication system with the added High Data Rate System shown within the dashed lines.

7.5.3.1 High Data Rate S-Band System. As indicated in Figure 7.5-2, the system has two modes of operation; (1) the 30 mb/s MOMS output can be transmitted directly in real-time or, (2) the recorded data on the wideband tape recorder (Section 7.4.2) can be transmitted in a playback mode. The remainder of this system is identical to the S-Band data system of EOS A described above.

7.5.3.2 Steerable Antenna for LRGS. The EOS to LRGS system is justified and described in Section 9.6 and the link calculation indicates the spacecraft antenna gain must be 10 db or higher. The antenna proposed is a fan beam type with a 120° beamwidth parallel to the flight path and a 10° beam-width orthogonal to the flight path. The advantage of this type antenna is that continuous steering is not required with only one adjustment about the spacecraft roll axis required per station pass. The steering mechanism required is simple and reliable with less than twelve discrete pointing angles required.
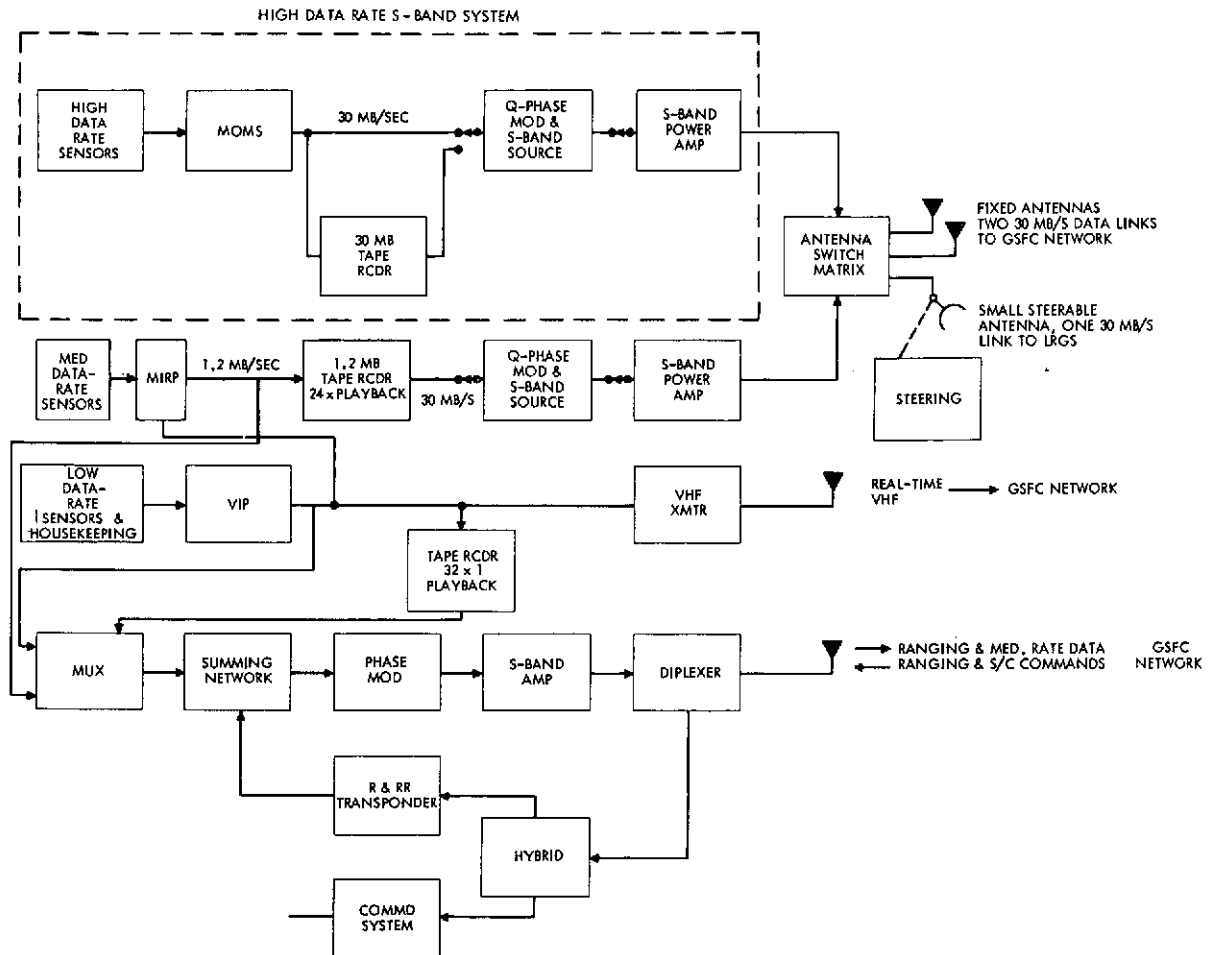
HIGH DATA RATE S-BAND SYSTEM

Figure 7.5-2. EOS B Communications System

7.5.4   EOS C AND D

The EOS C and D spacecraft are not clearly defined in terms of which sensors will be used, but it is projected that an increase in data rate from the 30 mb/s on EOS A and B to 100 mb/s or higher will be required. This section describes a communication system capable of transmitting the 100 mb/s data rate to both a ground station and a DRS. The rationale for the selected link frequency of 22 GHz is given in Section 9.5. Figure 7.5-3 is the blocked out version of this system with the medium-data rate system, the low data rate ranging and command system, and the real time VHF system being identical to the systems previously described. The spacecraft mechanical configuration proposed has two steerable K-band antennas. One is mounted under the main body of the spacecraft for transmission to ground stations, and the other is mounted above the main body in a position that allows   100 degrees of clearance from zenith for transmitting to DRS.

7.5.4.1   Quadriphase Modulator and K-Band Source.   The input to this unit is the 100 mb/s or higher data from the MOMS which is described in Section 7.4.2.3. The modulator is similar to that used in the S-Band units with only the frequency and the techniques used to accomplish the requirements being different. The specific type of K-Band source to be used for EOS will not be defined at this time since the technology for developing microwave sources is changing rapidly and two separate GSFC studies in this area will be complete prior to the EOS spacecraft design.
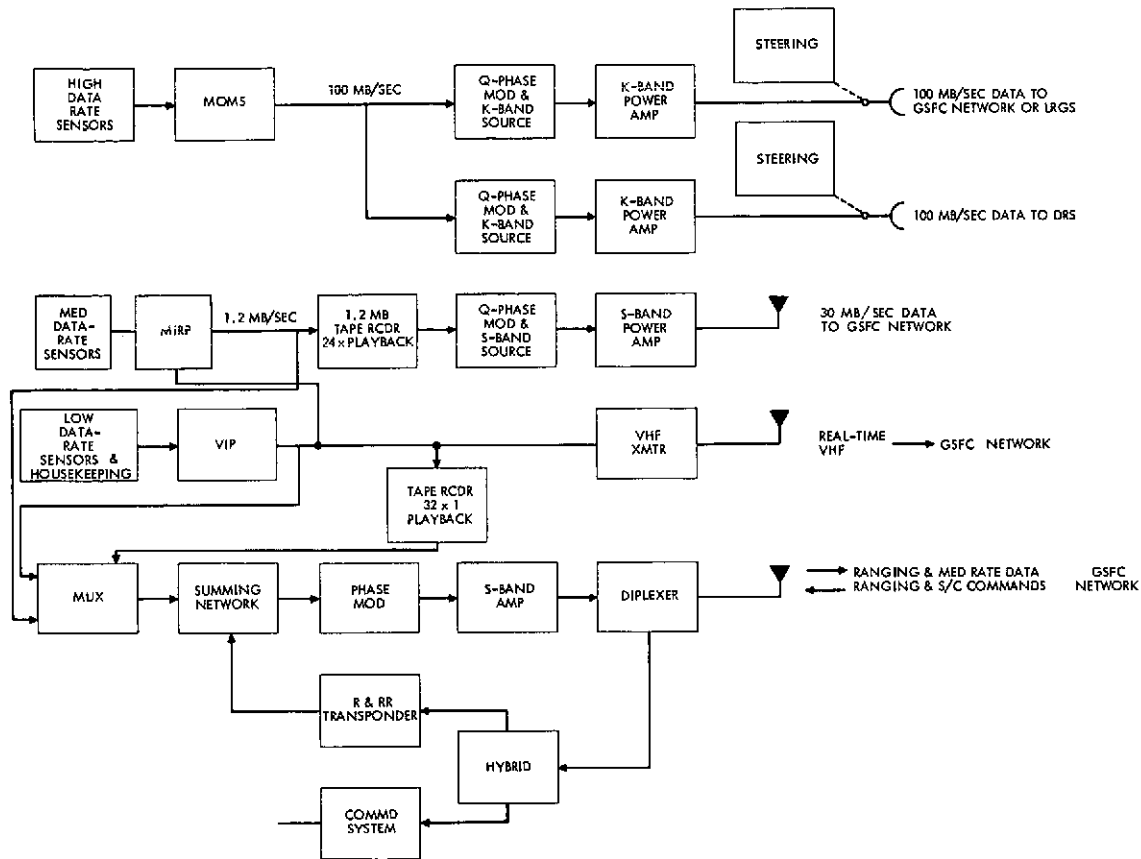
7-57

Figure 7.5-3. EOS C and D Communications System

7.5.4.2 K-Band Power Amplifier. To achieve the power required for the EOS K-Band link to ground, a transmitter with a 5.0 watt output is needed. A space qualified TWT with 5.0 watts output is presently available but a promising alternative is a solid state Transferred-Electron Amplifier (TEA). A K-Band TEA with a 10 watt output is presently under development for GSFC. This unit would have the advantage of operating on low voltage without the need for power converters. It would also be more compact and lighter than the bulky vacuum devices.

7.5.4.3 Steerable K-Band Antenna. A critical element in the 100 mb/s K-band link is the S/C antenna. For this application a steerable high gain antenna is an absolute requirement. The EOS-to-ground link was sized for a S/C antenna gain of approximately 45 db. This would require an aperature equivalent to a 1.0 meter parabolic reflector and have a beamwidth of 1.0 degree. The type of antenna and the mechanism for steering have not been decided at this time since GSFC is presently engaged in the development of a K-band spacecraft antenna and the results of this development will be factored into the decision on the type of antenna used.

7.5.4.4 100 MB/S Data System to DRS. The 100 mb/s link to DRS is identical to the K-band system described above with the exception of the transmitter power output required. The link calculation of Table 7.5-1 indicates that a K-Band EOS-to-DRS link would require approximately 50 watts of transmitter output power for the 100 mb/s data link. To achieve this power some development in space qualified TWT's or power combining techniques for TEA's is required. There is no known TWT presently available that meets the 50 watt c.w. requirement but this figure is well within the theoretical limits of space TWT's.

Table 7.5-1

K-Band Link Calculations for EOS to DRS

Item	Parameter	Level
1.	Transmitter Output Power	+47 dbm (50) watts
2.	Passive Loss	-2db
3.	S/C Antenna Gain (1 m dish)	+41db
4.	Propagation Loss	-209.5 db
5.	DRS System Temp.	500°K
6.	Received Noise Power in a 100 MHz Bandwidth	-91.5 dbm
7.	Antenna Gain DRS (9 ft. dish)	+50 db
8.	Signal Power at Receiver	-73.5 dbm
9.	S/N in 100 MHz Bandwidth	+18 db
10.	System Margin (BER of 10^{-5})	+8 db

7.5.5 WEIGHT, SIZE, AND POWER

This section tabulates the communications system weight, size, and power. Although redundant subsystems are not shown in Figures 7.5.1, 7.5.2, and 7.5.3, the weights and sizes in Table 7.5-2 do include redundant subsystems where required.

The physical parameters of the equipment covered in Section 7.4 will not be repeated here. The weight and power tabulations include the S/C antennas, but the antennas that are exterior to the main body of the S/C were not included in the size column.

Table 7.5-2

Summary of EOS Communication Systems Weight, Size, and Power Requirements

System	Weight kg. (lbs.)	Size cc (in. [3])	Power W
1. S-Band Data System Quadriphase Modulator, S-Band Source, Antenna and 10 WATT S-Band Power-amplifier	7.94 (17.5)	3,66.4 (224)	40
2. S-Band Real-Time Data, Ranging and Command Diplexer, Hybrid, Command Receiver, R & RR Transponder, modulator, Mux, Summing Network, Antenna and 5 watts S-Band Power Amplifier	17.4 (38.5)	1,900.0 (116)	39
3. 100 mb/s 5 Watt System Quadriphase Modulator and K-Band Source, Steerable Antenna and Controls, 5 watts K-Band Power Amplifier	179.0 (39.5)	5,630. (344)	50
4. 100 mb/s 50 Watt System to DRS Quadriphase Modulator and K-Band Source, Steerable Antenna and Controls, 50 watts K-Band Power Amplifier	242.2 (53.5)	7,300.0 (446)	275
5. LRGS System Antenna and Steering Mechanism	5.2 (11.5)	655 (40)	1

7.6 ATTITUDE CONTROL

7.6.1 INTRODUCTION

The Attitude Control System (ACS) is intended to stabilize the spacecraft to the desired earth-pointing mode, to provide control sensor and torquer data for attitude determination, and to control the solar array orientation.

The requirements on the ACS for attitude control, attitude determination accuracies and rate stability are primarily dictated by the nature and resolution capabilities of the payload sensors and the proposed orbit altitudes. Payload sensor data processing considerations indicate that the prime requirement on the ACS is good spacecraft rate stability to avoid distortions of the sensor field of view. Consideration of the structural properties of the spacecraft and the state-of-the-art in spacecraft control systems and components leads to a modular design concept with a baseline design meeting the minimum program requirements and having incremental growth capabilities to meet more stringent specifications. This baseline design will provide an attitude control accuracy of about 0.2 degrees 1 sigma (plus 0.5 degrees bias offset), rate stability of better than 0.005 degree per sec, and a ground-computed after-the-fact attitude determination accuracy of 0.1 degree 1 sigma in each axis. Further improvement in rate stability can be achieved by using better quality sensors (presently available) and paying close attention to structural design. Addition of a precision stellar-inertial attitude determination system would allow spacecraft inertial attitude determination to about 0.002 degree 1 sigma.

Two broad groupings of EOS instruments can be identified as: global sensors with a wide field of view (~ 400 nautical miles) and medium resolution (~ 2 km), and terrain mappers with a narrow field of view (~ 100 nautical miles) and very high resolution ($\leq$ 100 meters). Considering the global sensors first, it can be seen that an attitude accuracy of 0.5 degrees in a typical EOS orbit (1000 km) produces a neglible offset (10 km) in the field of view covered by the sensor. However, it is necessary to reference this sensor data to geographic coordinates to an accuracy of one resolution element, or 2 km. This can be accomplished with an attitude determination accuracy of 0.1 degree.

In the case of the very high resolution sensors, the 10 km offset produced by a 0.5 degree attitude error is satisfactory provided the selected orbit produces an overlap of at least 10 km in the sensor swath on a later orbit. However, an attitude determination accuracy of 0.1 degree is insufficient to permit referencing this sensor data to an accuracy of one resolution element (< 100 meters). The required geographical referencing is accomplished by landmark techniques and/or precision attitude determination (see Section 7.7).

It is also necessary to consider the requirement on ACS rates imposed by the very high resolution sensors. A typical sensor is the Thematic Mapper planned for EOS B. Each of six spectral bands has nine detectors to sweep out nine contiguous 66 meter swaths or 594 meters in a 1000 km orbit. The sweep cycle lasts about 0.1 second in order to maintain contiguity on the next sweep as the spacecraft advances in orbit. If it is desired to limit distortion of the sweep to 1/4 of a resolution element, or 16 meters, the vehicle pitch and roll rates would have to be limited to 160 μ rad/sec or about 0.01 deg/sec. The requirement in yaw is less stringent. Taking into account the increased resolution of future EOS sensors as well as the state-of-the-art in control system performance, a goal of 0.005 deg/sec maximum rate appears reasonable.

The approach in the control system design has been to use proven techniques in achieving the desired goals. The ERTS/Nimbus ACS design concept forms one logical basis for the EOS control system. This choice, with modifications and changes to improve performance, is capable of meeting EOS requirements.

7.6.2 ATTITUDE CONTROL SYSTEM (ACS)

The ACS aligns a body fixed reference frame (x, y, z) with the local vertical orbital reference frame (X, Y, Z). These frames are shown in Figure 7.6-1. The right handed XYZ reference frame has its origin at the spacecraft center of mass and has the + Z (yaw) axis directed down along the local vertical towards the center of the earth; the + X (roll) axis normal to the local vertical and in the orbit plane, nominally aligned with the velocity vector for a circular orbit; and the + Y (pitch) axis normal to the orbit plane completing the right handed triad.

The body reference set (x, y, z) has the same origin and is defined by the spacecraft geometry: yaw (+z) along the center line of the support tower directed downwards; roll (+x) along the length of the bays; and pitch (+y) completing the right handed triad.

The roll, pitch and yaw body axes (x, y, z) are nominally aligned with the corresponding local vertical orbital reference axes (X, Y, Z) by the attitude control system. The attitude errors are measured by a set of sequential right handed Euler rotations: roll ϕ, pitch θ, and yaw ψ.

The control axes, about which the attitude control torques are applied, are nominally the same as the body axes (x, y, z). The spacecraft principal axes of inertia form a right handed set centered at the actual center of mass of the spacecraft. These axes move with respect to the body axes with any change in mass distribution, the predominant component of such motion being at orbital frequency due to solar array motion. Based on Nimbus experience, this effect is expected to be small.
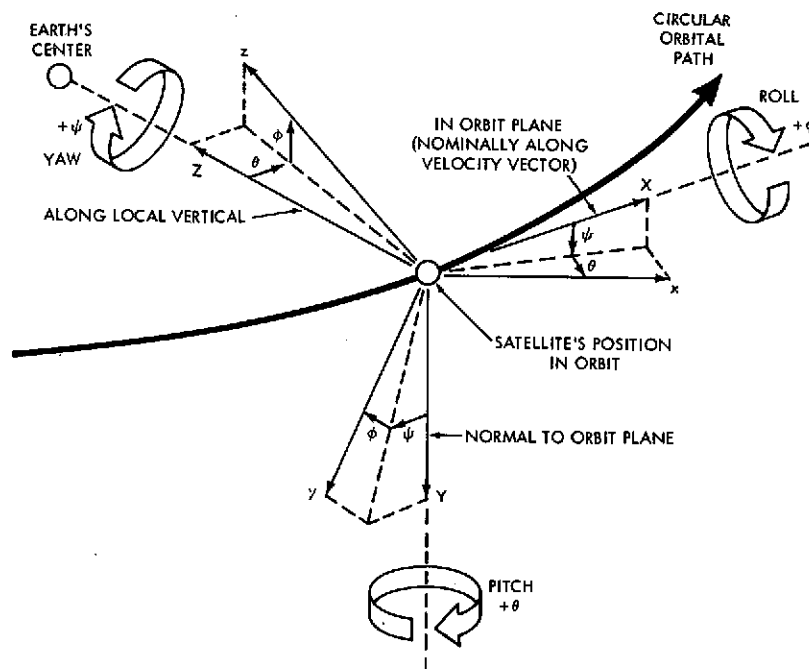

Figure 7.6-1.   EOS Orbit Plane Reference Coordinates

The ACS has three major modes of operation with smooth transition from one mode to the next:

- Launch Mode

- Acquisition Mode

- Normal Stabilized Mode (with infrequent short term perturbations caused by orbit control operations).

Operation of the ACS is as follows. During the launch mode, all the ACS components and subsystems are ready but inhibited. After separation from the launch vehicle and deployment of the bays and solar panels, the spacecraft tip-off rates are reduced to fractions of a degree per second by use of rate gyros. An earth-sun acquisition sequence using rate gyros, horizon sensors and sun sensors establishes the desired orientation. Any reacquisition would also use the same scheme. All launch vehicles under consideration have the capability of orienting the EOS to approximately the desired orientation following orbit injection and prior to separation of the spacecraft. For added reliability, the control system can acquire (reacquire) from any initial attitude.

During the normal stabilized mode, the spacecraft is controlled by reaction wheel torquers. Cold gas jets are used during acquisition and whenever the error or wheel speeds exceed certain threshold values. The EOS control system is essentially a redesigned ERTS/Nimbus type of system. Figure 7.6-2 is a functional block diagram of the proposed ACS.
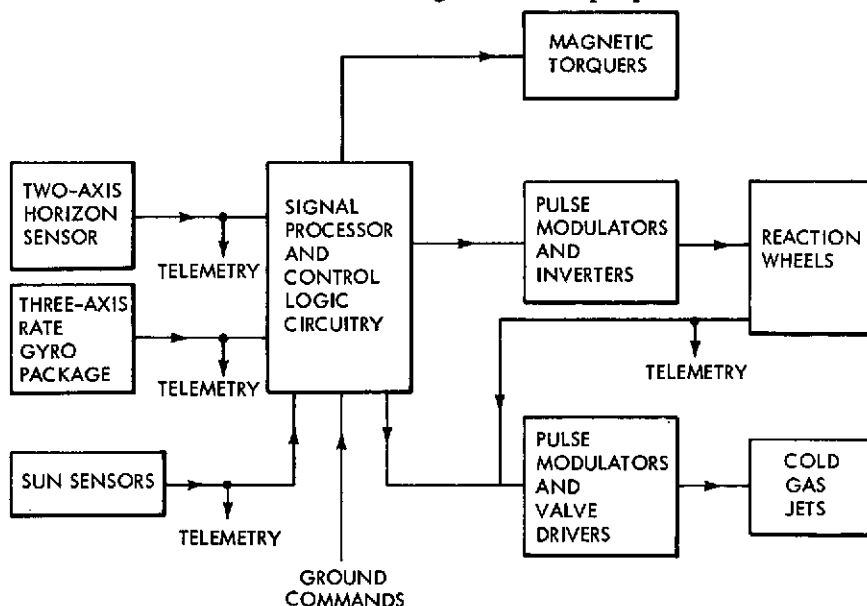

Figure 7.6-2. Attitude Control System Functional Block Diagram.

A two-axis earth sensor and a three-axis rate gyro package act as the primary sensors. Roll and pitch attitude information are provided by the earth sensor which senses the earth-space horizon defined by the sharp cut-off in the 15μ m CO_2 absorption band of the IR spectrum. A three-axis rate gyro package provides precise rate measurement which is less noisy than the rate information that can be derived from the horizon sensors.

Attitude information about the yaw axis is not directly available; however, the combination of roll and yaw rate and roll position information yields yaw attitude as shown in Appendix I. This is commonly called yaw gyrocompass control.

A coarse sun sensor system is used for the solar array orientation control. The same system, or another body fixed sun sensor system, may be used during initial acquisition and also as backup attitude sensors.

Inertia wheels are used in an orthogonal triad to produce three axis control torques in a momentum exchange system. The wheels are driven by 400 Hz two-phase servo-motors, the inverters being gated by pulse modulators to reduce the power required. The attitude and rate sensor outputs, suitably combined and passed through compensating networks, are fed to the pulse modulators. Cyclical momentum variations are absorbed by the inertia wheels while uni-directional or secular momentum buildups are limited by magnetic torquers and occasionally attenuated by the mass expulsion devices, i.e., the cold gas jets. As demonstrated by the Nimbus-4 spacecraft, the need for momentum dump may be considerably reduced by judicious use of the magnetic torquers and choosing an appropriate orientation of the spacecraft so as to minimize gravity gradient torques. This would produce some attitude bias which can be kept small by proper planning of the mass distribution in the spacecraft.

The present ERTS/Nimbus control system will be modified to accommodate the more stringent EOS requirements by using precise primary sensors to permit the design of an accurate control system. The improved sensors are within the present state-of-the-art. A detailed discussion of these sensors is found in Appendix I.

7.6.3 DISTURBANCE TORQUES

Spacecraft disturbance torques are of two kinds: those imposed from external sources and those produced internally.

7.6.3.1 <u>External Disturbance</u>. The external disturbance torques are produced by aerodynamic drag, magnetic and gravitational forces, and solar pressures. These torques are not easily predicted, but EOS, with its known orbits and attitudes, allows reasonable estimates. These disturbances vary slowly with predominant secular and orbit frequency components. Such torques must be counteracted by the control system. The momentum variation imposed by the external disturbance torques are absorbed by the reaction wheels (up to the limit of wheel momentum capacity). The time history of the wheel speeds should match that of the disturbance torque impulses. The wheel moments of inertia must be chosen large enough so that the speed variation is within acceptable limits. As the secular components of the wheel speeds build up with time the wheels must be desaturated by use of the gas jets.

The need for frequent jet firings may be reduced by stabilizing the spacecraft to its gravity gradient null to reduce the secular momentum buildup and by using the magnetic torquers to counteract both secular and cyclic torque variations. Nimbus spacecraft experience indicates that the spacecraft will not need jet firings for long periods of time when the above steps are taken. The structural design of the spacecraft and the location of the components determine the bias between the gravity gradient null and the nominal null with respect to the reference orientation. It is not unreasonable to expect that this may be kept below 0.5 degree.

7.6.3.2 <u>Internal Disturbance</u>. The internal disturbance torques are caused by the motion and vibration of spacecraft components, unwanted expulsion of mass through outgassing and venting, and thruster misalignment and crosscoupling of axes. These torques are more difficult to predict than the external torques and the induced spacecraft motions are usually of higher frequencies. The method for dealing with internal disturbances is therefore different. The frequencies of these torques and/or the resultant vibrations of the structure may be kept higher than 1 Hz. The control system bandwidth may be adjusted to be less than 0.1 Hz so that the control system does not interact with the high frequency disturbances. Since the pointing accuracy requirement is quite modest on the baseline design, the resulting performance is expected to be satisfactory.

The rate stability is a cause of some concern but it appears that with the control sensors and sensor processing schemes mentioned in this Section and in Appendix I, a rate requirement of 0.005 degree/sec can be met. Careful consideration should be given to rate stability during the actual design, particularly if flexible members (e.g., roll up solar arrays) are proposed for future EOS use.

The various disturbance torques, both external and internal, are analyzed in Appendix H. The results of these calculations are summarized in Table 7.6-1. The estimates for the 9:00 a.m. or 3:00 p.m. orbits represent the worst condition due to increased solar pressure disturbance torques. Maximum and minimum estimates of aerodynamic disturbance torques correspond to the maximum and minimum estimates of atmospheric density.

Table 7.6-1

Two-Year Torque Impulse Buildup for the 9 a.m. or 3 p.m. Orbits

Source	Altitude (nautical miles)	Affected Axis	Torque Impulse (ft-lb) sec	
			EOS A&B	EOS C & D
Orbit Adjust	400/600	mainly pitch	2070	3240
Aerodynamic	400	pitch	10400 (max)	14800 (max)
			315 (min)	420 (min)
	500		3150 (max)	4200 (max)
			75 (min)	100 (min)
	600		1240 (max)	1650 (max)
			32 (min)	42 (min)
Solar Pressure	400/600	roll	4500	8820
Gravity Gradient (Residual)	400/600	pitch	100	210
Magnetic	all	all	compensated	compensated
Total	400	all	17000 (max)	27000 (max)
			7000 (min)	12700 (min)
	500	all	9800 (max)	16500 (max)
			6800 (min)	12400 (min)
	600	all	7900 (max)	14000 (max)
			6700 (min)	12300 (min)

Approximately 80% of the aerodynamic, solar pressure, and residual gravity gradient disturbance torques can be compensated by the proposed magnetic torquers. This assumption is borne out by experience with Nimbus. The net torque impulse over a two-year life can be converted to required thrust impulse utilizing the control jet lever arms on EOS (8.0 ft in roll, 11.5 ft in pitch, and 4.0 ft in yaw). The required thrust impulse can be supplied by a Freon-14 cold gas system (I_{sp} = 46 sec) as on Nimbus. The results are shown in Table 7.6-2.

Table 7.6-2

Pneumatic System Thrust Impulse and Freon-14

(Two-year Mission Duration)

Source	Altitude nautical miles	EOS A&B		EOS C	
		lb sec	lb of gas	lb sec	lb of gas
Orbit Adjust	400/600	230		360	
Orbit Environment	400	300		480	
	500	170		300	
	600	140		250	
Acquisition & Contingency	400/600	230		360	
Total	400	760	16.5	1200	26.0
	500	630	14.0	1020	22.0
	600	600	13.0	970	21.0

It is recommended that the pneumatic system be capable of carrying up to 25 lb of Freon-14. This would permit a two-year operation in any EOS orbit. For EOS A and B spacecrafts the pneumatic system would be charged to 60% of capacity.

7.6.4 ATTITUDE DETERMINATION

Reconstruction of sensor imagery and referencing of sensor data to geographical coordinates become easier with more precise information about spacecraft attitude. This information is not required in real time, and the spacecraft does not have to be controlled to any great accuracy, though the rate stability should be adequate to allow accurate attitude determination.

The majority of EOS sensors have a resolution of about 2 km. It would be desirable to be able to geographically reference such sensor data to an accuracy of one resolution element. At a typical EOS orbit of 1000 km, this represents an attitude determination accuracy of 2×10^{-3} radians or about 0.1 degree.

Attitude determination to an accuracy of 0.1 degree 1 sigma, or better, may be obtained by ground processing of the telemetered horizon sensor, rate gyro, and tourquer data. No additional on-board hardware is needed.

The horizon sensor output has highly correlated (low frequency) errors caused by the oblateness of the earth and misalignments of the axes. The control system similarly has gravity gradient bias offsets, proportional errors to maintain wheel speeds, and axis misalignment. These errors, particularly the yaw attitude error, cross-couple into the horizon sensor output. These slowly varying components can be calibrated out to the accuracy with which they can be computed or measured. After-the-fact smoothing of discrete data points from the horizon sensor, the gyros, and the wheel tachometers should enable attitude determination to an accuracy of 0.1 degree 1 sigma.

Success of this scheme depends on the precision with which these calibratable components can be measured. The weakly correlated (high frequency) noise level must of necessity be low to permit accurate calibration. This noise arises from the following sources:

- Spacecraft jitter

- Sensor and electronics noise

- Horizon definition instability

Spacecraft attitude uncertainty of 0.2 degree 1 sigma and rates of 0.005 degree/sec 3 sigma appear adequately low. If rate variations (accelerations)are kept sufficiently small, the strapdown gyros should provide accurate rate information without having to resort to frequent sampling. The sensor electronics, signal processing quantization and round-off errors must be compatible with the projected accuracy. Some of the high frequency sensor noise can also be eliminated by the signal processing scheme described in Appendix I.

Horizon definition is usually unstable over a wide range of wavelengths but the 14 to 16 μm CO_2 absorption band offers an attractive choice. Available data indicate that at EOS orbit altitudes of 400 n.mi. and above, the instability in that band is less than 0.05 degree 3 sigma, including the effect of sensor noise. Since flight tested sensors have been built using this band it is within the present state-of-the-art. The horizon definition stability of 0.05 degree 3 sigma is adequate for attitude determination up to 0.1 degree 1 sigma.

7.6.5 SOLAR ARRAY DRIVE

Power available from the solar array varies with the cosine of the angle between the array normal and the sun line. The purpose of the proposed single axis (pitch) solar array drive is to minimize this angle to maintain maximum solar array power. The angle between the array normal and sun line is a function of the particular EOS orbit, time of year, and solar array drive accuracy. A solar array drive accuracy of ± 5 degrees results in a worst case array orientation angle of 15 degrees which produces a negligible loss in solar array power. Thus, ±5 degree accuracy for the solar array drive is considered adequate.

The proposed solar array drive for EOS consists of two independent drives about the pitch axis, one for each paddle. An ERTS/Nimbus type of drive system appears suitable. The drive would be at a bias speed between 2.9 and 3.75 degree/min depending on orbit altitude. During daylight, sun sensors would measure the orientation or error angles and modify the bias speed to minimize error. At night, the solar paddles would rotate at the nominal bias speed. This simplifies reacquisition of the sun as the spacecraft emerges into daylight.

The present ERTS/Nimbus drive employing a geared motor appears to be suitable for EOS. The estimated weight and power for each solar array drive are 30 pounds and 10 watts. Other choices include an adjustable low frequency synchronous motor or a stepper motor drive. These drives are desirable because of the absence of gearing. Further study relating to the choice of the solar array drives should be performed during the Phase B study.

7.6.6 SUMMARY

The proposed EOS attitude control system can acquire the desired orientation from any initial spacecraft attitude, stabilize the spacecraft to 0.5 degree with rates less than 0.005 deg/sec, provide sensor and torquer data to enable after-the-fact attitude determination to 0.1 degree, and orient the solar arrays to ± 5 degrees.

The ACS satisfies the requirements of all global EOS sensors, in addition to serving as the base for the precision attitude determination and/or control system to meet the need of the very high resolution sensors.

The ACS utilizes a horizon sensor and a three-axis rate gyro package to develop three-axis attitude and rate error data. These error signals are used to control three reaction wheels, via compensating networks and pulse modulators, so as to minimize attitude errors and rates. A cold-gas jet system is used for initial acquisition and for unloading the reaction wheels. A three-axis magnetic torquer is used to conteract known external disturbance torques to minimize the need for frequent jet firings.

The proposed ACS is based on proven techniques that pose no severe development problems; although further analysis of various aspects (in particular, the specifications for the performance and accuracy of the control sensors) is required. Further study of system redundancy should be made to insure a minimum of two-years life time. Effects of spacecraft flexibility on pointing accuracy and rate stability should also be studied.

The estimated power and weight of the ACS is given in Table 7.6-3. The ACS can be modularized by building the pneumatic system as one unit (to be mounted at the top of the tower) and another unit (except for the horizon scanners) to be located in the central body. The horizon sensors should be mounted near the bottom edge of the central body, in the pitch-yaw plane, so as to obtain an unobstructed field of view.

Table 7.6-3

Attitude Control System Weight and Power Summary

| Item	Weight (pounds)	Average Power (watts)
Horizon Sensor	20	10
Rate Gyros	40	20
Sun Sensors	5	1
Reaction Wheels	60	5
Magnetic Torquers	20	-
Pneumatic System	*60/70**	1
Electronics	20	8
Mounting & Wiring	30	-
Solar Array Drives	60	20
Total	*315/325**	65

*EOS A&B
**EOS C&D

7.7 PRECISION ATTITUDE DETERMINATION/CONTROL

7.1-1 PRECISION ATTITUDE DETERMINATION

For EOS flights containing the Thematic Mapper, it is necessary to determine the geographical location of the sensor ground track to about 100 meters. Landmark techniques, described in Section 10, provide a means of performing after-the-fact geographical referencing to very high accuracies. However, this requires rather complex ground processing. It is impractical to process all of the expected high resolution data (of the order of 10^{11} bits/orbit) via these techniques.

Precision attitude determination provides an attractive alternative or supplement to landmark techniques. Though not quite as accurate as landmark techniques, it provides a relatively simple method of automatically annotating all high resolution data (after-the-fact) to accuracies of about 100 meters rms.

The precision attitude determination scheme can be described as follows. Referring to Figure 7.7-1, let xyz be the spacecraft body fixed reference frame and let xyz represent a geocentric inertial
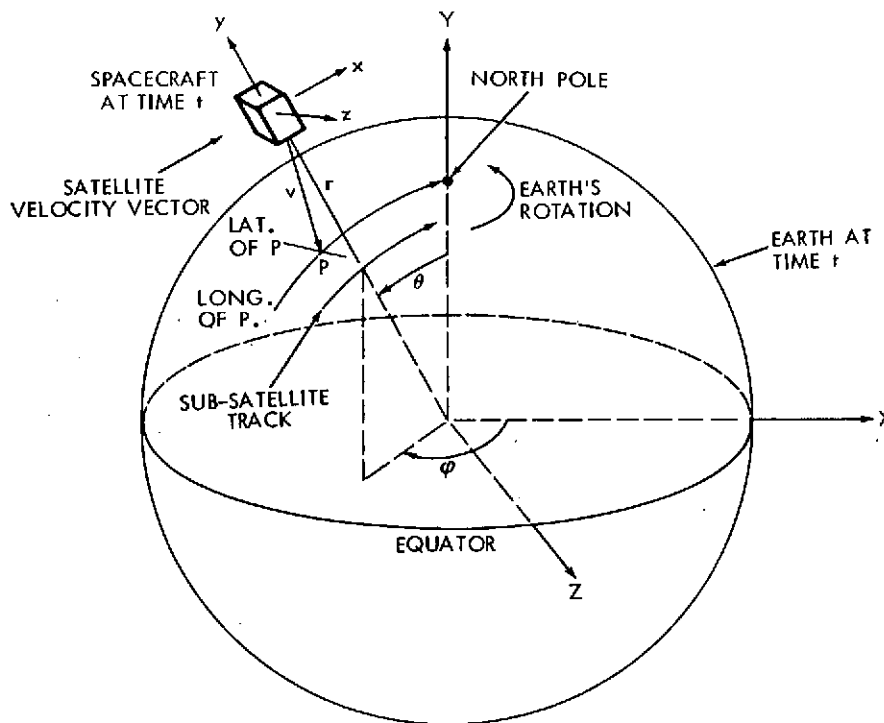
XYZ — Earth centered inertial axes

x y z — Spacecraft body axes — orientation relative to X Y Z at time t measured via Precision Attitude Determination System

V — Line of sight vector at time t of point scanner (or of a particular picture element of frame sensor) — known in xyz system.

r, θ, φ — Satellite position at time t — known from orbit determination

P — Earth surface point intersected by V — latitude and longtitude of P determinable from preceding and knowledge of earth orientation relative to XYZ at time t.

Figure 7.7-1. Geographical Referencing via Precision Altitude Determination

coordinate system (e.g., Y the earth's axis of rotation, X in the equatorial plane aligned with the vernal equinox, and Z in the equatorial plane completing the right handed triad). The two coordinate systems can be unambiguously related at time t if we know their relative angular orientation (via the precision inertial attitude determination system) and the spacecraft position (from orbit ephemeris estimation).

The line-of-sight of a point scanner, or of a particular picture element in a frame type of sensor, is a well-defined vector (denoted as V in Figure 7.7-1) in the spacecraft body frame of reference. The earth's geographical coordinate system at time t is related in a well known way to the inertial coordinate system defined above. Finding the intersection of the line-of-sight vector V with the geographical coordinate system, and hence determining the latitude and longitude of the sensor ground track point P, is a deterministic problem that is readily solved by ground computation.

In the above discussion, the spacecraft body axes refer to a reference block in the spacecraft to which the high resolution sensor is attached, or else to a reference block whose slowly varying mis-alignment with respect to the sensor is continuously measured (via a 3-axis autocollimator). The inertial orientation of this reference block (and hence of the sensor) is continuously measured by a 3-axis gyro system. Also attached to the reference block is a star sensor that obtains star updates at a frequency sufficient to correct for the gyro drift errors. The time history of gyro, star sensor and autocollimator readouts is stored and transmitted to the ground once per orbit, where computer processing reconstructs the time history of the inertial attitude of the sensor for that orbit. This is combined with orbit ephemeris information and sensor geometry to yield a geographical annotation for all of the sensor data in that orbit.

The hardware required aboard the spacecraft for the precision attitude determination system is the 3-axis gyro system, star sensor(s), and autocollimator if the sensor is remote from the reference block. There are several different techniques for mechanizing this inertial attitude measurement system. One way is to use three strapdown, single-axis rate integrating gyros and one or two passive star sensors, as is done by Honeywell for SPARS, an AIR Force program. Another way is to utilize a gimballed star tracker in place of the passive star sensor, as is done by TRW for PPCS, a Goddard program. Still another method is to utilize a 3-axis gimballed gyro system as well as a gimballed star tracker. There are pros and cons to each method which require further study.

At the present time, it appears that any one of these methods is suitable for the EOS application and should be capable of achieving an inertial attitude measurement accuracy of about 0.002 degrees. This represents an error of about 35 meters for a 1000 Km orbit. This error compares favorably with the error in orbit determination of about 30-100 meters. Other sources in this geographical referencing system include unknown axis misalignments in the sensor or between the sensor and the reference block. These fixed misalignments introduce bias errors which can be calibrated out by initial use of some simple landmark identification scheme. The remaining random component of sensor misalignments can be kept small (less than 0.002 degrees rms) by good mechanical and thermal design of the instrument and its mounting to the spacecraft. All in all, it would appear that geographical referencing of EOS data to an accuracy of about 100 meters rms is achievable by 1975 via a precision attitude determination system.

An interesting point to note is that the gyro portion of the precision attitude determination system can also be used in conjunction with landmark techniques to greatly reduce the frequency of landmarks required. This is worth further study.

7.7.2 PRECISION ATTITUDE CONTROL

A natural evolution of a precision attitude determination system would be a precision attitude control system to orient a high resolution sensor or sensors in real time. This requires an on-board computer to perform many of the functions that were previously performed on the ground. This computer would continuously generate its own estimates of orbit ephemeris based on ground tracking inputs once per orbit. There would be some degradation in the generated earth pointing reference because real time estimation of orbit ephemeris and spacecraft attitude is inherently less precise than

after-the-fact determination. Still, earth pointing to an accuracy of better than 0.01 degrees feasible without making the system unduly complex. This is equivalent to about 175 meters on the ground. This precision pointing could be done with respect to the local vertical or at some commanded latitude and longitude.

The precision orientation of a high resolution sensor to its individual target would be accomplished by a precision 3-axis servo platform to which the sensor is attached. In some cases, it would not be necessary to orient the entire sensor. For example, precision pointing control of the Thematic Mapper could be accomplished by 3-axis servo control of a mirror. If a particular alignment of the sensor field of view relative to the target is not required, then 2-axis servo platforms would be sufficient for precision orientation.

A precision attitude control system would permit precision orientation of high resolution sensors to their individual targets (local earth vertical, offset with respect to the vertical, or continuously at a commanded latitude and longitude) without affecting the earth orientation of the spacecraft as a whole. Thus, coarser sensors on the spacecraft would continue to be earth oriented within the accuracy of the coarse control system (about 0.5 degrees). Of course, the precision earth reference could also be used to upgrade the earth orientation accuracy of the coarse control system.

A great advantage of a precision attitude control system for high resolution sensors is that the sensor data can be geographically referenced in real time without any dependence on ground processing. Thus, a small local ground station could receive this data directly in a more useful form. Another advantage is the ability to orient a high resolution sensor to a particular geographical target (e.g. a hurricane) and to have it automatically follow the target as long as it remains within view of the satellite.

7.7.3 IMPLEMENTATION

The plan outlined in this section allows for an orderly mechanization of precision attitude determination and control which takes the form of add-on units to the basic spacecraft design. Thus the spacecraft hardware for precision attitude determination in no way complicates the basic coarse control system design. This added hardware could be omitted on EOS flights containing only coarse sensors that do not require precision attitude determination. (On such flights a simpler precision attitude determination scheme discussed earlier provides the required 0.1 degree accuracy. The next stage of precision attitude control requires the add-on units of a computer and precision servo drives for the high resolution sensors to be controlled. Again, this addition does not compromise the basic spacecraft control system and again, it can be omitted on any EOS flight not requiring precision attitude control of sensors.

7.8 THERMAL CONTROL

7.8.1 EOS CENTRAL BODY

7.8.1.1 Introduction. The basic requirement for the thermal design of the central body is that the electrical components must be maintained at 25°C ± 10°C (59°F to 95°F), while the batteries must be maintained at 20°C ± 10°C (68°F to 118°F).

7.8.1.2 Basic Design. Temperature control for the equipment of the proposed EOS spacecraft is achieved by employing a system of louvers, heat pipes, multilayer insulation, and thermal control coatings. The thermal design concept for the EOS central body is illustrated in Figure 7.8-1.
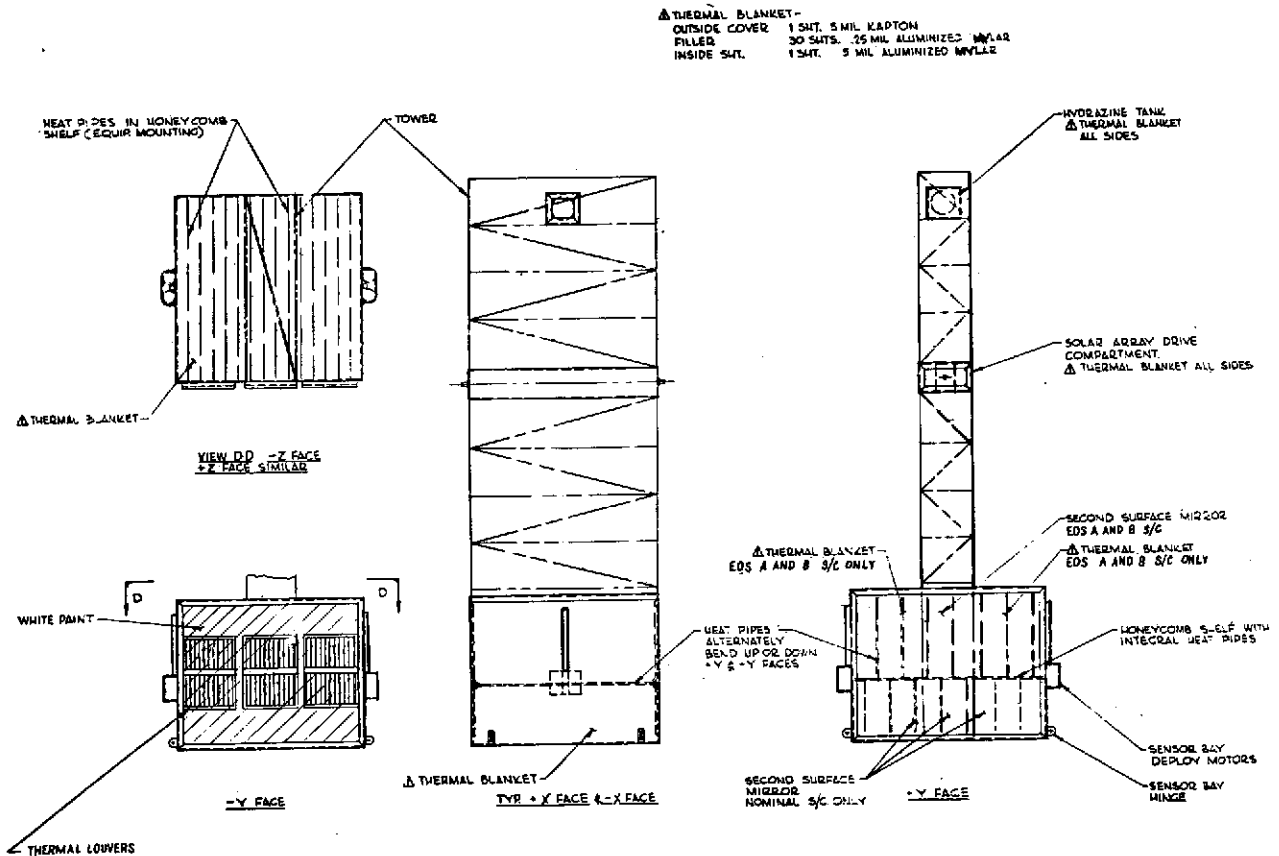

Figure 7.8-1. Thermal Control for Body and Tower

Assumming a square cross-section for the central body, the west side (-Y axis) of the spacecraft never has direct sun incident on it. This surface, along with the east side (+Y axis) of the central body serves as the primary thermal radiator for the central body. The east side is not as desirable as the west side as a radiating surface, but by necessity it must be used to dissipate the internally generated heat. Second surface mirrors are used on the east side to reflect the incident solar energy. The bulk of the electronic components are mounted to the equipment shelf which is connected to the radiators via heat pipes spaced about 4 inches apart. As shown in Figure 7.8-1, the equipment shelf and primary radiating surfaces consist of honeycomb panels with heat pipes embedded in them to distribute the heat load over the entire face.

The batteries must be controlled between 50°F and 86°F, while the remaining electrical components

should be held to between 59°F and 95°F. Due to this conflict in temperature requirements, the batteries are mounted to the west side radiator which will be slightly cooler than the equipment shelf. The batteries will be located as near as possible to the louvers on the west side.

Both the EOS A and B, and EOS C and D designs have 6 ft^2 (-55m^2) of louvers on the west side of the central body. In addition, for the EOS C and D spacecraft the east side is covered with Optical Solar Reflectors (OSR's),while the west side has 13.0 ft^2 of a fixed radiator finished with white paint. For the EOS A and B configuration, the east side has 9.0 ft^2 of OSR's while the west side has 14.0 ft^2 of a fixed radiator finished with white paint. All remaining central body areas, for both configurations, are covered with multilayer insulation.

The solar array drive and auxiliary propulsion fuel tank mounted in the solar array tower will have their own thermal control system. A reasonable thermal control scheme to assume at this point is multilayer wraps of insulation and use of a small heater to keep these items warm.

7.8.1.3 Thermal Model. To verify the thermal performance of the central body a small thermal model was developed for numerical solution[1] This model is illustrated in Figure 7.8-2. It consists of a node for each side of the central body, the equipment shelf, and the front and back of the solar cell panel.
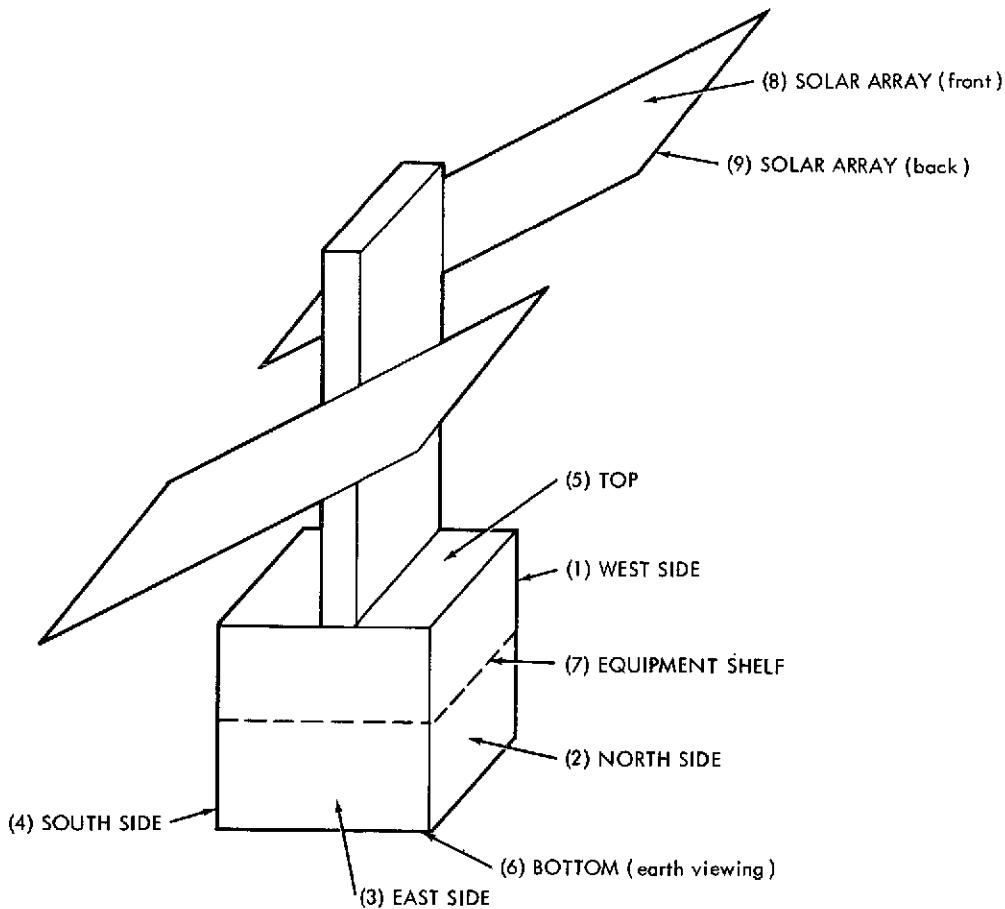

Figure 7.8-2.   EOS Thermal Model

As previously mentioned, the west side of the central body contains thermal louvers in both the EOS A and B and EOS C and D configurations. A plot of the effective emissivity vs temperature assumed in the model is shown in Figure 7.8-3. The assumed values for absorptivity and emissivity for the central body thermal computations are:

White paint west side radiators $\alpha/_\epsilon = 0.2/0.8$

OSR's $\alpha/_\epsilon = 0.1/0.8$

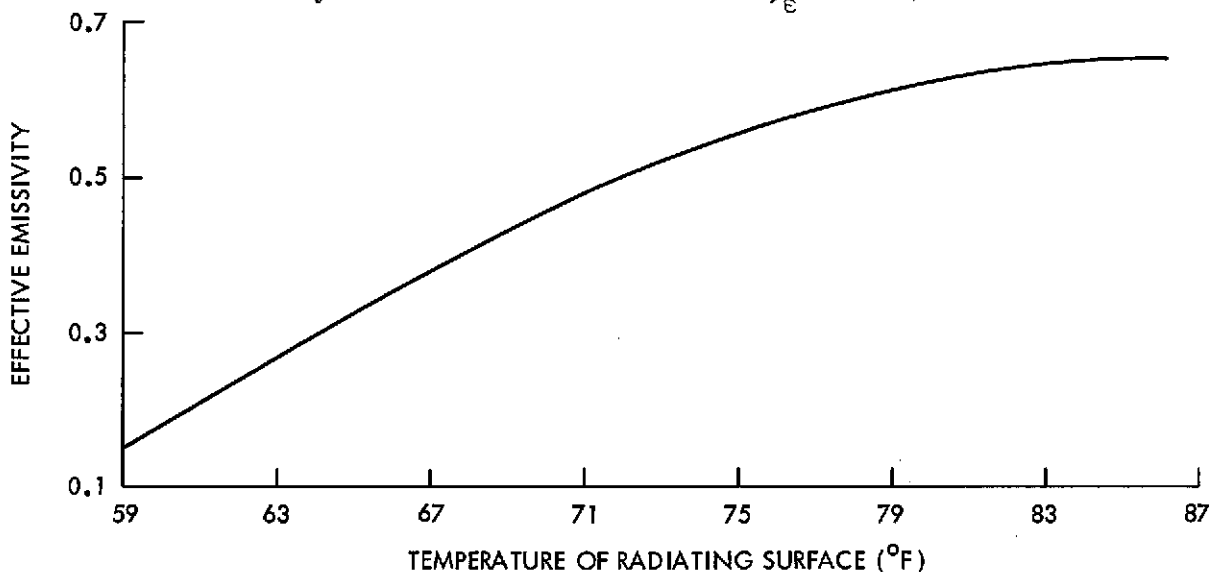multilayer insulation $\alpha/_\epsilon = 0.0075/0.015$

Figure 7.8-3. Louver Effective Emissivity vs. Temperature

Thermal computations for the EOS A and B, and EOS C and D central body were done for a 600 n.m, 9:00 o'clock orbit. For other orbits (i.e. noon or twilight) or altitudes (i.e. 400 n.m.) the results would be fairly close.

7.8.1.4 Heat Dissipation and Incident Fluxes. The estimated heat dissipation rates are shown in Table 7.8-1. Values shown in this table are estimates of maximum and minimum average regulated dissipation. Transient and peak load conditions were not considered. Furthermore, small deviations from the estimated totals in Table 7.8-1 would have little effect on the conclusions drawn from the thermal analysis.

Incident environmental heat fluxes were computed for each surface of the spacecraft.[1] To do this, the orbit plane inclination was assumed to be 100° and the sun-earth line assumed to make an angle of 45° with the orbit normal, at the equinox. The orbit plane was assumed not to precess in the computation of the incident fluxes for winter and summer solstice conditions. Table 7.8-2 shows the results of these calculations. The numbers in the table are the orbit-average incident radiation from either the sun, albedo, or earth for the equinox, summer solstice, or winter solstice conditions. These heat flux calculations ignore any shadowing effect of the spacecraft. For the purposes of the present calculations the equinox and summer solstice fluxes are taken as being equal.

7.8.1.5 Conclusion.

a. EOS C and D. Figure 7.8-4 shows a plot of the equipment shelf temperature vs total heat dissipation. From the figure, the maximum temperature is 90° F and the minimum is 61° F, thus satisfying the 59° F to 95° F requirement.

Table 7.8-1

Central Body Heat Dissipation (watts)

	EOS A and B		EOS C and D	
	Min	Max	Min	Max
Data Handling & RF Logic	150	350	200	500
Battery	58	65	160	122
Power Conditioning *	210	210	350	350
Controls	40	40	40	40
Orbit Adj.	10	10	10	10
Totals	468	675	706	10 22

*Assumes shunt dissipators to be outside spacecraft.

Table 7.8-2

Incident Heat Fluxes (orbit average - BTU/hr ft²)

	Equinox			Summer-Solstice			Winter-Solstice		
	Sun	Albedo	Earth	Sun	Albedo	Earth	Sun	Albedo	Earth
West	--	4.7	12.8	--	4.58	12.8	--	5.88	12.8
North	85.78	6.31	12.8	85.03	6.22	12.8	93.32	7.25	12.8
East	238.38	7.94	12.8	243.71	7.88	12.8	184.19	8.54	12.8
South	85.78	6.31	12.8	85.03	6.22	12.8	93.32	7.25	12.8
Top	98.47	--	--	96.97	--	--	113.51	--	--
Bot.	32.49	24.8	50.27	33.26	24.43	50.27	26.69	28.45	50.27
Paddle									
Front	337.12	2.22	15.4	339.51	2.2	15.4	313.43	2.31	15.4
Back	--	12.29	15.39	--	12.05	15.39	--	14.69	15.39
Period	107.44 min								
Suntime	0.766			0.771			0.724		

dissipation. From the figure, the maximum temperature is 90°F and the minimum is 61°F, thus satisfying the 59°F to 95°F requirement.
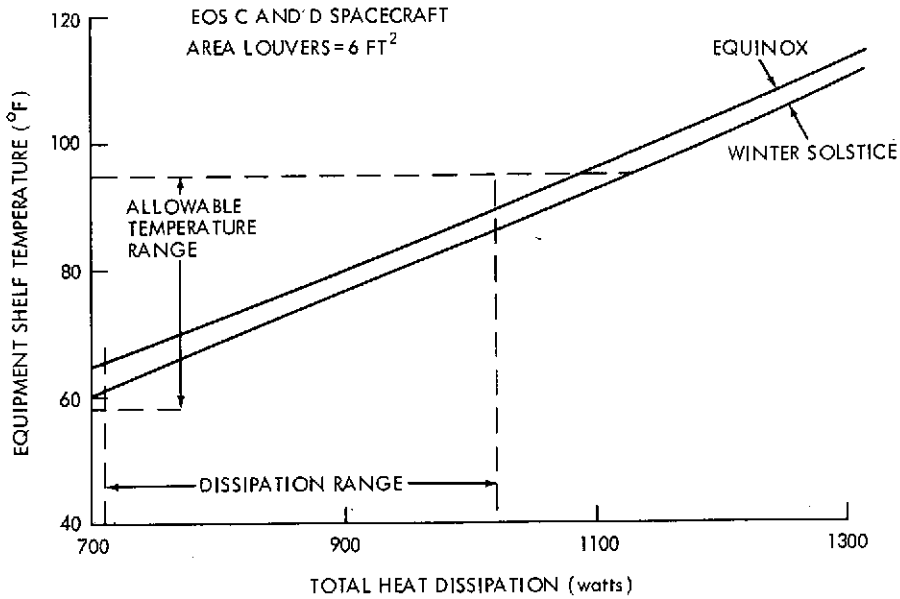

Figure 7.8-4.   Equipment Shelf Temperature vs. Total Heat Dissipation

Figure 7.8-5 shows the west side radiator temperature vs total heat dissipation. The maximum temperature is 81°F and the minimum is 57°F, which is well within the 50°F to 86°F range required for the batteries.
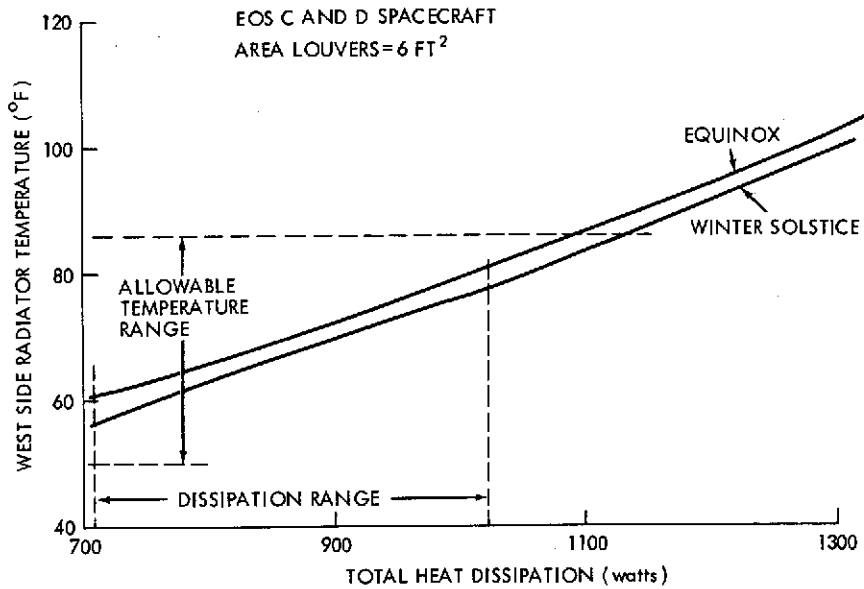

Figure 7.8-5.   West Side Radiator Temperature vs. Total Heat Dissipation

b. EOS A and B. The total heat dissipation vs equipment shelf temperature curve is shown in Figure 7.8-6. The temperature range in this case is from 80°F at the maximum dissipation point to 54°F at the minimum dissipation point. Hence, the maximum temperature is well below the allowable (95°F), but the minimum temperature is 5°F too low. This low temperature could easily be increased by employing an auxiliary heater during low dissipation periods, or using slightly larger louvers.
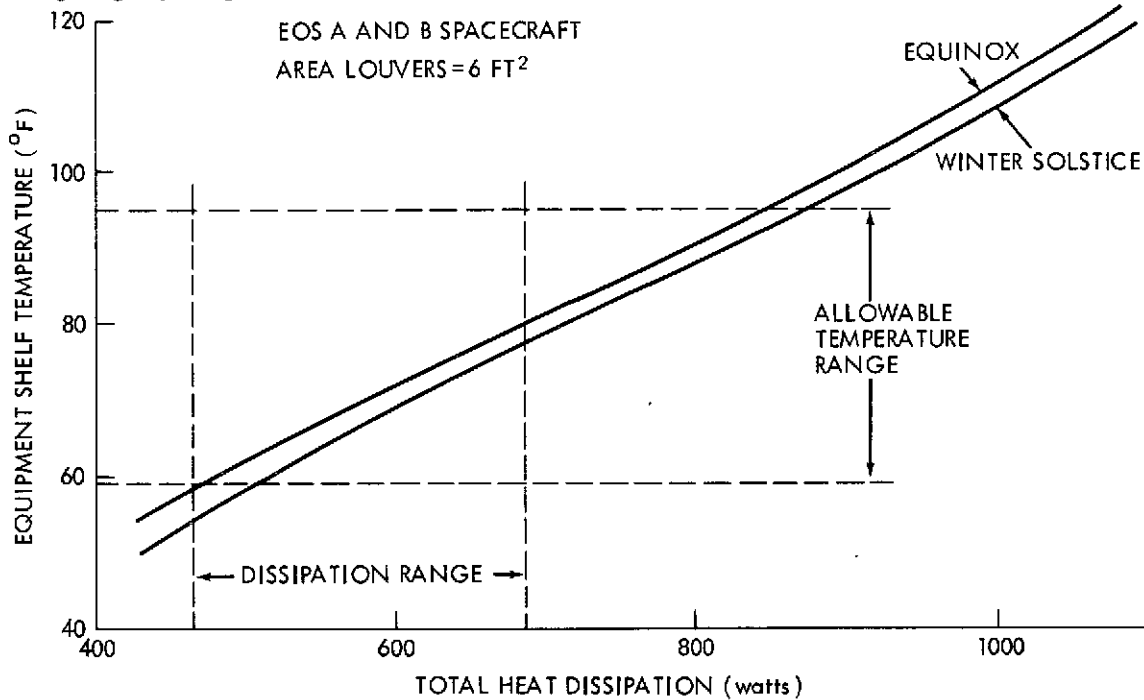

Figure 7.8-6. Equipment Shelf Temperature vs. Total Heat Dissipation

Figure 7.8-7 shows the west side radiator temperature vs total heat dissipation. The maximum temperature fluctuation is from 49°F to 69°F. Hence, the maximum temperature is well below the allowable maximum for the batteries while the minimum temperature falls 1°F less than the allowable minimum. The minimum temperature could be raised by the methods previously mentioned.

c. Summary. At this point there does not appear to be any inherent difficulty with the thermal design and control of the EOS central body. More detailed calculations must, of course, be done in the future.

7.8.2 SENSOR BAYS

7.8.2.1 Design Criteria. Table 7.8-3 shows estimates of the average heat dissipation loads for each bay for a noon orbit. These heat dissipation rates are approximations which are based on experiments proposed for EOS early in the study. There is enough flexibility in the thermal design of the spacecraft to accommodate changes in the heat dissipation rates as shown in Table 7.8-3.

It is necessary for each bay to dissipate their loads while maintaining the component temperatures between 25°C ± 10°C (or from 59°F to 95°F). In the following computations it is assumed that there is a constant 10°F temperature drop between the bay components and radiator surfaces. Hence, the radiator temperature limits are from 49°F to 85°F. Furthermore, it is assumed that only the west side (-y axis) of the bay can be employed as a thermal radiator, and that all of the bay surface areas not used for temperature control purposes are covered with multilayer insulation.
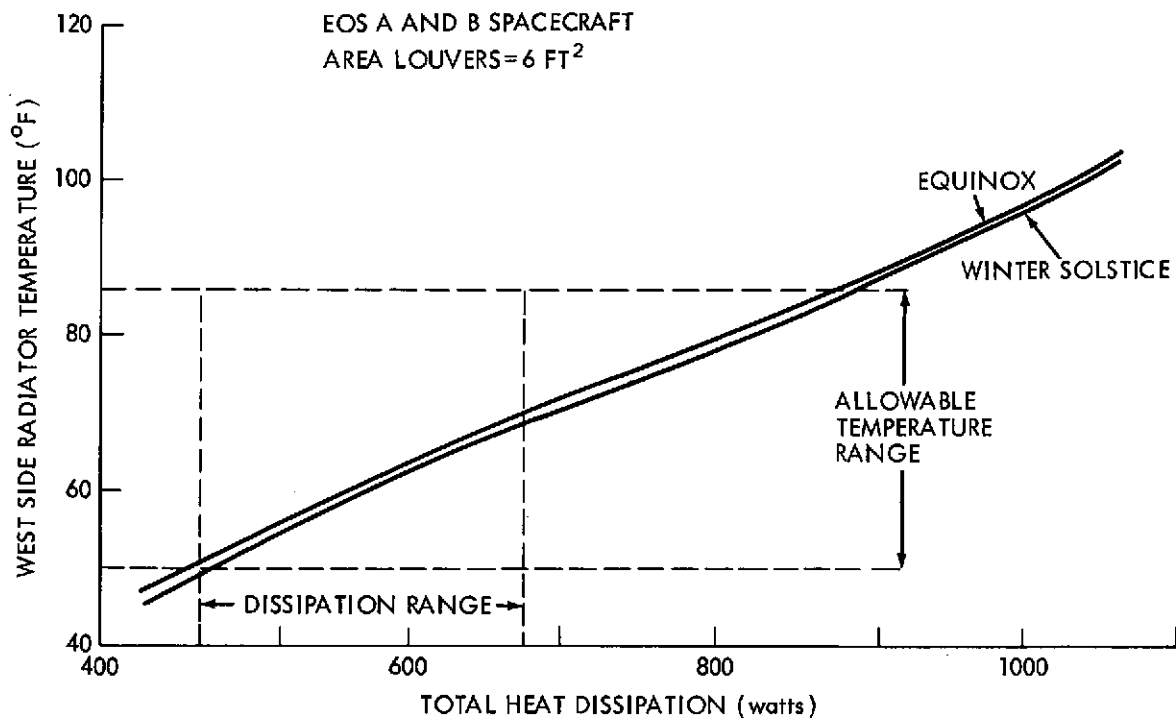
Figure 7.8-7. West Side Radiator Temperature vs. Total Heat Dissipation

Table 7.8-3

Bay Dissipation Loads - Noon Orbit (watts)

	EOS A and B			EOS C and D		
	Min	Nom	Max	Min	Nom	Max
Bay #1	0	21	35	111	139	165
Bay #2	115	122	141	140	140	200

7.8.2.2 Sensor Bay Radiator Sizing.

a. EOS A and B. The heat dissipation characteristics of a west facing radiator for a noon orbit are shown in Figure 7.8-8. The two curves represent the capacity of a new radiator in a minimum sun orbit (a) and the capacity of a degraded radiator (b) in a maximum sun orbit. Start of life radiator characteristics were that of a white coating having a solar absorptance of 0.20 and a thermal emittance of 0.85. After ageing the absorptance is assumed to be 0.35.

If thermal control louvers are placed over these radiators the absorptance and emittance characteristics will be as shown in Figure 7.8-9. The two pairs of curves again represent new (C_2, C_1) and degraded (d_2, d_1) performance with the additional restriction that the open louvers will absorb 40% of any incident sunlight. The dashed lines represent the approximate capacity of the louvers between fully open and fully closed positions.

Bay number one must dissipate 35 watts less whatever heat leak there is through the module insulation. To be conservative a minimum estimated heat leak of 7 watts is used. Therefore, 35-7=28 watts is the maximum heat to be dissipated by the radiators. The minimum heat is zero with the experiment turned off. This means that auxiliary heater
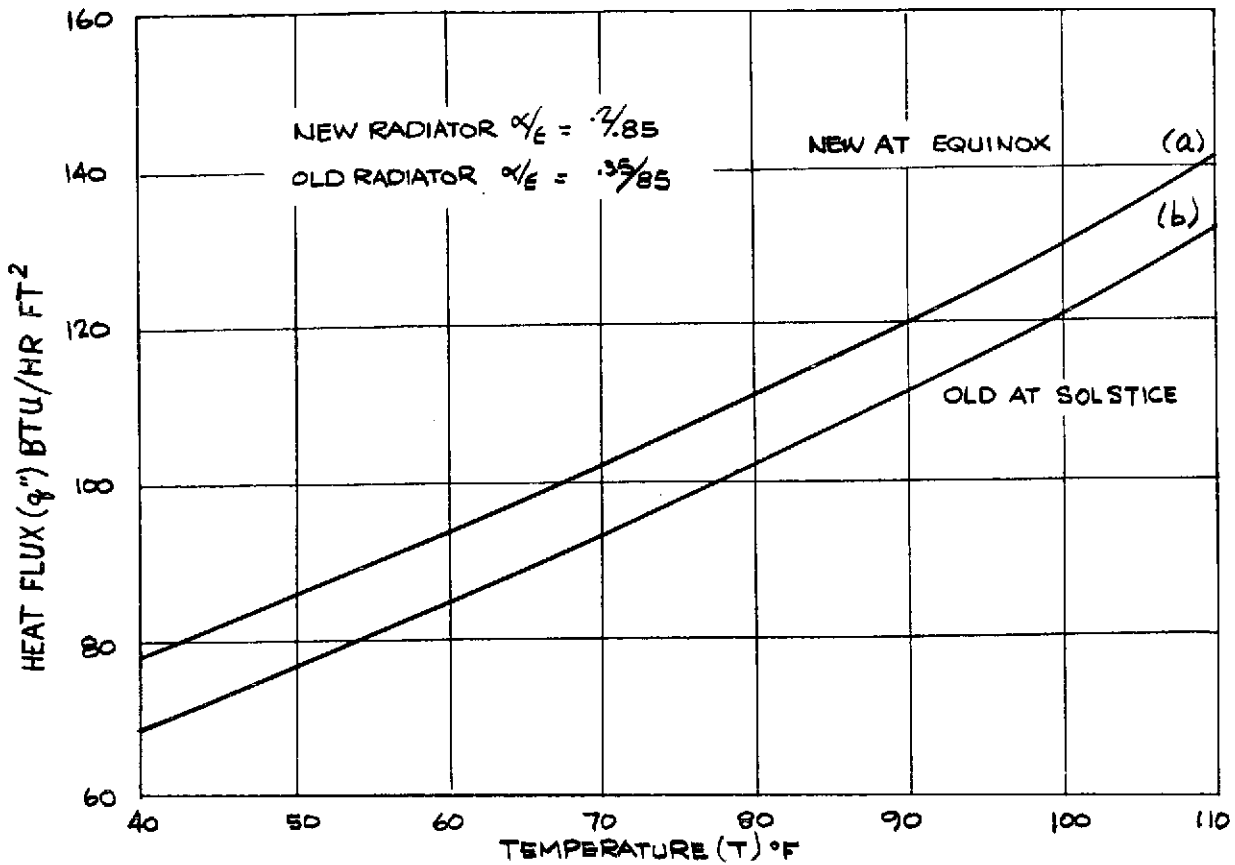
Figure 7.8-8. Characteristics of an Open EW Radiator in a 400 nm Noon Orbit

power must be used to maintain the module in the minimum standby temperature range. Louvers must be used to conserve this heater power. The required louver area is obtained with the use of Figure 7.8-9.

The $10^{\circ}F$ interior temperature rise to the $95^{\circ}F$ components requires the radiator to dissipate 96 BTU/hr (28 watts) at a temperature of $85^{\circ}F$. From Figure 7.8-9, point (A), q" for a degraded radiator is 90 BTU/hr ft^2. The required louver area is therefore $96/90=1.067$ ft^2.

At the cold condition with the equipment off, the radiator temperature must be maintained at $49^{\circ}F$. The louver q" from Figure 7.8-9 is 14 BTU/hr ft^2; therefore, (14) (1.067) 14.95 BTU/hr of heat is lost through the louvers. Combining this loss with a maximum estimated heat leak (78 BTU/hr), to be conservative, yields a net loss of 92 BTU/hr which must be made up with auxiliary power of 27 watts.

In the hot condition, bay number two must radiate 141 watts (482 BTU hr) less the minimum estimated heat leak of 24.4 BTU/hr, and in the cold case 115 watts (393 BTU/hr) less the maximum heat leak of 78 BTU/hr. Following the same procedure as for bay one yields 5.09 square feet of louvered radiator area. The cold case flux of 315 BTU/hr/5.09 ft^2 = 61.9 BTU/hr ft^2 will produce a radiator temperature of $65^{\circ}F$. This is well above the allowable $49^{\circ}F$ indicating that this louver design is feasible. Further calculations show that a free radiator of 3.58 ft^2 combined with a louvered radiator of 0.84^2 ft will maintain the number 2 bay radiator between $85^{\circ}F$ and $49^{\circ}F$.
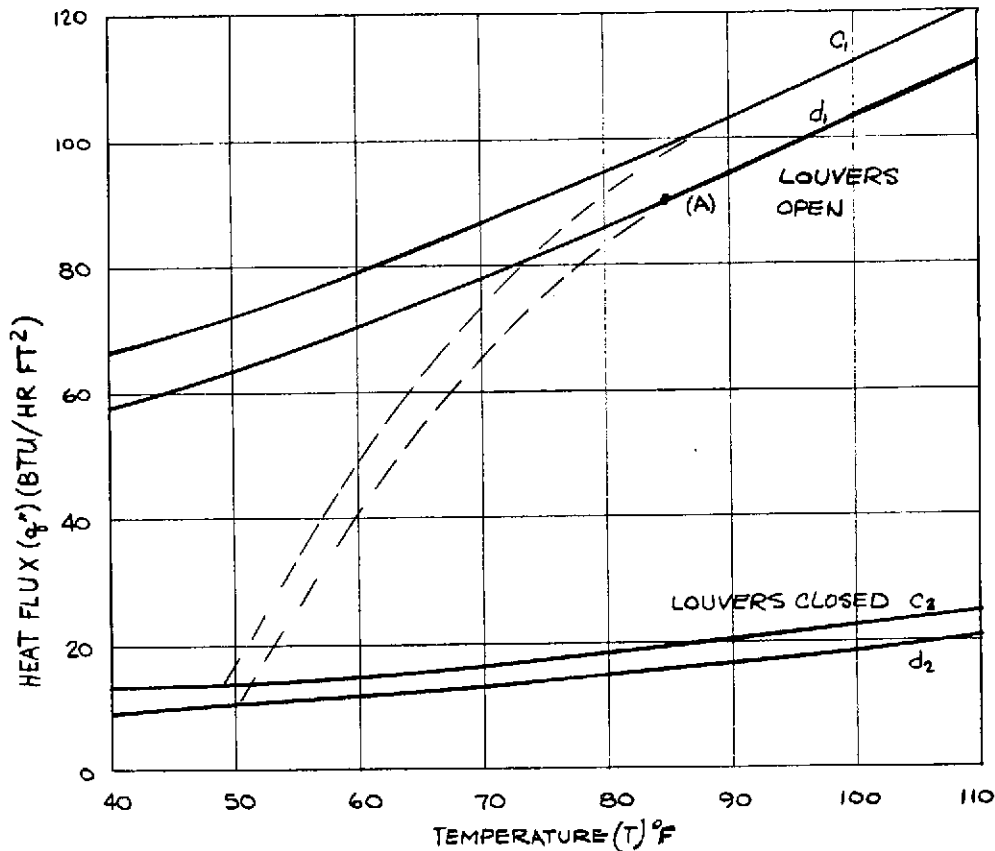
7-82

Figure 7.8-9. Heat Rate Characteristics of an EW Louver Set @ 400 nm Noon Orbit

b. EOS C and D. Bay number 1 has an estimated heat leak range from 7 to 131 BTU/hr. The radiator dissipation is therefore from a minimum of 249 BTU/hr to a maximum of 556 BTU/hr. Therefore, $556/90 = 6.25$ ft^2 of louvers keep the radiators at 85°F during the hot case and at 57°F during the cold case condition. While it would be theoretically possible to reduce the louvered area and use up the 8°F (57° - 49°) margin, it is rather pointless to do so at this phase in the spacecraft development.

Bay No. 2 has the same heat leak range but a higher heat dissipation load. The radiator dissipation is between 348 and 676 BTU/hr. Then $676/90 = 7.5$ ft^2 of louvers will maintain the 85°F maximum allowable radiator temperature while holding to 59°F during a cold, low power period.

7.8.2.3 Heat Pipes and Insulation. U shaped heat pipes could be used to thermally couple the east, top, and west bay surfaces. The experiment packages could then mount to the top sur- face of the bay where the heat pipes could cool them directly. These heat pipes could be spaced so that each one carries no more than 50 watts.

All bay surfaces but the radiators, and earth viewing operatives would be covered with multilayer insulation.

7.8.2.4 Effects of Twilight and 9 A.M. Orbits. The approximate thermal calculations as presented for the noon orbit would be changed very little for a twilight or 9 o'clock orbit. (Also, there would

be little difference in the calculations for a 600 n. m. orbit). Hence, the thermal design of the bays would be basically the same for either a 9 o'clock or twilight orbit.

7.8.2.5 Conclusion. It is concluded that basic thermal design and control of the bays present no particular difficulty, and that there is a margin to accommodate future changes. More detailed thermal calculations, including transient effects, will have to be made once the experimental packages become better defined.

7.8.3 SOLAR ARRAY TEMPERATURES

The thermal analysis of the solar cells panels consisted of evaluating the temperatures and the thermal gradients under various configurations considered. The results are applicable to all configurations considered because of the general method in which the calculations were made. The panel was considered to be 3/4" honeycomb structure with an effective conductance, which includes the effects of solar cells and associated substrates, of 10 BTU/hr °R. The back of the panel was assumed to be coated with a white paint having a stable absorptance to emittance ratio of 0.2/0.85. The relative low absorptance of this coating tends to reduce albedo effects and hence insures the operating temperature of the cells to be within acceptable limits.

Both 400 n. m. and 600 n. m. altitudes were considered for high noon, twilight, and 9 o'clock orbits. The solar cell side of the panels is normal to the solar vector during the sunlight portion of the orbit.

Standard analytical techniques were employed. An Orbital Heal Flux (OHF)[1] computer program was utilized to obtain solar, albedo and earth fluxes impinging on the panels. The OHF results were incorporated into an Orbital Transient Heat Transfer (THT)[1] computer program and temperature profiles were generated for the different cases considered. The results of these calculations are shown in Table 7.8-4.

Table 7.8-4

Solar Panel Temperatures and Gradients

400 n. m.	Solar Cell Temp. (°F)		Max Gradient	
	Max	Avg Sunlit	Min	°F
Twilight	135	135	135	15
High Noon	150	140	-102	12
9 o'clock	143	139	- 96	14
600 n. m.				
Twilight	131	131	131	15
High Noon	148	143	-105	12
9 o'clock	141	136	- 90	14

Changes due to solistice variations were assumed minor in this analysis, and thermal interchange between the panels and the spacecraft were not considered.

7.8.4 SENSOR COOLING

7.8.4.1 Introduction.

The Thematic Mapper has detectors, which must be maintained at $90^{\circ}K$ during operation. This sensor must be operative for one to three years; the precise duty cycle, however, is not defined at the present time. Furthermore, at this stage one could not predict the problems that would be encountered in either the sensor or cooling system due to intermittent cool-down throughout the EOS mission. Therefore, it is assumed in the following discussion that the sensor cooler is required to maintain the Thematic Mapper sensor at $90^{\circ}K$ continuously for two years. Furthermore, the discussion that follows would apply to the cooling of any sensors with temperature requirements in the $90^{\circ}K$ or lower range.

7.8.4.2 Types of Coolers.

a. Discussion. There are many spacecraft sensor cooling devices which are being investigated in the field at the present time. These include solid-cryogenic coolers, passive radiators, rotary or reciprocating Brayton and Claude cycle machines, Stirling refrigerators, and Vuilleumier (VM) refrigerators.

It was determined that a solid cryogenic cooler, passive radiator, or VM refrigerator would be the best sensor cooling device for EOS. This conclusion is based on the following considerations:
1) Rotary, Brayton and Claude cycle refrigerators require excessive electrical power for low cooling loads. These devices are more applicable to high cooling load requirements.
2) Reciprocating Brayton and Claude cycle refrigerators would be much larger, and probably heavier, than either a Stirling or VM cooler in the cooling load and temperature range of interest for EOS application. In addition, these machines require a large amount of electrical power (~ 100 W) and are mechanically complex.
3) Although the Stirling cycle refrigerator requires a relatively low amount of electrical power, it does not have the potential for a 2-year operation as does the VM refrigerator. This is primarily a result of the high differential pressures across the refrigerator pistons which usually necessitates the use of pressure seals and causes relatively high bearing loads.

The elimination of all possible sensor cooling methods for EOS but solid-cryogenic coolers, passive radiators, and VM coolers is further supported by Figure 7.8-10. This figure, extracted from Reference 7.8-2, shows the most probable areas of application of spaceborne refrigerators as a function of cooling load and temperature. In constructing this map, cooling system lifetime was not considered per se, but rather the criteria of minimum total system weight was employed. Considering the approximations inherent in a map of this nature, then, it is concluded that for a sensor temperature of $90^{\circ}K$, on a system weight basis, solid cryogenic coolers, passive radiators, and Stirling or VM cycle refrigerators should be considered for use on EOS. The Stirling refrigerator is eliminated, however, because of the two year continuous operation requirement.

b. Solid Cryogen. Solid cryogen refrigerators consist of a solid cryogen stored in a vented dewar, with the solid state maintained by evacuating the ullage space around the cryogen. The sensor to be cooled is mounted on a pedestal, which is in thermal communication with the solid cryogen. Cooling occurs due to the sublimation of the cryogen, with the resulting vapor vented to space.

The prime advantages of a solid cryogenic cooler for spacecraft application are that it requires no power and it is relatively simple in design with few or no moving parts. In addition, for relatively short duration missions it may have a weight and size advantage over closed cycle systems.

The disadvantages of a solid cryogenic cooler are that for a relatively long life-time operation its weight and size may be prohibitive, and its use may impose restrictions on detector mounting. Further complications in the operation of the coolers are in filling the dewar with the cryogen, and the vacuum requirement during pre-launch storage and during ascent into orbit. Also, the design of the cryogenic dewar requires a great deal of sophistication in order to reduce parasitic loads to a minimum. Hence, mounting and insulation considerations are of paramount importance.
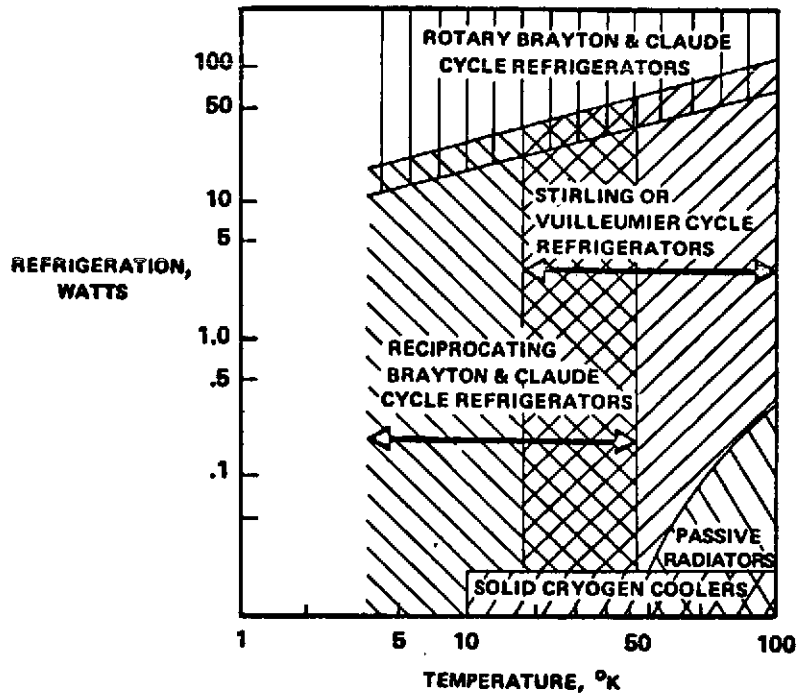
Figure 7.8-10. Most Probable Areas of Application of Various
Spaceborne Refrigeration Systems

Table 7.8-5 (from Reference 3) lists the properties of various cryogens which are applicable to
subliming refrigerators. For the EOS requirements (i.e. sensor temperatures about $90^\circ K$)
methane and argon are prime candidates. However, because of the hazards in handling methane
it is concluded that argon would be the best cryogen for an EOS subliming cooler.

If it is assumed that the detector and dewar heat leaks to the argon can be held to 50 MW, then
37.3 pounds of argon would be required for an EOS mission of two years. This argon would
occupy a volume of 604 in^3.

The total subliming-cooler weight is the sum of the argon, container, mounting, insulation, and
radiation shroud weights. For example, Figure 7.8.11 shows a solid argon subliming cooler
as reported in Reference 7.8-4. This cooler was designed for a total cooling load of 40 MW for a
one year operating lifetime. In this design solid carbon dioxide is employed to cool the copper
shroud surrounding the argon radiation shield in order to minimize parasitic load. As shown, the
argon volume (223 in^3) occupies less than one-half of the total dewar volume. The weight of the
argon for this cooler is 13.7 lbs vs 29.9 lbs for the whole system.

On the basis of the example cited, it appears that approximately 30 lbs should be added to the
weight of the argon for an EOS 2-year subliming solid cooler. This results in a total weight of
67.3 lbs. The volume of the cooler is estimated to be about 1 ft^3.

It is concluded that the solid cryogenic cooler should not yet be ruled out for use on EOS. However,
at this point the weight of the cooler appears quite high, and for a longer duration mission would
be prohibitive.

c. Passive Radiator. The use of a cryogenic radiator to cool spacecraft sensors is the most
direct way to utilize the low temperature sink of space. Ideally, the passive radiator requires
no power, has no moving parts, and should be capable of long-lived operation. However, there
are several very serious practical limitations with sensor passive coolers.

Table 7.8-5

Properties of Solid Cryogens*

Coolant	A	CO	H_2	CH_4	Ne	N_2
Temp range °K	55-83	51-68	9-13	67-88	16-24	47-63
Press range, torr	1-480	1-115	1-30	1-80	1-260	1-90
Heat of sublimation,						
cal/g	44	70	122	136	25	54
Btu/lb	80	126	219	245	45	97
Density						
g/cm³	1.7	0.93	0.09	0.52	1.4	1.02
lb/ft³	106	58	5.4	31.5	87.3	63.8
Heat absorbed						
cal/cm³	75.3	65.1	9.76	70.7	35	54.8
Btu/ft³	8460	7300	1090	7720	3930	6160
Thermal conductivity of solid						
mW/cm-°K	8.0	--	9.0	--	4.0	3.0

*Values given are approximate.

1) The radiator performance is very sensitive to radiant input from the sun, earth, or spacecraft structure and components. Hence, the cooler must be tailored to each particular spacecraft and orbit and, in fact, in certain cases it may be impossible to design a passive cooler to maintain a sensor temperature at 90°K.

2) The cooler must be mounted so that it is as thermally isolated from the spacecraft as possible. This is necessary in order to prevent the cooler from becomming prohibitively large and heavy due to high parasitic heat input.

3) The cooler surface must be protected from spacecraft effluents. This can be accomplished by either preventing effluent impingement through careful spacecraft design, or, more practically, making provisions for this problem in the cooler design. For example, in Reference 7.8-5 an anti-frost cover is provided which, when actuated, raises the temperature of the radiator surface by shielding it from cold space. In addition, the cooling patch in this cooler design is maintained in a controlled dry atmosphere for the period of major spacecraft outgassing (~10 days).

4) The passive coolers must be very carefully handled on the ground in order to prevent contamination of the cooler surface. Even a small amount of contamination could result in the cooler not achieving the specified sensor temperature.
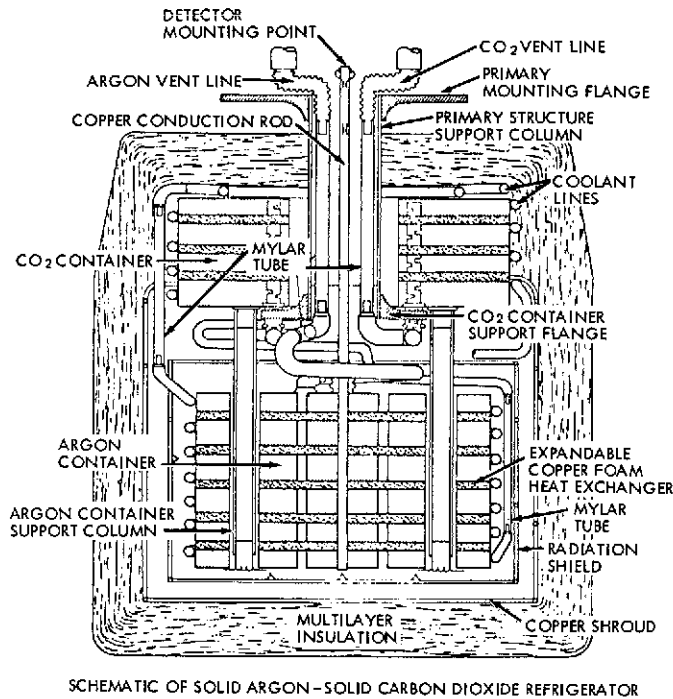
DETECTOR
MOUNTING POINT
ARGON VENT LINE
COPPER CONDUCTION ROD
CO₂ CONTAINER
MYLAR
TUBE
ARGON
CONTAINER
ARGON CONTAINER
SUPPORT COLUMN
CO₂ VENT LINE
PRIMARY
MOUNTING FLANGE
PRIMARY STRUCTURE
SUPPORT COLUMN
COOLANT
LINES
CO₂ CONTAINER
SUPPORT FLANGE
EXPANDABLE
COPPER FOAM
HEAT EXCHANGER
MYLAR
TUBE
RADIATION
SHIELD
MULTILAYER
INSULATION
COPPER SHROUD

SCHEMATIC OF SOLID ARGON-SOLID CARBON DIOXIDE REFRIGERATOR

Figure 7.8-11.   Schematic of Solid Argon-Solid Carbon Dioxide Refrigerator

5) The thermo-physical properties (i.e. absorptivity/emissivity) of many radiator surface coatings degrade with time. Thus, the radiator may cool the sensor patch to 90°K at the beginning of the flight, but the patch temperature may increase significantly after two years.

Preliminary basic geometric configurations for possible EOS sensor coolers have been constructed. As a ground rule it was assumed that the surface area of the cooler is 1.7 ft². Then, with an emissivity of 0.8, the radiator can dissipate about 1/2 watt at 90°K. This cooling load is a reasonable value for the sensor load, which is on the order of milliwatts, plus the parasitic load to the cooler.

Figure 7.8-12B shows the basic passive radiator cooler configuration for a 10:00 o'clock through noon orbit.[1] The cooler consists of radiating and reflecting surfaces. The purpose of the reflecting surface (low absorptivity and high directional reflectivity) is to reflect the input radiation from the solar paddle (when viewed), and hence minimize its effect on the radiating surface. This cooler configuration could be greatly simplified for a one paddle spacecraft design (Appendix C) because a reflecting surface would then not be required, and the radiator could be located anywhere on the paddleless side of the bay.

―――――――――――

[1]The cooler geometrics were constructed for the EOS A and B spacecraft configuration. For the EOS C and D spacecraft the cooler designs would be very similar, with only minor changes in the configurations shown. Also, Figure 7.8-12 merely shows the rudiments of passive coolers that would avoid viewing the sun or spacecraft. For example, the geometry of the cooler in the planes parallel to the top plane and bottom surfaces of the bays is not considered.
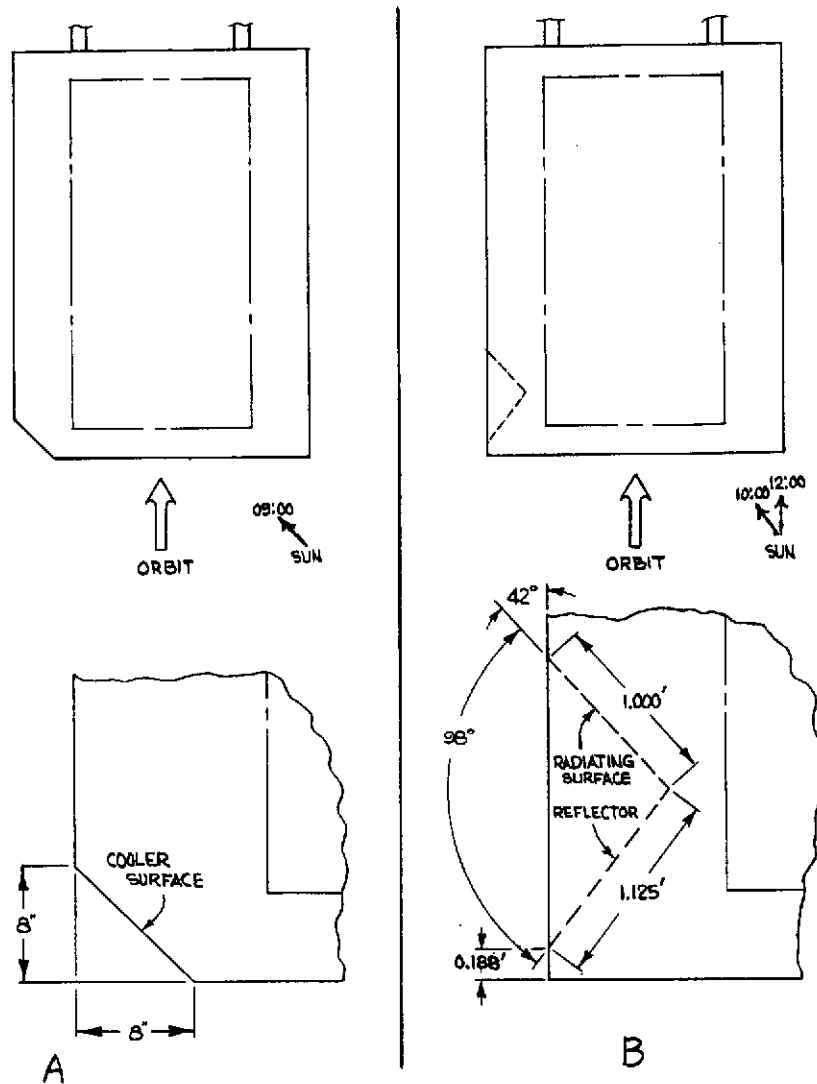
Figure 7. 8-12.   Basic Passive Cooler Geometry

It is noted that the final design of the two-paddle spacecraft, 10:00 through 12:00 o'clock orbit, radiator would be much more complicated than presented here. Nevertheless, at this point it at least appears feasible to design a passive cooler for the EOS sensor patch. Furthermore, it is noted that the area on the edge of the bay occupied by the cooler is not large enough to significantly alter the overall bay thermal design and control system, as presented in paragraph 7.8.2.

For a 9 o'clock orbit a more compact passive cooler design can be constructed. This concept is depicted in Figure 7.8-12A. With the dimensions shown in the figure, the radiator surface will only be exposed to cold space (i.e. the surface never views the sun, earth, paddles or spacecraft structure) throughout the orbit.

In summary, the use of a passive radiator cooler in EOS appears feasible at the present time. However, the design of this cooler for the two paddle spacecraft would be complex; it can be greatly

simplified for the one paddle spacecraft. The weight of the passive radiator would be significantly less than that of a solid cryogenic cooler, but all of the disadvantages of a passive radiator, which were previously discussed, would exist.

d. Vuilleumier Refrigerator (VM).

1) Description. The following discussion on the operation of a VM refrigerator is simplified in that only the predominant heat transfer processes at each crank position are considered; the pressure drops across the regenerators are ignored and hence the gas pressure at a given crank angle is the same throughout the refrigerator; thermal losses are neglected (ideal case) and consequently the gas temperature in each section is constant and the regenerators heat or cool the gas to the corresponding existing cylinder gas temperatures.

The VM refrigerator consists of a hot cylinder, to which heat (Q_H) is transferred from a heat source (i.e. either from spacecraft electrical power or an isotope heat source), a cold cylinder, to which heat (Q_C) is transferred from the load (the sensor), and a sump (or ambient section) from which heat (Q_A) is rejected. The operating fluid (e.g. helium gas) in these three sections is at three different temperatures ($T_H > T_A > T_C$) and flows through the regenerators into or out of each section, due to the motion of the displacers as the crank rotates (refer to Figure 7.8-13). The gas temperature differences between the sections is maintained by the displacers (which are thermal barriers), the regenerators (which heat or cool the flowing gases to the appropriate temperatures) and the heat transfer to or from each of the three sections.
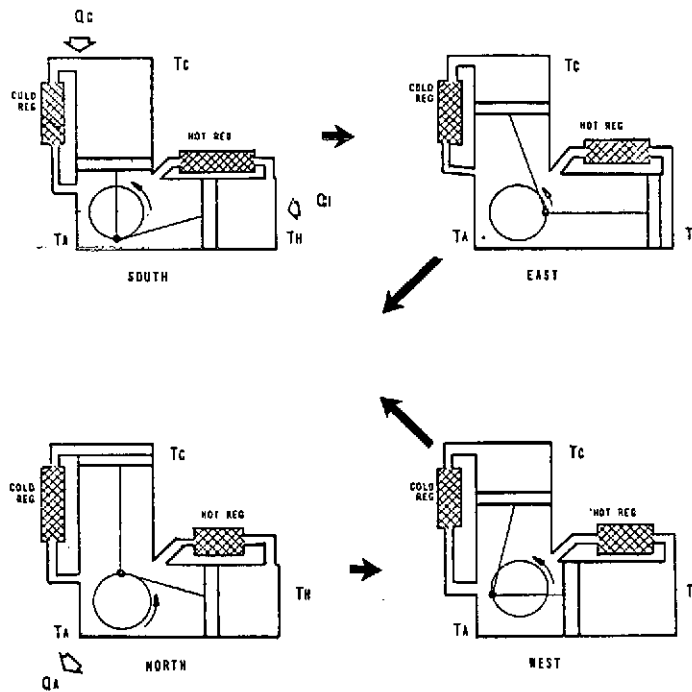

Figure 7.8-13.   Vuilleumier Refrigeration

When the crank is in the south position, the cold displacer is at its maximum displacement position and the hot displacer is only at the half-maximum position. The mean gas temperature in the VM refrigerator is relatively low and consequently the gas pressure is low. Since this low pressure is the result of the west-south expansion process (as will be shown) heat is absorbed from the refrigeration load and heat source.

As the crank turns to the east position, both the hot and cold cylinder volumes decrease. Part of the cold gas is forced through the cold regenerator, where it is heated to T_A before entering the ambient section. Part of the hot cylinder gas is forced through the hot regenerator where it is cooled to T_A before entering the ambient section. Heat, which is to be used later in the cycle, is thus stored in the hot regenerator. Finally, since both the hot cylinder volume and cold cylinder volume have decreased, the mean gas temperature and, consequently, the gas pressure do not change very much during this process. Nevertheless, the gas pressure does decrease somewhat, resulting in gas expansion and heat absorption from the load.

As the crank moves from east to north, the hot cylinder volume increases and the cold cylinder volume decreases. The cold gas which is forced through the cold regenerator is heated to T_A, while part of the ambient gas flows through the hot regenerator, is heated (from storage energy) to T_H, and enters the hot cylinder. The net effect of the hot cylinder volumetric increases and the cold cylinder decrease is an increase in the mean gas temperature and gas pressure. Hence, this process is one of gas compression and, in order for the temperatures to remain constant, heat is rejected at the ambient section.

As the crank turns from north to west, both the hot cylinder and cold cylinder volumes increase. Part of the ambient gas moves through the cold regenerator, releases heat to it, and enters the cold volume at T_C. On the hot side, part of the ambient gas moves through the hot regenerator, absorbs heat, and enters the hot volume at T_H. Since both the cold volume and hot volume increase, the system pressure does not greatly change. Nevertheless, there is some compression with a corresponding heat rejection at the ambient section.

The crank now turns from west to south, decreasing the hot cylinder volume while increasing the cold cylinder volume. Part of the hot cylinder gas is forced through the hot regenerator where it is cooled to T_A, while part of the ambient gas is forced through the cold regenerator where it is cooled to T_C. The mean gas temperature and, consequently, gas pressure decreases, resulting in gas expansion. Heat absorption at the cold and hot ends thus results.

The net effect of the above processes is that heat is absorbed at the cold and hot cylinders and rejected at the sump. Typically, for a real VM with a cold cylinder temperature of $75^\circ K$, a hot cylinder temperature of $1200^\circ F$, and a sump temperature of $140^\circ F$, a 1/4-watt cooling load can be attained with about 70-90 watts power input at the hot cylinder with a 5-10 watt motor required to drive the crank.

2) Advantages. The following are the projected significant advantages of a Vuilleumier refrigerator system for spacecraft sensor cooling:

  1) Flexibility

      Compared to a passive-radiator cooler the VM refrigerator system provides for flexibility with respect to sensor location within the spacecraft, and in overall spacecraft design. The reasons for these advantages are that the VM refrigerator, with the cold cylinder interfaced with the sensor, does not have to be located close to the ambient radiator because heat pipes can readily be employed to transfer waste ambient-section heat to the radiator; and the location of the ambient radiator is not as critical as the location of a passive-radiator cooler because the ambient radiator is relatively insensitive to viewing the spacecraft structure or paddles. The reason for the insensitivity of the ambient radiator is that it is a relatively high temperature, high heat load device. Furthermore, changes in the ambient temperature radiator could readily be compensated for by changing the hot cylinder power and temperature, or adjusting the RPM of the VM refrigerator.

  2) Reliability of Ambient Radiator

      In addition to being relatively insensitive to viewing other radiating surfaces, the ambient

radiator is relatively insensitive to alterations in its thermo-physical surface properties. For example, it can readily be shown that for an isothermal radiator

$$\frac{T'}{T} = \sqrt[4]{\frac{1-\xi}{1-\xi'}\left(\frac{\epsilon}{\epsilon'}\right)} \qquad [1]$$

where T is the radiator design temperature, ϵ is the design emissivity, ξ is the design point ratio of radiator energy absorbed to the energy emitted. The primed variables represent these values for a radiator dissipating the same load with altered surface properties. Now, suppose a radiator surface degraded as follows:

New Radiator	Old Radiator
emissivity = 0.85	emissivity = 0.85
absorptivity = 0.2	absorptivity = 0.35

For a passive-radiator cooler, a reasonable value for ξ would be about 0.5, and hence ξ' = 0.5 (0.35/0.2) = 0.875. If we take T=90°K, then, from equation (1) T' = 117°K. This is a serious degradation in performance.

For a VM ambient radiator the total heat rejected for a one sensor load would be about 100 watts. The radiation input from the spacecraft and environment is estimated to be about 20 watts. Therefore, ξ = 0.2, ξ'= 0.2 (0.35/0.2) = 0.35, and from equation (1) it can be found that the radiator temperature changes from 140°F (design) to 173°F. This change in ambient radiator temperature could easily be compensated for by increasing the power to the hot cylinder by about 5 watts. Thus, the sensor temperature would remain the same.

3) Controllability

The VM cooler system can be adjusted to compensate for increased cooling loads, due to higher than anticipated parasitic loads, by varying the hot cylinder power or the VM RPM. This controllability does not exist for the passive radiator. For a solid cryogen system an increased cooling load would result in a more rapid depletion of the cryogen.

4) Long-lifetime Operation

Although not demonstrated to date, the VM refrigerator has the potential for long lifetime operation. The main reason for this is that the RPM is relatively low, the bearing loads are low, and non-rubbing seals can be used on the displacers.

3) Disadvantages. The prime disadvantage of a VM cooler system is that from 70-90 watts of thermal power, and about 10 watts of electrical power are required. The thermal power could be supplied from an isotope heat source, but, if this is not practical, it must be supplied from the spacecraft electrical power via an electric heater.

Furthermore, since the VM cooler is an active refrigerator, care must be taken in its mounting and in the sensor/cooler interface design to insure that refrigerator vibrations do not interfere with sensor alignment.

4) VM State of the art.

a) Operational Models. Although a long-lived VM refrigerator has not yet been built, many shorter-lived machines have been successfully tested. For example, a Hughes Aircraft Corporation VM refrigerator was tested at GSFC with cold cylinder temperatures of 90°K, 100°K and 110°K, and refrigeration loads of 1/4 and 1/2 watt, to determine the required

power input. The results of these tests are shown below:

Motor Speed (rpm)	Refrigeration (watts)	Cold Temp. (°K)	Thermal Input Power (watts)
500	0.245	91	77
500	0.245	102	71
500	0.245	112	63
600	0.240	90	87
600	0.240	98	75
600	0.240	110	64
600	0.500	88	97
600	0.500	98	88
600	0.500	110	77

b) Development Program. An engineering model (Reference 6) of a 5-watt VM refrigerator for spacecraft application is being developed under a GSFC contract at Garrett Airesearch Corp. A preliminary design has been completed and design analyses, component tests and final design drawings are nearly complete. The purpose of this development is to improve the VM operational lifetime over that of existing units. It is scheduled for acceptance testing during October, 1971.

An extensive bearing materials test program is included in the Airesearch contract. Many different combinations of materials were tested on an ASTM test machine. The most attractive materials from this program are now undergoing wear tests in a helium atmosphere at elevated temperature to simulate the conditions under which the bearings on the high temperature displacer of the VM must operate. Other component tests are underway to verify design characteristics and life expectancy.

The design analyses and component tests indicate that a VM cryogenic refrigerator can successfully meet spacecraft life requirements by incorporating the following features: (1) The bearings must consist of very hard materials running against a very hard compacted solid lubricant which will not decompose or outgas at the hot cylinder temperatures. To date, the results (Reference 7) obtained have shown that the coefficient of friction and wear rates are lower than expected and that flame sprayed tungsten carbide on Inconel 718, with Boeing compact 6-84-1, is a promising bearing materials pair. (2) The helium working fluid should be contained by an all welded structure. (3) Displacer seals should be of the non-contact type.

After delivery, extensive performance and life tests will be performed on the 5-watt refrigerator at GSFC to further prove vacuum operation. The technology from this program could readily be used to design smaller long-lived VM coolers.

c) Math Model. A comprehensive mathematical model (analysis and computer program) of the Vuilleumier refrigerator was developed at GSFC during the past year (Reference 8).

The basic features of the analysis which distinguish it from the ideal analysis heretofore employed in the field are: (1) Equations are developed to calculate cylinder gas temperatures, thus eliminating the constant cylinder gas temperature assumption of the ideal model. (2) Hot and cold regenerator thermal inefficiencies and gas pressure drops are accounted for. (3) Thermal conduction losses are included. (4) Hot and cold displacer gas leakage losses are included with respect to both thermal inefficiencies and displacer/wall friction. (5) Equations for the calculation of steady state regenerator gas temperatures and pressures, and gas internal mass flow rates are developed.

The VM math model program (Reference 9) solves the system of partial differential equations developed in the analysis. For a given refrigerator design and fixed cylinder temperatures, the performance program calculates the cooling load and hot cylinder power requirement, instantaneous values of cylinder gas temperatures and pressures, hot and cold regenerator temperature profiles, and internal gas mass flow rates. Comparisons of the program results with available test data show good agreement.

A VM refrigerator scaling study, using the math model, is presently underway at GSFC. The goals of this investigation are to obtain performance curves for the present 5-watt refrigerator; to study the effect of the refrigerator ambient temperature on refrigerator performance, ambient heat pipe design, and ambient radiator design; and to scale the present 5 watt refrigerator down to a 1/4 - 1/2 watt cooling load design.

5) VM Cooler Applicable to EOS. Figure 7.8-14 shows a 1/4 watt (cooling load) VM refrigerator design which is applicable to the EOS spacecraft. This machine is a scaled-down version of the 5-watt unit currently being developed at Garrett Airesearch Corporation. Hence, it has all of the long lifetime features incorporated into the 5-watt design.

A design - schematic of a possible VM refrigerator sensor cooling system for the EOS spacecraft is shown in Figure 7.8-15. This system is located in the corner of a bay, as shown. The thermal power in this design is supplied to the VM refrigerator from an isotope heat source, which is in the form of a 4" diameter sphere. (The isotope would not necessarily have to be spherical.) As recommended in References 10 and 11, the isotope could be a 150 watt modified form of either
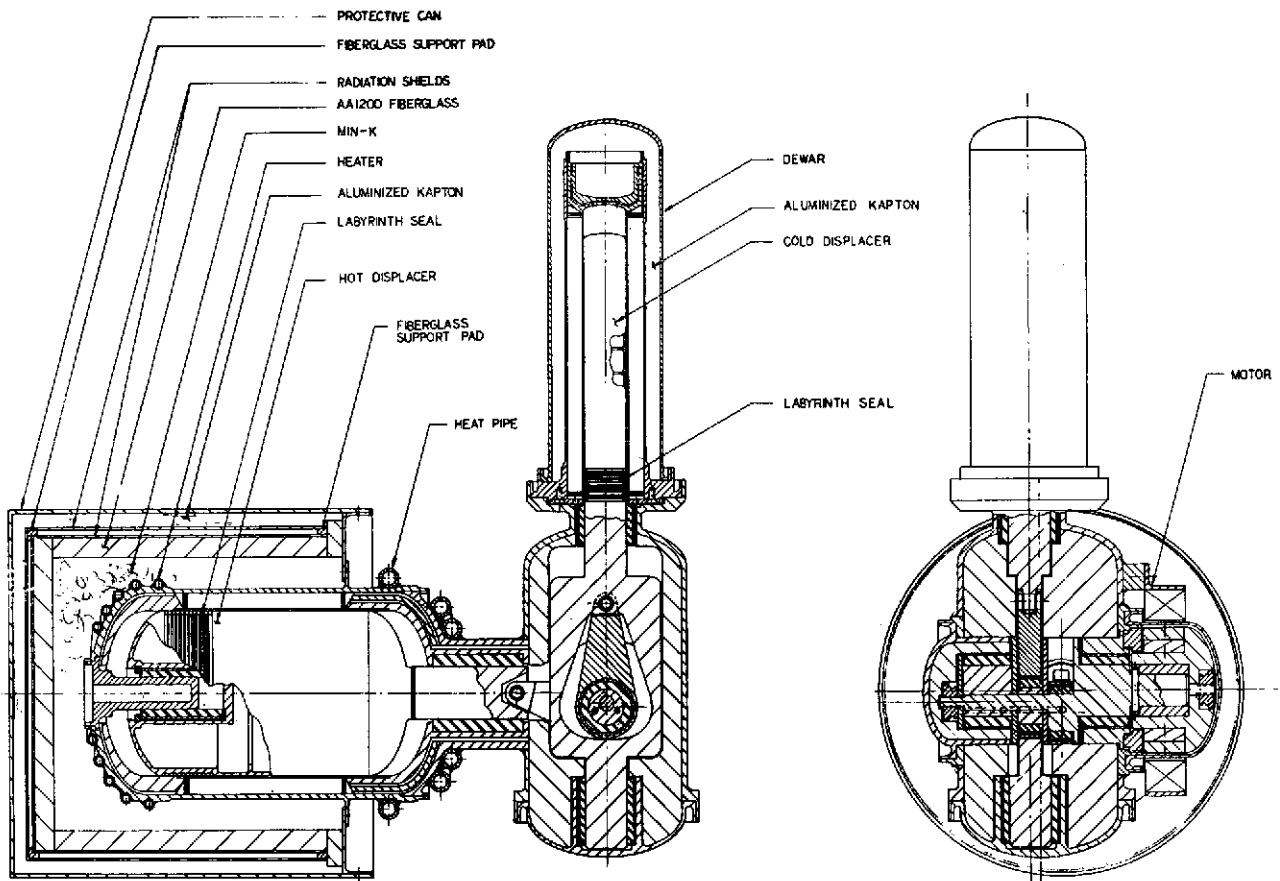

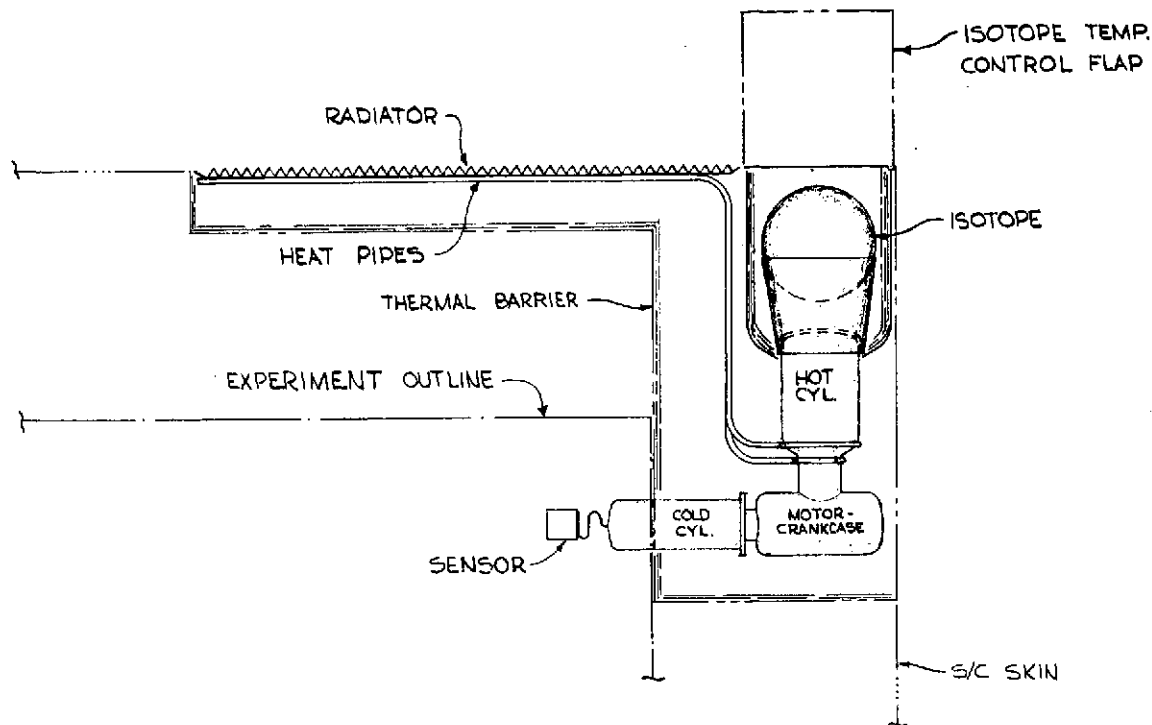Figure 7.8-14. 1/4 Watt VM Refrigerator

7-94

Figure 7.8-15.   VM Refrigeration System

SNAP - 19 (Modified IDRHS) or the isotope being developed for the Transit spacecraft. Both of
these heat sources use Pu-238 as fuel. The isotope heat is transferred via a radiation interface
to the hot cylinder; studies in Reference 10 show that this type of interface is preferable. From
70-90 thermal watts are required at the hot cylinder in order to sustain the 1/4 watt cooling load,
Two ambient temperature heat pipes transfer the wast heat from the VM crankcase (i. e. ambient
section) to the radiator. These heat pipes are 3-4 feet long and use either ammonia or water as
the working fluid. The radiator dimensions are 1.75' by 143' (2.5 ft^2). From the overall thermal
analysis of the bay (Section 7.8.2) it can be concluded that this area is available on the edge of·
the bay; that is the VM radiator does not interfere with the overall bay thermal control system for
either the EOS A and B or C and D spacecrafts. The VM refrigerator drive motor in this design
requires about 5-10 watts of electrical power which would be supplied by the spacecraft. The
interface between the cold cylinder and sensor (shown schematically in Figure 7.8-15) would be a
flexible thermal connector.

Several other orientations of the EOS VM cooling system are shown in Figures 7.8-16 A through D.
In these figures the bay, thematic mapper experiment (phantom lines), and VM cooling system are
shown to scale, for the A and B spacecraft.   Note that in Figures 7.8-16 B-D the cold cylinder /
hot cylinder phase angle is 180°, as opposed to 90° in Figures 7.8-15 and 7.8-16 A. This angle is
of little consequence to the basic VM design and hence provides for flexibility in packaging and
sensor location.

Figure 7.8-16 D shows one possible location for a VM cooler with an electric heat supply. The
electrically heated VM could be located almost anyplace in the bay provided that the ambient
section is within 3 - 4 feet of the ambient radian. Although 80 -- 100 watts of electrical power
would have to be supplied from the spacecraft, it is felt that at this point an electrically powered
VM should not be ruled out.

The weight of the VM refrigeration system employing an isotope heat source would be about 20 to
25 lbs. An electrically powered VM system would weigh about 8 lbs less than the isotope system.
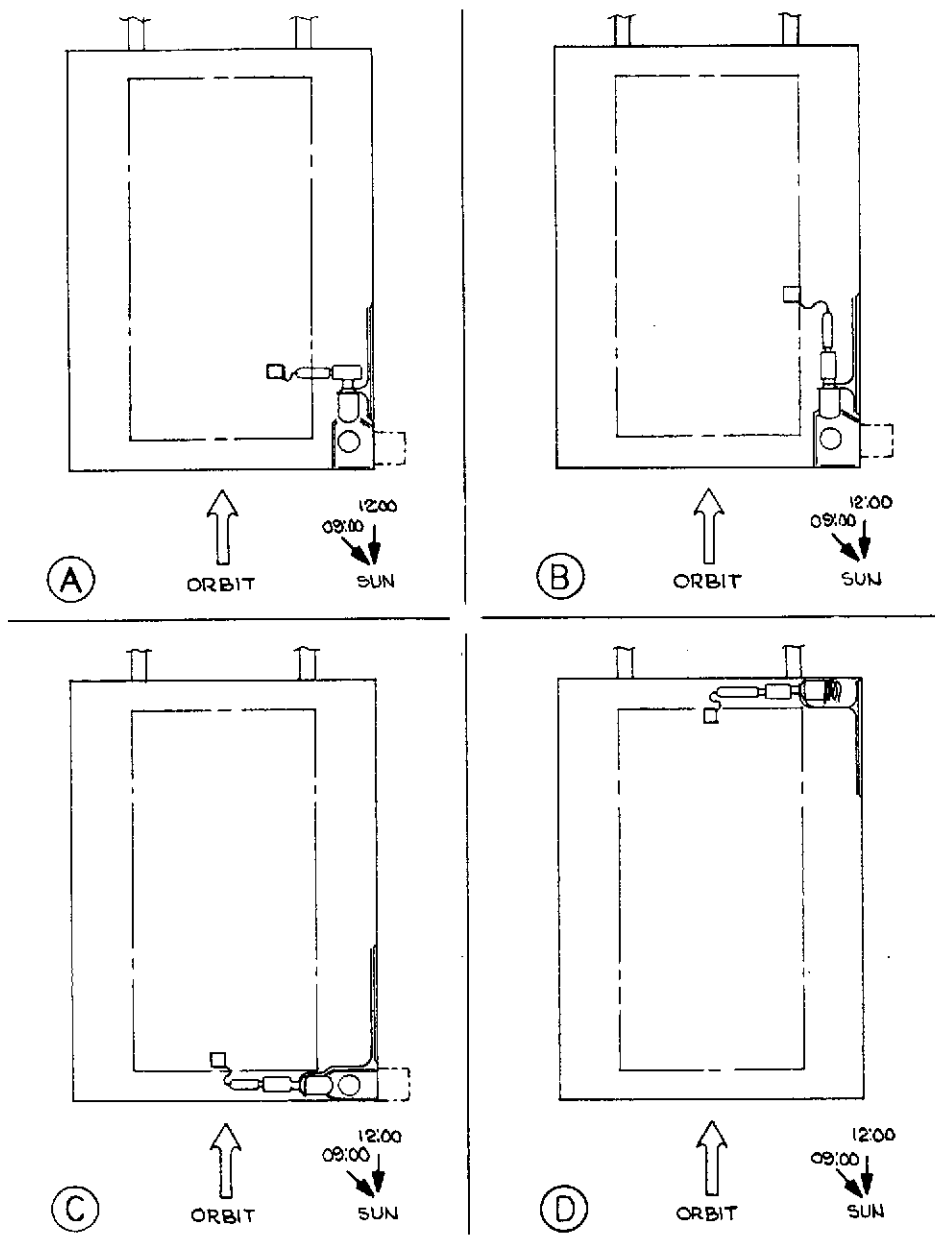
Figure 7. 8-16.   VM Refrigeration Systems in A and B Spacecraft Bay - To Scale

7.8.4.3 Conclusion. It is too early to make a firm decision as to the sensor cooling method to use for the EOS spacecraft. It is recommended that further study be done on the three systems proposed, and that the sensor/cooler interface design be studied once the experimental hardware configurations are better defined. It should be noted, however, that if an isotope heat-source VM refrigerator is to fly on EOS, the isotope specifications would have to be written by the first or second quarter of fiscal year 1972.

7.8.5 REFERENCES

1. Fairchild Hiller Corp., Unpublished Study, December, 1970.

2. Brenkenridge, R.W., "Spaceborne Refrigeration Systems," presented at Cryogenics and Infrared Detection Systems - a Technical Colloquium, Frankfurt Am Main, West Germany, April 17-18, 1969.

3. Fowle, A.A., "Cooling with Solid Cryogens - A Review," Advances in Cryogenic Engineering, Vol. 11, Plenum Press, N. Y., P. 198, 1966.

4. Caren, R.P. and Caston, R.M., "A Solid Cryogen Refrigerator for 50°K Infrared Detector Cooling," Advances in Cryogenic Engineering, Vol. 13, P. 450, 1968.

5. Amnable, R.V. and Lodder, J.F., "Design of a Dual Patch Multi-Element Radiant Cooler," ITT Aerospace / Optical Division, Electro-Optical Operations, Fort Wayne, Indiana, July 1970.

6. Yoshikawa, D.K., "75° Miniature Vuilleumier Cryogenic Engine", Final Report for Task I, Contract NAS5-21096, The Garrett Corporation, Torrance, California, October, 1970.

7. Garrett Corporation, "75° Miniature Vuilleumier Cryogenic Engine", Fifteenth Monthly Technical Letter Report, Contract NAS5-21096, February 10, 1971.

8. Sherman, A., "Mathematical Model of a Vuilleumier Refrigerator", GSFC X-763-71-125, Goddard Space Flight Center, Greenbelt, Maryland, 1971.

9. Simmons, E., "Vuilleumier Engine Modification 1 Support", Technical Direction 734-102, Computer and Software, Inc., Goddard Space Flight Center, Greenbelt, Maryland, April, 1970.

10. RCA Final Report, "ICICLE Feasibility Study", Contract NASA 5-21039, RCA Corporation, Cambridge, N. Y., February, 1970.

11. Hittman Associates, Inc., "Preliminary Investigation - ICICLE System Nuclear Heat Source", HIT-416, Hittman Associates, Inc., Columbia, Md., Sept. 1969.

7.9 PROPULSION SYSTEMS FOR ORBIT ADJUST

7.9.1 INTRODUCTION

The orbit adjust system is necessary to (1) obtain initial orbit acquisition and (2) provide subsequent orbit adjustments throughout the useful lifetime of the spacecraft. The orbit adjust system proposed for both the EOS A and B and the EOS C and D spacecraft is described in this section.

7.9.2 SYSTEM DESCRIPTION

To obtain an initial system design, a conservative velocity increment (ΔV) of 200 feet per second was selected in order that all possible spacecraft maneuvers would be accounted for. Table 7.9-1 lists the total impulse required for each spacecraft based on this ΔV selection. The system designs were based on a nominal steady state thrust of 5 pounds force for each spacecraft and the tabulated total impulse corresponds to the particular spacecraft.

Current auxiliary propulsion state of the art for orbit adjust, in many applications, utilizes systems based on hydrazine propellant with a Shell 405 catalyst type thruster. Both the EOS A and B and the EOS C and D spacecraft will utilize hydrazine orbit adjust systems. However, since these spacecrafts are not of the spinning variety, all tankage systems will contain diaphragms to assure a positive separation between the propellant and pressurant gas as well as to maintain the propellant in the appropriate location within the tank.

Hydrazine systems have a rated average specific impulse (a performance factor of propellants) of 200 seconds upon which the system design is based. Two systems were designed and analyzed to show that either one can be used for the EOS A and B and EOS C and D spacecraft. The basic variation between the two systems is the number of propellant tanks used. One system uses two 16.5 in. diameter tanks and the other a single 22.5 inch diameter tank. Table 7.9-1 tabulates the results of the system designs and shows only a nominal weight difference between a one and two tank system.

The basic advantage of a two tank system is that should a leak occur in one tank it can be isolated from the other tank by closing a valve. Therefore, to take advantage of this redundancy a two tank system has been proposed for both the EOS A and B and EOS C and D spacecraft and is discussed in Section 7.2. A schematic of the single tank system is shown in Figure 7.9-1 and a schematic of the two tank system is shown in Figure 7.9-2. The single tank system is included here as an optional choice for either spacecraft. For either system the tanks are qualified off the shelf hardware and should present no problem in special fabrication requirements. An itemization of the component weights for each system is presented in Table 7.9-2.

The freezing point of neat hydrazine is 36° F. However, since this system will be placed within the confines of the central body, there will be no danger of the propellant freezing. The thermal design of the central body, section 7.8, provides for the temperature to be no lower than 59° F thereby providing an adequate margin of safety above the propellant freezing point.

Operation of these proposed tankage systems is based upon filling one side of the diaphragmed tanks with the hydrazine propellant. The other side of the diaphragms is pressurized with gaseous nitrogen to the appropriate pressure. When the thrusters are operated the pressurized gas forces the hydrazine through the catalyst beds and out the nozzles. One effect of this procedure is that the gas pressure decreases as the propellant flows out the tank resulting in a corresponding decrease in thrust. This relationship is shown in Figure 7.9-3. This effect can be easily corrected for because the required correction impulse bit can be obtained by operating the thrusters for increasing lengths of time. There will be adequate telemetered information from the thruster systems to determine tank pressures at any given time.
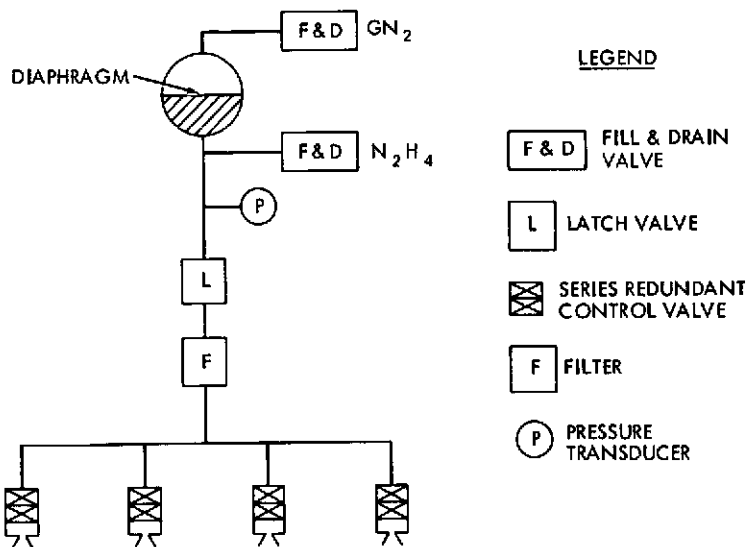
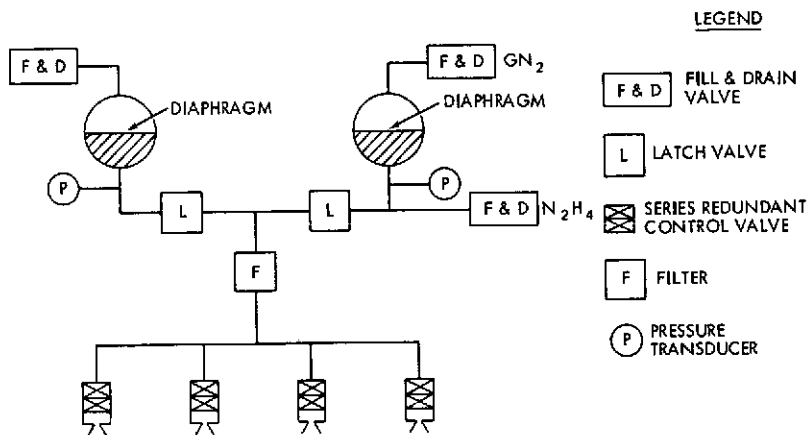PRECEDING PAGE BLANK NOT FILMED

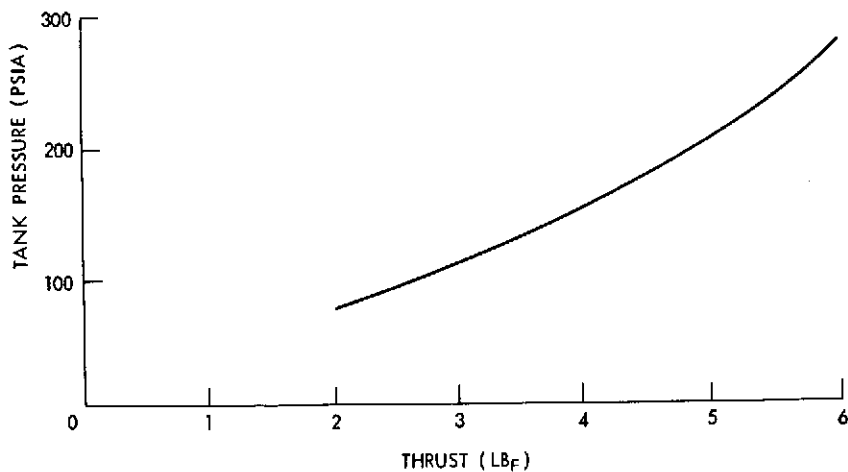Figure 7.9-1.   One Tank System

Figure 7.9-2.   Two Tank System

Figure 7.9-3.   Tank Pressure vs. Thrust

Table 7.9-1

Orbit Adjust System Design Parameters

Parameter	EOS A&B	EOS C&D
Spacecraft weight (lb)	2,500	3,800
Total Impulse (lb-sec)	15,500	23,800
Number of 16.5 inch dia. tanks	2 (two tank system)	2 (two tank system)
Number of 22.25 inch dia. tanks	1 (one tank system)	1 (one tank system)
Number of 5 lb force thrusters	4	4
Blow down thrust decay (lb force)		
a) 16.5 inch dia. tank	6.0 to 4.0	6.0 to 2.5
b) 22.25 inch dia. tank	6.0 to 4.4	6.0 to 3.2
Thruster power (watts/thruster valve)	18	18
Number of valves		
a) one tank system	5	5
b) two tank system	6	6
Propellant weight (lbs)	77.5	119.0
Total system weight (lbs)		
a) one tank system	105.5	146.1
b) two tank system	119.4	159.9
Minimum impulse bit (lb-sec)	.15	.15
Latch valve power (watts/100 millisec)	80	80

7.9.3 SUMMARY

The basic system proposed for all the EOS spacecraft is based on hydrazine propellant utilizing a Shell 405 catalyst type thruster. It utilizes two 16.5 inch diameter diaphragmed tanks. Each tank weighs 14.0 pounds and together with associated hardware and electronical components has a dry weight of 39.7 pounds. The EOS A and B spacecraft requires 77.5 pounds of propellant and 2.2 pounds of gas for a total weight of 119.4 pounds and the EOS C and D spacecraft requires 119.0 pounds of propellant and 1.2 pounds of gas for a total weight 159.9 pounds. A schematic of the two tank system is shown in Figure 7.9-2.

Table 7.9-2

EOS Orbit Adjust System Component Weights (lb)

Spacecraft	EOS A&B		EOS C&D	
Tank System	#1	#2	#1	#2
Tanks	15.0	28.0	15.0	28.0
Thruster and valves (1.2 lb each)	4.8	4.8	4.8	4.8
Isolation Valves	1.2	1.8	1.2	1.8
Filters	.4	.4	.4	.4
Fill Drain Valves	.4	.6	.4	.6
Transducers	.3	.6	.3	.6
Wiring & Connectors	1.0	1.0	1.0	1.0
Tubing & Miscellaneous	2.0	2.5	2.0	2.5
Dry Weight	25.1	39.7	25.1	39.7
Hydrazine (N_2H_4)	77.5	77.5	119.0	119.0
GN_2	2.9	2.2	2.0	1.2
Total Weight	105.5	119.4	146.1	159.9

Tank System
#1—One 22.25 inch diameter tank
#2—Two 16.50 inch diameter tanks

SECTION 8

LAUNCH VEHICLES

SECTION 8

LAUNCH VEHICLES

ILLUSTRATIONS

TABLES

SECTION 8

LAUNCH VEHICLES

8.1 INTRODUCTION

Of all the launch vehicles that could be considered for use in the EOS programs, only the Delta could be supported by the facilities available at the Western Test Range (WTR). Indeed, the Delta 2910 appears destined to become the standard vehicle for launches from WTR after 1975. Since launch from WTR is essential to the sun-synchronous orbits required of the EOS missions, the Delta 2910 is proposed for launch of both EOS A and B.

One conclusion resulting from the orbit studies is that an orbital altitude of about 530 nm for EOS A and B is the best choice for all factors considered to date. The orbital altitudes selected for launch vehicle considerations were 400, 600, and 1000 nm for which the sun-synchronous requirement dictates orbit plane inclinations of about 98, 100, and 104 degrees, respectively.

Table 8.1-1 includes the on-orbit weight capabilities of the Delta 2910 tailored to the EOS A and B requirements. At 530 nm altitude the inclination angle would be about 99 degrees, and the on-orbit weight capability is about 2600 pounds.

Table 8.1-1

Sun-Synchronous Orbit Launch Vehicle Capability

Launch Vehicle	Payload Weight (lb)		
	400 nm orbit	600 nm orbit	1000 nm orbit
Delta 900	2300	2000	1500
Delta 2910	2700	2500	2000
Thor Agena A-4	3100	2900	2600
Atlas/TE 364-4	3960	3150	2040
Titan III BS/Burner II [1]	4350	3700	2550
Titan III C/Transtage [2]	14000	7000	--
Shuttle	18000	18000	18000

[1] TE 364-2 used in Burner II for 400 and 600 nm orbits. TE 354-4 used for 1000 nm orbit.
[2] Direct ascent.

Since the payload selections for EOS C and D as projected by this study indicate a potential orbit-weight requirement of about 3800 pounds, Table 8-1 also includes a tabulation for other potential launch vehicles. The Delta capability can be expected to continue to grow in the future as it has in the past. However, should the EOS C and D requirements exceed the growth of the Delta, Table 8.1-1 shows the other launch vehicles with adequate capability.

8.2 DELTA LAUNCH VEHICLE

8.2.1 INTRODUCTION

The Delta 2910 launch vehicle (Figure 8.2-1) has an overall length of approximately 115.6 feet and a maximum body diameter of 8 feet. A brief description of the vehicle characteristics follows.
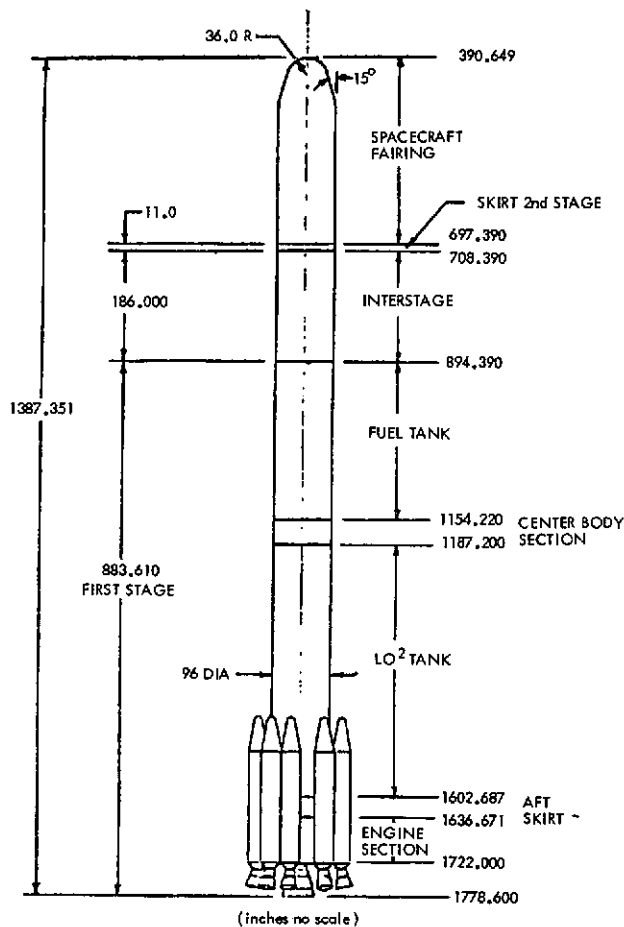

Figure 8.2-1. Delta Vehicle

8.2.2 FIRST STAGE

The first stage Delta is a McDonnell Douglas Astronautics Company (MDAC) modified Thor Booster incorporating strap-on thiokol solid fuel rocket motors. The booster is powered by a Rocketdyne H-1 engine using liquid oxygen and liquid hydrocarbon propellants. The main engine is gimbal mounted to provide pitch and yaw control from lift-off to Main Engine Cutoff (MECO). Two liquid-propellant vernier engines provide roll control throughout first stage operations, and pitch and yaw control from MECO to first stage separation.

8-8

8.2.3 SECOND STAGE

The second stage is powered by an Aerojet General Corporation AJ10-118F liquid fuel, pressure-fed engine employing aerozine-50 and N_2O_4 propellants. The second stage main engine is also gimbal-mounted to provide pitch and yaw control through second stage burn. A nitrogen gas system using eight fixed nozzles provides roll control during powered and coast flight, as well as pitch and yaw control after Second Stage Cutoff (SECO). Propellant settling (ULLAGE) before second stage restart is achieved by thrust from two nitrogen gas jets. Two fixed nozzles fed by the propellant tank helium pressurization system provide retro thrust after spacecraft separation.

8.2.4 ATTACH FITTING

The EOS Spacecraft will be attached to the Delta vehicle by means of a Delta attach fitting that incorporates the sequencing and separation system shown in Figure 8.2-2.
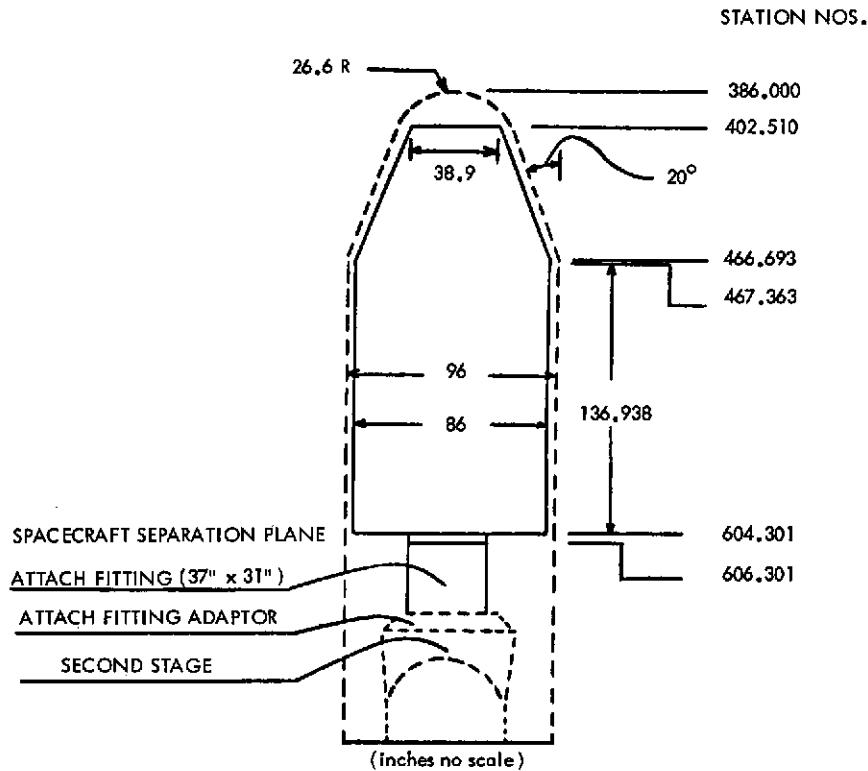

Figure 8.2-2. Payload Envelope

8.2.5 SPACECRAFT FAIRING

The Delta 8 foot fairing will protect the spacecraft from aerodynamic heating during the boost flight. It is jettisoned as soon as the vehicle leaves the sensible atmosphere shortly after second stage ignition.

8.2.6 GUIDANCE AND CONTROL

The Delta vehicle for the EOS launch will utilize the Delta Inertial Guidance System (DIGS). The DIGS system, consisting of an inertial sensor package and digital guidance computer, controls the vehicle and sequence of operations from lift-off to spacecraft separation. The sensor package provides vehicle attitude and acceleration information to the guidance computer. The guidance

computer generates vehicle steering commands to each stage to correct trajectory deviations by comparing computed position and velocity against prestored values.

In addition, the guidance computations perform the functions of timing and staging as well as issuing preprogrammed command attitude rates during the open loop and coast guidance phases. For a second stage restart mission, the second burn is also performed under the control of the inertial guidance system.

8.3 SHUTTLE

8.3.1 INTRODUCTION

The Space Shuttle System envisions an air-breathing boost stage, and an orbiter stage with a cargo bay capable of accommodating payloads up to 15 ft in diameter and 60 ft in length. The all-azimuth launch capability of the Shuttle system makes polar and retrograde orbits accessible. However, sun-synchronous circular orbits are not accessible above 270 nm with useful payload using the orbiter air-breathing engines. For the EOS mission, the shuttle without orbiter air-breathing engines is indicated, and for orbit altitudes above 340 nm, the Shuttle Upper Stage Mode may be required. The Shuttle payload data of Table 8.1-1 are based on this mode.

In this mode of operation, the shuttle orbiter is ejected into a 50 x 100 nm elliptical orbit with the proper inclination. The orbiter would then transfer to a parking orbit at between 100 and 270 nm; and, finally the expendable Shuttle Upper Stage (Tandem Burner II) would deliver the EOS to its final orbit. All maneuvers would be co-planar.

8.3.2 SHUTTLE LAUNCH AND OPERATIONS

The new capabilities represented by the Space Shuttle System are expected to be made available in two stages. The earlier stage (currently programmed for the late 70's) will require an expendable shuttle upper stage to reach the EOS destination. The major payoffs of retrieval or on-orbit refurbishment will have to await the manned space tug or teleoperator, or a plan to provide extra propellant tanks in the cargo bay for particular missions.

In the initial stage, shuttle operations bear many similarities to launch operations with an expendable booster (see Figures 8.3-1 and 8.3-2). One contribution of the Shuttle will be the opportunity for verification of spacecraft operational status after launch while the orbiter stage is in its parking orbit prior to commitment to final insertion by the expendable Shuttle Upper Stage (Figure 8.3-3). For this checkout, the Shuttle telemetry will be capable of transmitting the EOS housekeeping telemetry to earth (probably via a Data Relay Satellite Link) so that the EOS Project Manager, supported by the spacecraft development team, can make the final launch decision.

In later stages of development of the Shuttle System, where the Shuttle Upper Stage is replaced by a Space Tug, similar considerations would apply. A final check of spacecraft performance could be made after sensory bay and solar array deployment, but prior to separation from the Tug. The EOS configuration selected in this study is fully compatible with this mode of operation, and with retrieval by the Tug (Figure 8.3-4). Space is reserved for a docking ring on the base of the central body, the sensor bay deployment is reversible, and solar arrays can either be retracted, or cut loose.

The EOS configuration is also compatible with a space operating system in which on-orbit refurbishment is accomplished through replacement of major elements by means of a teleoperator (Figure 8.3-5). The configuration is also compatible with shuttle retrieval, Figure 8.3-6). The sensor mounting bays of EOS are nearly independent systems through most of their development cycle. The mechanical, electrical, and thermal interfaces are simple and are adaptable to teleoperator manipulation. Detailed in-house GSFC analyses of these interfaces will be available for inclusion in the System Design Phase proposal request.
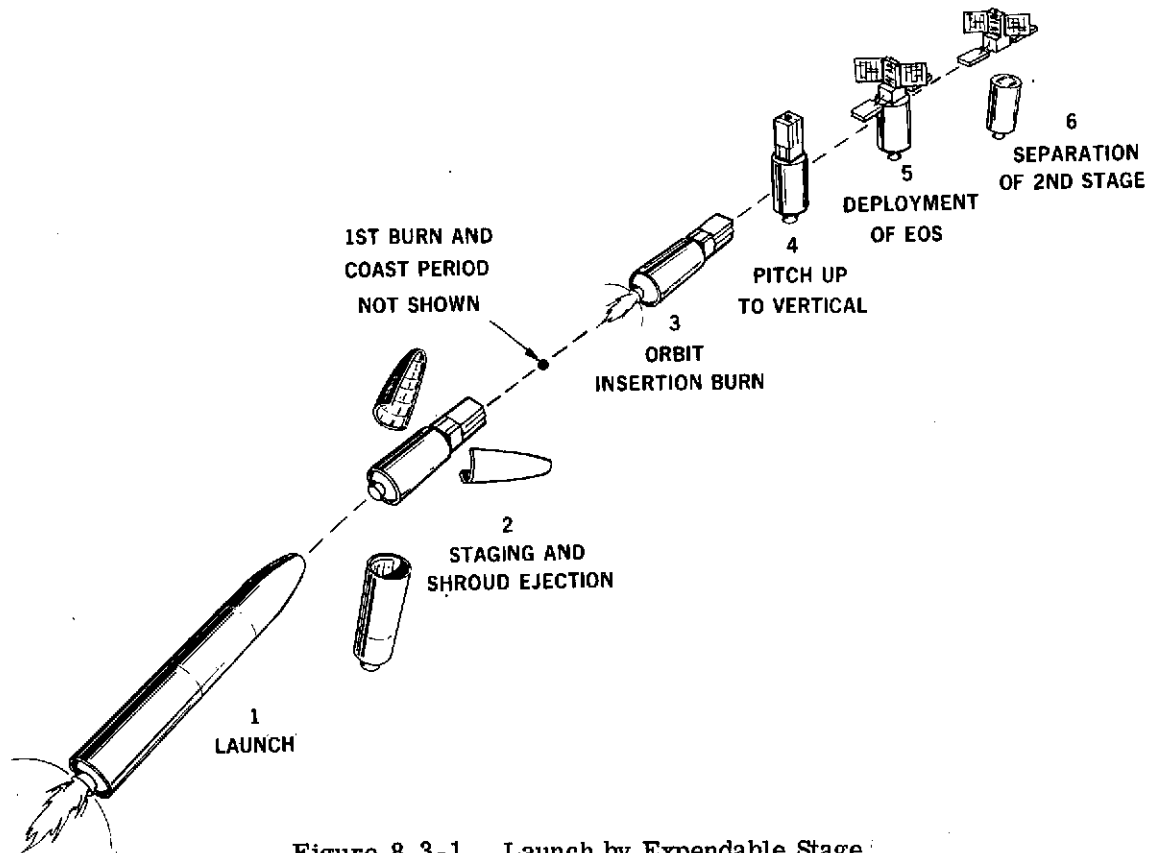
Figure 8.3-1. Launch by Expendable Stage

8.4 ORBIT INJECTION ERRORS

For orbits where precise control of sensor swathing patterns is required, there is a close relationship between the characteristics of the launch vehicle guidance system and the orbit adjust system required to trim out any orbit errors. For the Delta Inertial Guidance System (DIGS), the precision with which the desired orbital altitude, inclination, and eccentricity can be obtained is specified by the Delta Project to be the 99 percent probability levels given in Table 8.4-1.

The impulse required to correct for these errors is given in Section 7.9; the orbit adjust system to provide this impulse, and to provide for drag make-up, is also discussed in Section 7.9.

Table 8.4-1

Delta Injection Errors

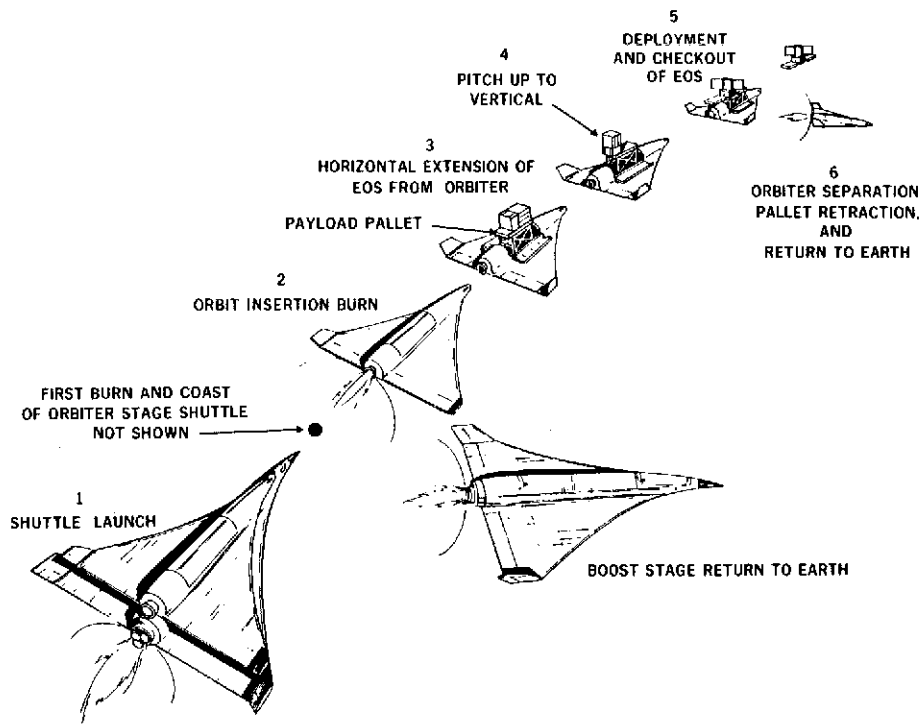| Parameter	99 Percent Probable Deviation
Semi major axis Inclination Eccentricity	± 15 nm (± 28 km) ± 0.065 deg. 0 to 0.002

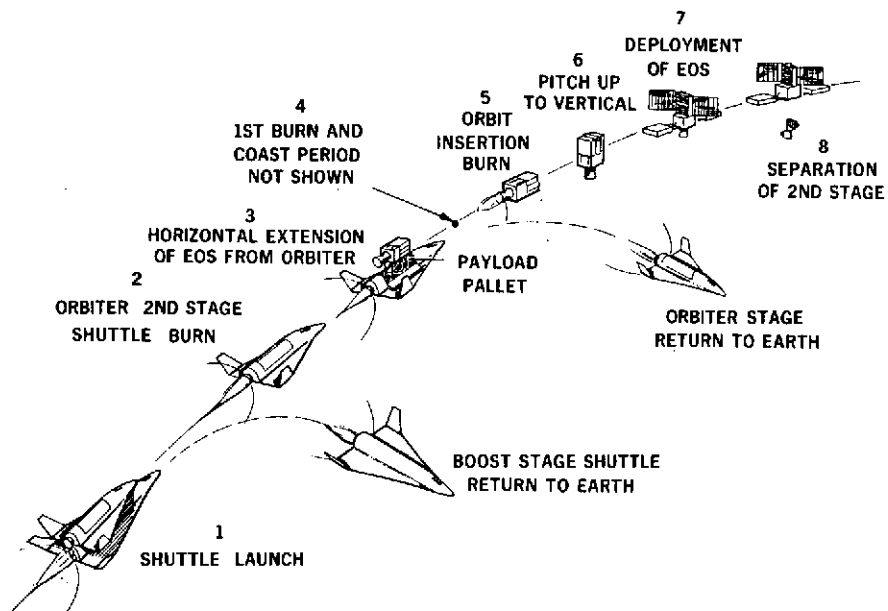Figure 8.3-2.   Shuttle Launch, Direct Insertion
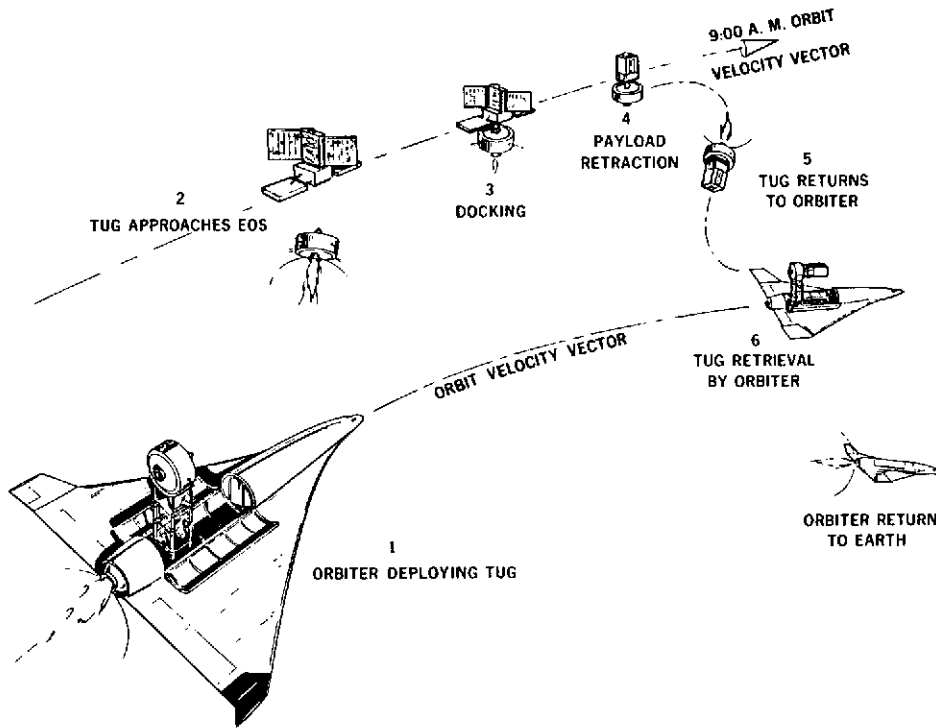

Figure 8.3-3.   Shuttle Launch, Expendable Upper Stage

8-12

Figure 8.3-4. Retrieval by Tug
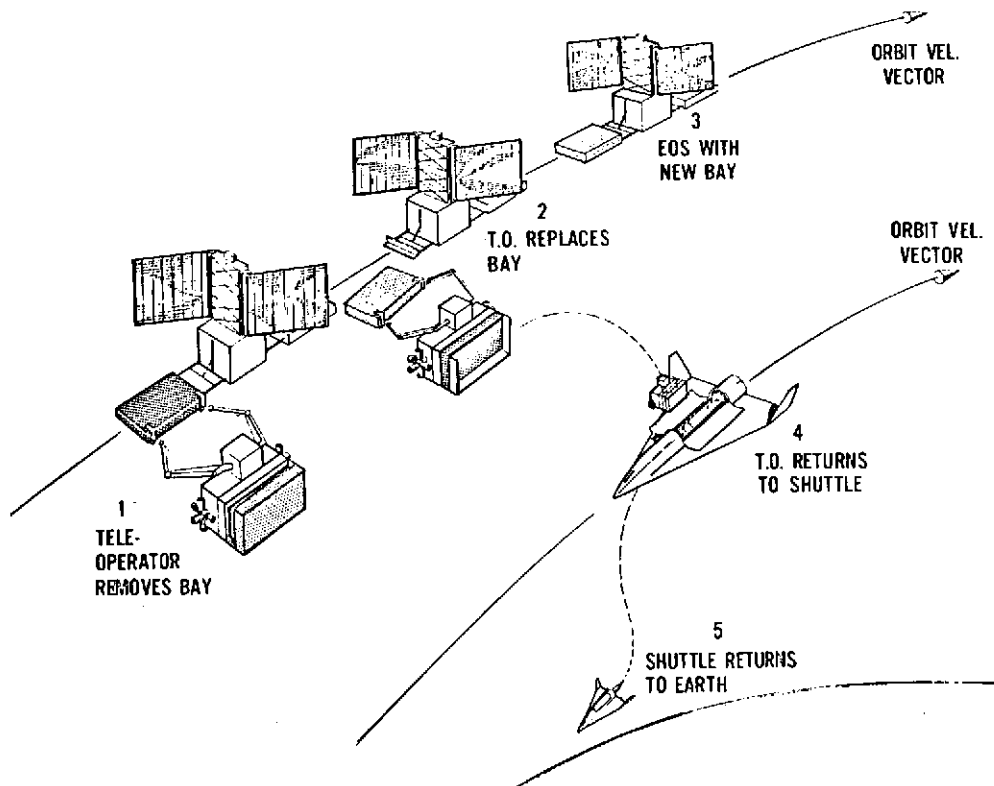
Figure 8.3-5. Teleoperator

5
EOS IS TURNED
HORIZONTAL
AND STOWED

4
PAYLOAD
RETRACTION

6
ORBITER
RETURNS
TO EARTH

3
DOCKING

2
ORBITER EXTENDS PALLET

1
ORBITER APPROACHES
DEPLOYED EOS
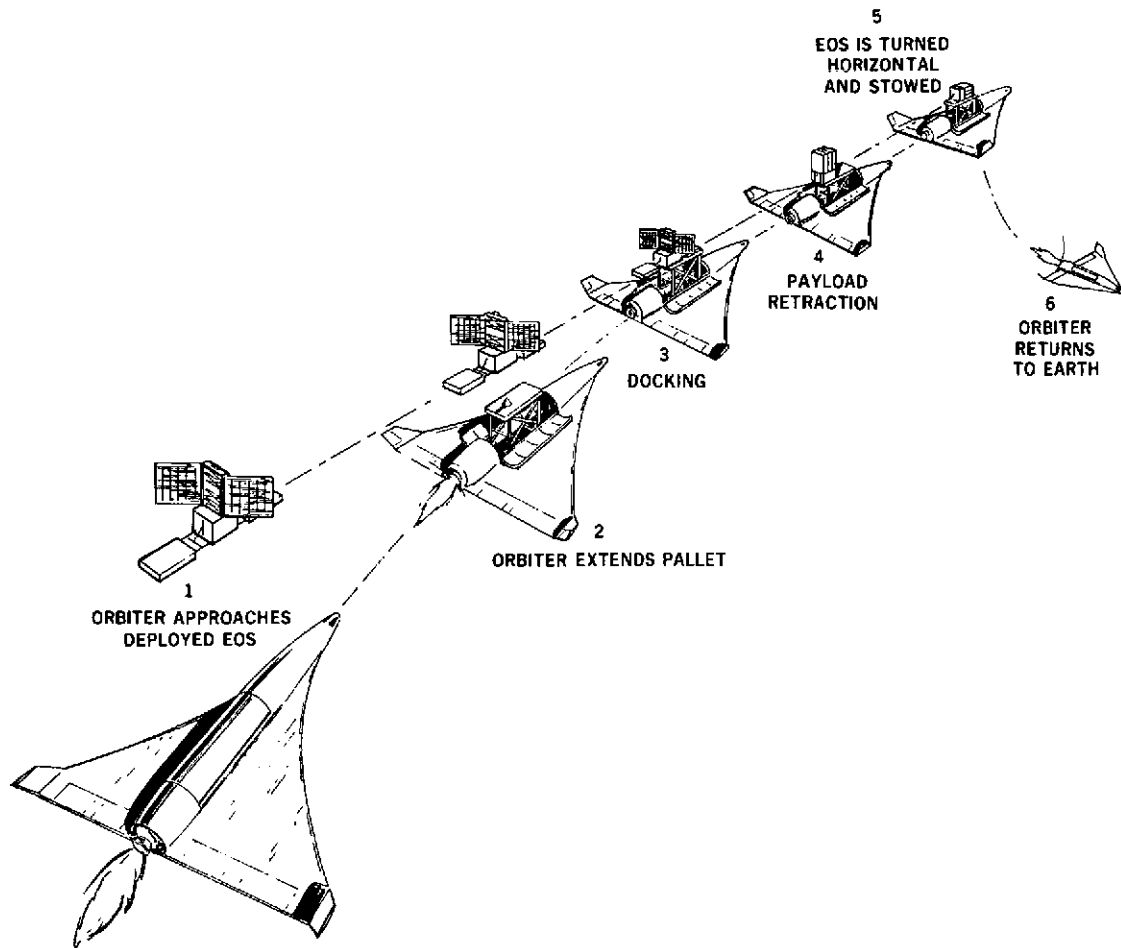
Figure 8.3-6.   Retrieval by Shuttle

SECTION 9

TRACKING AND DATA ACQUISITION

ILLUSTRATIONS

9.1 INTRODUCTION

The objective of this section is to present the ground tracking and data acquisition systems. Rationale for selection of various link parameters are discussed with emphasis on using existing ground support systems. Consistent with the spacecraft data handling system (described in 7.4) equipments may be separated into six separate links.

        1. S-Band data link

        2. VHF Telementry

        3. Command

        4. Ranging

        5. K-Band data link

        6. Local Readout Ground Stations (LRGS) special
           data link

To take advantage of existing and planned ground equipments, links 1 through 4 above will be made compatible with the existing GSFC stations. Links 5 and 6 will require new antenna tracking and data acquisition systems. K-Band and LRGS systems are proposed and the rationale for selecting the system parameters are included in this section.

9.2 S-BAND DATA LINK

9.2.1 RF BANDWIDTH AND FREQUENCY

The first system parameters to be determined are the RF bandwidths and the RF carrier frequencies. Selection of the bandwidth required by the 30 mb/s sec digital transmission system is determined by several factors; RF band-widths available in existing receiving equipments, bandwidth allocations practices and availability of an efficient digital modulation technique. A study of existing documentation (Ref. 1, 2, and 3) on digital communications indicates a quadriphase modulation system is an appropriate choice. This technique offers excellent energy efficiency and requires half the bandwidth of ordinary PSK. The quadriphase system will result in a link RF bandwidth of 30 MHZ which is the maximum available RF bandwidth (projected to 1975) in the STADAN and the Manned Space Flight Network (MSFN). The RF carrier frequency proposed for the EOS mission is in the S-band (2200-2300 MHz). This selection is justified by the fact that both STADAN and MSFN will be instrumented (antenna feeds, parametric amplifiers, down converters and receivers) to support a carrier in this band with an RF bandwidth of 30MHz. It should be noted here that an additional frequency in the S-band (2500-2690 MHz) for Earth Scientific Satellite Services will be requested by the United States at the World Administration Radio Conference for Space Telecommunications to be held at Geneva in 1971. If this band were assigned to EOS, the MSFN would require extensive modifications to its antenna systems (STADAN antennas are already being modified). Both MSFN and STADAN stations would require additional parametric amplifier/converter systems to support the 2550-2690 MHz band.

9.2.2 STADAN COVERAGE AND EQUIPMENT

The Space Tracking and Data Acquisition Network (STADAN) is presently undergoing an extensive antenna and receiver modification program. This program, scheduled for completion in 1973, will instrument the antennas listed below with a broadband feed system covering the frequency bands of 1690-1710 MHz, 2200-2300 MHz and 2550-2690 MHz. In addition all sites will be equipped with the wideband (30 MHz 3 db bandwidth) Multifunction Receiver System (MFR). Figure 9.2-1 is a block diagram of a typical STADAN site and the site and the equipment required to support the EOS 30 mb/sec S-band link.
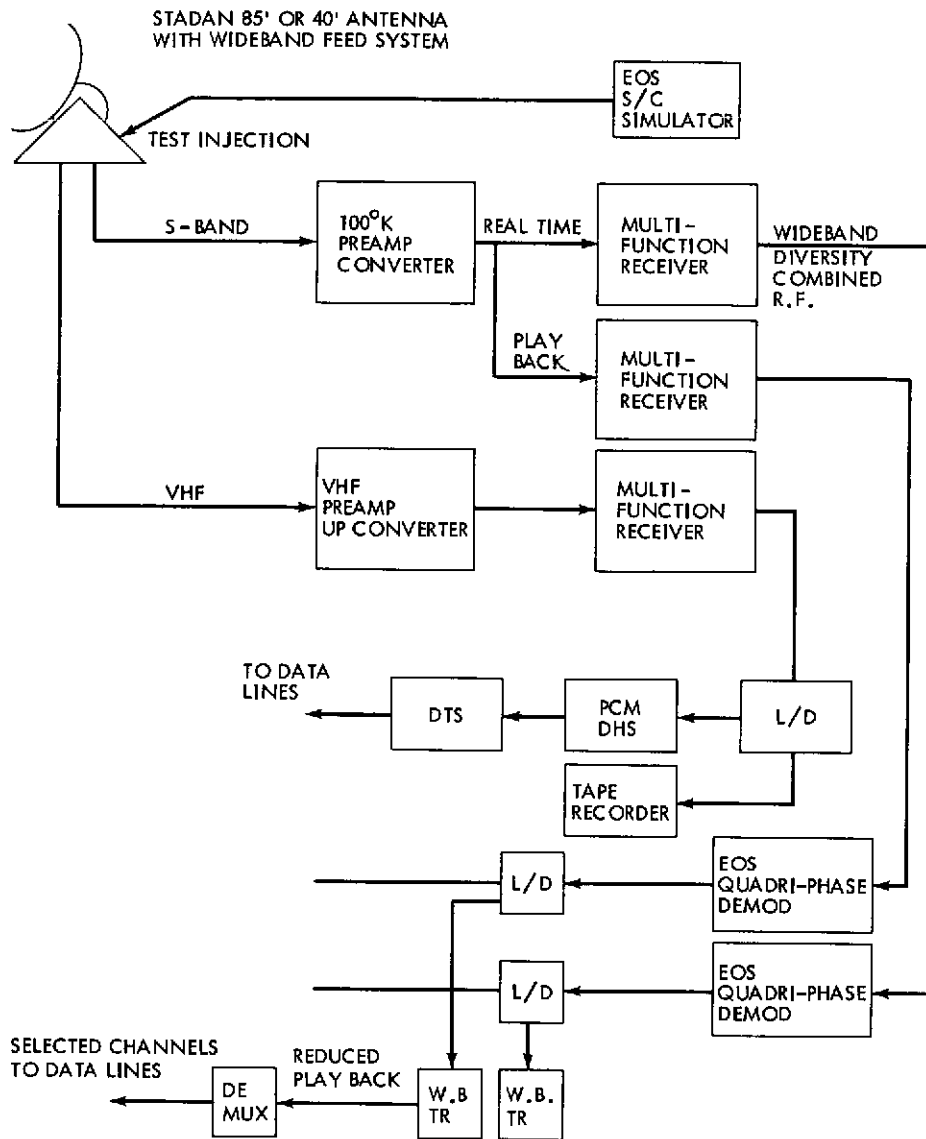
Figure 9.2-1. Configuration for a Typical STADAN Station

Site Location	Antenna Size (ft)
Fairbanks, Alaska	84
Fairbanks, Alaska	40
Orroral, Australia	85
Johannesburg, South Africa	40
Quito, Ecudaor	40
Santigo, Chile	40

Site Location	Antenna Size (ft)
Tananarive, Madagascar	40
Rosman, N. C.	85
Rosman, N. C.	85
NTTG, GSFC	40

Figures 9.2-2 and 9.2-3 are the station profiles for 740 km and 1100 km orbits including local terrain and mechanical restrictions on the antenna. Actual S-band coverage is somewhat less than the areas indicated due to a finite acquisition time for both the antenna and the data.
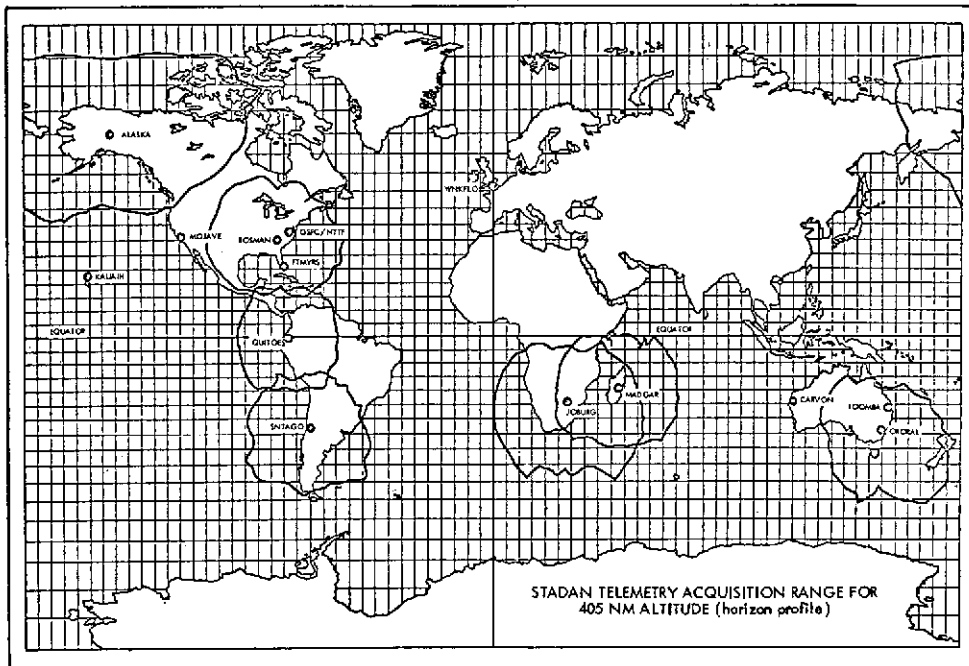
Figure 9.2-2. STADAN Station Horizon Profiles for 400nm (740 Km) Orbit

-9.2.3 MSFN COVERAGE AND EQUIPMENT

The MSFN Manned Space Flight Network is also engaged in a modification program. This program, scheduled for completion in 1971, will instrument the antennas listed below with the RF equipment required to support the EOS 30 mb/sec S-Band link. Figure 9.2-4 is the configuration for a typical MSFN station.

Site Location	Antenna Size (ft)
Goldstone, Calif.	85
Canberra, Australia	85
Madrid, Spain	85
Guam	30

9-9

Site Location	Antenna Size (ft)
Carnarvon, Australia	30
Bermuda	30
Hawaii	30
Merritt Island, Florida	30
Grand Canary	30
Ascension Island	30
Corpus Christi, Texas	30

STADAN TELEMETRY ACQUISITION RANGE FOR
600 NAUTICAL MILES (horizon profile)
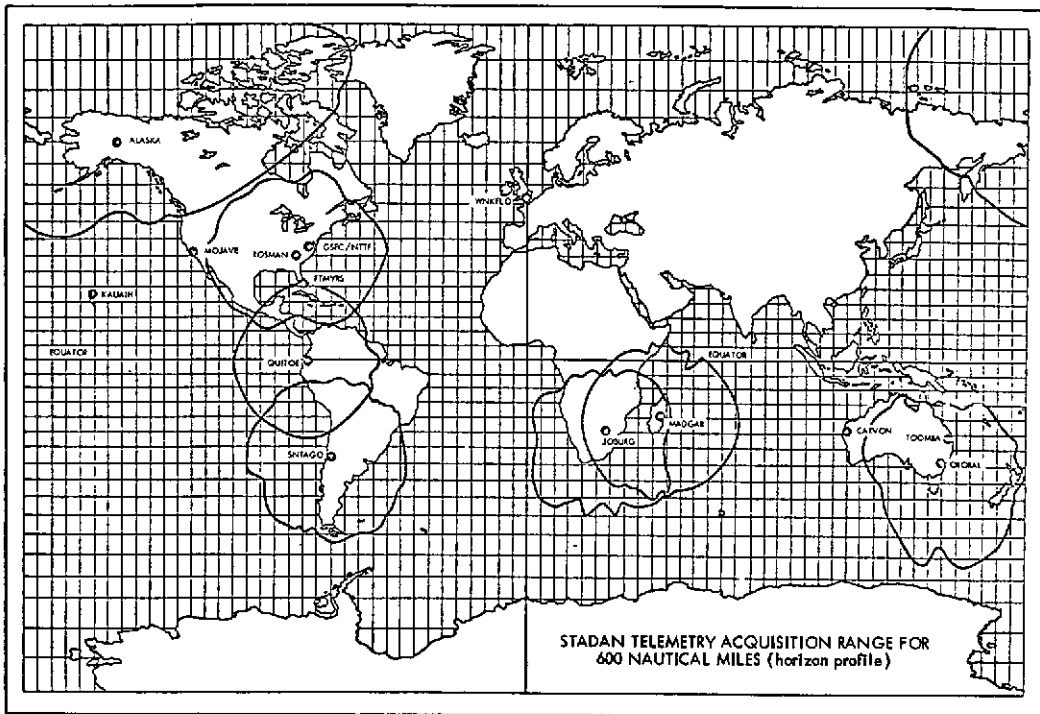
Figure 9.2-3.   STADAN Station Horizon Profiles for 600nm (1100 Km) Orbit

Figures 9.2-5 and 9.2-6 are station profiles for the MSFN stations.

9.2.4 S-BAND LINK

Table 9.2-1 is a S-Band link calculation which shows the spacecraft power required (see section 7.5.2.2) for existing ground station parameters. It should be noted that the calculations are made for a worst case situation since the maximum slant range coincides with the highest antenna temperature and greatest propagation loss. The results indicate that a 10 watt spacecraft transmitter is adequate for a 30mb/sec data link with a maximum BER of 10^{-5}.

9.2.5 EOS UNIQUE EQUIPMENT

The major advantage of selecting the S-band RF link and the 30 Mhz RF bandwidth is the availability of equipment at both STADAN and MSFN sites. However, several items of EOS unique ground

Table 9.2-1

S-Band Power Budget

Parameter	Worst Case	Best Case
Required signal-to-noise ratio for BER of 10^{-5} (db)	+10.0	+10.0
Receiver system noise temp. (Kelvin)	170.0	155.0
Receiver noise density (dbm/Hz)	-176.2	-176.6
Receiver noise power in a 30 MHz bandwidth (dbm)	-101.5	-101.9
System loss margin (db)	-3.0	-3.0
Signal level required (dbm)	-88.5	-88.9
Path loss (db)	-169.6	-160.8
Spacecraft antenna gain (db)	+4.0	+4.0
Ground antenna gain 30'aperature (db)	+44.0	+44.0
Required spacecraft transmitter power with no margin (dbm)	+33.1	--

Signal margin will change as indicated below when other GSFC antennas are used.

30' antenna with cryogenic parametric amplifier	+2.5 db
40' antenna	+1.3 db
85' antenna	+7.3 db
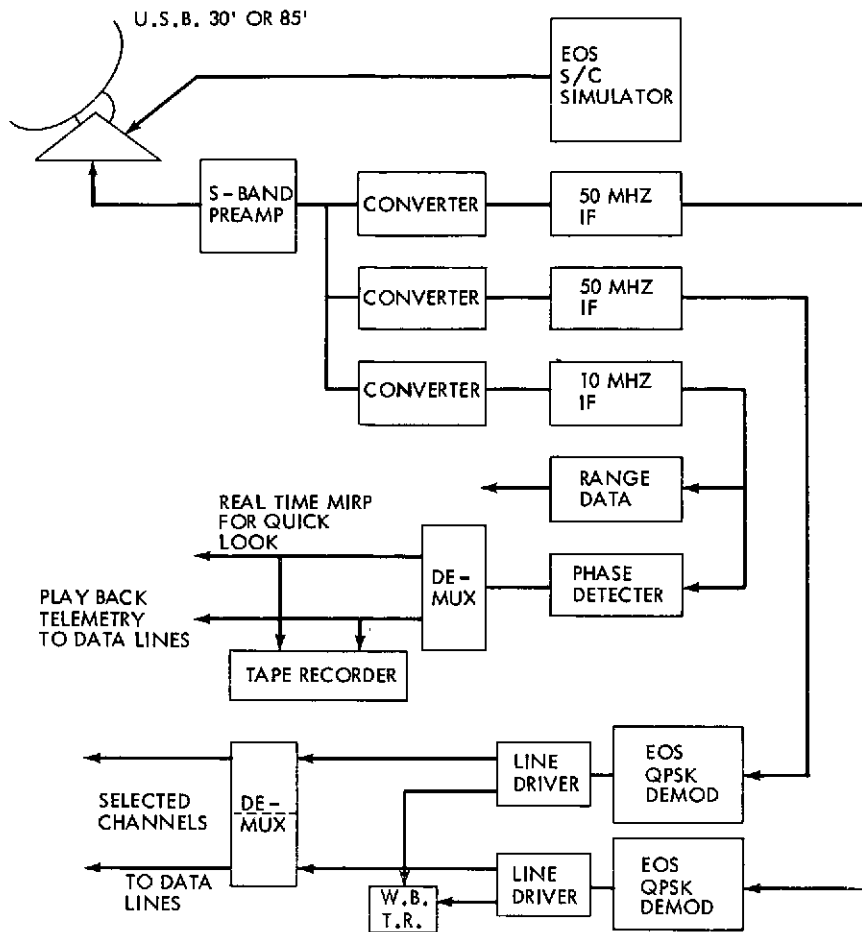
Figure 9.2-4. Configuration for a Typical MSFN Station

'equipment must be procured for the sites selected to support EOS. Listed below is the equipment required and the estimated unit costs assuming no development costs.

Equipments	Units/Site	Cost/Unit	Total
Wideband Tape Recorder	3	$100K	$300K
EOS Quadriphase Demodulator (including detectors and bit synchronizer)	3	50K	150K
EOS Spacecraft Simulator	1	50K	50K

9.3 VHF TELEMETRY

The VHF telemetry system will be modeled on systems used for the Nimbus and ERTS programs. The STADAN stations listed in section 9.2.2 are equipped to support the EOS VHF telemetry system when in contact with the GSFC control center.

Table 9.3-1 presents a link calculations for the proposed VHF downlink. A transmitter output power of 500 mw is selected as this transmitter is adequate and is readily available without expenditure of development funds.
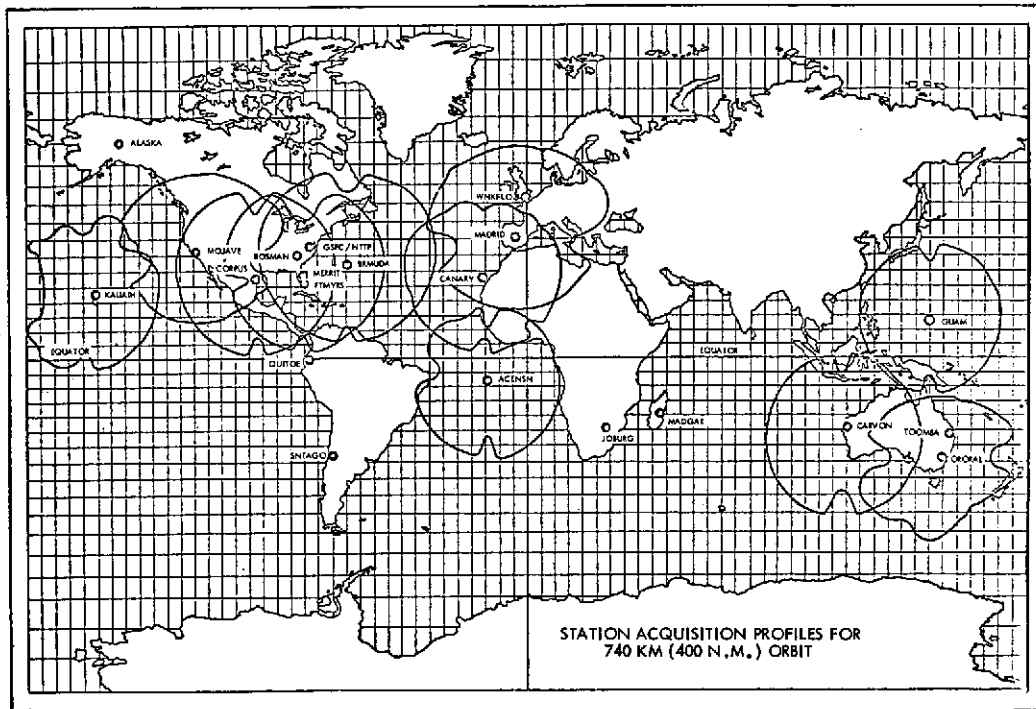
Figure 9.2-5. MSFN Station Profiles for 400nm (740 Km) Orbit

˙9.4 COMMAND

9.4.1 INTRODUCTION

There are three systems that could be utilized with EOS; VHF only, VHF and S-Band combined, and S-Band only. The first system, VHF only, has several disadvantages; the major one being that the MSFN sites are not equipped for VHF command and could not support the spacecraft if this system where selected. Other equally critical reasons for elimination of VHF only as the EOS command system are: difficulties with on-horizon commanding; atmospheric and noise problems and band crowding. The second system, VHF and S-Band combined as used on ERTS utilizes separate VHF and S-Band receivers. A disadvantage of this system is the increased complexity in the spacecraft. This system naturally enjoys the advantages of both the VHF and S-band command systems.

The third and recommended system is S-Band only. This system has the advantage of all site support with no additional ground equipment required (all STADAN's will have 2025-2120 MHz command-band capabilities by 1973). Other advantages are that a single spacecraft command receiver is required and VHF atmospheric and noise problems are avoided. The only unfavorable factors for the S-Band only commanding are: higher doppler frequencies resulting in increased receiver predetection bandwidth, and larger S/C antenna-pattern troughs. These items are not only reduced by increased antenna gains at S-Band but are outweighed by absence of VHF atmospheric anomalies and near-horizon pointing capabilities.

9.4.2 COMMAND LINK

Table 9.4-1 is a S-Band link calculation for the proposed command link. The calculations are based on the proposed STADAN system that will consist of a 500 watt transmitter and a 3 meter dish slaved to an antenna with autotrack, Reference 5. Table 9-3 indicates that adequate S/N will exist for commanding EOS with the proposed STADAN S-Band command link.

9-13

STATION ACQUISITION PROFILES FOR
1100 KM (600 N.M.) ORBIT
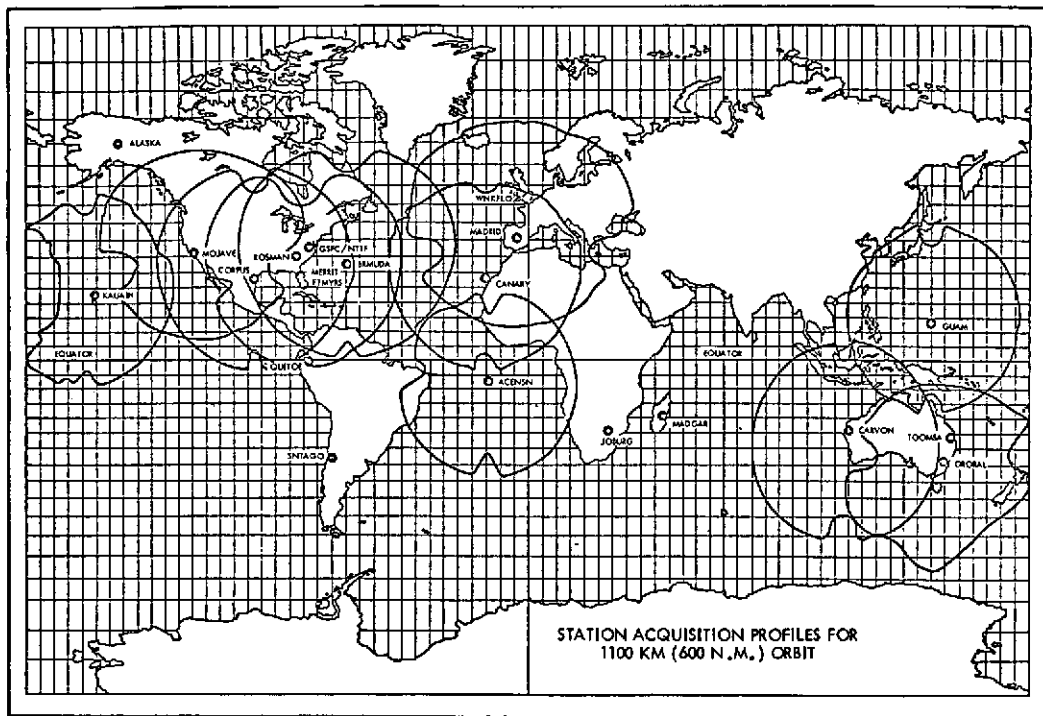
Figure 9.2-6.   MSFN Station Profiles for 600nm (1100 Km) Orbit

9.4.3 MSFN COMMAND

The MSFN command system uses both the 30-foot and 85-foot antennas and was designed to operate with spacecraft at lunar distances. A link calculation for a 30-foot dish is also included in Table 9.4-1 and it is obvious that the transmitter power will have to be reduced to avoid over-loading the spacecraft receiver.

9.5 RANGING

9.5.1 BACKGROUND

The Goddard Range and Range Rate (GRARR) system and the Unified S-Band (USB) systems are high accuracy, worldwide tracking systems which determine spacecraft range, range rate and angular position for orbit determination. The GRARR system presently operates in the 1750-1850 MHz transmit band and 2200-2300 MHz receive band. Plans are in progress to change to the 2025 to 2120 MHz transmit band which will result in frequency compatibility with the MSFN USB system.

9.5.2 TRANSPONDER SELECTION

The USB system uses a phaselock loop (PLL) transponder which phase locks the uplink signal and transmits a carrier signal back to the ground at a coherent frequency ratio of 240/211. At the completion of the transmit frequency modification, the GRARR system will also operate using a PLL transponder with a 240/221 frequency ratio. This transponder is the obvious selection for EOS since it will give full station coverage from both MSFN and GRARR sites. An additional advantage of the PLL mode is reduced transponder bandwidth and the resulting increased signal-to-noise ration available for transmission back to the ground station. The only disadvantage of the PLL mode is that additional acquisition time is required to sweep the transmit frequency to acquire phase lock of the PLL transponder and then return the transmit frequency to its nominal value.

9-14

Table 9.3-1

VHF Power Budget

Parameter	Worst Case 3050 km	Best Case 1080 km
Transmitter power (dbm)	+27.0	+27.0
Spacecraft Antenna gain (db)	-10.0	-7.0
Path Loss (db)	-145.0	-136.0
Spacecraft Circuit Loss (db)	-1.0	-1.0
Ground Antenna Gain (db)	+22.0	+22.0
Received Signal Power (dbm)	-107.0	-95.0
Received Sideband Power for PCM/PM at 1 rad. (dbm)	-108.5	-96.5
Receiver Noise Power (dbm) (in 15 khz Bandwidth)	-125.0	-125.0
System Loss Margin (db)	-3.0	-3.0
Signal-to-Noise Ratio Required for BER of 10^{-6} (db)	-10.5	-10.5
System Margin (db)	+4.0	+15.0

Two additional transponder modes were examined (crystal coherent mode with 240/221 ratio and crystal coherent mode with 60/55 ratio) and rejected since they are only compatible with the GRARR sites and not the MSFN sites. The only advantage the crystal coherent transponder has is instant acquisition. This feature is outweighed by the combined network coverage.

9.5.3 OTHER CONSIDERATIONS

Of interest to spacecraft planners of the 70's will be The Data Relay Tracking Experiment that will be conducted in 1973 using the GRARR and Applications Technology Satellite Ranging (ATSR) systems and the ATS-F and Nimbus E spacecraft. A comparison will be made of the tracking data obtained by the GRARR system tracking the Nimbus E spacecraft and the modified ATSR system tracking the Nimbus E spacecraft through the ATS-F synchronous spacecraft. The Nimbus E will fly a two channel crystal coherent GRARR transponder which may be tracked simultaneously by ATS-F and a ground station. For projects which may wish to participate in a similar experiment and still obtain support from the MSFN, a dual PLL/crystal coherent transponder could be developed. The dual transponder is an alternative available to projects which require unique features of both PLL and crystal coherent transponders.

9.5.4 RANGING LINK

The range and range rate signals will share a down link with the real time MIRP and the VIP playback signals (see Fig. 7.5.1). The system will be similar to that employed on ERTS with a PCM/PSK/PM modulation format. The final modulation indices for the various channels (ranging and data) cannot be determined until the MIRP and VIP bit rates are finalized, but it is expected that relatively low power (5W) will satisfy the link requirements.

Table 9.4-1

Command Power Budget

Parameter	STADAN		MSFN
	Worst Case 3050 km	Best Case 1080 km	Worst Case 3050 km
Transmitter Power (dbm)	+57.0	+57.0	+73.0
Ground Antenna Gain (db)	+34.0	+34.0	+43.0
Line Loss (db)	-1.0	-1.0	-1.0
Path Loss (db)	-169.4	-160.4	-169.4
Spacecraft Antenna Gain (db)	+4.0	+4.0	+4.0
Received Level on S/C (dbm)	-75.4	-66.4	-49.4
Receiver Noise Level in a 160 kHz Bandwidth (dbm)	-111.6	-111.6	-111.6
Signal-to-Noise Ratip Required (db)	+12.0	+12.0	+12.0
Signal-to-Noise-Ratio (db)	+35.2	+36.9	+62.2
System Margin (db)	+23.2	+24.2	+50.2

9.6 K-BAND DATA LINK

9.6.1 FREQUENCY SELECTION

There are multi-level modulation techniques available that would allow the higher date rates (100 mb/sec or higher) to be transmitted in the S-Band region. But, an investigation revealed that both the spacecraft transmitter power required and modulation circuit complexity is undesirable. Therefore the S-Band region was eliminated as a carrier frequency. The remaining possible bands are 8.025-8.500 gHz, 14.4-15.25 gHz, 15.25-15.35 gH and 21.2-22° gHz. The 21.2-22 gHz region is recommended and the K-band link calculations were based on this selection. It should be stated that the final frequency selection cannot be made until the results of the World Administrative Radio Conference for Space Telecommunications are made final. This conference is scheduled for the summer of 1971 in Geneva, and the results will be available by the fall of 1971. The rationale for selecting the 21.2-22.0 gHz frequency band is based on the availability of adequate bandwidth for expansion and the probability that the 8.025 to 8.500 gHz band would have to be shared with the operational Earth Resources satellites. The disadvantages of this band selection are twofold, one, some expenditures will be required for the development of new hardware for both the spacecraft and the ground data systems, and two, the attenuation due to water vapor and oxygen absorption is high at this frequency.

9.6.2 GROUND SUPPORT SYSTEMS

9.6.2.1 Existing Ground Support Antennas. The existing STADAN and MSFN antennas are not presently implemented for K-band. In addition, it should be emphasized here that the capabilities

of the STADAN and MSFN antennas to track and take data at 21.0 GHz is unproven at this time. An exhaustive, numerical, error analysis of a tracking system cannot be performed until further data are available to supplement and verify theoretical evaluations and predictions. Data must be taken over a period of time and under various environmental conditions and target parameters similar to the mission to be supported. Contributions to tracking errors that are not accurately known at this time are antenna surface tolerances, (and degradation of surface tolerance due to wind velocity, precipitation and temperature) static and dynamic structural errors, drive systems errors and dynamic servo errors.

For reasons stated above, a statement of fact concerning the ability or inability of the STADAN and MSFN antennas to track and take data at 21.0 GHz cannot be made at this time. It is recommended that this item be the subject of additional study and possibly actual measurements of the critical parameters be made under various environmental conditions. For the purpose of this report it will be assumed that the existing antennas are not available and an entire new ground system must be utilized.

9.6.2.2 K-Band System

The purpose of this section is to illustrate the system design considerations and economics involved in selecting system parameters for a K-Band 100 mb/sec data link. The first system parameter to be determined, once the carrier frequency is defined, is RF bandwidth. As in the 30 mb/sec system there are many ways to digitally modulate a carrier. The selected type of modulation, based on bandwidth and power efficiency, is again quadriphase modulation. The required bandwidth is therefore 100 MHz.

In performing a link calculation for a non-defined system, assumptions must be made and trade-offs considered to arrive at a reasonable solution. The size of the spacecraft antenna has arbitrarily been limited to one meter, the required signal for a given BER is fixed, the space loss is fixed, and a maximum attenuation due to water vapor and oxygen absorbtion can be determined. This leaves as variables, ground antenna gain, ground system temperature and spacecraft transmitter power.

The first trade-off to be considered is the spacecraft transmitter power. The theoretical limitation of RF power output for space TWT's at K-Band is 100 watts (Reference 6). There are many problems associated with the development of a tube at K-Band with a 100W output but all of these problems are amenable to solution by spending the required development time and money. Tubes operating at 20 GHz have been developed with output power in the 4 watt and 2 watt region respectively. Therefore, in the EOS time frame, it is logical to expect a TWT can be available with an output RF power of 5 watts with minimal expenditures of development funds. A possible alternate for a spacecraft transmitter is the solid state Transferred-Electron Amplifier (TEA). GSFC is presently sponsoring development of a TEA at 15 GHz with an output power in the 5 to 10 watt region. For the reasons stated above a 5 watt spacecraft transmitter is selected for the K-Band link calculations.

The next parameter to determine in the link calculation is the maximum atmospheric attenuation due to meteorological conditions. Several reports (References 7 & 8) contain models that permit estimation atmospheric attenuation for the standard atmosphere and for the atmosphere with precipitation. These reports indicate the maximum attenuation due to meteorological conditions at an acquisition angle of 10° is approximately 25 db. The attenuation reduces rapidly as the elevation angle is increased (20 db at 15°, 10 db at 25°). Using 5 watts S/C output power, a maximum attenuation of 25 db coupled with a space loss of 189.5 db and a spacecraft antenna gain of 44.5 db gives a signal level of -134 dbm at the ground antenna. The required receiver signal-to-noise ratio of +10 db in a 100 MHz bandwidth can be achieved with a ground system G/T of 28.3. Implementation of a ground antenna system with a 28.3 G/T involves a trade-off between antenna size and antenna system noise temperature. There are three possible preamplifiers that could be incorporated. Table 9.6-1 is a listing of the three along with projected cost, noise

Table 9.6-1

Comparison of Three (3) K-Band Preamps

Preamp Type	Preamp Noise temp (Kelvin)	Preamp Cost/unit ($K)	Antenna Size		Antenna Cost ($K)	System Cost ($K)
			(m)	(ft)		
TDA	1500	10	9.15	30	490	500
Paramp	200	75	4.0	13	320	395
Cryogenic Paramp	25	125	2.55	7.7	280	405

temperature and antenna size required to obtain the G/T. The antenna cost was derived from a cost model constructed by Bell Telephone Laboratories under contract to GSFC. It is recommended that a 4 meter dish antenna with an uncooled paramp be used.

Reasons for this recommendation are:

It is the least expensive system and future development in uncooled parametric amplifiers and medium size antennas could reduced the price by 50%.

It is more reliable than the cyrogenic amplifier.

It has an important technical advantage over a system using a Tunnel Diode Amplifier which requires a significantly larger antenna.

In addition to the above comparisons, the TDA and Cryogenic paramp systems offer little opportunity to improve the stated noise temperature while the uncooled paramp temperature could be reduced by 100K by the development of a high-quality varactor chip. An additional feature of the system using a 4 meter antenna and the room temperature paramp is the antenna could be instrumented at a later date with a cryogenic paramp. This modification would improve the G/T by 4.4 db and allow the system to support future spacecraft with data bandwidths up to 250 MHz.

Table 9.6-2 is a link calculation of the proposed K-Band 100 mb/sec communication link.

It should be noted that the -25 db allocated to atmospheric attenuation is for an extraordinarily heavy rain of 25 mm/hr. and could total as little as a few hours per year depending on the location of the station. If the mission requirements concede loss of data while operating in a heavy rain, this attenuation figure could be reduced to 10 db, equal to a link gain of 15 db. If this were the case the system parameter recommended for change is spacecraft antenna gain. A gain reduction of 15 db in the spacecraft antenna would widen the 3 db beamwidth from 1.4 degrees to 8.0 degrees and alleviate the stringent pointing requirements for the high gain antenna.

In summary, all parameters listed in Table 9.6-2, with the exception of path loss, are interdependent and the optimum values for each parameter cannot be determined until the mission requirements are finalized.

9.7 EOS TO LOCAL READOUT GROUND STATION (LRGS)

Government agencies, both U.S. and foreign, as well as private industry and institutions have a need for the EOS data. Therefore, a system capable of transmitting data directly to a local readout ground station (LRGS) is proposed.

Table 9.6-2

K-Band Power Budget

Parameter	Worst Case 30 km	Best Case 1080 km
Transmitter output power (dbm)	+37.0	+37.0
Spacecraft loss (db)	-2.0	-2.0
Spacecraft antenna gain (db)	+44.5	+44.5
Path loss (db)	-189.5	-180.5
Atmospheric attenuation (db)	-25.0	0
Ground system temperature (Kelvin)	275.0	215.0
Ground system noise power in a 100 MHz bandwidth (dbm)	-94.3	-95.0
Ground antenna gain (4M dish) (dbm)	53.0	53.0
Signal power at ground receiver (dbm)	-82.0	-48.0
Signal-to-noise ratio in ground receiver (db)	+12.3	+47.0
Signal-to-noise ratio for BER of 10^{-5} (db)	+10.0	+10.0
Signal margin (db)	+2.3	+37.0

The purpose of this system is to distribute sensor data directly from the EOS satellite to the user equipped with a LRGS. The LRGS should be simple, low cost, transportable and self sufficient in the sense that, except for antenna steering information it can receive, demodulate, process and display data without support from the EOS Control Center. In designing a system of this type there are a multitude of parameters that can be varied to meet the requirements. The delineation of optimum parameters will be left to Phase-B studies and other studies now in process at GSFC.

9.7.1 BACKGROUND

The proposed RF system for the EOS-B could be used to support a LRGS with a minimum of change. The Power available to the spacecraft transmitter for this purpose is 60 watts. This amount limits the transmitter output power to about 20 watts and this will be the starting point of the RF link calculation. The spacecraft transmission frequency and method of modulation has already been described in Section 7.5.

9.7.2 LINK DEFINITION

9.7.2.1 Introduction. The S-Band Link Calculations of Table 9.2-1 indicate that a 10 watt space-craft transmitter allows a margin of 4 db for the MSFN 30-ft. antenna system and even more for the 40 and 85-ft. STADAN antennas. This transmitter power could be increased by 3 db to 20 watts if a LRGS is to be supported. To determine the minimum size LRGS antenna that could support EOS, a graph of spacecraft transmitter power vs. ground antenna size was constructed (Figure 9.7-1) with the following parameters held constant.

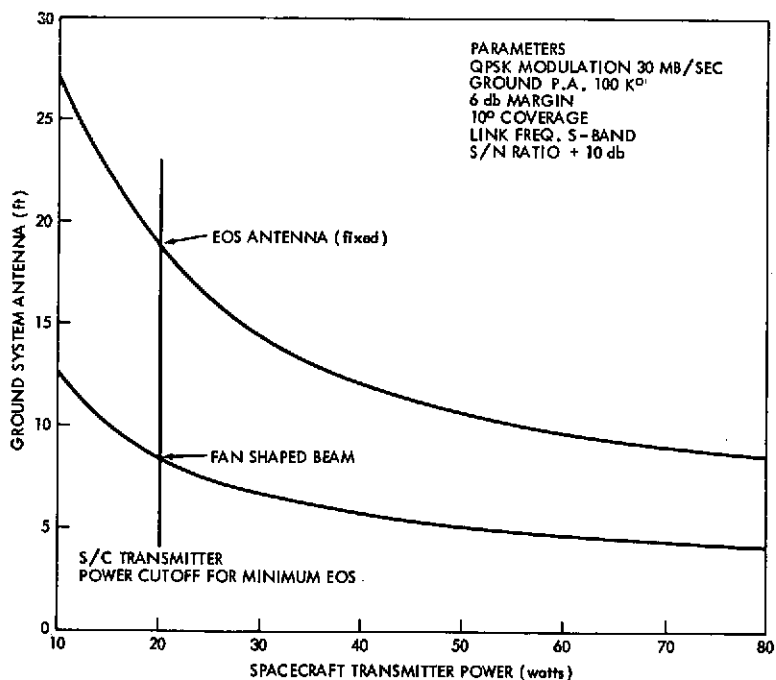|	
Link Frequency	2250 MHz
Modulation	QPSK (30 mb/sec)
Required Signal-to-Noise Ratio	+10 db
Preamp Temperature	100 K
Station Coverage	10° above horizon
Link Margin	6 db

Figure 9.7-1. S-Band LRGS Link

9-20

The minimum size LRGS antenna that could be used with the proposed S/C antenna requires an equivalent aperature of 5.8 meter (18 ft.). Although there is no definitive cut-off on antenna size for a low-cost, transportable LRGS, a ground antenna of 5.8 meters is considered excessive and means of improving other link parameters should be investigated. The only variable parameter now existing in the link is the spacecraft antenna and this must be examined for possible increased gain.

A promising concept for this application is a fan-beam type antenna pattern with a 120° beam-width parallel to the flight path and narrow beamwidth orthogonal to the flight path. The advantage of this type antenna is that only one adjustment about the spacecraft roll axis is required per station pass. The fan beam antenna could be implemented by either of three basic configurations; fixed electronically switched antennas, (2) mechanically steerable antennas and (3) electronically steerable (phased arrays) antennas. All three types will result in some increase in spacecraft complexity as well as in operational problems. The final selection will be made after more detailed study, but electronically pointed system is perhaps best suited for this mission. For a 10 db antenna gain, the beamwidth in the cross direction will be 10°. The lower curve in Figure 9-7 represents an antenna with the above parameters.

9.7.2.2 User Antenna. As indicated in Figure 9.7-1 a 9 foot (approx. 3 meter) parabola has sufficient gain to support the 30 mb/sec S-Band data link with a 10 db gain S/C antenna. A 4 meter antenna is recommended (to allow for degradation caused by a radome for all weather operation.) and for increased operation and system margin. The system antenna criteria could be met with an array of smaller parabolas and all possible antenna configurations will be examined prior to final selection.

9.7.2.3 Tracking. Three methods of tracking a orbiting satellite are program tracking, auto-tracking and manual tracking. An antenna with an equivalent aperature of 4 meters has a 3 db beamwidth of 2.5° at 2250 MHz and the proposed EOS orbit would have a maximum angular velocity of approximately 0.4°/ second. Past experience has shown that manual tracking will not be acceptable to this system. A selection between program and autotracking will be determined by the availability of a computer on site for other purposes, such as data processing, that could be shared for program tracking. Of the monopulse tracking systems, one, two, and three channel systems will be examined for cost-effectiveness and performance.

9.7.2.4 Low Noise Front End. The selection here is obvious; a room temperature parametric amplifier with a noise performance of 100 Kelvin. This unit can be made small (1,950 cu cm, 120 cubic in.). light (2 kg, 4 lb.) and reliable. When procured in quantities in excess of 10 units, the price could be less than $4,000.00 per unit.

9.7.2.5 Receiver and Demodulator. The remainder of the RF system (receiver and demodulator) presents no design problems, but there is not "off the shelf" inexpensive system available for demodulating a 30 mb/sec QPSK signal. An effort should be made to organize all users to a common system, so all could benefit from one development, and production and the resulting cost saving.

9.8 TRANSFER OF DATA FROM DATA ACQUISITION SITES TO NASA DATA PROCESSING FACILITY (NDPF)

9.8.1 INTRODUCTION

The manner in which the data will be transferred from the data acquisition site to the NDPF cannot be defined until the user requirements are better defined. Three possible modes, exist for data transfer from a data acquisition site; real-time wide band transmission, near real-time reduced speed transmission, and tape transmission via postal service.

9.8.2 REAL TIME

The technology utilized by common carriers to transmit wide band data is rapidly expanding. Facilities for handling EOS data rates (30 and 100 mb/sec) are technically achievable, but the cost for a link of this type would be prohibitive. An estimate for a 30 mb/sec data line, via common carrier, from Mojave to GSFC is 1.5 million dollars per month. It is obvious that economics eliminate the use of wideband real-time data transmission. If selected channels are required real time they could be demuxed at the site and transmitted at a bandwidth equal to the data rate of the channel.

9.8.3 NEAR REAL-TIME

This method consists of recording the data on a wide band tape recorder and playing back the data at a reduced tape speed. This method has excellent efficiency as the speed ratio can be selected for continuous use of the data lines. In a high priority or perishable variation of this method, selected channels can be demuxed at the site and transmitted to the NDPF at further reduced data bandwidths.

9.8.4 TAPE TRANSFER

A data transmission method based on Postal service is the most economical but involves a delay in receipt at NDPF. For operational planning current indications are 4 to 5 days from ALASKA or MOJAVE to NDPF.

9.8.5 EOS DATA TRANSFER

As previously indicated, the data transfer modes will be dictated by the needs of the data users. The most likely mode would be a combination of all three of the described methods with a high percentage of the data being mailed to NDPF and selected data channels being played back in both real-time and reduced speed. It should be noted here that a two year lead time is required to implement a special data transfer requirement via common carrier. Although there is no standard configuration of NASCOM Network circuits to and from data acquisition sites, existing data circuits from selected sites are listed in Table 9.7-1

Table 9.7-1

Characteristics of Existing Data Links

From	To	Link	Bandwidth	Max Data Rate
NTTF	GSFC	Coaxial		
MOJAVE	GSFC	Common Carrier	7.2kHz	7.2 kb/sec
Alaska	GSFC	Common Carrier	(Two)-48kHz	(Two)-38kb/sec
Rosman	GSFC	Common Carrier	1.5 MHz	240 kb/sec
GSFC	Suitland	Common Carrier	48 kHz	Analog only

9.9 REFERENCES

1. "Digital Communications at Gigahertz Data Rates", Parts 1 and 2; C. L. Cuccia, J. L. Spilker and D. T. Magill, Microwave Journal, January and February 1970.

2. "Report on a 400 Megabit/sec Digital Modem", IEEE International Communications Conference, Boulder, Colorado, June 1969, J. H. Polson, and M. Kerrigan.

3. "Quadri-Phase Communication System Design", Philco-Ford Corp., Technical Memo #135, D. T. Magill.

4. "GSFC Mark 1 Tracking and Data Relay Satellite (TDRS) System Concept" Phase A Study Final Report, November 1969.

5. TIROS-N S-Band Command Feasibility Study, NASA Internal Memo from R. T. Fitzgerald Senior Staff Engineer, Code 570 to Mr. C. Hunter, TIROS-N Study Manager, dated September 1970.

6. "Latest Advances in Space TWT's", J. Benton, H. Smith, and P. Wolcott, presented at the AIAA 3rd Communication Satellite Systems Conference, Los Angeles, California, April 1970.

7. "K_u - Band Tracking and Data Relay Satellite Ground Antenna Study", X-525-70-200, June 1970, GSFC.

8. "Earth-to-Space Communications at Millimeter Wavelengths", Altshuler, Edward E., Air Force Cambridge Research Laboratories Report, AF CRL-65-566, August 1965.

SECTION 10

GROUND DATA PROCESSING SYSTEM

SECTION 10

GROUND DATA PROCESSING SYSTEM

PRECEDING PAGE BLANK NOT FILMED

ILLUSTRATIONS

TABLES

SECTION 10

GROUND DATA PROCESSING SYSTEM

10.1 GENERAL

The Earth Observatory Satellite NASA Data Processing Facility (EOS NDPF)[1] user requirements are based on the currently evolving requirements for the Earth Resources Technology Satellite (ERTS). The general EOS data flow concept is shown in Figure 10.1-1. The regional data distribution centers will serve the general user community and operate separately from the EOS project. These centers will be considered as primary users to the EOS NDPF. The primary users will include the user agencies as well as the approved prime investigators.

10.2 INPUT DATA

Input data to the NDPF have been classified into three categories according to data rates and their corresponding transmission links, (1) high data rate sensors, (2) medium data rate sensors, and (3) low data rate sensors and housekeeping. Since the imaging sensors are not fully defined at this time, nominal assumptions have been made about their sampling rates and quantization levels. It is expected that the NDPF will have the flexibility to process data with a variety of formats and data rates.
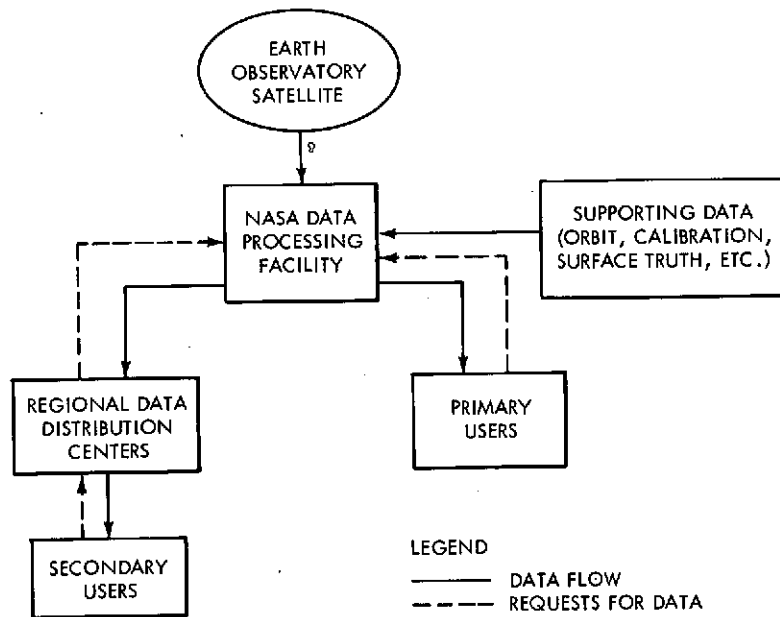

Figure 10.1-1. Data Flow Chart

---

1. The EOS facility is considered an extension or modification of the ERTS NDPF.

10.2.1 HIGH DATA RATE SENSORS

The Thematic Mapper has the highest data rate of the EOS sensors. For each 185 x 185 km scene this instrument will generate six spectral images of about 4200 x 4200 pixels[1] (66m IFOV) each, and one spectral image of about 1300 x 1300 pixels (200m IFOV). The pixels will be encoded using seven bits each. To size the ground data processing system requirements let us assume a typical orbit as shown in Table 10.2-1 (orbital data were chosen from the ERTS B and C study reports). The EOS satellite would pass over 185 km (ground distance) in 28.6 seconds and generate 26.25 mbits/second of image data.[2]

Table 10.2-1

Typical Orbit

Period	103.3 min
Semi major axis	7290.4 km
Eccentricity	0.001
Inclination	99.098 degrees

The Thematic Mapper, intended for scanning land and coastal regions in daylight, may be considered useful within 150 degrees latitude. For such usage a typical day would consist of 200 minutes of data. This assumes 190 minutes a day of land coverage and an additional 5 percent for coastal regions.

The stations equipped to record the EOS data are the ERTS stations at Goldstone, Goddard, and Alaska. The daily data volume for the Thematic Mapper is summarized in Table 10.2-2 for three possible telemetry configurations. To allow for a 10 percent overlap in the 185 x 185 km format, the number of scenes, images, and pixels include an extra 10 percent. For comparison, ERTS is being sized for 188 scenes or 1316 images per day.

Table 10.2-2

Daily Data Volumes for Thematic Mapping

Communication Link	Minutes	Scenes	Images	Total Pixels
Data Relay Satellite (or on-board recording)	200	462	3234	5.0×10^{10}
NASA Ground Stations	135	311	2177	3.3×10^{10}
Alaska, Goldstone & GSFC	20	46	323	5.0×10^{10}

---

1. A pixel is the number representing the intensity of a scene within the Instantaneous Field of View (IFOV) of a detector. The number of bits used for this value will be six to ten bits. An image is defined as an array of pixels which may be recorded on tape or film.
2. Image scanners do not transmit image data all the time. Sometimes the line retrace time can be a significant amount relative to the scan time. Unless data buffers are used, image data are not transmitted during this retrace time. Therefore the efficiency of the data is defined as the ratio of actual image bits to the total bits transmitted. If the sensor is only 85 percent efficient, then the total data rate will be about 31 megabits/second. If the scan efficiency is only 20 or 30 percent, then the data rates will be about 100 megabits/second, but the average real-time image data rate will still be 26.25 megabits/second.
3. If the Instantaneous Field of View (IFOV) were decreased from 66m to 40m, the data volume would increase by a factor of (66x66)/(40x40) = 2.7. The total number of pixels would increase by this factor. However, with the same format, the number of scenes recorded on film would be the same, but with 2.7 times as many pixels/cm².

10.2.2 MEDIUM RATE SENSORS

The Oceanic Imaging Spectrophotometer (OIS) will generate twenty spectral images of a 926 x 926 km scene every 143 seconds. Each image will consist of 695 x 695 pixels (2 km IFOV) of eight bits each which will produce a 0.54 megabit/second image data rate. The sensor will operate during daylight between ± 75 degrees latitude, the number of scenes each day will be

$$\frac{150°}{360°} \quad \text{x} \quad \frac{86400 \text{ sec/day}}{143 \text{ sec/scene}} \quad \text{x} \quad 1.10 \text{ (10\% overlap)} = 277 \text{ scenes/day}$$

Each scene has 20 spectral images so that there will be 5540 images/day or 5540 x 695 x 695 = 2.7 x 10^9 pixels/day. One assumption is that telemetry coverage will be available when required using on-board tape recorders with playback as well as real-time transmission.

The Multispectral Imaging Radiometer (MIR) has four detectors operating continuously in the emissive region. The detectors will generage four images of 1600 x 1600 pixels (2 km IFOV) each representing a 2870 x 2870 km scan swath every 444 seconds. Each pixel will be represented by ten bits so that the image data rate will be 230 kbits/second. The number of scenes each day will be

$$\frac{86400 \text{ sec/day}}{444 \text{ sec/scene}} \quad \text{x} \quad 1.10 \text{ (10\% overlap)} = 195 \text{ scenes/day}$$

Six daylight channels will have approdimately the same resolution. Therefore, the number of scenes between ± 75 degrees latitude during daylight will be

$$\frac{150°}{360°} \quad \text{x} \quad \frac{86400 \text{ sec/day}}{444 \text{ sec/scene}} \quad \text{x} \quad 1.10 \text{ (10\% overlap)} = 81 \text{ scenes/day}$$

The image data rate for these detectors will be 347 kbits/second; therefore, the total MIR image data rate will be 577 kbits/second. The daily data volumes for these sensors are summarized in Table 10.2-3.

Table 10.2-3 Daily Data Volumes for the Oceanic Imaging
Spectrophotometer (OIS) and Multispectral
Imaging Radiometer (MIR)

Sensor	Minutes	Scenes	Images	Total Pixels
OIS	600	277	5540	2.7x10^9
MIR (4 detectors)	1440	195	780	2.0x10^9
MIR (6 detectors)	600	81	486	1.2x10^9
Total			6806	5.9x10^9

10.2.3 LOW RATE DATA

Standard telemetry low data rate sensors and housekeeping data will not contain image type data. Spacecraft housekeeping, including attitude measurements and spacecraft clock time, will be put on computer compatible tapes by the Operations Control Center (OCC) and sent to the NDPF for processing. Attitude measurements will be calculated in the NDPF and used with orbit data to map images onto a standard projection. If the desired position accuracy of each pixel is approximately the same as the IFOV then the instrument on the spacecraft with the smallest IFOV will determine the accuracy required for the orbit and attitude calculations. For example, if EOS A has a medium rate sensor with 2 km IFOV's, then an angular attitude measurement error of seven minutes could be tolerated. This does not allow for errors in the orbit ephemeris calculation which will cause additional errors in the ground position calculation.

10.3 USER OUTPUT REQUIREMENTS

General mission requirements and practical instrumentation technology combine to define data needs. It is desirable to maintain as much flexibility as possible to support changing user requirements. Various disciplines will require different output products of the same data. Output formats should be categorized according to the data rates of the sensors being considered.

10.3.1 HIGH DATA RATE SENSORS

The Thematic Mapper characteristics are similar to the ERTS multispectral scanner for which the user requirements are being defined. The higher signal to noise ratio planned for the EOS sensor will be degraded by film recording, consequently digital data will be the preferred output for analytical purposes. Emphasis should be directed toward formatting digital data so that the user will not have to perform routine processing such as geometric and radiometric correction.[1] More than one digital output product should be produced. For example, the small volume user could have standard computer compatible digital tape, and the large volume user could have special high density digital tapes. Another consideration is the selection of specific geographic areas and spectral bands.

Film data will continue to be a primary output for some experimenters (e.g. photogrammetrist and geologist) and experimenters not equipped to process digital data. Film data, like the digital data, should have geometric and radiometric errors removed with images presented on standard projections such as Transverse Mercator and Polar Stereographic projections.

Most of the applications for thematic mapping data will not require near real-time processing. Like ERTS users, most EOS users can tolerate delays of a week or more. Near real-time data will be required for major disasters such as earthquakes or hurricanes. On a more regular basis, near real-time data will be required for fishing fleets, pollution monitoring, and iceberg detection. Though EOS is a research and development satellite, quasi-operational uses must be supported to obtain correlative ground truth data. The user requirements are summarized in Table 10.3-1.

10.3.2 MEDIUM RATE SENSORS

The OIS data will be used primarily for research which will not require near real-time output to most users. A limited amount of near real-time data could be processed in the NDPF without the refined orbit and attitude computation. The primary form of output data will be digital since

---

1. Sensors will be calibrated to remove geometric and radiometric errors. Geometric corrections include spacecraft attitude measurements (in-flight), spacecraft alignment (preflight) and internal sensor geometric measurements (pre and in-flight). Radiometric measurements include preflight and in-flight calibration data.

Table 10.3-1

High Data Rate Output Requirements

Digital Data	
Output Medium	Computer compatible digital tapes
	High density digital tapes
Format Selection	By spectral bands
	By geographic areas
Features	Geometrically corrected
	Radiometrically corrected
	Standard projection
Timeliness	One week or more for most applications
Film Data	
Output Medium	Black & white positives & negatives
	Color positives & negatives
Format Selection	185 x 185 km scenes at 1:1,000,000 scale
	Smaller areas at larger scale
Features	Geometrically corrected
	Radiometrically corrected
	Standard projection
Timeliness	One week or more for most applications
	Less than one day for special requirements

analysis of the 20 spectral channels is difficult to process from film. Film data, however, will be required for general assessment of the image quality and cloud cover. One or two black and white film images and one color film image should be available for each area. Images may be single channel or of several channels. For example, each of the three film image colors (red, blue and green) may be represented by weighted averages from the 20 spectral channels.

The MIR data will be used in digital form and processed by the users. Initial screening of the data by users will require black and white film outputs. The specific spectral bands selected will depend on user requirements; therefore, flexibility in film formats should be provided.

10.3.2.1 Medium Data Rate Formatting. Medium rate sensor data should be projected onto a standard format, such as a Mercator projection or polar projection, for both the digital and film outputs. The data will have overlap between adjacent swaths with the overlap increasing as the distance from the equator increases. Initially, duplicated data will be required by the users, and algorithms will be developed to eliminate redundant data so that the most useful information will be retained. For the sampling density of paragraph 10.2.2 there are 1.2×10^8 distinct pixels (no redundancy) between ± 75 degrees latitude or 2.4×10^9 distinct pixels for 20 channels. This is about one-fourth the number of pixels for full earth coverage

compared to the sensor data without redundancy removal. This assumes four days of complete coverage at 2.7 x 10^9 pixels/day (see Table 10.2-3).

10.4 PROCESSING REQUIREMENTS

10.4.1 RECORDING MEDIUMS

Large volumes of EOS data will require recording techniques not commonly used. The standard computer 9 track, 1600 bits/inch, 2400 foot reels of tape is limited to 3.5 x 10^7 pixels. This assumes 4000 pixels/record with a 0.75 inch record gap. Nonstandard high density tape recorders such as the 28 channel Ampex recorder uses a 3600 foot tape and can record 20 K bits/inch/track with 30 tracks across the one inch width. Assuming 8 bits/pixel plus one parity bit/pixel, one tape will hold 2.3 x 10^9 pixels. Other higher density recording techniques such as laser beam writing on film have been tested, but a standard commercial recorder of this type is not available.

Film data will continue to be an important recording medium for image data. Geometric distortions and modulation transfer function deterioration will not be significant for a 70 mm format. However, gray level accuracy may not be maintained above five or six significant binary bits. These parameters are currently being analyzed for the ERTS system; the experience gained on the ERTS operations will be incorporated into the EOS film processing system.

10.4.2 HIGH DATA RATE SENSORS

The maximum daily data volume is 5.0 x 10^{10} pixels (see para. 10.2.1). To record this data digitally would require 1430 standard digital tapes or 22 high density tapes per day. A one year archive would require about 8000 high density tapes. Users may want data for a small area overlapping two image swaths; the processing system should be able to mosaic from several high density tapes if necessary.

The demand for near real-time data can be met by the regular processing equipments using priority assignments. For near real-time data to be useful, it must be transmitted to the user in a timely manner. For example, a 4000 x 4000 pixel image (6 bits/pixel would require 12 hours to transmit over a 2400 bit/sec telephone line. For practical implementation, either smaller areas must be selected or wider band data lines used.

10.5 DATA HANDLING FACILITIES

The NASA Data Processing Facility for EOS (NDPF) will adopt most of the data handling functional concepts of the ERTS system since the data processing requirements are similar. The NDPF will respond to requests from the users and perform routine processing and quality control checks. The conceptual design described in this section consists of six major subsystems (see Figure 10.5-1).

- Bulk Processing

- Digital Image Processing

- Custom Processing

- Support Services

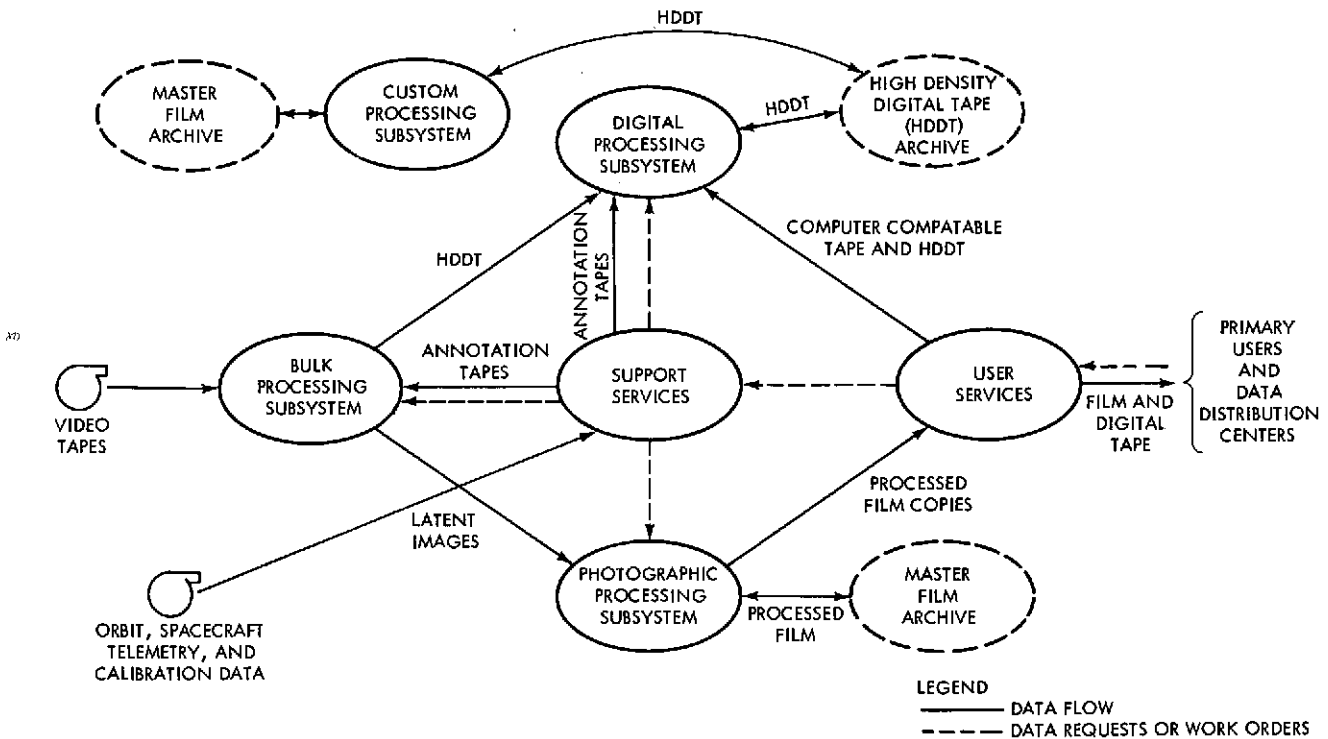- User Services

- Photographic Processing

Figure 10.5-1.   NASA Data Processing Facility

10.5.1   BULK PROCESSING SUBSYSTEM

This subsystem could be a modification of the ERTS Bulk Processing Subsystem.   This subsystem will receive the Image Video Tapes (IVT)[1], the Image Annotation Tapes (IAT), and operator instructions to produce film images via the Electron Beam Recorder (EBR) and the High Density Digital Tape (HDDT) for use by other subsystems.   Radiometric and geometric corrections which are available will be applied to the bulk processed data.   The block diagram of this subsystem is shown in Figure 10.5-2.   The IVT will be separated into two data rate categories.   The assumption is that the high rate data and the medium rate data with their corresponding 30 megabit/sec and 1.2 megabit/sec data rates may be recorded on different types of tape recorders; however, these recorders would require similar playback recorders and controllers.   To utilize the EBR and HDDT effectively, the high rate sensor data could be played back at a slower than real-time rate and the medium rate sensor data would be played back faster than real-time.   In this manner the Bulk Processing Subsystem would process all data at the same rate.   The Ampex 1928 high data rate recorders could operate at 30 megabits/second; another possibility would be a new development for a 100-200 megabit/sec recorder using laser beam, electron beam, or holographic recording on film.   There have been proposed designs for such recorders.   The medium rate data recorder could also use the Ampex 1928 which could easily handle the 24 megabit/second rate required when the satellite tape recorder is played back at twenty times real time.

The Image Annotation Tape (IAT) will be generated by the Support Services group.   Orbit and spacecraft attitude data will be used by Support Services to compute the appropriate annotation data and control information for the Bulk Processing Subsystem.   Long term radiometric and geometric calibrations may be included on the IAT or may be conveyed directly from Custom Processing.   The VTR Controller equipments will provide the necessary controls for the tape

---

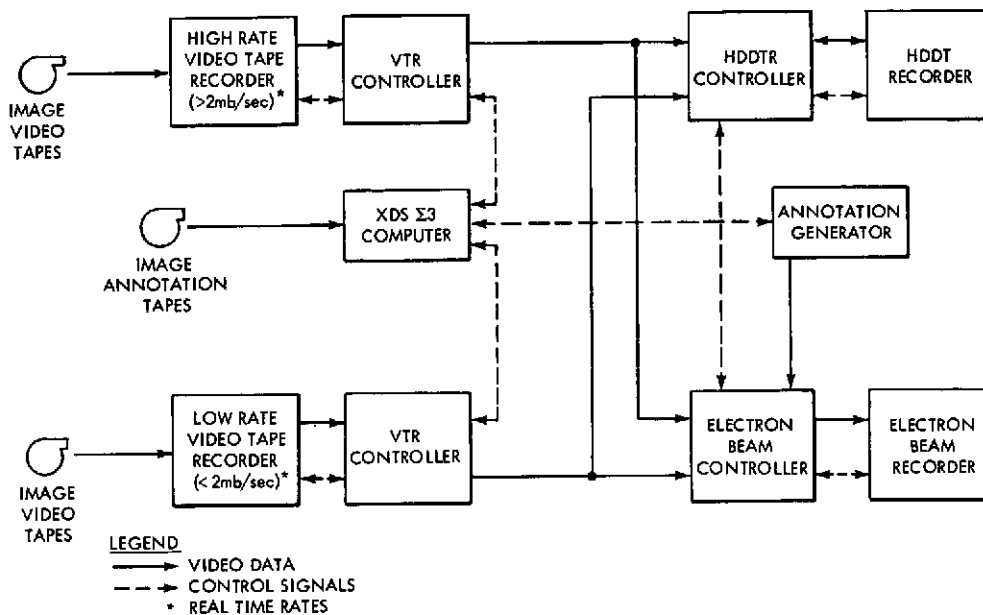1.   IVT tapes are recorded at the receiving sites.

Figure 10.5-2. Bulk Processing Subsystem

recorder operation such as start, stop, rewind, etc., and provide frame and line synch detection, calibration detection and extraction, and formatting for the HDDT recorder and the EBR. The controller equipments will also perform decommunication of the various spectral channels of the different scanners. These controllers should be designed to accommodate formats specified in the video data standards to be developed.

The EBR and its associated controller and annotation generator will produce latent film images for processing by the Photographic Processing Subsystem. The EBR beam will be deflected in a nonlinear manner to generate a standard projection of the scene on film. Even with an ideal attitude control system, nonlinear deflections would be required to produce a standard projection. The electron beam will make reference marks to maintain precise correspondence between the image and the reference marks. The data required by the EBR and EBR controller for proper beam deflection and annotation will be provided by the IAT.

The HDDT recorder and controller will record data from the IVT as well as play back HDDT's to form an image on film. This latter capability allows film recording from HDDT's generated in the The Digital and Custom Processing Subsystems. The ERTS NDPF uses the Newell recorder for the HDDT; another possibility is the Ampex 1928 recorder.

The Sigma 3 Computer will control the system, receiving its instructions from the IAT and the operator. Where possible, the processing instructions will be contained on the IAT thus minimizing operator errors. The computer will verify that the proper tapes have been mounted and will search the tapes for the required data. The computer will process calibration data that have been multiplexed with the image data, merge this calibration with the long term calibration from the IAT, and send correction data to the EBR and HDDT recorder controller.

10.5.2 DIGITAL IMAGE PROCESSING SUBSYSTEM

This subsystem could be a modification of the ERTS Special Processing Subsystem. The Digital Image Processing Subsystem will produce HDDT's that have been radiometrically and geometrically corrected. Computer compatible tapes will also be generated which will contain the same information as the output HDDT's. In addition, output HDDT's can be played back to generate computer compatible tapes. Correction data may be contained on the HDDT, the IAT, or a calibration tape.

This subsystem will not process pixel data within the computer. The computer will control the special equipment which performs the actual computation for each pixel.

This subsystem consists of input and output HDDT recorders and controllers, a Sigma 3 computer, and a special purpose digital processor that will perform radiometric and geometric corrections (see Figure 10.5-3). The HDDT recorders will be the same as the ones used in other subsystems; however, one of the HDDT recorders must have speed control since this is a continuous operation.
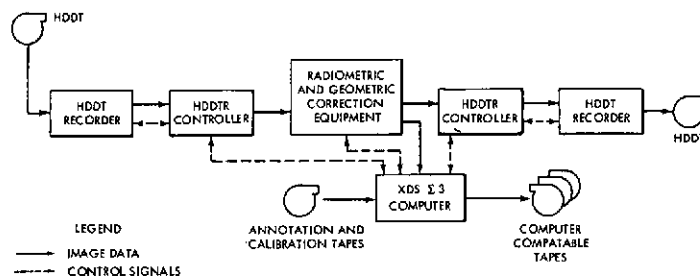

Figure 10.5-3. Digital Processing Subsystem

The special processor for radiometric correction and geometric warping will consist of a memory which contains one or two hundred lines of image data. Each new line coming in will replace the oldest line in memory. An output line will be formed by indexing through the memory in a nonlinear pattern. The computer will provide the indexing control data; indexing will be linear over short segments so that the computer will provide indexing data for each segment, not for each pixel. Radiometric corrections will be performed on each pixel again using error corrections that are position dependent but linear over small regions.

The Sigma 3 computer will be the controlling unit providing the appropriate signals for the special equipment. The computer will read calibration data from the HDDT, the IAT, or the calibration tape and from these data will compute the indexing values required by the special processor.

10.5.3 CUSTOM PROCESSING SUBSYSTEM

This subsystem could be a modification of the ERTS Precision Processing Subsystem. The Custom Processing Subsystem performs all processing not normally required on all data. One example is correlation with ground truth data to perform precise geometric correction and orientation for film data as well as to provide correction factors to the Digital Processing Subsystem for precise digital geometric corrections. Ground truth correlation is a method used for precise geometric orientation of the images. This method is used to obtain precision better than that obtained from attitude measurement systems. Points of known latitude and longitude are located within the image very accurately. Only a few points have to be located if the errors within the image are smooth. For example, if the error within the image area is one of shift in the north-south and east-west directions, one point is required. If there is rotation, two points are required. Non-linear errors caused by unmeasured changes in the attitude as the satellite moves will require more points to correct. These reference points can be located by automatically cross correlating the image and a reference image that has been previously measured manually. A set of reference images will be available from the ERTS program.

10.5.4 SUPPORT SERVICES

This subsystem could be a modification of the ERTS Support Services Subsystem. Support Services will form the nucleus of the NDPF operations. It will consist of an XDS Sigma 5 computer, quality control instruments, storage space, and software. The primary input and output products and services are shown in Table 10.5-1. All data received, as well as processed, will be stored

Table 10.5-1

Support Services Input and Output Products

Inputs	Outputs
Data Requests	Production Control
Orbit Tapes	Annotation Tapes
Spacecraft Telemetry	Digital Data
Video Tapes	Information Retrieval
Coverage Requests	Management Reports
Station Contacts	Data Accounts
Image Data	Logistics
Management Requests	Quality Control Information

in the Support Services. Support Services can be used for the following functions:

● Inventory

● Quality evaluation

● Cloud cover

● Abstracts

● Data requests

● Coverage requests

● Process completion

The low rate data including housekeeping and sensor data will have basic processing performed in the OCC. Support Services will receive these data from the OCC on computer compatible digital tapes and respond to user requests and output the requested data in the appropriate format. Support Services will also make copies of computer tapes for distribution to one or more user.

Support Services will maintain eleven basic files. These files are listed in Table 10.5-2.

10.5.5 USER SERVICES

User Services will provide direct support for the user and advise him of the NDPF output products. User Services will contain various equipments such as: viewing tables, multispectral display systems, and an interactive terminal into the Sigma 5 computer. It will also contain catalogs and a browse file and provide personnel to assist the users with their special problems.

10.5.6 PHOTOGRAPHIC PROCESSING SUBSYSTEM

This subsystem could be a modification of the ERTS photographic facility. The Photographic

Table 10.5-2

Support Services Data Base Files

Main Image File	Work Order File
Swath File	Data Received File
Image Annotation Data File	User Address File
User Profile File	Remote Batch Queue File
Spacecraft Coverage File	Historical Processing File
Data Request File	

Processing Subsystem processes all latent images produced in the Bulk Processing and Custom Processing Subsystems. The Photographic Processing Subsystem receives duplicating requests from Support Services and makes film copies as required.

ATTACHMENTS

ATTACHMENT A

NIMBUS G AND H

PRE-PHASE A STUDY

A-3

UNITED STATES GOVERNMENT

Memorandum

TO　　:　John F. Clark, Director　　　　　　　DATE: December 29, 1969

FROM　:　Chairman, Meteorology Program Working Group

SUBJECT:　Nimbus G and H Pre-Phase A Study

eference:　Memorandum to NASA Headquarters, Attention: Office of Space Science
and Applications - Dr. Naugle, from Goddard Space Flight Center,
Office of the Director, dated October 6, 1969, Subject: "Supplement
to POP 69-2 Cover Letter dated August 15, 1969; Phase A activities
and FY'70; Proposed Redefinition of Phase B New Starts."

　　　　In response to the referenced memorandum, the report Nimbus G

and H Mission Requirements and Concepts (Pre-Phase A) Study dated

20 December 1969 is hereby submitted by the Meteorology Program

Working Group.

William R. Bandeen, Head
Planetary Radiations Branch

cc:　Members of METWG
　　　Dr. Pieper
　　　Mr. Stroud
　　　Mr. Spencer
　　　Mr. Bourdeau
　　　Mr. Press
　　　Dr. Tepper

PRECEDING PAGE BLANK NOT FILMED

A-5

NIMBUS G and H

Mission Requirements and Concepts

(Pre-Phase A) Study

Meteorology Program Working Group
Goddard Space Flight Center

20 December 1969

A-7

Foreword

This report was prepared by the Goddard Space Flight Center
Meteorology Program Working Group in response to a request set forth
in a Memorandum to NASA Headquarters, Attention: Office of Space
Science and Applications - Dr. Naugle, from Goddard Space Flight
Center, Office of the Director, dated October 6, 1969, Subject:
"Supplement to POP 69-2 Cover Letter dated August 15, 1969; Phase A
activities and FY'70; Proposed Redefinition of Phase B New Starts."

The Meteorology Program Working Group consists of the following
members:

W. Bandeen, Code 622, Chairman

H. Butler, Code 480

Dr. B. Conrath, Code 622

W. Gould, Jr., Code 733

Dr. W. Nordberg, Code 620

H. Ostrow, Code 731

Dr. I. Rasool, Code 630

J. Schulman, Code 731

W. Shenk, Code 622

A-9

Summary

The Meteorology Program Working Group has identified five
areas requiring further research involving the application of
advanced observing techniques from near Earth satellites beyond
Nimbus F. These areas of research and the types of instrumenta-
tion required for their investigation are: (A) Sea Surface
Phenomena — passive imaging microwave radiometers, active pulse
radars (scatterometers), and imaging multispectral infrared and
visible radiometers of high spatial resolution; (B) Structure
and Phenomena of the Atmosphere above 30 km — advanced vertical
sounders (of high spectral and spatial resolution, sensing at
infrared and microwave wavelengths, and employing both frequency
and limb scanning techniques) and multichannel high precision
photometers; (C) Cloud Structure and Composition — imaging
multispectral infrared radiometers of high spatial resolution
and passive imaging microwave radiometers; (D) Spectral, Spatial,
and Temporal Characteristics of Significant Earth Features —
synthetic aperture radars, passive imaging microwave radiometers,
and imaging multispectral infrared and visible radiometers of
high spatial and spectral resolution; and (E) Interactions
Between Different Levels in the Earth-Atmosphere System —
combinations of the instrumentation in (A), (B), (C), and (D).

Because of an apparent overlap of the meteorological
requirements set forth in (A) and (D) above with Earth resources
objectives, strong consideration should be given to combining
the Nimbus G and H and ERTS E and F missions into single Earth
observations missions.

Requirements having a major impact on the design of the
satellite system are: large microwave antennas (1-to-10 meters
in diameter) with scanning capability, several hundred watts of
average power for the active radars, high pointing accuracies
($\sim$0.02 degrees), a high capacity data storage/transmission system,
and a sun-synchronous orbit not necessarily noon-midnight (e.g.,
4:00 a.m. - 4:00 p.m.).

Contents

I. INTRODUCTION.

The meteorological satellite program is now ten years old. The initial attempt at making meteorological measurements from space was from the Vanguard II satellite launched on 17 February 1959 with a detector intended to map reflected sunlight from the Earth's cloud cover. Several months later on 13 October 1959 the Explorer VII satellite was launched with an omnidirectional radiometer which made the first measurements of the short- and long-wave radiation balance over the Earth. The full-fledged meteorological satellite program began with the launch of TIROS I on 1 April 1960. A total of ten TIROS and three Nimbus satellites has been orbited as of this writing. Perhaps it is well at this point to recount briefly where we have been and what we have accomplished and are about to accomplish before considering the Nimbus G and H missions of the mid-1970's.

TIROS I carried two vidicon cameras and demonstrated the usefulness of space-borne television systems in meteorological research. Research with the early television pictures led to many discoveries concerning the organization and movement of cloud patterns and their relationship to meteorological processes, and limited operational use of the television pictures in weather forecasting was begun soon after the launch of TIROS I. The value of the cloud cover pictures was initially so firmly established that at least one type of imaging device has been included on every meteorological satellite flown to date and will be included on all meteorological satellites now being planned for the future (NASA, 1966).

Subsequent to TIROS I, nine additional TIROS satellites were flown. Some of these carried low resolution or omnidirectional sensors responding to reflected solar radiation and long-wave thermal emission for the purpose of investigating the radiation balance of the Earth-atmosphere system. Some of these also carried a medium resolution, five-channel, scanning radiometer responding to selected wavelength intervals in the visible and in the infrared between about 6 and 30 microns. The scanning radiometer data were applied in many different ways, including cloud cover mapping, the tracking of storms, the determination of surface temperatures and cloud top heights, radiation balance studies, the inference of mean tropospheric water vapor content, and the mapping of mean stratospheric temperatures and their associated circulation patterns (Bandeen, 1969).

The first of the second generation R&D satellites, Nimbus I, was launched on 28 August 1964. It carried an advanced vidicon camera system and a new scanning High Resolution Infrared Radiometer (HRIR). The instantaneous field of view (IFOV) of the HRIR was 0.5 degrees (an order of magnitude smaller than the 5-degree IFOV of the TIROS radiometer). To achieve this IFOV the HRIR utilized a PbSe detector, cooled to 200°K by a single-stage radiative cooler. The HRIR responded to thermal emission between 3.6 and 4.1 microns and, with its spatial resolution of about 7 km at the nadir, yielded imagery that approached the quality of the television cameras. Nimbus II, launched on 15 May 1966, carried the same sensors as Nimbus I, plus a scanning Medium Resolution Infrared Radiometer (MRIR). The MRIR was an advancement over the TIROS five-channel radiometer, having a smaller IFOV (2.9 degrees) and improved spectral and signal-to-noise characteristics.

Nimbus III, launched on 14 April 1969, departed markedly from its predecessors by carrying three new classes of experiments. One, the Monitor of Ultraviolet Solar Energy (MUSE) experiment, monitored wavelengths important to the photochemical processes affecting the generation and destruction of ozone. A second, the Interrogation Recording Location System (IRLS), demonstrated the feasibility of locating moving platforms, such as balloons and buoys, and of collecting in-situ measurements from them and determining atmospheric winds and ocean currents from their movements. The third class, represented jointly by the Infra-Red Interferometer Spectrometer (IRIS) and the Satellite Infra-Red Spectrometer (SIRS), was perhaps most dramatic in demonstrating the ability to sense remotely vertical profiles of temperature in the atmosphere. This is accomplished by suitably "inverting" spectral radiances measured over the 15 micron absorption band of carbon dioxide. The success was so dramatic that vertical temperature profiles from SIRS have been used operationally by ESSA for numerical weather prediction since May 1969 (Wark and Hilleary, 1969). IRIS acquires spectra at a resolution of 5 cm^{-1} from 5-to-20μ; hence in addition to temperatures, vertical profiles of water vapor and ozone have been achieved by inverting radiances measured over the 6.3 micron and rotation water vapor bands and the 9.6 micron ozone band (Hanel and Conrath, 1969). In addition to these new experiments, Nimbus III also carried an Image Dissector Camera System (IDCS), an HRIR, and an MRIR.

Nimbus D, scheduled to be launched in the 1st Quarter of 1970, will carry four vertical sounders, i.e., improved versions of IRIS and SIRS plus a Selective Chopper Radiometer (SCR) and a Filter Wedge Spectrometer (FWS). The SCR will make measurements in the 15 micron band, but the FWS will for the first time acquire spectra in the 4.3 micron band of carbon dioxide. A new Backscattered Ultra Violet (BUV) experiment on Nimbus D will remotely sense vertical profiles of ozone by means of the inversion of radiances measured in the near ultraviolet part of the spectrum. Also a new two channel (at 11 microns and 6.7 microns) Temperature Humidity Infrared Radiometer (THIR) will be flown on Nimbus D in addition to the IDCS, IRLS, and MUSE experiments.

Nimbus E, scheduled to be launched in the 2nd Quarter of 1972, will for the first time carry experiments sensing emission in the microwave part of the spectrum. An Electrically Scanning Microwave Radiometer (ESMR) having an IFOV of $\sim$1.5 degrees will sense emission at 1.55 cm (19.3 GHz). A Nimbus E Microwave Sounder (NEMS) will measure radiances over the oxygen absorption lines near 5 mm (60 GHz) to yield vertical temperature profiles. A new Infrared Temperature Profile Radiometer (ITPR) obtaining radiances in the 15 micron band but having a step-scanning capability and a much higher IFOV (1.5 degrees) than SIRS (12 degrees) or IRIS (8 and 5 degrees), allowing it more readily to see through holes in the clouds, will be tested. A new two-channel scanning Surface Composition Mapping Radiometer (SCMR) designed to sense reststrahlen features near 10 microns and, hence, to distinguish between "acidic" and "basic" surface materials will be tested. The SCMR will employ a HgCdTe detector cooled to 80°K by a two-stage radiative cooler, and will have a very high IFOV (0.6 mrad), thus viewing a spot having a diameter of about 600 meters from an orbital altitude of 1000 km. In addition a Tracking and Data Relay System (T&DRS), an updated version of the SCR, and the THIR will be flown.

Nimbus F is scheduled to fly in the 2nd Quarter of 1973. Its payload has not been completely established yet but in all probability will include advanced vertical sounders (sensing in the 15 micron and 4.3 micron carbon dioxide bands and the 5 mm oxygen band), an Earth radiation balance experiment, a differential doppler constant-level balloon tracking system, a microwave scanning radiometer, and a multispectral imaging infrared radiometer.

Thus, the R&D meteorological satellite program, beginning with the TIROS series and continuing with the Nimbus series through Nimbus F, has developed, or is currently developing, a vast array of sensors which may be divided into the following six categories:

a. Framing devices (television cameras).
b. Non-scanning radiometers (omnidirectional or low spatial resolution).
c. Scanning multispectral radiometers (medium-to-high spatial resolution).
d. Moving platform (e.g., balloon/buoy) location and data collection systems.
e. Indirect vertical atmospheric sounders.
f. Instruments to monitor the direct radiation from the sun (e.g., ultraviolet radiation important in the photochemistry of ozone).

The space technology represented in categories a.-through-e. above and techniques of data analysis and interpretation developed in the R&D satellite program, in large part have been or are being incorporated into the Environmental Survey SAtellite (ESSA) operational system. These developments have emphasized the remote sensing of the troposphere and lower stratosphere, the regions having the most immediate impact upon weather processes affecting man's environment. These developments will also provide the technology upon which the space-based part of the Global Atmospheric Research Program (GARP) of the mid-1970's will draw to provide world-wide measurements of the mass, wind, and moisture fields from the surface to 10 mb (a height of ∿31 km) (COSPAR WG VI, 1969; NAS, 1969). In contrast to the other categories, sensors in category f. heretofore have been intended solely for research purposes without any parallel prospect of their being incorporated into the operational system.

We believe that a significant milestone will have been reached in the applications of space techniques to meteorology after Nimbus F. Up to that point the major thrust of the Nimbus program will have been focussed on making observations for the purpose of describing the initial conditions which must be used in the models for long range numerical forecasts. Specifically, techniques to measure the mass and motion fields on a global scale will have been developed to a degree such that they will be utilized in observing systems for the GARP. After Nimbus F the Nimbus program may continue

to facilitate the refinement of these techniques, but it is not expected that this alone would justify the flying of follow-on observatories.

However, it is also expected that the first global experiments for the GARP will only be the first attempt at making long range weather forecasts and that many gaps in our knowledge of atmospheric processes will render this first attempt less than perfect. Some of these gaps have already been identified in the present planning for the GARP. For example, there are gaps in our understanding of how kinetic energy is generated in the tropical atmosphere and how this energy is transferred to higher latitudes, of how energy is transferred at the air-surface boundary and through the upper layers of the atmosphere, and of what role radiation plays in energy transfers throughout the atmosphere. Undoubtedly, as the GARP progresses many more such gaps will be identified. We believe that new approaches to space-borne observational techniques will be necessary to fill some of these gaps. These techniques will place increasing demands on spacecraft technology to accommodate antennas and telescopes and to provide the required power, data storage, and data transmission capacities. The Nimbus G and H missions should be devoted to these new observational techniques, and the spacecraft should be designed to fulfill the increased demands of the sensor systems.

II. RESEARCH MISSIONS AND CONCEPTS FOR NEAR-EARTH METEOROLOGICAL
     SATELLITES BEYOND NIMBUS F.

The broad objectives of the R&D program in meteorology include:

a. increasing our understanding of processes occurring in
    the Earth-atmosphere system, and
b. developing systems of potential use in the operational
    meteorological satellite system:
(Earth Surveys Planning Panel, 1969).

With respect to item a., a number of critically important parameters have been identified that warrant the development of observational techniques which should be flown on Nimbus G and H. These parameters are the structure of the atmosphere above 30 km, the state of the

surface underlying the atmosphere, especially the sea surface, and the structure, composition and dynamics of clouds.

Observations of interactions between different levels of the atmosphere and between the atmosphere and the land and sea beneath are of comparatively recent origin. It was somewhat of a surprise when in 1912 Dines showed from statistical studies of European balloonsondes that high surface pressure is associated with a warm troposphere and a high cold stratosphere and that low surface pressure is associated with a cold troposphere and a low warm stratosphere. This tendency for the atmosphere to be correlated in the vertical has spurred the use of empirical orthogonal and other statistical functions in many recent applications, a notable one being their application to the problem of indirectly inferring vertical temperature profiles from satellite radiance measurements. Using such functions, it has been shown that the temperature profile throughout the troposphere may be inferred reasonably well from an incomplete set of radiances, say values pertaining only to the upper half of the troposphere and the lower stratosphere (Smith 1969). Similar correlations have been observed in the horizontal, e.g., the surface pressure has been shown to be negatively correlated between the Eastern and Western Pacific Ocean. As numerical models of the atmosphere have become more sophisticated, the necessity to refine the treatments of the turbulent exchange within the atmosphere, the effects of friction of the ocean and land upon the surface boundary layer, and the exchange of sensible heat, water vapor, and momentum between the surface and the atmosphere has become increasingly more important. For example, recent evidence indicates that in order to make a weather forecast of more than about 10-days duration, properties of the ocean from the surface to a depth of about 100 meters must be known (World Weather Program Plan for FY 70, 1969). This point of view is supported by the National Academy of Sciences Plan for U. S. Participation in the Global Atmospheric Research Program. In a discussion of requirements for atmospheric wind, temperature, pressure, and water vapor measurements and for sea-surface temperatures for numerical weather prediction, that report continues ... "The list of variables is not complete. Ocean temperatures and currents above the thermocline, ozone, soil moisture (evapotranspiration), and ice and snow cover are among other variables that must eventually be measured. Estimates of tolerable errors for these are not yet known..." (p. 17 of NAS, 1969).

With respect to Item b. we note that most of the components of the operational satellites have evolved or have been adopted directly from the R&D program. It is evident that many advanced instruments and components for future operational spacecraft must also come from the R&D program of the future.

The Working Group has identified five specific areas requiring further research involving the application of advanced observing techniques from near Earth satellites beyond Nimbus F. These are discussed below.

A. Sea Surface Phenomena.

   1. Sea surface temperature.

   The sea surface temperature (in conjunction with the air surface temperature) is perhaps the most important single parameter in meteorology. It is not only a direct measure of the total amount of energy available at the Earth's surface for driving the atmosphere but also controls the flux of water vapor from ocean to the atmosphere. A knowledge of its variation in time and space is therefore essential to the understanding of the energetics of the ocean-atmosphere system. Scanning radiometers looking down in infrared atmospheric windows have already demonstrated their ability to measure sea surface temperatures in clear skies quite accurately. But obscuration by clouds and other particulate matter and absorption by gases (principally water vapor) tend to give spurious results. Increasing the spatial resolution and employing multispectral measurements should increase the ability of infrared radiometers to see through "holes" in clouds and to apply corrections for gaseous absorption. But in order to make sea surface temperature measurements through an overcast, a passive microwave radiometer operating at a wavelength $(\lambda) > 5$ cm is required. To achieve spatial resolutions of 10-20 km, for measurement at these wavelengths, a large antenna (2 to 3 meters) would be required. The effects of water salinity and sea-surface roughness tend to complicate this type of measurement, but additional research is in progress to resolve this point.

   2. Sea surface roughness.

   The sea surface roughness spectrum contains information from which surface winds may be derived. This information may be of relevance to studies of the exchange of heat, momentum, and moisture

A-19

between ocean and atmosphere. Passive microwave radiometers flown on airplanes have already shown that there is some correlation between roughness and emission at centimeter wavelengths. But ambiguities exist. An active pulse radar (scatterometer) operating at a wavelength (λ) of 2.3 cm (13 GHz) and a passive radiometer operating at a λ of 1.5 cm (20 GHz) have been proposed to eliminate the ambiguities. Such a system might entail one or two large antennas (1-to-2 meters in diameter).

B. Structure and Phenomena of the Atmosphere Above 30 km.

The upper stratosphere and mesosphere (i.e., the region between about 30 km and 90 km) has been largely neglected in our efforts to consider first the lower atmosphere immediately around us with its obvious importance to daily weather. But the entire atmosphere is one, and there is increasing evidence that it is a highly correlated medium.

1. Temperature.

Recent rocket flights indicate that at high latitudes a strong correlation exists between upper air temperature variations and the upward propagation of gravity waves from the troposphere (Theon and Smith, 1970). Also, Wallace and Kousky (1968) have found evidence from an analysis of radiosonde data of downward propagating Kelvin-like waves in the tropical stratosphere accompanied by temperature fluctuations of 3°-5°C. This type of wave produces an upward flux of westerly momentum which may be large enough to account for the westerly accelerations associated with the quasi-biennial oscillation. Vertical sounders in the infrared having very high spectral resolutions (or effectively high spectral resolutions obtained by selective chopping techniques) could determine temperatures up to about 50 km. Vertical microwave sounders sensing in the 5mm (60 GHz) or 2.5mm (120 GHz) absorption bands of oxygen could determine temperatures possibly to about 80 km. A problem in the analysis of the microwave data is caused by Zeeman splitting of the absorption lines in the magnetic field. More work is required in this area to assess this problem adequately. A limb scan technique in say the 15μ carbon dioxide band also appears promising for determining upper atmospheric temperatures to about 60 km. For this technique high pointing accuracies of the order of $\pm$ 0.02 degrees are required.

2. Composition.

Investigations of the composition of the upper air will increase our understanding of atmospheric processes, such as dynamics and photochemistry. For example, recent investigations of the ozone content of the atmosphere, inferred from Nimbus III spectra in the 9.6µ ozone absorption band, indicate a high correlation between ozone in the upper air and tropospheric weather systems (Prabhakara, 1969). We feel that the sensing of ozone profiles and total content on a global scale will be of increased importance as similar studies progress. The measurement of airglow and scattering in the ultraviolet, visible, and near infrared can reveal information regarding the constituents of the high atmosphere and the atomic and molecular transitions resulting in the observed emissions. The possibility of detecting trace constituents by optical occultation techniques appears to be attractive. For example the water vapor distribution in the upper air might be determined by viewing the direct rays of the sun in suitably chosen absorption bands in the visible or infrared. Such information would be applicable to studies of transport mechanisms such as the possibility that large quantities of water vapor are injected into the stratosphere by cumulus towers, especially in the tropics. High precision pointing multichannel photometers with modest sized telescopes (2-to-3 inches in diameter) would be required for this purpose.

C. Cloud Structure and Composition.

Determining the structure of clouds (e.g., their thickness, droplet size distribution, ice-water content, etc.) is important in increasing our understanding of cloud physics and in increasing our ability to treat clouds quantitatively in problems involving atmospheric dynamics, thermodynamics, and radiative transfer. Infrared spectral imaging in the region 1.5µ to 2.5µ has already demonstrated its ability to discriminate between ice clouds and liquid water clouds in aircraft tests. It may be possible to determine the thickness (ice particle content) of cirrus clouds by multispectral sensing at wavelengths having different absorption characteristics due to water vapor and ice particulates, for example at 6µ and 50µ. Such observations of reflected and emitted infrared radiation may be combined with observations of emitted microwave radiation in the 0.5 - 3 cm range (of the type that will be made with Nimbus E and F) to yield a complete

and global picture of cloud structure. The technique would probably consist of three instruments, one for each of the three spectral regions. Instruments would be scanning to produce images of cloud structure. The reflected (solar) infrared instrument would be simplest, with a small multispectral scanning telescope. The emitted IR instrument would require larger optics and would be comparable to the Nimbus E THIR. The microwave sensor would be the most complex, requiring an antenna configuration similar to that on Nimbus F, but with multispectral capability.

D. Spectral, Spatial, and Temporal Characteristics of Significant Earth Surface Features.

The discussion in Section A above illustrates that in many investigations of sea surface phenomena and of air-sea and air-land interactions of meteorological importance, there are coincident Earth resources applications. For example, measurements of sea surface properties are of importance to meteorology regarding air-sea interactions but are also of importance to Earth resources regarding marine food and other resources for man's use. The latter requires high resolution (500 m) multispectral images of solar radiation reflected from the sea surface with a capability to acquire and transmit such data nearly globally and daily. As far as the sensor is concerned this can be accomplished with an instrument of probably lesser complexity than the Multi-Spectral Scanner (MSS) on ERTS A and B; however, it requires an on-board data system of much greater capacity than on ERTS A and B. Measurements of soil moisture and heat capacity are of importance to meteorology regarding their effects on the atmosphere but are also of importance to Earth resources regarding agriculture, hydrology, and geology. Similarly, measurements of ice and snow cover are of importance to meteorology regarding the albedo and heat balance but are also of importance to Earth resources regarding hydrology.

To obtain high resolution measurements of soil moisture, a combined long wave ($\lambda > 5$ cm) imaging microwave radiometer and synthetic aperture radar system appears to be required. Such a system would demand a hundred watts of power or more on the average and entail one or two large antennas of 5-to-10 meters in diameter. Also, to obtain visible and infrared measurements with respect to

ocean and land surface temperatures and to land heat capacity and reststrahlen features, high spectral and spatial resolution imaging spectroradiometers would be required. It would seem purposeful, therefore, to join the Nimbus G and H missions and their contemporary Earth resources missions (ERTS E and F) into combined Earth observations missions.

E. Interactions Between Different Levels in the Earth-Atmosphere System.

Measurements performed in A, B, C, and D above can be utilized in studies of the energy exchange among various levels in the Earth-atmosphere system. For example the vertical soundings of temperature and composition discussed in B, along with a knowledge of the incident solar flux, allow calculations to be made of the radiative energy flux in the upper atmosphere. The flux divergence gives the radiative heating and cooling rates for the various atmospheric levels. Measurements of surface phenomena of the types described in A and D will be useful in establishing the lower boundary conditions of the system. In addition, measurements from a visible radiometer can be used to determine the reflectance properties of the boundary. Measurements described in C for determining cloud structure can be used in calculating radiative energy exchange between cloud layers and between clouds and other atmospheric levels.

III. NIMBUS G AND H SPACECRAFT SYSTEM AND ORBITAL REQUIREMENTS.

The high spatial resolution instruments discussed in Section II. will acquire enormous quantities of data; it appears, therefore, that new methods of data transmission, storage, display, and analysis will be required. For example on-board storage requirements might be eliminated in favor of a real-time relay via a geostationary satellite system to a ground station.

The current Nimbus pointing accuracy is $\pm$ 1 degree along each axis and the body rates are $\pm$ 0.03 degrees/second. There have been infrequent occasions with current Nimbus satellites where large excursions of 5-to-15 degrees in yaw have occurred. For research requiring accurate positioning, it has usually been necessary to identify a coastline or other landmark. To accommodate the much higher spatial resolutions discussed in Section II. improved pointing accuracies and body rates appear to be necessary. But in particular a method of determining the instantaneous attitude of the spacecraft

and of incorporating this information in the data reduction is
a clear requirement.

The orbital height should be rather low for maximum spatial
resolution (∿600 n. mi.), and a high inclination orbit is required
for global coverage. A sun-synchronous orbit, as in the past,
seems to be advantageous to facilitate the analysis of day-to-day
variations (apart from diurnal variations). There appears to be
no scientific reason why the orbital nodes should remain at local
noon and midnight as in the past. In fact there appear to be
valid arguments for shifting the nodes to say a 4:00 a.m. - 4:00 p.m.
position for the purpose of maximizing the diurnal spread of such
measurements as surface temperatures.

The size and power requirements of some of the sensors dis-
cussed in Section II. bring forth the question of whether the
current Nimbus spacecraft will be suitable for the proposed missions.
It appears that a wholly new and larger spacecraft may be required.

IV. CONCLUSIONS.

The following conclusions have been reached in this study:

A. A significant milestone will have been reached in the
applications of space techniques to meteorology after Nimbus F.
By the time Nimbus F is launched in 1973, techniques to measure
the mass and motion fields on a global scale will have been developed
to a degree such that they will be utilized in observing systems for
the GARP. We believe that new approaches to space-borne observational
techniques will be necessary to fill the gaps in our knowledge of
atmospheric processes that have already been identified in the
present planning for the GARP and those that will undoubtedly be
identified in increasing numbers as the GARP progresses.

B. The observational techniques discussed in this report are
necessary to fill some of the gaps in our knowledge. They will place
increasing demands on spacecraft technology to accommodate the re-
quired antennas and telescopes and to provide the necessary power,

data storage, and data transmission capacities. The Nimbus G and H missions should be devoted to these new observational techniques, and the spacecraft should be designed to fulfill the increased demands of the sensor systems.

C. The areas of science and technology discussed in this report should receive additional emphasis in the SRT and AAFE programs in order to prepare the concepts adequately for flight experiments.

D. Because of the apparent overlap of meteorological and Earth resources missions, strong consideration should be given to combining the Nimbus G and H and ERTS E and F missions into single <u>Earth observations missions</u>.

E. The Nimbus G and H orbit should be near the Earth and of high inclination, probably sun-synchronous. It very possibly may be advantageous to have the nodal times at other than noon and midnight as in the past. A suggested combination is 4:00 a.m. - 4:00 p.m.

V. REFERENCES.

Bandeen, W. R., 1969: Experimental Approaches to Remote
Atmospheric Probing in the Infrared from Satellites,
pp. 465-506 in Atmospheric Exploration by Remote Probes,
Vol. 2; Proceedings of the Scientific Meetings of the
Panel on Remote Atmospheric Probing. National Academy
of Sciences, 698 pp. [Also available as GSFC Document
X-622-68-146.]

COSPAR Working Group VI, 1969: Systems Possibilities
for an Early GARP Experiment. Report to the Joint
Organizing Committee (JOC) (January), 55 pp.

Dines, W. H., 1912: The Statistical Changes of Pressure
and Temperature in a Column of Air That Accompany Changes
of Pressure at the Bottom. J. Roy. Meteorol. Soc., 38,
41-50.

Earth Surveys Planning Panel, 1969: Earth Surveys Program
Documentation. NASA Hqtrs., (April 22), 154 pp.

Hanel, R. A. and B. Conrath, 1969: Interferometer Experiment
on Nimbus 3: Preliminary Results. Science, 165, 1258-1260.

National Academy of Sciences, 1969: Plan for U. S.
Participation in the Global Atmospheric Research Program.
U. S. Committee for the GARP, 79 pp.

NASA, 1966: Significant Achievements in Satellite Meteorology
1958-1964. Publication Sp-96, 141 pp.

Prabhakara, C., 1969: Global Ozone from Nimbus III. Paper
in GSFC Science and Technology Presentation (December 3).

Smith, W. L., 1969: Statistical Estimation of the
Atmosphere's Geopotential Height Distribution from
Satellite Radiation Measurements. ESSA Technical Report,
NESC 48, 29 pp.

Theon, J. S. and W. S. Smith, 1970: Seasonal Transitions
in the Thermal Structure of the Mesosphere at High Latitudes,
J. Atmos. Sci. (To be published.) [Also available as GSFC
Document X-621-69-393.]

Wallace, John M. and V. E. Kousky, 1968: Observational
    Evidence of Kelvin Waves in the Tropical Stratosphere.
    J. Atmos. Sci., 25, 900-907.

Wark, D.Q. and D. T. Hilleary, 1969: Atmospheric
    Temperature: Successful Test of Remote Probing.
    Science, 165, 1256-1258.

World Weather Program Plan for FY 70, 1969: Submitted
    on March 13 to The Congress by the President. Reprinted
    in Bull. Amer. Meteor. Soc., 50, 658-686.

ATTACHMENT B

FOLLOW-ON MISSIONS TO

ERTS A AND B

(Report of the GSFC Earth Resources

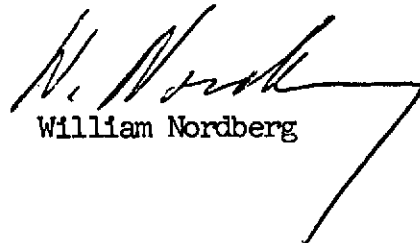Working Group)

UNITED STATES GOVERNMENT

Memorandum

TO   :   Members, GSFC Earth Resources Working Group   DATE: April 20, 1970

FROM :   Chairman, GSFC Earth Resources Working Group

SUBJECT: Outline of Follow-on Missions to ERTS A&B

       The Earth Resources Working Group agreed on 16 April
on the attached outline of follow-on missions to ERTS A and
B. These discussions took into account, in particular, the
excellent report generated by the Meteorology Working Group
on Nimbus G and H which reflects very strongly on ERTS A and
B follow-on missions. Therefore, the results of the Earth
Resources Working Group discussions deal only with additions
to or modifications of the Meteorology Working Group report
on Nimbus G and H.

William Nordberg

Attachment

cc:
Mr. Gubin - Code 730
Dr. Vonbun - Code 550
Mr. Bandeen - Code 622
Mr. Laughlin - Code 733

Dr. Clark - 100
Dr. Pieper - 600
Mr. Stroud - 110
Dr. Stampfl - 401
Mr. Press - 450
Mr. Weiland - 450

OUTLINE OF FOLLOW-ON MISSIONS

TO ERTS A&B BY

GSFC EARTH RESOURCES WORKING GROUP

April 16, 1970

I. Summary

The Earth Resources Working Group believes that there is no basic requirement inherent in Earth surface observations that would necessitate a spacecraft platform which is different or separate from that outlined broadly by the Meteorology Working Group for the Nimbus G & H missions. Also, the variation and occasional conflict in requirements for orbit height, hour angle, and coverage are often greater among Earth surface observation experiments than they are between meteorological and Earth surface observation experiments. For example, thermal infrared observations of soil moisture require almost a twilight orbit, while high resolution visible imagery for the same purpose requires a nearly high noon orbit. Thus, meteorological and Earth Surface observation experiments can be combined on one observatory spacecraft, but requirements for all experiments cannot be met with one mission.

In addition to remote sensing with TV cameras, scanners and radiometers, there is a strong requirement for obtaining photographic images with very high resolution and fidelity. Recoverable film cameras must be flown for that purpose. The Working Group recommends, therefore, that planning for the ERTS C & D missions as film recovery satellites should be continued, while ERTS E & F missions should be planned for electro-optical and radio sensors. From a technological point of view, these two rather diverging objectives could be met by one single spacecraft. However, since there is no compelling scientific requirement to have film recovery and scanners on the same spacecraft, the Working Group does not quarrel with present Agency planning to have two programs for this purpose, but, the ERTS E & F observations should be performed with the same basic spacecraft as the Nimbus G & H missions. This spacecraft should be designated the "Earth Observation Spacecraft" (EOS) combining meteorology and Earth surface experiments.

Two types of Earth surface observations must be distinguished: (a) those requiring high spatial resolution but which may tolerate very limited coverage; and (b) those which require extensive coverage (horizon to horizon) but do not require high spatial resolutions. Differences between these two observation types reflect strongly on the spacecraft data system, on sensor scanning or pointing control and orbit adjust requirements. Both types of observations will be needed with the EOS. Type (a) observations will be largely based on further developments of the ERTS A & B Multispectral Scanner. Advanced sensors, such as imaging radars and very high resolution microwave radiometers could also be used for this type of observation. But, since both the design of these instruments for spacecraft use will be very difficult

and since the physics of the measurements is as yet very poorly understood, we are not very optimistic that radars and microwave radiometers with high spatial resolution will be available for flight in the time frame of 1974/75. Radiowave sensors will be applicable primarily to type (b) observations where both the size of radiometer antennas and the power consumption of radars can be kept within reasonable limits, namely, 10-20 feet and several hundred watts, respectively.

II. Objectives

1. Mapping of spectral, spatial, and temporal characteristics of significant solid earth, vegetation, and hydrographic features including those of snow and ice.

a. Thermatic mapping of reflected sunlight and emitted terrestrial radiation with a spatial resolution greater than that on ERTS A & B but in similar spectral bands will continue to be required for geology, geography, hydrography, demography and agriculture.

b. Extension of imagery to longer wave lengths (microwaves, radio waves) in both the active (radar) and passive (radiometer) modes will be most useful for surveys of soil moisture, ice and snow. Such surveys would be largely independent of cloud cover. In the area of geology, it is questionable whether images from radiowave sensors will be of value, since the spatial resolution at these wavelengths will be orders of magnitude poorer than for visible imagery, and since for geology no rapid repetition of observations will be required. Cloud cover is therefore not as great a problem as it is in other disciplines where repetitive observations are required. Radiowave sensors could be used in geology possibly for the mapping of faults and similar geological features under heavy vegetation cover. However, this would require imaging radars with immense power consumption. Large scale vegetation characteristics and agricultural patterns could be mapped with microwave radiometers.

2. Survey of sea surfaces.

a. Measurements of sea surface temperatures on a global scale, possibly independent of cloud cover and atmospheric conditions, are required for a variety of oceanographic applications. It would be highly desirable to obtain temperature profile measurements of the upper few hundred feet of the oceans; however, no technique for such a measurement from spacecraft can as yet be conceived.

b. Measurements of the composition of the sea surface such as salinity, contaminants (e.g., oil slicks), plant and animal life are required for the study of the ocean circulation as well as for tracking pollutants and for the management of sea food resources.

c. Measurements of sea surface structure, e.g., roughness, depth patterns, etc., are required for study of the ocean dynamics and for aid to navigation.

III. Resolution and Coverage

The Working Group believes that observation coverage must extend at least over an area of about 100 X 100 miles. If coverage is restricted to smaller areas much of the advantage inherent in satellite observations would be lost. Because of data system limitations, objective 1.a., namely, the very high resolution (20 meter) mapping of earth surface features can be fulfilled only with extremely limited areal coverage.

Furthermore, sensor limitations would make it necessary to obtain any larger area coverage through image mosaics. In view of these technical difficulties, it is not expected that the spatial resolution of observations for early Earth Observation Spacecraft will be substantially better than for ERTS A & B.

High resolution measurements, even if limited to the resolution of ERTS A & B, will pose stringent requirements on orbit adjust and spacecraft pointing control, although in some cases the latter may be incorporated into the sensor pointing and scanning mechanism. Orbit contiguity such as is required for ERTS A & B will not necessarily be required for these observations. Some experiments may require, for example, covering the same area, instead of contiguous strips, on consecutive days. In either case, a orbit adjust system will be necessary to fulfill these coverage requirements. This particular coverage requirement would also necessitate steerability of the sensors. With orbit adjust to provide strip contiguity for some sensors, other sensors could cover a given area consecutively for about three days if the sensors are steerable.

Long wave imagers (microwave radiometers and radars) will provide much poorer spatial resolution than cameras and optical radiometers. The Working Group believes that for land surface observations such as mentioned under objective 1.b. the poorest resolution tolerable will be about one kilometer. Higher spatial resolutions are very much desired if possible. Radiowave observations over the sea surface (especially for sea surface temperature measurements) can tolerate much poorer spatial resolutions, of the order of 50 to 100 kilometers for sea surface temperatures on a global scale.

IV. Orbit

In contrasts to meteorological requirements, earth surface observations almost always require the lowest possible orbit height since maximum spatial resolution is often required. However, there is a practical limit to that height since acquisition of wide bandwidth data requires a certain minimum observation time at readout stations. This consideration probably limits the satellite height to no lower than about 400 miles or so. The Earth Observation Spacecraft should therefore be configured so that it can be placed into orbits ranging in height from about 400 to 1,000 miles, depending on the individual mission.

In general, most earth surface observations make it desirable to have a sun synchronous orbit because of coverage, sun angle, and similar considerations. However, the hour angles of these orbits will not necessarily be near high noon. For example, observations of terrestrially emitted infrared radiation from which information on heat capacity of the earth surface would be inferred, require a twilight orbit to make measurements just before sun rise and sun set. Radar observations might also favor such a twilight orbit although the observations physically may not require sunlight but, from a spacecraft point-of-view, a twilight orbit would provide maximum electrical power.

V. Instrumentation

Objective l.a. requires the development of bigger telescopes than on ERTS A & B, more sophisticated scan mechanism, and possibly steering and pointing control for the sensors but does not require fundamentally new developments for optics, detectors, and electronics.

Objective l.b. requires development of microwave radiometers and radars, expecially antennas, which were generally specified in the Nimbus G & H report by the Meteorology Working Group. For polar ice surveys, where thick rain cloud cover is generally not a problem, high frequency (greater than 15 GH_z) microwave radiometers could be employed. Such radiometers would not require excessively large antenna sizes (less than 20 ft.) and could be similar to those now planned for Nimbus F; they might, however, employ multi-frequency and dual polarization. For measurements of soil moisture and for snow surveys very high spatial resolution, although limited coverage, is required. Also, these measurements should be made largely independent of cloud cover over land regions which requires low frequencies (lower than 5 GHz). In that case, antenna sizes of greater and possibly much greater than 20 feet will be needed for radiometers. For the active mode (radars) large power requirements (several hundred watts, if not kilowatts) will be called for.

B-10

A dual approach could be pursued for objective 2.a., sea surface temperature observations. Existing infrared radiometers on ITOS and Nimbus could be modified to provide appropriate spatial resolution, dynamic range, scan rates and data handling to measure sea surface temperatures with very high accuracy (1°C) and high spatial resolution (500 m) in cloud free areas but with limited coverage. These infrared radiometers would be supplemented by microwave radiometers at frequencies lower than 5 GHz, possibly at several frequencies, to measure sea surface temperature with much poorer spatial resolution but globally and independent of cloud cover. Because of the lesser spatial resolution required for that purpose, antenna size here is much less of a problem than for objective 1.b. and a 10 ft. diameter antenna would probably be satisfactory. Physically, measurements would be interpretable in terms of sea surface temperatures over the open oceans, while near coastal areas, salinity patterns could be measured.

To meet objective 2.b. (oil slicks, plant and fish life, etc.) one would probably have to rely primarily on scanners, imaging reflected solar radiation with a spatial resolution of about 1 km. These would be of similar design, but smaller than those used for objective 1.a. Also, the spectral range of the sensors would be different for this ocean-ographic purpose than it was on ERTS A & B or than it would be to meet objectives 1.a.: While for land observations, especially for vegetation and water contrasts, the near infrared part of the spectrum is preferred, sea surface observations require a spectral range at shorter wavelengths, in the green and blue. Wide area coverage will be possible, because of the less stringent spatial resolution.

No sensors are known at this time to determine ocean depth from spacecraft. This can be done only to a limited extent by observing reflected sunlight with the same technique as described for 2.b. above. Roughness of the sea surface might be measured with a radar-radiometer combination in the 10-15 GHz range or perhaps completely passively with the surface temperature radiometers described for 2.a. above. Instrumentation would be similar to that proposed for Nimbus F and for the Saturn Workshop. Since spatial resolution requirements are not very stringent (about 100 km) the antenna sizes would be about 10 ft. and power consumption in the order of 100 watts.

VI. On Board Data System

The high resolution multispectral scanner (objective 1.a.) will require the system to support data rates in excess of 100 million bits per second. The MSS being developed for ERTS A has a ground resolution in the order of 250 feet and with data in four spectral bands generates data at a rate of 15 million bits per second. If the advanced MSS sensors were to have a

ground resolution of 125 feet in eight spectral bands the required data rate would be 120 million bits per second. If a resolution of 60 feet in eight spectral bands was to be achieved the instrument would generate data at a rate of 480 million bits per second. These data rates are beyond the capacity of any on-board data recording system that could be available in time to support the first EOS missions and, as a matter of fact, the higher rate quoted is almost five times the capacity of any ground recording system currently under development.

The lack of on-board storage will require the real time transmission of high resolution data either directly to a ground station or via a data relay satellite system. The availability of a data relay satellite system by 1975 with channel capacities of 100 million bits per second or greater, is very unlikely and would also impose very severe constraints on the spacecraft in terms of the large, high frequency antennas that would be needed to send the data to the relay satellite. The most probable transmission will be directly to a local receiving station via a medium gain, directive antenna on the spacecraft. This antenna will have a gain from 10 to 30 db and be less than one meter in diameter. The radio frequency used will probably be between 6 and 15 GHz since a channel bandwidth in excess of 100 MHz will be required. The transmitter power required to send the data to a 15 to 30 foot antenna on the ground would be on the order of 10 watts. It is probable that any other sensors in the system will have a data rate that is low compared to the advanced high resolution scanner and could be time division multiplexed into the PCM data with a minor increase in the data rate.

The sensors for the oceanographic data (objectives 2.a., b. and 2.c.) will require full coverage and thus require on-board storage or data relay, but fortunately, generally have a much lower data rate. For example, a sensor with a 1 Km resolution over a 1,000 Km field of view will generate data at a rate of 7,000 points per second with a spacecraft ground velocity of 7 Km per second. If the system has 70% scan efficiency and has data in three spectral bands requiring 10 bit precision, it will generate data at approximately 300,000 bits per second. An improved video recorder, similar to that under development for ERTS A, could be developed to have a record to playback speed ratio of 1 to 30 and since a playback data rate of 15 million bits per second is achievable it could record data at 500,000 bits per second for an entire orbit and dump all of the data in a single pass over a ground station. This storage system should be adequate to support all of the sensors requiring "full earth" coverage.

Other aspects of the data system such as command or housekeeping telemetry must meet requirements similar to the existing ERTS or OAO missions and will present no significant problems.

The major problem in the system described is in the developing of a PCM telemetry system capable of multiplexing the many sensor outputs of a high resolution scanner into a PCM data stream at rates greater than 100 million bits per second. The ground recording and reproducing system for this high rate data is also a significant problem.

ATTACHMENT C

SUMMARY OF AAFE

STARTS IN FY-70 AND FY-71

5.1 SUMMARY OF ADVANCED APPLICATIONS FLIGHT EXPERIMENTS

(FY 70 STARTS)

Visible Radiation Polarization Measurement From a Satellite (Sekera; University of California)

Determines atmospheric aerosol content, concentration, distribution, turbidity, by measuring intensity and polarization of light emerging from atmosphere in visible region. Uses a polarimeter at different view angles and sun angles.

Satellite Microwave Radiometry to Sense the Surface Temperature of the World Ocean (Ilidy; North American Rockwell)

Measures sea surface temperature on global basis. Uses a passive microwave radiometer at 2.65 GHz. Thermal resolution is $1°K$ and spatial resolution is 270 nautical miles. Frequency is chosen to be independent of cloud cover (except heavy rainfall).

MIT Aeronomy Experiment (Newell; MIT)

Determines vertical distribution of atmospheric density and temperature, ozone density and atomic oxygen density on a global scale. Measures earth's limb radiances (at several UV and visible wavelengths) using a spectrophotometer. Also uses a star tracker-occultometer for attitude reference and star attenuation profiles.

Radiometric Vertical Sensor (Grauling; Westinghouse)

Determines the local vertical for orienting a space platform. Uses four, 60 GHz radiometers coupled to four $1° X 8°$ antennas in two orthogonal axes. The radiometers are used in a null seeking mode to equalize antenna temperature. System looks at earth's oxygen mantle.

Microwave Occultation Experiment (Lusignan; Stanford University)

Determines atmospheric pressure (density) profile through occultation of a transmitted 5 GHz signal between master-slave satellites. Transmission through earth's atmosphere (at different path lengths, due to different orbits) will alter the phase velocity of the carrier signal and the path of the carrier wave.

Composite Microwave Radiometer-Scatterometer (Pierson; New York Univ.,
Moore; Univ. of Kansas, and Tomiyasu; GE)

Provides information on ocean waves, winds, precipitation, ice
movement, surface temperature, land snow cover, ice fields, flooded areas.
Uses a microwave radiometer and a radar scatterometer. Interlaced
measurements are made of radar differential scattering cross section and
microwave emissivity. This offers a more complete definition of surface
properties and temperature. Frequencies under consideration are 9.3 GHz,
11.7 GHz, and 13.9 GHz.

Carbon Monoxide Pollution Experiment (Bortner; General Electric)

Determines the vertical profile of CO and CO_2 into the mesosphere
and obtains geographic mapping of CO concentrations. Measures earth and
earth's limb radiances at 2.3 or 4.6 microns. Uses a CO Michelson
correlation interferometer. Investigate CO sink mechanisms in the
atmosphere.

Phase-Synchronization of Remote Oscillators (Thompson, Wood; OT/ITS)

Studies the synchronization of remote oscillators by means of a
master-auxiliary-slave station combination. Phase synchronization
over a 65 Km ground track at X-band will be monitored as a function
of atmospheric and other system variables.

Propagation Characteristics of the Atmosphere Near the 22 GHz Water
Vapor Line (Thompson; OT/ITS)

Studies the dynamics of attenuation and dispersive characteristics
of the atmosphere in the 22 GHz region. Phase and amplitude fluctuation
measurements on signals at 9.9, 19.8, 22.2, 24.7, and 34.5 GHz, over a
terrestrial path, will be made and the data anlayzed in terms of spectral
and cross-spectral densities of the variables as well as the statistics
of their distribution. Valuable in assessing the usefulness of 22 GHz
region for space communications.

Ultraviolet Atmospheric Ozone Profile Experiment (Barth, University of
Colorado)

Global measurement of ozone concentrations in the 30 - 55 km
altitude region. Ozone concentrations will also be measured as a
function of spatial and temporal variables. The instrument consists
of a 125 mm. focal length Ebert type monochrometer which will scan
the spectral range 2,000 A to 3000 A with 2 A resolution.

Cloud Physics Radiometer (Flight Tests) (Hovis; NASA-GSFC)

Flight tests of dual channel infrared radiometer. Will determine loud particle type and size using channels around 1.6 and 2.1 microns and cloud altitude using "A" band of oxygen near 0.76 microns. Tests will be made aboard a Lear Jet out of Ames Research Center up to altitudes of 45 K feet. Data will be correlated with available radiosonde data to determine temperature at cloud height.

Fraunhofer Line Discriminator (FLD) Experiment (Hemphill; Dept. of Interior, USGS)

Measures the ratio of central intensity of selected Fraunhofer absorption line to intensity of continuum adjacent to the line; both are measured in incident sunlight and in light from a target (ground, water, or atmosphere) suspected to luminesce. Used to detect luminescent materials such as marine plant chlorophyll, some water pollutants, or aerosols and hydrocarbons in the atmosphere.

Multi-Channel Ocean Color Sensor (MOCS) Experiment (White; TRW)

Incorporates spectrometric measurement of ocean surface for mapping distribution, concentration, and type of organic matter. Uses unique all electronic multispectral line scanner over the visible wavelength range, 4000 A - 7000 A with 150 A spectral resolution. Ground coverage to be 150 x 1 nautical miles. Determine location and concentration of plankton, water pollution, oil slicks, upwellings, sediment, and ocean dynamics.

Global Air Pollution (Ludwig; General Dynamics/Convair)

Measure concentrations of CO, CO_2, SO_2, NO, NO_2, NH_3, and CH_4 to as low as 0.001 ppm and up to 350 ppm on a global basis using a remote gas filter correlation analyzer. The instrument utilizes optical correlation of gases to selectively measure the change in infrared radiation in the 2 - 20 micron range due to specific pollutants. Will afford continuous day and night measurements of isopleths of tropospheric pollutant concentrations to determine dispersal rates and long term buildup, to forecast regional pollution, and to establish relationships with global meteorology. Will also measure pollutant concentrations in the upper atmosphere to study chemical processes and sink mechanisms.

Global Survey of Atmospheric Trace Constituents and Pollutants Using a High Speed Interferometer (HSI) (Farmer; JPL)

Identify minor or trace molecular constituents in the atmosphere over latitudes containing a majority of populated areas by means of measurements conducted with a high speed Fourier interferometric spectrometer. Measurement of absorption spectra in the 1 to 5 micron region will indicate trace pollutant distribution which exhibit a marked degree of localization. Determine sources and sinks of constituents with this high resolution (0.12 cm^{-1}) instrument and study evolutionary cycle of variable materials.

Microwave Temperature Sounding of the Mesosphere and Upper Stratosphere (Staelin; MIT)

Invert radiometric measurements of thermal microwave emission in the upper atmosphere (15 - 80 km) to obtain temperature. Measurements will be taken in four bands near 60 GHz corresponding to weighting function peaks near 70, 50, 40, and 18 km. Instrumentation is a multi-channel passive super-heterodyne Dicke radiometer utilizing one antenna and one local oscillator. Microwave-inferred temperature profiles will be compared with those measured by rocketsondes and collected to produce global temperature profiles in the upper stratosphere and mesosphere.

Atmospheric Propagation Measurements in the 50 to 70 GHz Band (Liebe; OT/ITS)

Determine shape function, strengths, self-and-foreign-gas pressure broadened widths and shifts, and nonlinear overlap correction of $^{16}O_2$ using quantitative microwave refraction spectroscopy (dispersometry) in the 50 - 70 GHz band. Refine atmospheric transmission response in this frequency band by measuring parameters to better than 1 percent. Laboratory tests will be conducted under well defined atmospheric conditions with simulated altitudes between 0 and 200 km over the temperature range 240° K to 350° K.

Microwave Hologram Radar Techniques and Their Application to Earth Resources Study (Zelenka; Univ. of Michigan)

Study expected performance of an orbital microwave hologram radar in a mapping application. Optimize systems parameters to determine capabilities and limitations of this technique for application to earth resources.

Interferometer Position Location (Tsitsera; IBM)

Determine the location of mobile platforms to an accuracy of 1 to 2 km (1σ) using long baseline microwave (L-band) interferometry techniques. Determine feasibility of attaining accuracy through design and ground test of major functional elements. Key components in the three antenna system (one movable and two calibration) include antenna, extendable boom and signal processing and will be developed and tested individually and combined in system operation.

Development of a Nd: YAG Laser for Space Application and a Laser Altimeter (Randall; NASA-MSFC)

Develop an electroluminescent diode-pumped Nd:YAG laser with: (a) 1/2 to 1 watt output at 5300 A; (b) 1 percent or greater efficiency; (c) 1 percent amplitude stability; (d) room temperature operation; (e) 1,000 hour lifetime; and (f) mode-locked operation. Laser will be used in optical communication and altimeter systems which permit 100 megabit/sec data rates and 1 foot accuracy, respectively.

Mode-Locked Laser Radar System (Leonard; Aerospace Corp.)

Measure satellite-to-ground distances to ±5 cm using a mode-locked Nd:YAG laser operating at 1.06μ. The laser will emit 30 p sec pulses at a repetition rate of 300 MHz. A pulse be picked periodically for ranging. Time of flight to a retroreflector will be measured and corrected to 0.1 n sec accuracy by means of an electro-optic light deflector-light detector array. Engineering model development will include field tests over ground-to-ground distances of 10 km. Atmospheric corrections will be applied.

Laser Space Communication Experiment (Goodwin; Hughes Aircraft)

Develop a laser communication system for use between low altitude and synchronous satellites. Will include wide angular tracking and 10.6 micron communication link with doppler compensation.

Only the modulator portion will be developed under the AAFE program. The modulator, cadmium telluride, has better modulator characteristics than the gallium arsenide previously used, and will be used in the heterodyne system to rotate the plane of polarization of the emitted beam.

Laser Gyro Experiment (Kilpatrick; Honeywell)

Establish the integrity, long life, and precision rate performance of a laser integrating rate gyro. Emphasis is placed on long life and low power resulting from the use of high quality materials and operation, and strobed discharge operation, respectively. Aircraft flights will be performed and the laser gyro compared to a highly sensitive torqued gyro. Accelerated life tests will also be performed.

Performance Evaluation of a Strapdown Electrically Suspended Gyro (ESG) (Elwell; Honeywell)

Develop an electrically suspended gyro with 0.0001 degree/hour total drift error, a system readout accuracy of 15 arc seconds and a system life of greater than 30 days. The gyro consists of a highly polished spinning mass which is electrically suspended. A great circle is circumscribed on the rotor and light source-sensors are mounted on three mutually perpendicular axes to generate the direction cosine signals for angular reference. Emphasis is on rotor uniformity (mass balance), rotor polish (signal-to-noise ratio), line scribing (calibration), and line detection (accuracy) techniques.

Multiple Beam Antenna Experiment (Damonte; Lockheed)

Demonstrate practicality of an antenna system capable of providing high gain point-to-point communications and/or area coverage by shaped beams. Will serve as a prototype for future space applications. Work will include analysis of applications configured from existing requirements, construction of suitable feeds and associated feeding network, measurement of radiation patterns, analysis test results, and extrapolation to potential space applications.

Multiple Shaped Beam Antenna Experiment (Ward; Fairchild-Hiller)

Design, develop, and test a 12 GHz antenna system capable of generating multiple shaped beams of r.f. energy from satellite. Will use offset feed to a 4-foot section of a parabola to minimize feed element blockage and reduce sidelobe levels. Beam shape can be chosen by the selection of the feed horns used in the feed matrix.

High Resolution Microwave Sea-Ice Mapping Radiometer (Gloersen; NASA-GSFC)

Measure temperature differences in 1 km square area with a high resolution microwave radiometer to determine percent of ice in a broken field of ice. Emphasis on study and design of electrically scanned high resolution radiometer, including gain, beamwidth, sidelobe levels, and low noise amplification.

Electro-Optic Direction Sensor (Johnston; JPL)

Determine characteristics and limitations of an optical direction sensor based on the anisotropy of crystals. The device would be useful for satellite attitude control or acquisition and pointing. Use as a horizon sensor is also indicated.

Orbiting Gravity Gradiometer (Forward; Hughes Research Labs)

Measure variations in earth's gravity in order to improve the precision of the mathematical description of the earth's gravitational field. The rotating gravimeter consists of two orthogonal, torsionally coupled "dumbbells" whose frequency of rotation is "tuned" to specific harmonic terms. High sensitivity is attainable through the use of computer analysis of resulting data.

ATTACHMENT D

SPACECRAFT TEST CONSIDERATIONS

EOS Test Considerations

The EOS Project will utilize the protoflight development approach which provides a flight spacecraft system tested at Prototype environment levels.* This approach is recognized by the GSFC General Environmental Specification for Spacecraft and Components, S-320-G-1 and has been completely successful through eight launchings of other spacecraft. Orbital performance has indicated no adverse effects from application of the higher test levels as compared to flight spacecraft developed and tested at levels equivalent to the expected mission environment. The Protoflight approach was selected for EOS because it is believed to be cost effective and a proven, reliable spacecraft development process.

Structure and thermal design qualification at the spacecraft level will be accomplished using a combined structural/thermal model spacecraft. Testing the model at prototype levels will provide proof of design margins. Inputs for analytic model manipulation and validation will be obtained to establish flight dynamic loads and expected flight temperatures.

New component and sensor designs will follow a conventional development approach utilizing prototype and flight models

---

*Prototype levels are approximately equivalent to 1.5 times launch stress and ±10°C beyond mission temperature extremes.

for design qualification and acceptance respectively. The Protoflight approach will be used on hardware designs having a successful prior flight history.

Functional testing at the component, sensor, subsystem and system levels during bench, integration, environmental and special tests will be stressed. Sensor and component verification of functional capability will be required at all levels of higher assembly and will be demonstrated under environments simulating the mission, e.g., equipment normally operating during launch would also be operating during simulated launch vibration tests. Sensor/component operation during special tests at ambient pressure and temperature such as system RFI will be a design goal.

The EOS design offers alternatives for the selection of specific test configurations and test flows. For example, it is probable that the thermal design of the major spacecraft elements, appendages, mainbody and sensor bays could be made sufficiently independent to permit thermal balance testing at the major element level as opposed to the full systems configuration. Acoustic testing at the major element level may also be an acceptable alternative for flight qualification of Protoflight Spacecraft. Trade-offs between spacecraft design accommodation and facility capability have been made on Projects such as ATS-F and will be required for EOS in order to surface an adaptive cost-effective and reliable

evaluation program. Competing test flows will be studied during Phase B to define preferred spacecraft configurations.

Technology and facilities for environmental and special tests such as RF, deployment, etc. appears to be limited but within state-of-the-art for EOS. Special stimulus are expected to be necessary for functional testing of the sensors during thermal balance and thermal vacuum test but have not been defined. This latter area is the greatest unknown affecting test program definition and will be studied during Phase B.

From an overall point of view, test guidelines from S-320-G-1 and test experience from prior Observatory programs appears usable for EOS. The need is to optimize cost/reliability.